United States Department of Agriculture

Agricultural Research Service

STREAM CHANNEL EVOLUTION OF LITTLE SALT CREEK AND NORTH BRANCH WEST PAPILLION CREEK, EASTERN NEBRASKA

Prepared by:
Eddy J. Langendoen and Andrew Simon
United States Department of Agriculture
Agricultural Research Service
National Sedimentation Laboratory
P.O. Box 1157
Oxford, MS 38655

Prepared for:
Lower Platte South Natural Resources District, Lincoln, Nebraska
Papio-Missouri Natural Resources District, Omaha, Nebraska

February 2000

EXECUTIVE SUMMARY

The CONCEPTS numerical model was used to assess the channel stability of Little Salt Creek between Raymond and Bluff Roads, Lancaster County, Nebraska, and the North Branch West Papillion and West Papillion Creeks between Fort and West Center Streets, Douglas County, Nebraska. These creeks have incised and widened, and are threatening saline wetlands (Little Salt Creek) and urban infrastructure (West Papillion Creek) adjacent to the channels.

The CONCEPTS model was enhanced to simulate the evolution of cohesive streambeds, which are found in Little Salt and West Papillion Creeks. Field studies were carried out to determine the erodibility of the cohesive streambed-material, the shear strength of the cohesive streambank-material, and the channel geometry. Instantaneous discharge hydrographs were constructed to realistically simulate channel response.

Channel evolution of Little Salt Creek was simulated for a 60-year period. The effects of channel roughness and grade control structures on channel incision and widening were studied. Channel evolution of the North Branch West Papillion and West Papillion Creeks was simulated for a 16-year period. The effects of channel roughness, erodibility of streambank material, discharge, and grade control structures on channel incision and widening were studied.

The simulations indicate that: (1) the modeled reach of Little Salt Creek will degrade over its entire length, varying from 5 ft (1.5 m) near Raymond Road to 13 ft (4.0 m) near Bluff Road; and (2) the modeled reach of the North Branch West Papillion and West Papillion Creeks will degrade between Fort and Maple Streets with an average incision of 9 ft (2.8 m) upstream of Fort Street. Along Little Salt Creek the widening rates are largest near Mill Road, the average widening at the bank top is 5 ft (1.5 m) and the maximum widening is 14 ft (4.3 m). Near the saline wetlands the average widening at the bank top is 2.1 ft (0.6 m) and the maximum widening is 3.9 ft (1.2 m). Along the North Branch West Papillion Creek the average widening of the bank top near Fort Street is 4.1 ft (1.3 m) and the maximum widening is 11.2 ft (3.4 m).

Controlling the streambed at the following bridge crossings along Little Salt Creek is recommended: Raymond Road, North 1st Street, Mill Road, North 14th Street, and Waverly Road. This would reduce channel incision significantly. Channel incision upstream of Raymond Road is prevented, thus protecting the saline wetlands. Incision upstream of Mill Road and Waverly Road is reduced from 6.9 ft (2.1 m) to 2.5 ft (0.8 m) and from 9.6 ft (2.9 m) to 4.1 ft (1.2 m), respectively.

It is recommended to thoroughly examine the nature of the channel bed of the North Branch West Papillion Creek upstream of Maple Street. Present data on the erodibility of the surface of the streambed are inadequate to accurately simulate the evolution of this creek. The increase in resistance to erosion with depth of the streambed must be determined. Grade control structures only reduce erosion in their upstream vicinity. Installing grade control structures 0.38 mi (0.6 km) upstream of Fort Street, at Fort Street, and halfway between Fort and 168th Streets, would reduce average channel incision by approximately 40 percent. However, the maximum channel incision is only reduced by 25 percent. Considerations should be given to prevent extensive wetting of the streambanks along the North Branch West Papillion and West Papillion Creeks downstream of Maple Street. Although the streambed is stable, an increase in water content of the streambank material would cause mass failure of several streambanks.

This report and database can be downloaded from the enclosed CDROM.

ACKNOWLEDGMENTS

The data at the Little Salt Creek were collected by Brian Bell, John Cox, Andrea Curini, and John Massey of the USDA-ARS National Sedimentation Laboratory, Oxford, Mississippi, Gregory Hanson of the USDA-ARS Hydraulic Engineering Unit at the Plant Science and Water Conservation Research Laboratory, Stillwater, Oklahoma, and David Rus, Phil Soenksen, and Vincent Walczyk of the USGS Water Resources Division, Lincoln, Nebraska. Mr. Heath Trost assisted in the preparation of this report and the performing of the simulations. The National Sedimentation Laboratory management and the Channel and Watershed Processes Research Leader Carlos Alonso are acknowledged for providing the resources to carry out this study. The support of the Lower Platte South Natural Resources District, Lincoln, Nebraska and Papio-Missouri River Natural Resources District, Omaha, Nebraska is highly appreciated. This work was performed under Reimbursable Cooperative Agreement No. 58-6408-8-034 between the Papio-Missouri Natural Resources District and the National Sedimentation Laboratory.

TABLE OF CONTENTS

LIST OF FIGURES

LIST OF TABLES

1. Introduction

1.1 Problem Description

Many stream channels in eastern Nebraska were altered in the early 1900's to help alleviate flooding problems. Channel straightening has long been recognized as a cause of channel instability problems (for example, Simon and Rinaldi, 2000), such as downstream deposition, upstream degradation, and widening of the channel, which pose hazards to roads and bridges. In addition the channel banks, which comprise highly erodible soils, were severely eroded by extended periods of saturation following the floods of 1993. Many small county bridges failed or were closed following the floods.

Clearing of large tracts of land during settlement of the region prior to and after the Civil War (Brice, 1966) resulted in increases rates of surface runoff, erosion of uplands, and gullying of floodplains and terraces. Removal of woody vegetation from streambanks resulted in decreased hydraulic roughness, increased flow velocities and stream power, and contributed to increased peak discharges. Much eroded material was deposited in channels, resulting in loss of channel capacity and frequent and prolonged flooding of agricultural lands (Moore, 1917). Moore (1917) reports that aggradation was almost continuous along the trunk streams of southeastern Nebraska.

As a result of ubiquitous channel filling, local drainage districts implemented programs to dredge, straighten, and shorten stream channels (channelize) to reduce flooding and thereby increase agricultural productivity (Moore, 1917). Work was undertaken in southeastern Nebraska around 1910 (Moore, 1917). Dredging and straightening significantly increased bankfull discharge and channel gradient, resulting in a proportionate increase in bed-material discharge and rapid morphologic changes. These changes included upstream degradation, downstream aggradation (in the sand-bedded streams), and bank instabilities along altered streams and adjacent tributaries. In combination with the low resistance to erosion exhibited by the loess-derived channel materials, it is the increase in the erosional force (stream power) by channel dredging and straightening near the turn of the 20th century that caused the deep entrenchment, general states of instability, and present day problems in the channel systems in the loess area of the midwestern United States.

1.2 Purpose

In a cooperative effort, the U.S. Geological Survey-Nebraska District (USGS), the Papio-Missouri River and the Lower Platte South Natural Resources Districts, Nebraska Department of Roads, Federal Highway Administration, University of Nebraska, Lincoln, U.S. Army Corps of Engineers (USACE), and the U.S. Department of Agriculture-Agricultural Research Service-National Sedimentation Laboratory (NSL) are examining the effects of channel instabilities on bridge structures and floodplain resources in a 23-county area of eastern Nebraska.

One aspect of the NSL's role includes numerical channel-response modeling of parts of Little Salt Creek near Lincoln (Figure 1.1), and West Papillion Creek near Omaha (Figure 1.2). Initially, the numerical model study reaches were located on: (1) Little Salt Creek, reach extending from 0.25 mi (0.4 km) upstream of Raymond Road to Raymond Road, Lancaster County; and (2) North Branch West Papillion Creek, (a) a reach extending from Fort Street to 0.5 mi (0.8 km) downstream of Fort Street, Douglas County, and (b) a reach extending from Blondo

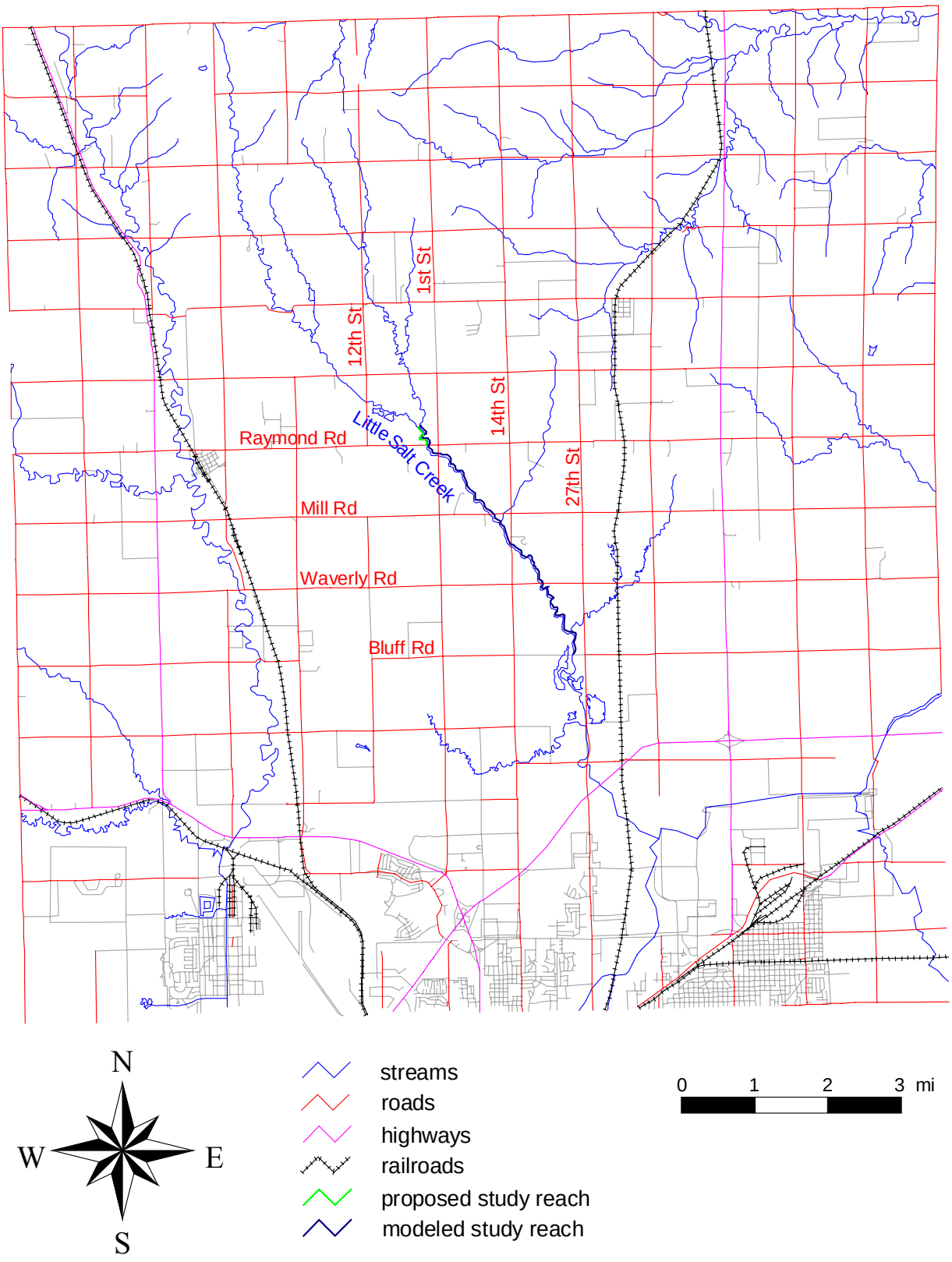

Figure 1.1 Map of the Little Salt Creek, Lancaster County, Nebraska.

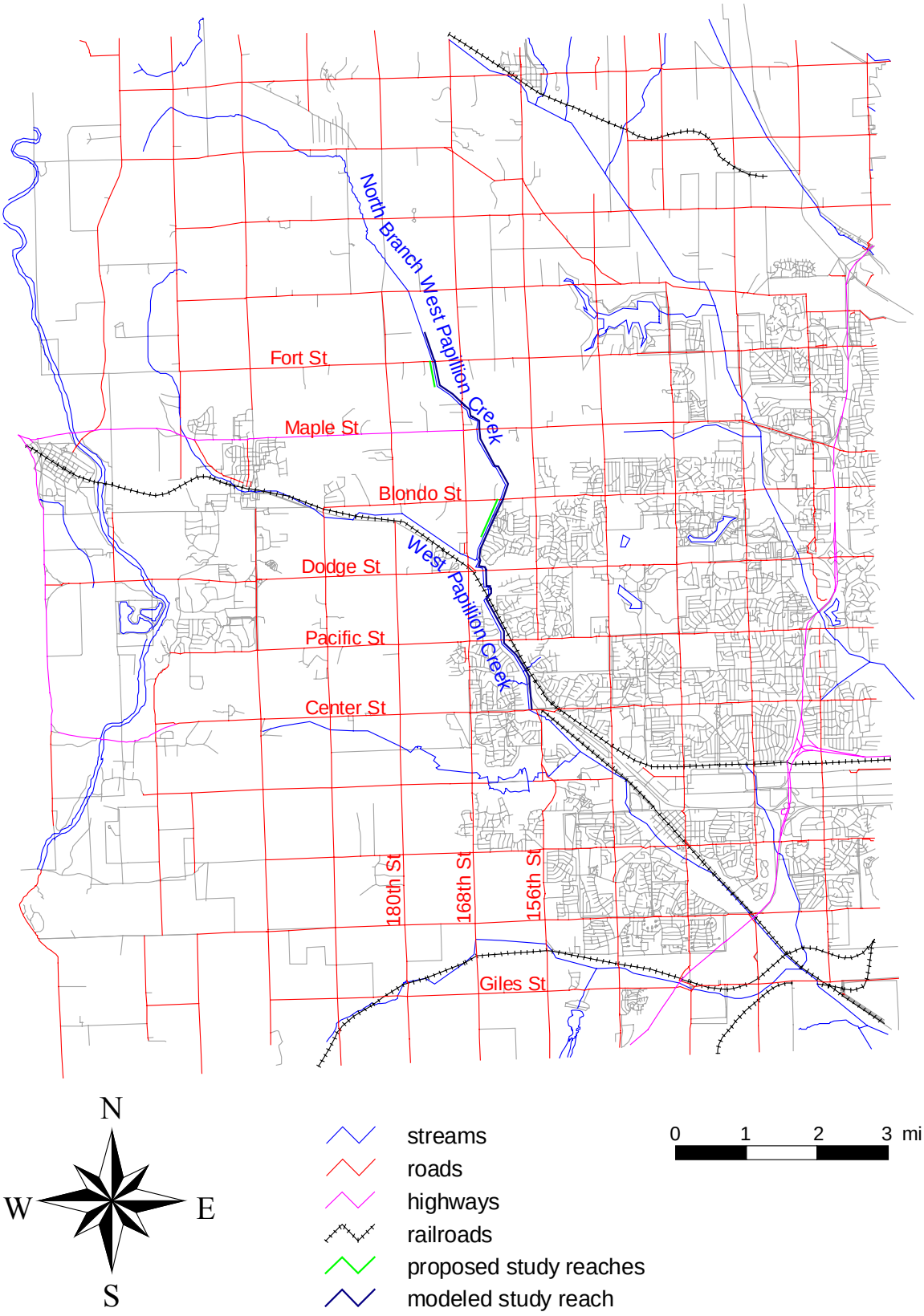

Figure 1.2 Map of the West Papillion Creek, Douglas and Sarpy Counties, Nebraska.

Street to 0.6 mi (1.0 km) downstream of Blondo Street, Douglas County. Early model simulations showed that these reaches were too short to obtain satisfactory results. It was decided to extend the modeling reaches as follows (see Figures 1.1 and 1.2):

1. Little Salt Creek: 0.25 mi (0.4 km) upstream of Raymond Road to Bluff Road. The total channel length is 4.9 mi (7.9 km).
2. West Papillion Creek: 0.45 mi (0.7 km) upstream of Fort Street to West Center Street. The total channel length is 7.3 mi (11.8 km).

The purposes of the modeling efforts are:

1. Evaluate the ability of alternative types and placements of mitigation measures to enhance channel stability (Papillion Creek and Little Salt Creek Basins).
2. Evaluate the effects of urbanization on channel stability (Papillion Creek basin).

1.3 Description of Problem Areas

1.3.1 Little Salt Creek

The Little Salt Creek is a tributary of Salt Creek and drains approximately 46.5 mi^2 (119 km^2). The average channel slope along the modeling reach is 0.0015. Saline wetlands in the Salt Creek basin have diminished from 16,000 acres originally to approximately 1,200 acres (Lower Platte South Natural Resources District, 1999). They hold a diversity of wildlife and contain rare plant communities. A saline wetland north of Raymond Road (Figure 1.3) is endangered by channel incision, which may lead to draining of the wetland. Channel incision may also lead to additional streambank failures and loss of wetland area (Figure 1.4).

1.3.2 West Papillion Creek

The West Papillion Creek is a tributary of the Big Papillion Creek and drains approximately 63 mi^2 (163 km^2) just upstream of the confluence with South Papillion Creek and Hell Creek. The average channel slope along the modeling reach is 0.0023. The West Papillion Creek has been severely impacted by urbanization. The channel has incised and widened significantly (Figures 1.5 and 1.6). Urbanization in the West Papillion Creek watershed is continuing north of Blondo and Maple Streets. It is expected that runoff will increase, leading to continuing incision and streambank failures along the North Branch West Papillion Creek (Figures 1.7 and 1.8).

Figure 1.3 View of Little Salt Creek and wetlands upstream of Raymond Road.

Figure 1.4 Streambank failure along Little Salt Creek north of Raymond Road.

Figure 1.5 Urbanization and streambank failure along the West Papillion Creek between Dodge and Pacific Streets.

Figure 1.6 Streambank failure along West Papillion Creek between Dodge and Pacific Streets.

Figure 1.7 Streambank failure along North Branch West Papillion Creek north of Fort Street.

Figure 1.8 Streambank failure along North Branch West Papillion Creek downstream of Blondo Street.

2. CONCEPTS Model Overview

2.1 Description

The CONCEPTS (CONservational Channel Evolution and Pollutant Transport System) model is being developed to evaluate stream-corridor restoration designs. The basic components of the model are channel hydraulics and morphology. CONCEPTS is designed to simulate unsteady, one-dimensional flow, graded-sediment transport, and streambank-erosion processes. It is capable of simulating the response of channels to instream hydraulic structures such as culverts, bridge crossings, and drop structures. Stage-discharge relations are computed using diffusion or dynamic-wave technology providing a computationally efficient and accurate model (Cunge *et al*., 1980). Channel evolution is computed by tracking bed-elevation changes and channel widening. Streambank erosion accounts for basal scour of bank-material particles by flow and mass wasting of unstable cohesive banks. The following subsections briefly describe the model as it applies to this study. A more detailed description of CONCEPTS can be found in its documentation (Langendoen, 2000).

2.1.1 Hydraulics

Channel flow is computed by relating stage and discharge at cross sections along the channel using laws of mass and momentum conservation. These relations are better known as the Saint Venant equations, which describe unsteady, gradually-varying one-dimensional open-channel flow (Cunge *et al*., 1980). Discharge and stage are directly computed at cross sections along the modeled reach. Hydraulic parameters such as flow top width, flow area, conveyance, or friction slope are a function of stage and discharge, and are determined using look-up tables based on cross-sectional geometry. CONCEPTS simulates the flow at the following hydraulic structures: culverts, bridge crossings, drop structures, and any structure for which a rating curve is available.

2.1.2 Sediment Transport

Flowing water induces sediment transport. Rates of sediment transport are a function of flow variables, composition of the bed material, and upstream sediment supply. The composition of the channel bed may change as particles are eroded or deposited on the bed, thereby changing flow hydraulics and transport rates of various particle sizes (fractional transport rates).

Sediment load is computed by size fraction. There are thirteen prescribed sediment-size classes ranging from clay and very-fine silt particles (wash load) to coarse gravel (Table 2.1). Sediment loads are calculated using a mass-conservation equation with erosion and deposition rates that depend on the type of bed material, that is whether the streambed material is cohesive or cohesionless. Sediments that contain clay particles are commonly cohesive due to the electro-chemical forces between particles, whereas coarse-grained sediments are cohesionless because these forces are absent. In the case of cohesionless streambeds, the local erosion or deposition rate is proportional to the difference between the sediment transport rate and sediment transport capacity. In the case of cohesive streambeds, erosion and deposition rates are based on local shear stress and erodibility of the material.

The modeling reaches have cohesive streambeds. The erosion rate (E) of a cohesive streambed can be defined as:

Table 2.1 Grain size classes used by CONCEPTS.

class	upper bound (mm)	representative diameter (mm)	description
1	0.010		clay – very fine silt
2	0.025	0.016	fine – medium silt
3	0.065	0.040	medium – coarse silt
4	0.250	0.127	fine sand
5	0.841	0.458	medium – coarse sand
6	2.000	1.297	very coarse sand
7	3.364	2.594	very fine gravel
8	5.656	4.362	fine gravel
9	9.514	7.336	fine gravel
10	16.000	12.338	medium gravel
11	26.909	20.749	coarse gravel
12	38.055	32.000	coarse gravel
13	50.000	43.713	very coarse gravel

$$E = K(\tau - \tau_c) \tag{2.1}$$

where K is an erodibility coefficient, τ is the shear stress exerted by the flow on the streambed and τ_c is a critical shear stress at which bed material will be entrained.

2.1.3 Streambank Erosion

In the study reaches streambank erosion has occurred by channel bed lowering followed by mass failure. Erosion of cohesive streambanks is a combination of: (1) lateral erosion of the bank toe by fluvial entrainment of bank-material particles, and (2) mass failure of the bank.

Lateral erosion is calculated following the procedure of Osman and Thorne (1988), which computes erosion rates based on excess shear stress similarly to Eq. (2.1). Osman and Thorne assume that erodibility coefficient K is a function of τ_c following the work of Arulanandan *et al.* (1980). Though the method is process based, it is quite a simplification of nature. The effects of vegetation on the rate of lateral erosion must be accounted for through the critical shear stress.

Streambank failure occurs when gravitational forces that tend to move soil downslope exceed the forces of friction and cohesion that resist movement. The risk of failure is expressed by a factor of safety defined as the ratio of resisting to driving forces:

$$F_s = \frac{\text{Resisting Force}}{\text{Driving Force}} = \frac{\text{shear strength}}{\text{gravity}} \tag{2.2}$$

Shear strength (s) is a combination of cohesion (c') and friction:

$$s = c' + \sigma \tan\phi' - (u_a - u_w)\tan\phi^b \tag{2.3}$$

where σ is the total stress normal to the base of the failure block (slip surface), ϕ is the angle of internal friction, u_a is pore-air pressure, u_w is pore-water pressure, and ϕ^b is an angle indicating the increase in shear strength for an increase in matric suction $(u_a - u_w)$. When driving forces exceed resisting forces, that is $F_s < 1$, the bank will fail.

CONCEPTS computes factor of safety for unsaturated streambanks taking into account the effects of positive and negative pore-water pressures, and confining pressures (Simon *et al.*, 1999). The failure surface does not need to intersect the bank toe. A search algorithm finds the failure-block configuration that has the smallest factor of safety.

2.2 Data Requirements

The accuracy of the calculated hydrographs depends on channel geometry, roughness characterized by Manning's *n*, and upstream and downstream boundary conditions. In CONCEPTS, the upstream boundary condition is a flow hydrograph, and the downstream boundary condition is a looped rating-curve. The model automatically computes the latter condition.

Calculations of sediment load and resulting degradation or aggradation of the streambed depend on flow variables, bed-material properties and composition, and erodibility of cohesive bed material. Computed streambank erosion depends on local flow variables, bank-material properties and composition, bank-material shear strength, and the elevation of the groundwater table to compute pore-water pressures.

2.2.1 Channel Geometry

CONCEPTS divides the channel into computational reaches connected by cross sections. The cross-section geometry is defined by a set of station and elevation points covering the floodplain, streambank, and streambed. From these, tables of flow area, top width, wetted perimeter, hydraulic radius, conveyance, and channel roughness are calculated as a function of stage.

2.2.2 Channel Roughness

Channel roughness is parameterized by Manning's *n*. Channel roughness can be determined from measured stage profiles for given discharge or from *n* values reported in the literature for given channel configurations. Manning's *n* is separately inputted for streambed, streambank, and floodplain.

2.2.3 Sediment-related Properties

Fractional content and unit weight of bed and bank material is required for each of the 13 size classes (see Table 2.1). The erodibility coefficient and critical shear stress to entrain cohesive bed material are needed to compute the erosion rate of the streambed (Equation 2.1).

Fluvial entrainment of bank-material particles is determined using a critical shear stress to entrain bank material particles. An erodibility coefficient is not necessary because it is a function of the critical shear stress. This critical shear stress is inputted by the user.

Streambank-stability analysis uses the effective cohesion and angle of internal friction, and the bulk unit weight of the bank material. To compute the contribution of matric suction to the

factor of safety an angle indicating the increase in shear strength for an increase in matric suction is required.

3. Characterization of Study Sites

NSL scientists visited the study sites on November 1997, August 1998, and March 1999 to collect data in cooperation with the USGS on streambank shear-strength parameters and streambed erodibility. In addition, the USGS surveyed the modeling reaches, took bed and bank material samples, and collected discharge data. Figures 3.1 through 3.7 show the locations where data was collected.

3.1 Channel Geometry

Figures 3.1 to 3.7 show the locations were cross sections were surveyed. Appendix I contains plots of the geometry of each surveyed cross section and the surveyed thalweg profile.

3.1.1 Little Salt Creek

Seven cross sections were surveyed upstream of Raymond Road on December 18, 1997 (Figure 3.1). These cross sections were resurveyed on October 15, 1998 to obtain a more detailed profile of the streambed. On March 15-16, 1999 six cross sections were surveyed upstream of Mill Road (Figure 3.2) and seven cross sections were surveyed near Bluff Road (Figure 3.3).

There are two reaches that could not be surveyed because they were inaccessible:

1. A reach extending from Raymond Road to the first surveyed cross section upstream of Mill Road. The length of this reach is 1.1 mi (1.7 km). Seven simulated cross sections were inserted along this reach with equidistant spacing. Their geometries gradually varied from that of the most downstream surveyed cross section at Raymond Road to that of the most upstream surveyed cross section at Mill Road.
2. A reach extending from Mill Road to the most upstream surveyed cross section near Bluff Road. The length of this reach is 2.2 mi (3.6 km). Seventeen simulated cross sections were similarly inserted along this reach between Mill and Bluff Roads.

Furthermore, two simulated cross sections were inserted between the third and fourth surveyed cross section near Bluff Road to represent a drop in the streambed. The total number of cross sections covering the modeling reach is 46.

3.1.2 North Branch West Papillion and West Papillion Creeks

The following reaches along the North Branch West Papillion Creek and West Papillion Creek were surveyed: (1) 21 cross sections downstream of Fort Street (September 11, 1997, Figure 3.4); (2) 9 cross sections upstream of Fort Street (November 19, 1997, Figure 3.4), which were resurveyed on October 20, 1998 to obtain a more detailed profile of the streambed; (3) 19 cross sections downstream of Blondo Street (September 12, 1997, Figure 3.5); (4) 4 cross sections upstream of West Center Street (November 25, 1997, Figure 3.7); (5) 6 cross sections near North 168th Street (March 17-18, 1999, Figure 3.6); (6) 2 cross sections upstream of Blondo Street (March 18, 1999, Figure 3.5); and (7) 2 cross sections downstream of Dodge Street (March 19, 1997, Figure 3.7).

The following reaches have simulated cross sections inserted because they were not accessible or because the distances between surveyed cross sections were too large to obtain accurate simulation results. In each case, the simulated cross sections were equidistantly spaced and their

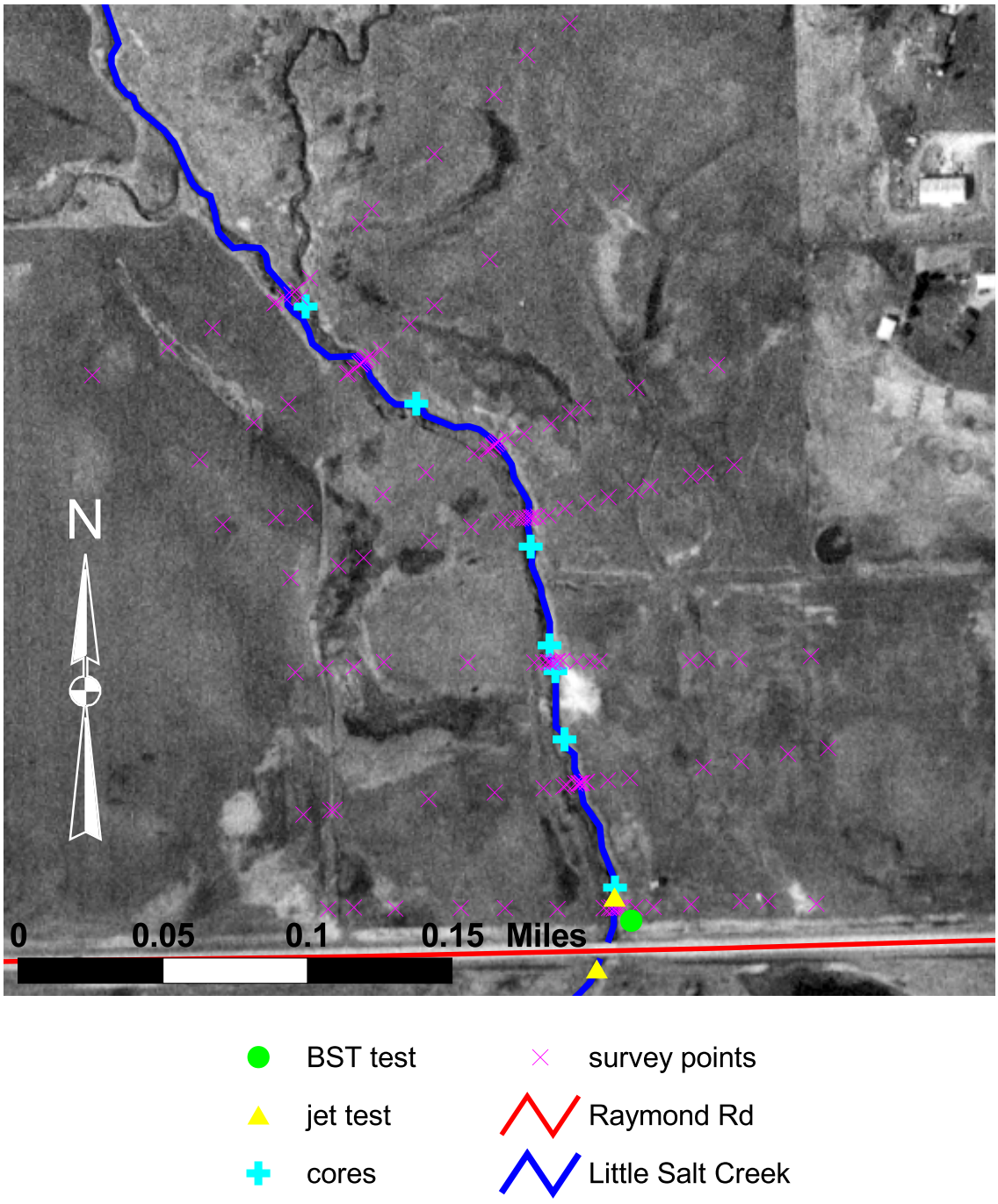

Figure 3.1 Data collection locations at Little Salt Creek near Raymond Road

geometries varied from the most downstream to most upstream surveyed cross sections at the subreach.

1. Two simulated cross sections were inserted near North 168th Street because distances between surveyed cross sections were too large: one cross section between the two most upstream surveyed cross sections near 168th Street, and a second cross section just downstream of 168th Street. The space steps were reduced from 0.344 mi (0.553 km)

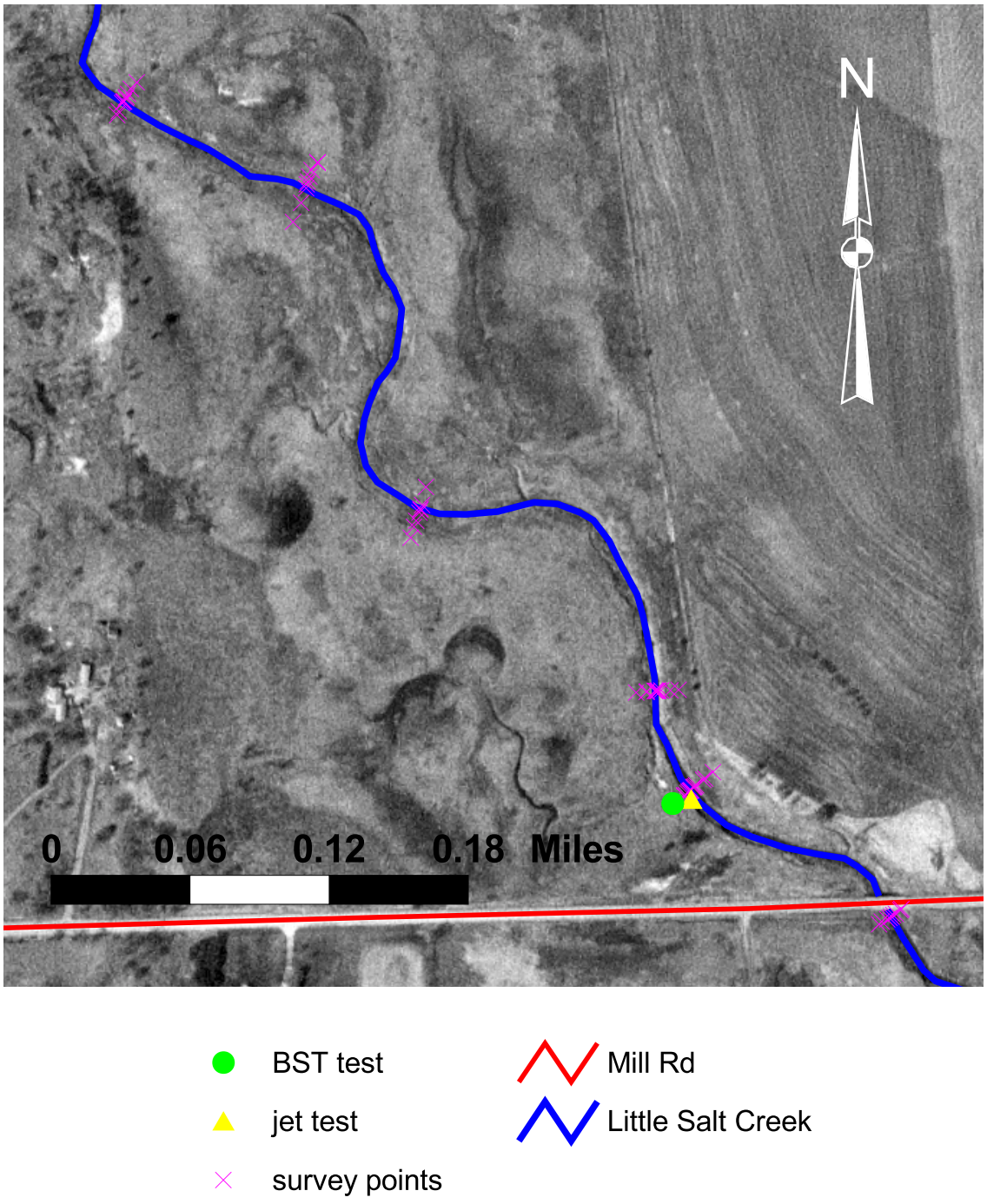

Figure 3.2 Data collection locations at Little Salt Creek near Mill Road.

originally to 0.172 mi (0.276 km) and from 0.239 mi (0.384 km) originally to 0.119 mi (0.192 km), respectively.

2. Nine simulated cross sections were inserted between Maple Street and Blondo Street covering a reach extending from the most downstream surveyed cross section at 168th Street

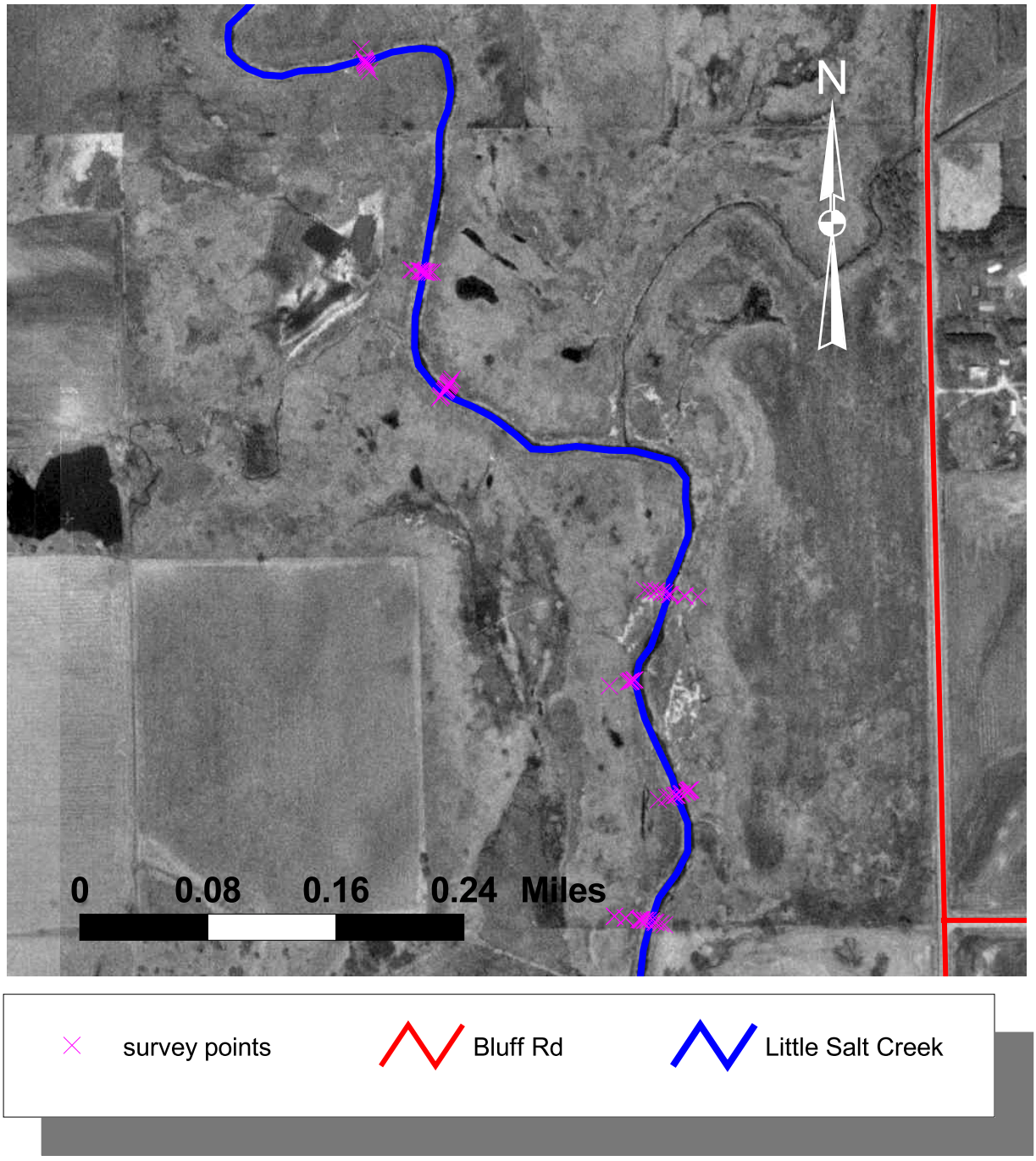

Figure 3.3 Surveyed cross sections along Little Salt Creek near Bluff Road at North 27th Street.

to the most upstream surveyed cross section near Blondo Street. The length of this reach is 1.35 mi (2.17 km).

3. Eight simulated cross sections were inserted along the reach between the most downstream surveyed cross section at Blondo Street and the upstream surveyed cross section downstream of Dodge Street. The length of this reach is 1.19 mi (1.91 km).

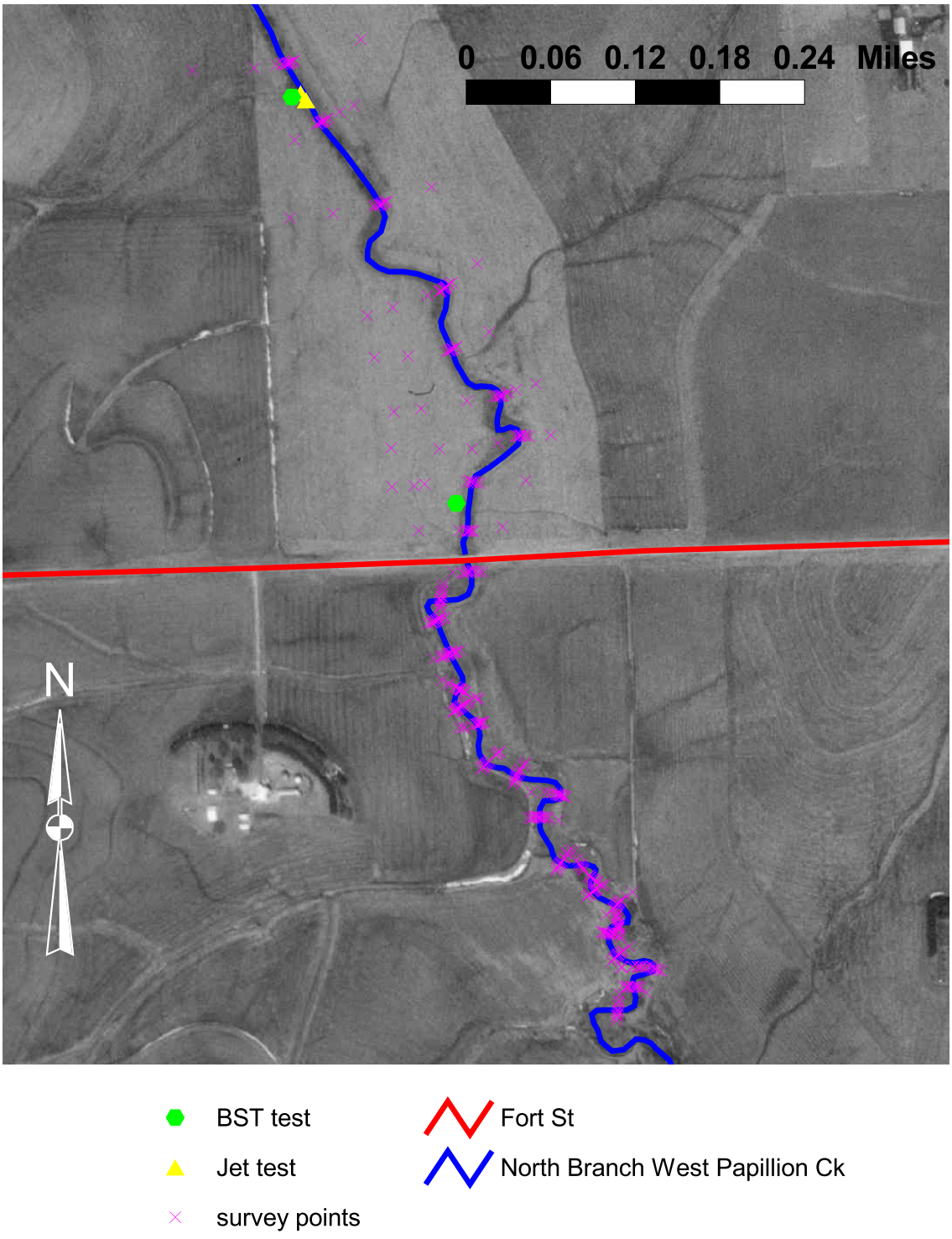

Figure 3.4 Data collection locations along North Branch West Papillion Creek near Fort Street.

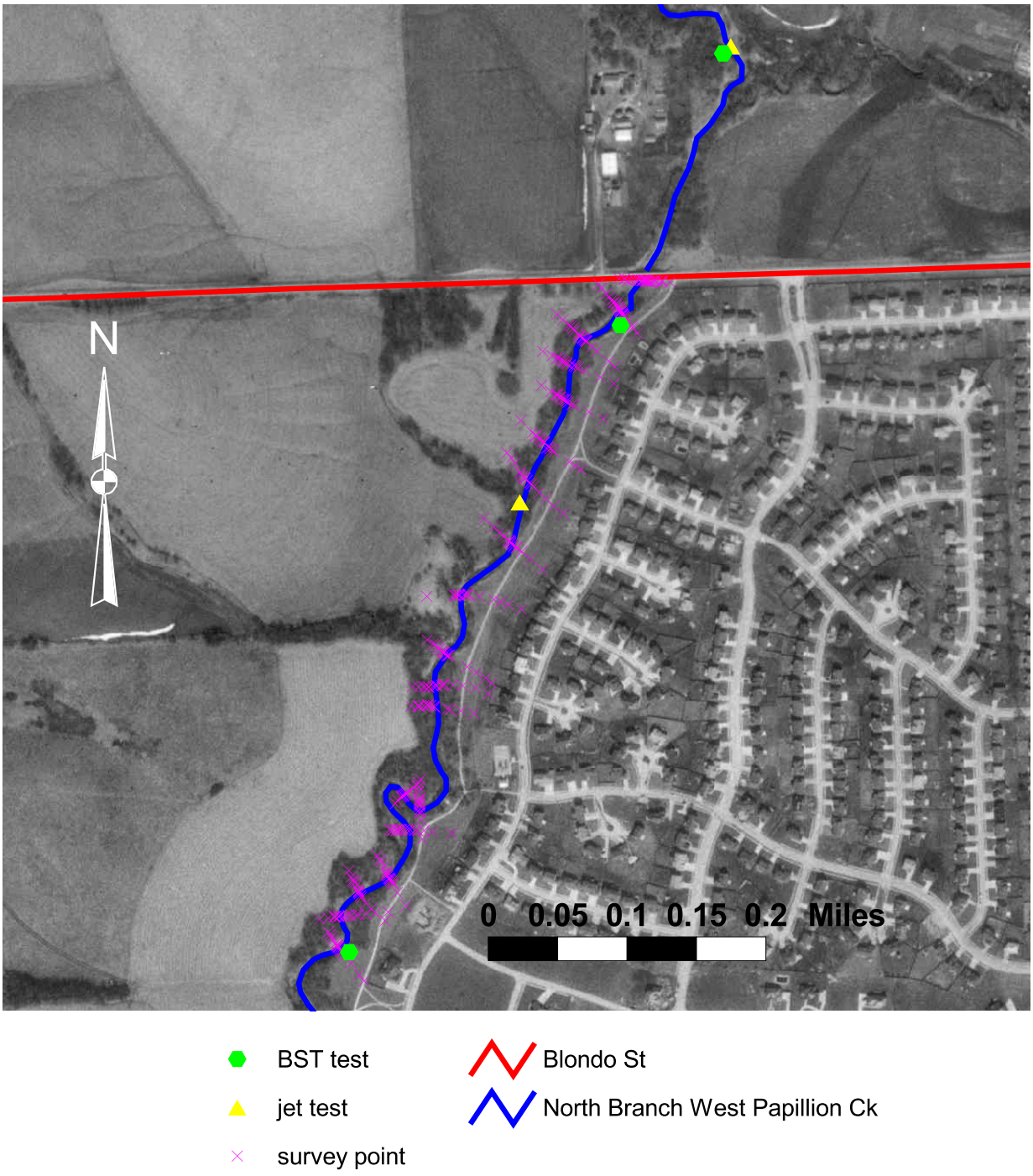

Figure 3.5 Data collection points along North Branch West Papillion Creek near Blondo Street.

4. Twelve simulated cross sections were inserted along a reach from the downstream surveyed cross section downstream of Dodge Street to the most upstream cross section near West Center Street. The length of this reach is 1.64 mi (2.63 km).

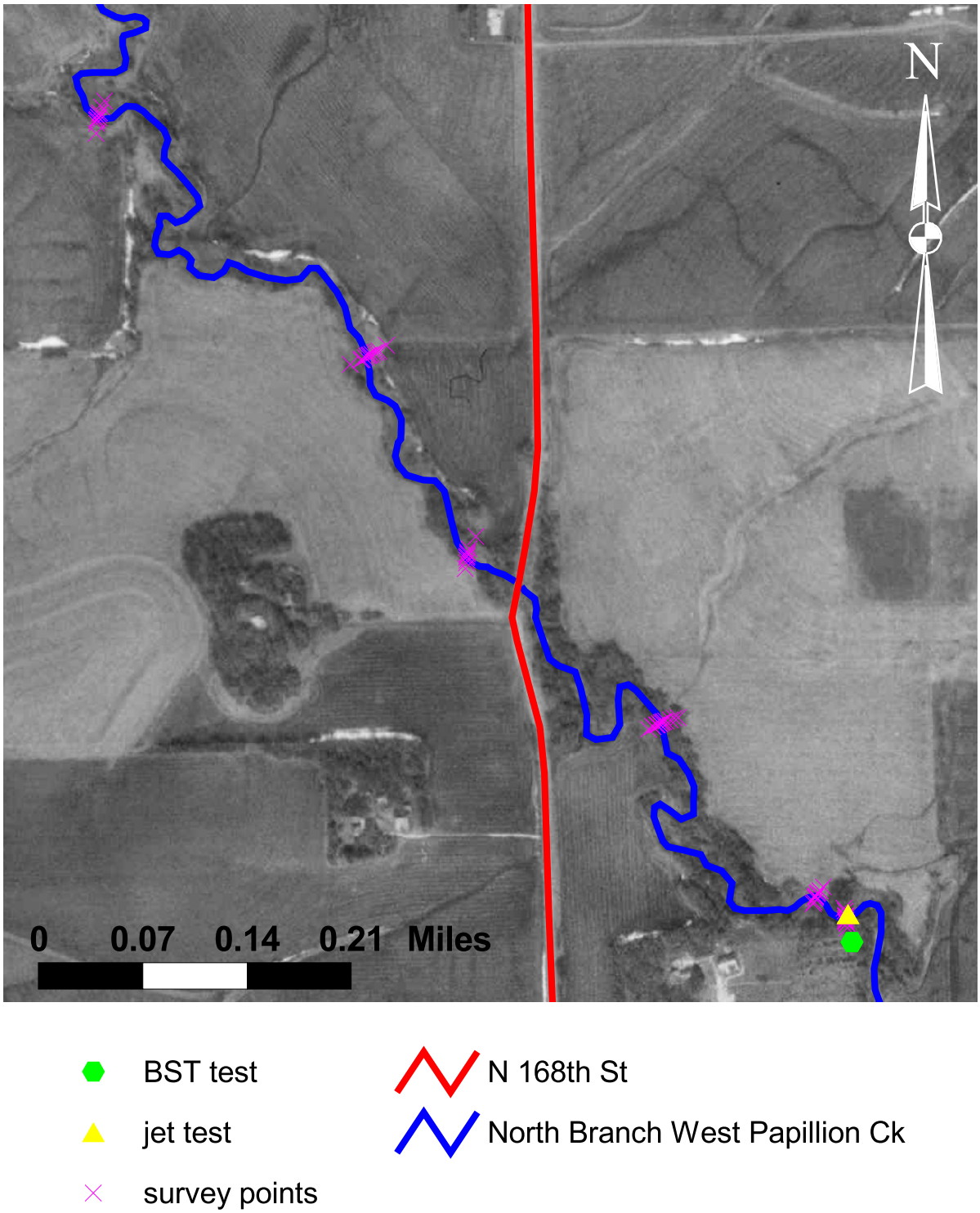

Figure 3.6 Data collection locations along North Branch West Papillion Creek near North 168th Street.

Figure 3.7 Data collection locations along West Papillion Creek between Dodge Street and West Center Street.

3.2 Hydrographs

3.2.1 Little Salt Creek

A USGS gaging station is located at Arbor Road on Little Salt Creek. Daily discharges were provided by the USGS for water years 1969 through 1998. Peak-flow data above a base discharge of 550 cfs (15.6 cms) were available for the same time period. Half-hourly instantaneous discharges were provided by the USGS for water years 1991-1994 and 1996-1998.

Mean daily discharges may not, however, be a good representative of the actual flow because they cannot account for the peak discharge and the commonly rapid rise from base flow to peak flow. The largest shear stresses exerted by the flow on the streambed often occur near peak flow. It is important to properly predict the bed shear stress to accurately predict the evolution of the streambed. The following procedure was used to convert the daily discharges to unsteady flow hydrographs:

1. A base flow discharge of 6.4 cfs (0.18 cms) was selected after analysis of the daily discharge values.
2. Using the available peak-flow data, a ratio between peak discharge and its corresponding daily discharge was determined for each of the 90 peak discharges. The average of all ratios was 3.9.
3. Runoff events were traced from the daily discharges. Discharges smaller than the base-flow discharge were set equal to the base-flow discharge. The maximum daily discharge in a runoff event was then multiplied by 3.9 to obtain the peak discharge. For known peak discharges the calculated peak discharge was replaced by that observed. This resulted in breakpoint data for each runoff event. It was assumed that each discharge value occurred at noon of that day. Two breakpoints were added to the day of peak flow to preserve runoff volume.

CONCEPTS requires discharge hydrographs to be imposed at the most upstream cross-section of the modeling reach. Using drainage-area analysis, the discharges at the gaging station were converted to those at the upstream boundary near Raymond Road. Figure 3.8 shows the drainage area of Little Salt Creek at Raymond Road (16.9 mi^2 (43.8 km^2)) and at the gaging station (43.6 mi^2 (112.9 km^2)). Assuming that discharge is related to drainage area through a power function (Leopold, 1994), the discharge at Raymond Road (Q_R) can be expressed as a function of the discharge at the gaging station (Q_g) and their respective drainage areas (DA_R and DA_g):

$$Q_R = Q_g \left(\frac{DA_R}{DA_g} \right)^{\xi} \tag{3.1}$$

The exponent ξ varies between 0.7 and 1.0 (Leopold, 1994). Similarly, we can determine discharge at the most downstream cross-section near Bluff Road (Q_B). If we neglect attenuation of runoff, the total lateral inflow into the channel is defined as:

$$Q_{lat} = Q_B - Q_R = \frac{Q_g}{DA_g^{\xi}} \left(DA_B^{\xi} - DA_R^{\xi} \right). \tag{3.2}$$

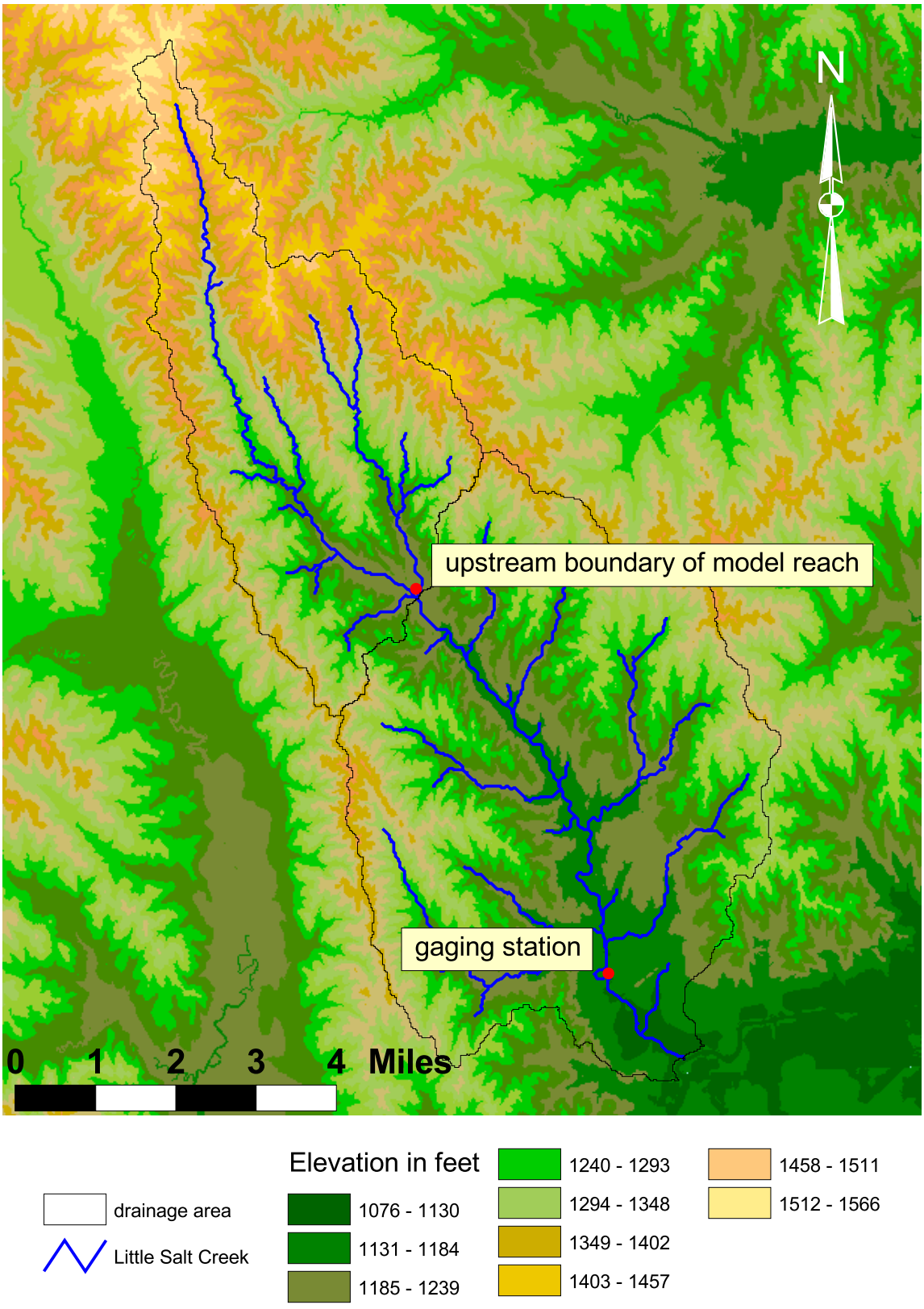

Figure 3.8 Drainage areas of Little Salt Creek at the upstream boundary of the model reach and near the gaging station.

Eliminating Q_g using (3.1) we have for the lateral discharge per unit channel length:

$$q_{lat} = \frac{Q_R}{L}\left(\frac{DA_B^{\xi}}{DA_R^{\xi}} - 1\right) = C_q Q_R, \tag{3.3}$$

where L is the channel length between the most upstream and downstream cross sections of the modeling reach. We see from (3.3) that q_{lat} equals Q_R times a coefficient. Using $DA_R = 16.9\,\text{mi}^2$ ($43.8\,\text{km}^2$), $DA_B = 33.1\,\text{mi}^2$ ($85.8\,\text{km}^2$), $\xi = 0.8$, and $L = 4.88$ mi (7.86 km) we get:

$$Q_R = 0.47 Q_g, \text{ and} \tag{3.4}$$

$$q_{lat} = 9.07\times10^{-5} Q_R. \tag{3.5}$$

Appendix II contains plots of the runoff events used in the model simulations for water years 1969 through 1998.

Additionally, model simulations were carried out with a constant discharge imposed at the upstream boundary. Using the peak-flow data, flood frequency was determined at the gaging station, and flood discharges were converted to those occurring at Raymond Road. The following discharges have been used: 1.05-year recurrence interval, 126.6 cfs (3.58 cms); 2-year recurrence interval, 559.2 cfs (15.84 cms); and 5-year recurrence interval, 1332.4 cfs (37.73 cms).

3.2.2 North Branch West Papillion and West Papillion Creeks

A USACE gaging station is located near Giles Road on West Papillion Creek. Daily discharges are available for water years 1965 through 1977. Hourly instantaneous discharges were available for calendar years 1997 through 1999. Nineteen peak-flow discharges are available for the above time periods.

The procedure outlined above was followed to convert the daily discharges to breakpoint data. Drainage-area analysis was used to convert the discharges to the upstream boundary near Fort Street. Figure 3.9 shows the drainage area of West Papillion Creek above the gaging station. First the discharges at the gaging station ($DA_g = 62.5\,\text{mi}^2$ ($161.9\,\text{km}^2$)) were converted to discharges immediately downstream of the confluence of North Branch West Papillion Creek and West Papillion Creek ($DA_c = 32.8\,\text{mi}^2$ ($85.1\,\text{km}^2$)). This discharge was then partitioned into a discharge from West Papillion Creek ($DA_W = 17.3\,\text{mi}^2$ ($44.9\,\text{km}^2$)) and a discharge from North Branch West Papillion Creek ($DA_N = 15.5\,\text{mi}^2$ ($40.2\,\text{km}^2$)) using their respective drainage areas. Thus, 53 percent of the discharge downstream of the confluence is contributed by West Papillion Creek and 47 percent by North Branch West Papillion Creek. The discharge at the North Branch West Papillion Creek just upstream of the confluence is then converted to the upstream boundary near Fort Street ($DA_F = 11.4\,\text{mi}^2$ ($29.5\,\text{km}^2$)). This yields:

$$Q_F = 0.22 Q_g \tag{3.6}$$

where Q_F is the discharge at the upstream boundary of the model reach.

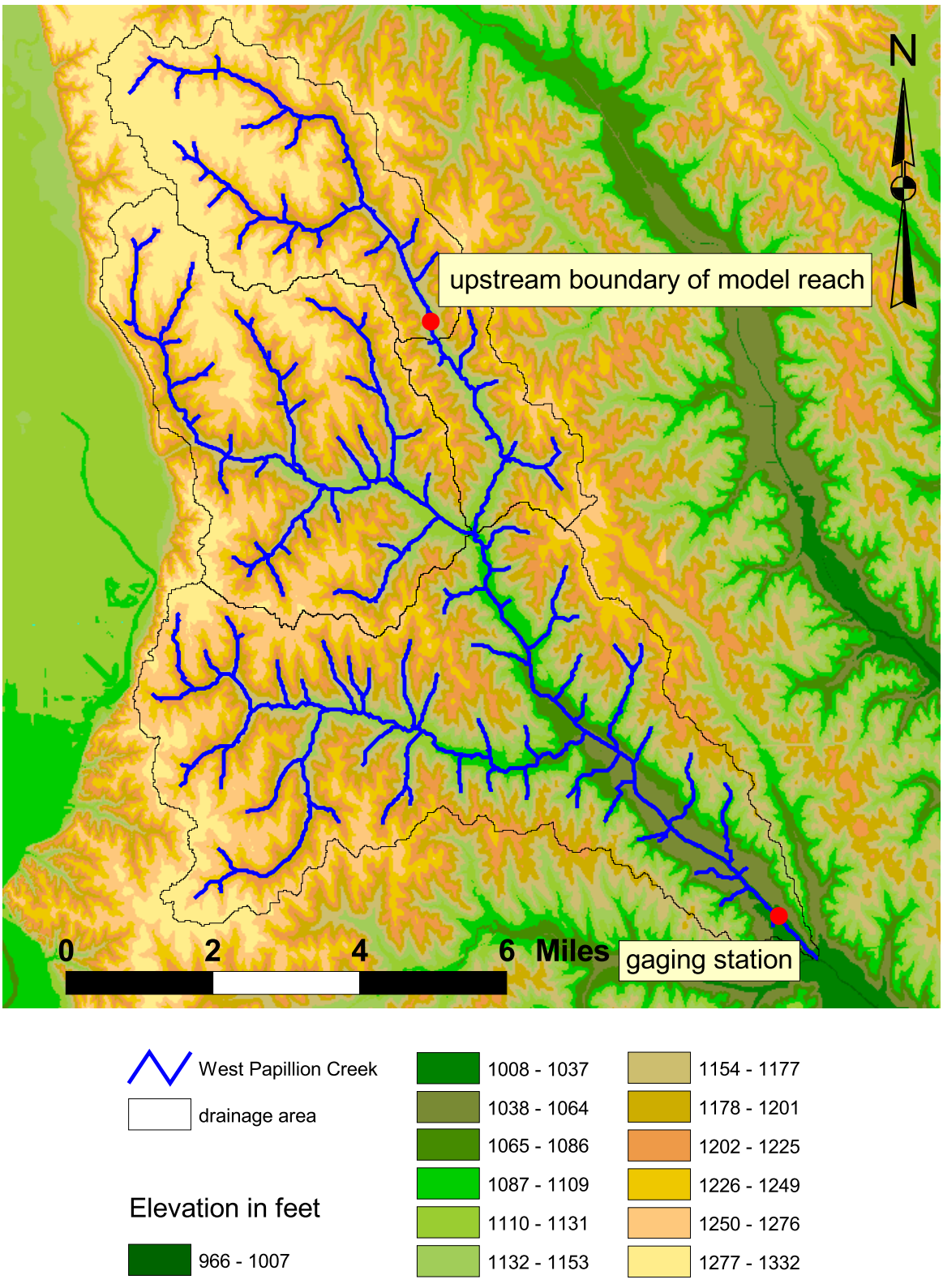

Figure 3.9 Drainage areas of West Papillion Creek at the upstream boundary of the model reach, near the gaging station, and the confluence of West Papillion Creek and North Branch West Papillion Creek.

The lateral inflow per unit channel length is then given by

$$q_{lat} = 5.04 \times 10^{-5} Q_F \tag{3.7}$$

Appendix II shows plots of the runoff events used in the model simulations for water years 1965 through 1977 and calendar years 1997 through 1999.

Additionally, model simulations were carried out with a constant discharge imposed at the upstream boundary. Using the peak-flow data, flood frequency was determined at the gaging station, and flood discharges were converted to those occurring at Fort Street. The following discharges have been used: 1.05-year recurrence interval, 277.9 cfs (7.87 cms); 2-year recurrence interval, 1384.3 cfs (39.20 cms); and 5-year recurrence interval, 2805.0 cfs (79.43 cms).

3.3 Bed-Material Properties

In situ field experiments were performed using a submersible jet device (Hanson, 1990) to measure the erodibility coefficient (K) and critical shear stress (τ_c) of the cohesive streambed material of Little Salt Creek and West Papillion Creek (Figure 3.10). The apparatus consists of a submerged jet with a nozzle diameter of 13 mm, set at a height of 0.22 m above the initial soil surface. Monitoring the depth of scour during a test yields the erodibility coefficient and critical shear stress. Bed-sediment samples were collected to determine particle size distributions.

3.3.1 Little Salt Creek

Jet tests were carried out upstream and downstream of Raymond Road on November 3 and 4, 1997 (Figure 3.1). At each location two bed material samples were collected. Seven cores, up to 2.5 ft long, were obtained from the streambed upstream of Raymond Road to characterize the bed material (see Figure 3.1). Two jet tests were carried out upstream of Mill Road on March 15, 1999 (Figure 3.2), and one jet test just downstream of Waverly Road on March 16, 1999.

Table 3.1 lists the results of the jet tests. Table 3.2 lists the composition of the bed material samples.

3.3.2 North Branch West Papillion and West Papillion Creeks

Jet tests were performed: (1) downstream of Blondo Street (November 5, 1997, Figure 3.5); (2) upstream of Fort Street (November 6-7, 1997, Figure 3.4); (3) downstream of 168th Street (March 17, 1999, Figure 3.6); (4) upstream of Blondo Street (March 18, 1999, Figure 3.5); and (5) downstream of Dodge Street (March 19, 1999, Figure 3.7). Bed material samples were collected at the 1997 test sites (downstream of Blondo Street and upstream of Fort Street). Table 3.1 lists the results of the jet tests. Table 3.2 lists the composition of the bed material samples.

Table 3.1 Results of jet tests.

site	critical shear stress τ_c (psf)	(Pa)	erodibility K, $\times 10^{-6}$ (ft / psf s)	(m / Pa s)
Little Salt Creek				
Raymond Rd upstream	0.00	0.0	419.1	2.67
Raymond Rd downstream I	0.13	6.3	50.2	0.32
Raymond Rd downstream II	0.17	7.9	105.2	0.67
Mill Rd upstream I	0.13	6.0	18.8	0.12
Mill Rd upstream II	0.22	10.7	9.4	0.06
Waverly Rd downstream	0.00	0.2	351.6	2.24
West Papillion Creek				
Blondo St downstream I	1.34	64.0	1.1	0.007
Blondo St downstream II	0.94	45.0	1.4	0.009
Fort St I	0.00	0.02	78.5	0.50
Fort St II	0.00	0.05	588.7	3.75
Fort St III	0.05	2.6	56.5	0.36
168th St I	0.20	9.6	14.1	0.09
168th St II	0.21	10.0	28.3	0.18
Blondo St upstream I	1.52	72.6	1.6	0.010
Blondo St upstream II	0.36	17.3	3.6	0.023
Dodge St I	1.12	53.7	1.6	0.01
Dodge St II	3.83	183.4	3.1	0.02

Table 3.2 Bed-material composition.

site	% clay	% very fine silt	% fine silt	% coarse silt	% total sand	textural class
West Papillion Creek						
Fort St Bed I	16.52	3.09	22.17	26.81	31.41	silt loam
Fort St Bed II	21.23	4.14	27.94	30.01	16.69	silt loam
Fort St Bed III	17.03	2.06	25.78	38.15	16.98	silt loam
Fort St Bed IV	18.58	2.58	26.81	36.60	15.43	silt loam
Blondo St Bed I	25.73	5.77	40.41	23.09	5.00	silt loam
Blondo St Bed II	27.77	4.19	39.79	22.51	5.75	silty clay loam
Blondo St Bed III	29.81	5.23	36.58	21.43	6.96	silty clay loam
Little Salt Creek						
Raymond Rd Bed I	11.74	1.02	17.32	18.34	51.58	loam
Raymond Rd Bed II	14.87	2.05	21.51	33.80	27.76	silt loam
Raymond Rd Bed III	10.69	2.03	10.16	8.13	69.00	sandy loam
Raymond Rd Bed IV	20.63	0.52	6.70	51.01	21.14	silt loam

Figure 3.10 Submersible jet device at left and borehole shear test device at center.

Figure 3.11 Borehole shear test device being lowered into the borehole.

3.4 Bank Material Properties

A series of in situ field experiments were performed using a borehole shear test (BST) device (Luttenegger and Hallberg, 1981, see Figure 3.11) to determine the shear strength of the cohesive streambank material of Little Salt and West Papillion Creeks. The shear-strength parameters determined by the BST device are apparent cohesion and angle of internal friction. Bank material samples were collected at the BST locations to determine bank material composition and unit weight.

3.4.1 Little Salt Creek

Successful BST experiments were carried out upstream of Mill Road on March 15, 1999 (see Figure 3.2 for their location) and downstream of Waverly Road on March 16, 1999. Bulk density of the bank material was determined at these sites as well as at a failed test site upstream of Raymond Road (Figure 3.1). Bulk densities varied from 2.39 slug/ft^3 (1.23 g/cm^3) to 3.51 slug/ft^3 (1.81 g/cm^3). The average bulk density is 3.07 slug/ft^3 (1.58 g/cm^3). Bank material composition was determined for a sample collected at the test site upstream of Raymond Road. Table 3.3 lists the shear-strength parameters of the bank material measured with the BST. Table 3.4 lists the composition of the bank-material sample.

3.4.2 West Papillion Creek

Successful BST test were carried out downstream of 168th Street on March 17, 1999 (see Figure 3.6 for their location), upstream of Blondo Street on March 18, 1999 (Figure 3.5), and downstream of Dodge Street on March 19, 1999 (Figure 3.7).

Bulk density of the bank material was determined at these sites as well as sites where BST tests failed: upstream of Fort Street (Figure 3.4) and downstream of Blondo Street (Figure 3.5). Bulk densities varied from 1.92 slug/ft^3 (0.99 g/cm^3) to 3.36 slug/ft^3 (1.73 g/cm^3). The average bulk density is 2.81 slug/ft^3 (1.45 g/cm^3). Bank material composition was determined of samples collected upstream of Fort Street and downstream of Blondo Street. Table 3.3 lists the shear-strength parameters of the bank material measured with the BST. Table 3.4 lists the composition of the bank-material samples.

Table 3.3 Results of BST tests.

site	effective cohesion (psf)	effective cohesion (kPa)	effective angle of internal friction (degrees)
Little Salt Creek			
Mill Rd, 3.3 ft (1 m) below soil surface	35.5	1.7	26.6
Mill Rd, 8.2 ft (2.5 m) below soil surface	108.7	5.2	32.2
Waverly Rd, 6.6 ft (2 m) below soil surface	112.9	5.4	31.0
Waverly Rd, 9.8 ft (3 m) below soil surface	98.2	4.7	33.8
West Papillion Creek			
168th St, 3.3 ft (1 m) below soil surface	96.1	4.6	27.5
168th St, 6.6 ft (2 m) below soil surface	148.4	7.1	28.8
Blondo St, 3.3 ft (1 m) below soil surface	167.2	8.0	26.1
Blondo St, 8.2 ft (2.5) m below soil surface	12.5	0.6	32.2
Dodge St, 9.8 ft (3 m) below soil surface	77.3	3.7	30.5

Table 3.4 Bank-material composition.

site	% clay	% very fine silt	% fine silt	% coarse silt	% total sand	textural class
Little Salt Creek						
Raymond Rd	20.43	2.03	24.32	31.42	21.77	silt loam
West Papillion Creek						
Fort St I	24.86	4.66	35.19	26.39	8.91	silt loam
Fort St II	18.95	2.05	26.61	38.89	13.51	silt loam
Blondo St I	28.46	6.21	41.37	19.65	4.31	silty clay loam
Blondo St II	25.24	2.06	35.00	27.79	9.91	silt loam
Blondo St III	21.06	4.11	37.46	26.17	11.21	silt loam

4. Little Salt Creek Study Results

4.1 Setup of Simulations

The computer model CONCEPTS was used to study the long-term stability of Little Salt Creek between Raymond Road and Bluff Road, Lancaster County. Seven model runs were performed (Table 4.1). Runs 1 through 4 simulated the response of the channel to the 30-year breakpoint discharge for various bed roughnesses. Runs 5 through 7 simulated the response of the channel to the 1.05-year, 2-year, and 5-year runoff events, respectively.

Table 4.1 Simulations performed for the Little Salt Creek study

run	discharge	Manning *n*
1	30-year breakpoint	0.025
2	30-year breakpoint	0.020
3	30-year breakpoint	0.015
4[†]	30-year breakpoint	0.015
5	1.05-year flood: 127 cfs (3.58 cms)	0.025
6	2-year flood: 559 cfs (15.8 cms)	0.025
7	5-year flood: 1330 cfs (37.8 cms)	0.025

[†]Channel-stabilization alternative

The following parameters were the same for all runs and all cross sections:

- Manning's *n* of streambanks and floodplains were selected as 0.06 and 0.15, respectively. However, the streambanks upstream of Raymond Road had *n* values of 0.08, because of the level of vegetation overgrowth.
- The critical shear stress to entrain bed material was 0.16 psf (7.7 Pa). This is the average of the values measured by the jet test device after dropping those with negligible τ_c (Table 3.1). The erodibility coefficient is the average of the four selected jet-test values, 43.5×10^{-6} (ft/psf s) (0.28×10^{-6} m/Pa s). Because the knickpoint upstream of Bluff Road was protected by stones, the critical shear stress was set to an arbitrary large value not exceeded by the shear stress exerted by the flow on the streambed.
- Data on the critical shear stress to entrain bank-material particles was unavailable. Therefore, it was assumed equal to that of bed material particles, that is 0.16 psf (7.7 Pa).
- Shear-strength parameters, effective cohesion and angle of internal friction, of the bank material were selected as 94.1 psf (4.5 kPa) and 30 degrees, respectively. The average measured effected cohesion is 89 psf (4.3 kPa) and average measured angle of internal friction is 30.9 degrees. The bulk unit weight of the bank material is assumed 108.2 lb/ft^3 (17 kN/m^3), which is a 10 percent increase over the average dry bulk unit weight to include water content of the streambank material. The angle indicating the increase in shear strength for an increase in matric suction is set to 17 degrees. The groundwater table at each streambank was 3.3 ft (1.0 m) above the bank toe elevation.

In the following sections the distance downstream of the upstream boundary of the modeling reach is referred to as "model mile."

4.2 Sensitivity to Bed Roughness

The shear stress exerted by the flow on the bed depends on the roughness of the bed. It is difficult to determine the roughness of cohesive streambeds if stage profiles for various discharges are unavailable. For cohesive streambeds, conventional methods that relate the resistance parameter Manning's *n* to a characteristic grain size estimate unrealistically small *n* values. Simulation runs were performed for three different values of Manning's *n*: 0.025 (run 1), 0.02 (run 2), and 0.015 (run 3) to determine the effect of Manning's *n* on channel evolution.

Figures 4.1 through 4.3 show the predicted thalweg profiles of the modeling reach at various points of time. The elevation of the channel bed at the downstream boundary of the modeling reach was not kept constant during the simulation. Therefore, the downstream end of the modeling reach is degrading like the rest of the reach. In reality, the downstream boundary of the reach is controlled by processes occurring further downstream, such as at the confluence of Little Salt Creek with Salt Creek. However, the bed protection at the drop (0.35 mi (0.56 km) upstream of the downstream boundary) prevents any incision at the downstream boundary from propagating upstream.

The figures show that the modeling reach is degrading. The rate at which degradation progresses decreases with decreasing roughness of the bed. Also, the depth of incision slightly decreases with decreasing bed roughness. The channel incision varies from about 14 ft (4.3 m) at the downstream end of the channel (model mile 4.4 (7.1 km)) to 5 ft (1.5 m) at the upstream end of the channel.

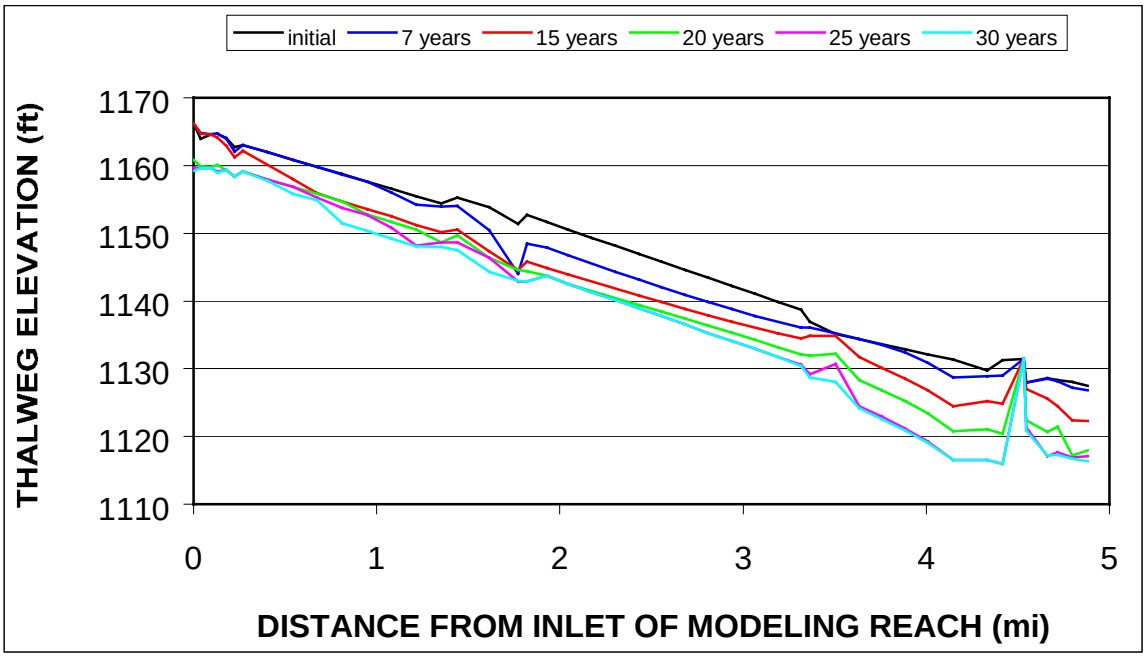

Figure 4.1 Simulated evolution of the thalweg profile, Little Salt Creek, for a 30-year period with *n*=0.025 (run 1).

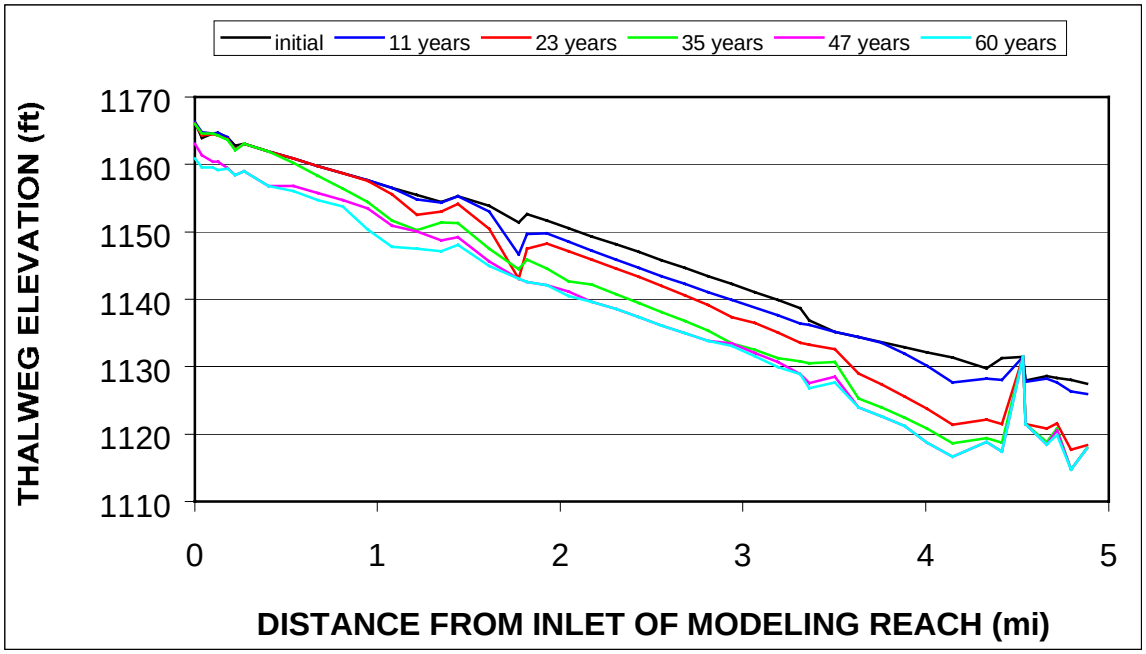

Figure 4.2 Simulated evolution of the thalweg profile, Little Salt Creek, for a 60-year period with *n*=0.02 (run 2).

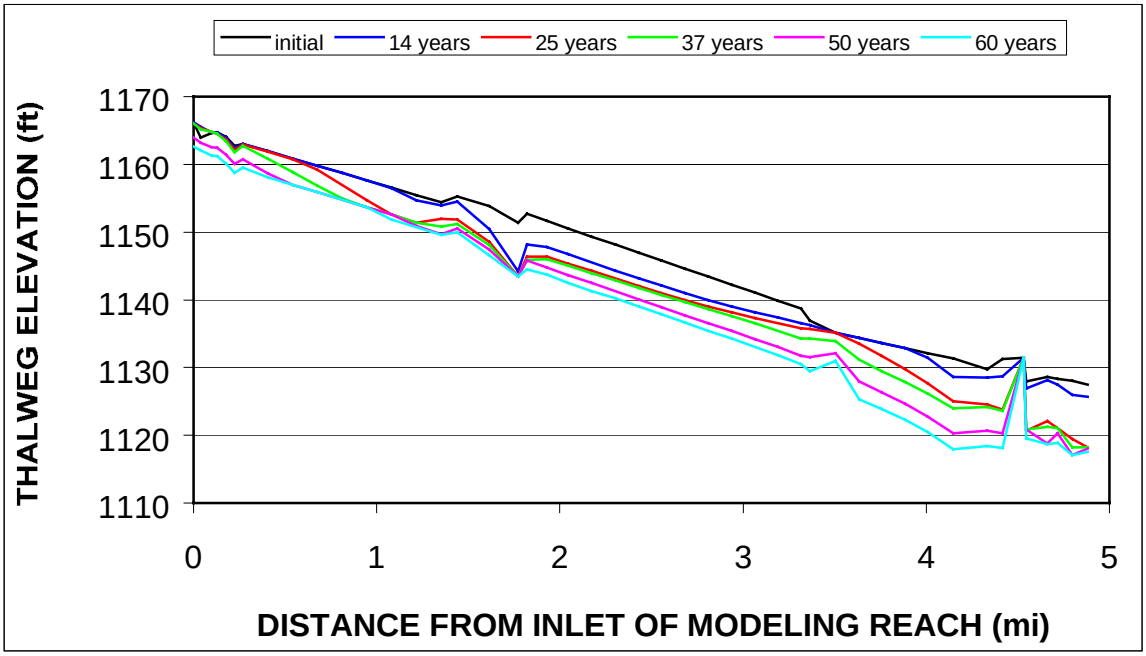

Figure 4.3 Simulated evolution of the thalweg profile, Little Salt Creek, for a 60-year period with *n*=0.015 (run 3).

It is important to note that the depth of incision may be overestimated. We assumed that the critical shear stress to entrain bed material particles and the erodibility coefficient are constant across the depth of the streambed. The bed material cores collected upstream of Raymond Road show that the bed becomes firm at a depth of approximately 1 ft (0.3 m). Therefore, the critical shear stress should increase and the erodibility coefficient decrease. Consequently, the rate and amount of degradation will be smaller than predicted here.

The increase in bank height associated with incision leads to a series of bank failures along the entire channel. Figures 4.4 through 4.6 show the changes in cross-sectional geometry at cross sections upstream of Raymond Road, upstream of Mill Road, and near Bluff Road.

Although, the critical shear stresses to entrain bed and bank material are the same, less bank material is entrained than bed material. Osman and Thorne's (1988) method computes the bank material erodibility coefficient as a function of the critical shear stress. The resulting erodibility coefficient is much smaller than that measured of the streambed. Consequently, channel incision prevails over bank retreat at the bank toe.

4.3 Sensitivity to Imposed Discharge

Commonly, the long-term stability of a channel is determined by using a project or design flood representing the channel-forming discharge, which usually coincides with the 1.5-year to 2-year runoff event. This theory, however, is highly empirical and may not predict the correct equilibrium morphology of the channel. Simulating each runoff event, although computationally more demanding, can be more accurate. For comparison, three runs were made with different design floods (the following flow rates are at the upstream boundary of the modeling reach): (1) run5, 1.05-year discharge of 127 cfs (3.58 cms); (2) run 6, 2-year discharge of 559 cfs (15.8 cms); and (3) run 7, 5-year discharge of 1330 cfs (37.8 cms).

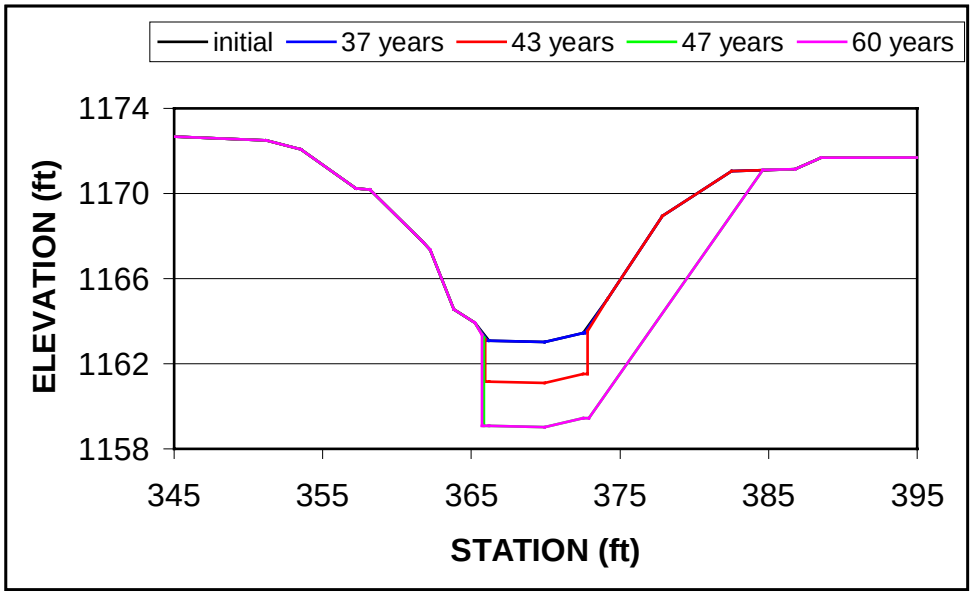

Figure 4.4 Computed changes in geometry of cross section 7 upstream of Raymond Road, Little Salt Creek (model mile 0.27 (0.43 km)), for a 60-year period with n=0.02 (run 2).

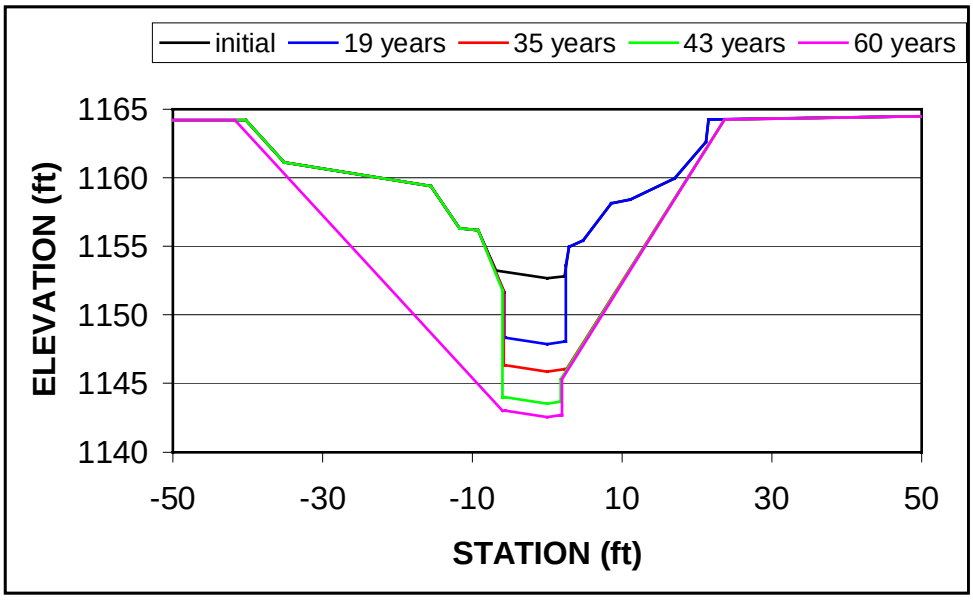

Figure 4.5 Computed changes in geometry of cross section 5 upstream of Mill Road, Little Salt Creek (model mile 1.82 (2.93 km)), for a 60-year period with *n*=0.02 (run 2).

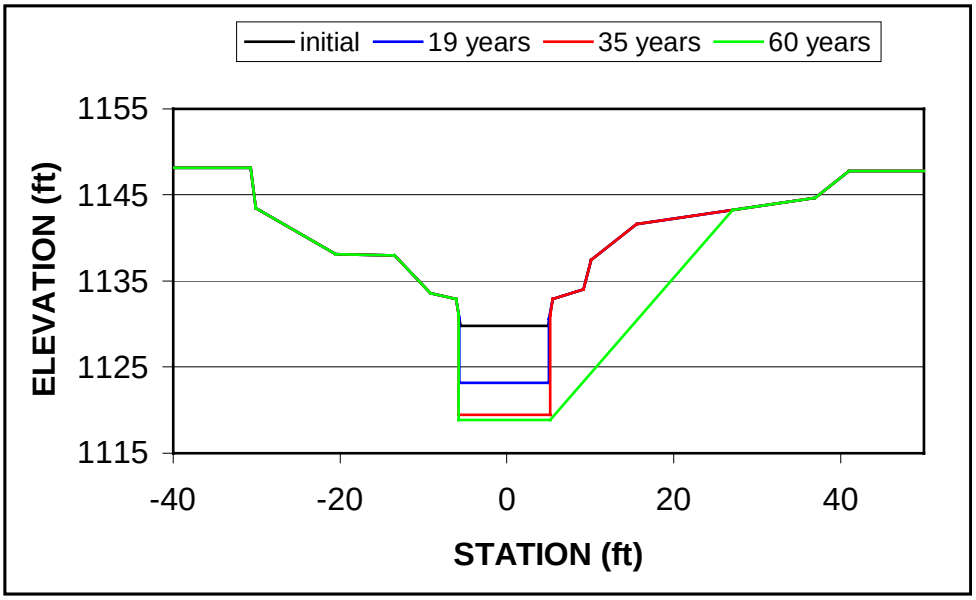

Figure 4.6 Computed changes in geometry of cross section 2 near Bluff Road, Little Salt Creek (model mile 4.33 (6.98 km)), for a 60-year period with *n*=0.02 (run 2).

Figures 4.7 through 4.9 show the predicted thalweg profiles of the modeling reach at various points in time. The equilibrium channels differ greatly with those from runs 1 through 3 (cf. Figures 4.1 through 4.3).

The 1.05-year flood only causes channel incision between Mill Road (model mile1.9 (3.1 km)) and Waverly Road (model mile 3.3 (5.3 km)). Only along this reach, shear stresses exerted by the 1.05-year flow exceed the critical shear stress.

In case of the 2-year flood, the amount of channel incision between Waverly Road and the knickpoint near Bluff Road is similar to that of runs 1, 2, and 3. However, incision is much larger upstream of Waverly Road. Here, the shear stress exerted by the 2-year flood on the bed is much larger than the average shear stress exerted by the breakpoint discharge.

The rate and amount of channel incision are much larger throughout the entire modeling reach in case of the 5-year design discharge.

4.4 Stabilization Alternative

The above simulations show that given the observed erodibility of the surface of the streambed and types of flows occurring between 1969 and 1998, Little Salt Creek will incise further. Figures 4.1 through 4.3 show that incision progresses from the middle and downstream end of the modeling reach to its upstream end. Hence, incision may be deterred by controlling channel grade at selected locations.

A simulation has been performed for the case where the grade of all bridge crossings along the modeling reach was kept constant. Figure 4.10 shows the resulting simulated evolution of the thalweg profile.

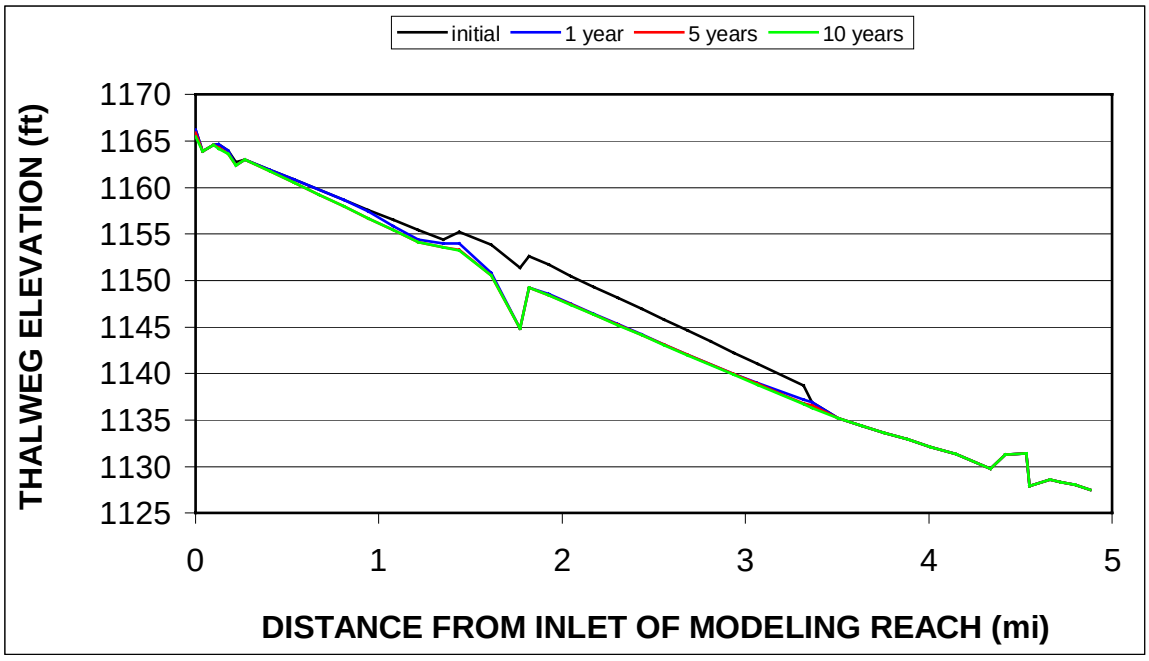

Figure 4.7 Simulated evolution of the thalweg profile, Little Salt Creek, for a 10-year period and the 1.05-year discharge (run 5).

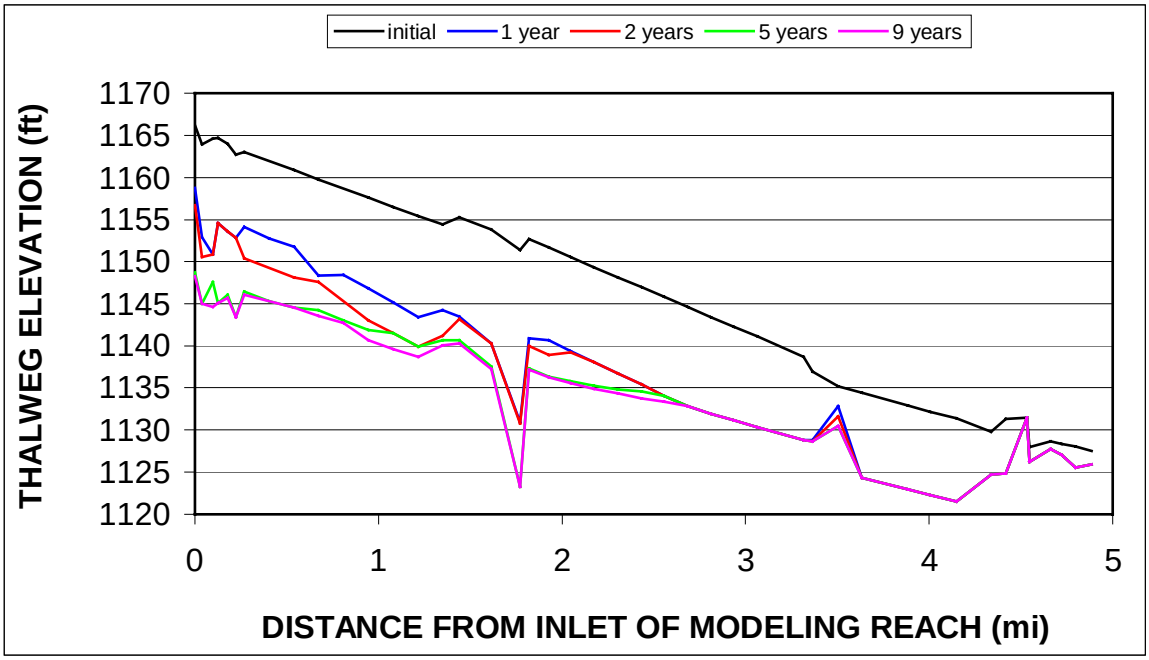

Figure 4.8 Simulated evolution of the thalweg profile, Little Salt Creek, for a 10-year period and the 2-year discharge (run 6).

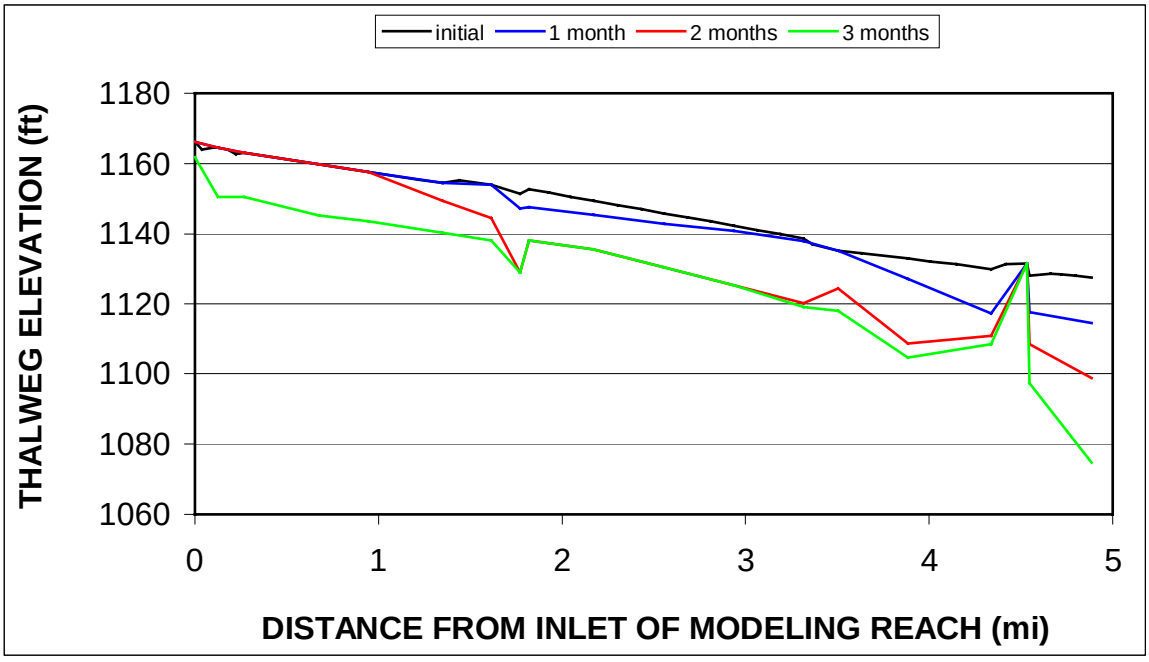

Figure 4.9 Simulated evolution of the thalweg profile, Little Salt Creek, for a 1-year period and the 5-year discharge (run 7).

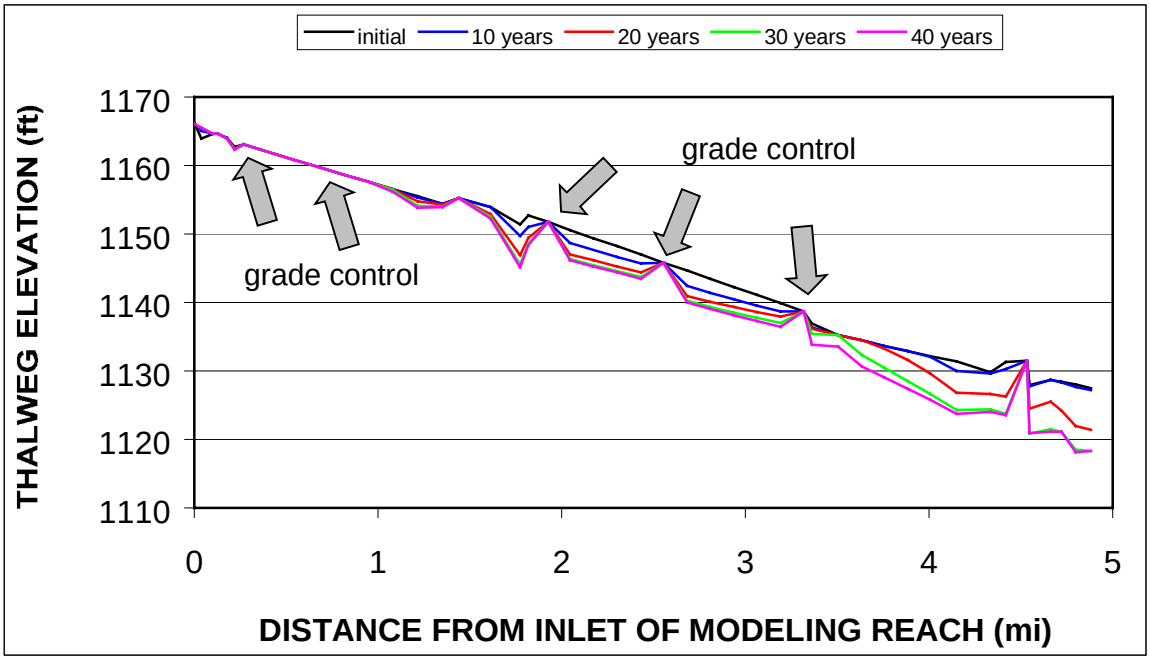

Figure 4.10 Simulated evolution of the thalweg profile, Little Salt Creek, for a 60-year period and the streambed controlled at each bridge crossing (run 4).

With the addition of the simulated grade-control structures at the bridges there is no or only minor channel incision upstream of Mill Road. Incision has been reduced between Mill Road and Bluff Road. Figure 4.10 also shows that the second grade-control structure, bridge crossing at North 1st Street may be omitted.

4.5 Summary and Interpretation

Table 4.2 summarizes the amount of channel incision and widening along the modeling reach of Little Salt Creek over a 60-year period using discharge data from 1969 through 1998. The morphology of the modeling reach is governed by the erodibility of the streambed material. In situ field experiments with a jet-test device suggest that erodibility of the streambed material is similar along the modeling reach. In the model simulations, constant erodibility coefficient and critical shear stress to entrain bed material are therefore assumed. As a result, channel incision increases along the modeling reach (Figures 4.1-4.3). The resulting increase in bank height leads to bank failures along the entire modeling reach.

Because incision at the downstream end of the modeling reach is larger than that at the upstream end, the thalweg profile steepens, causing incision to progress from downstream to upstream. Therefore, incision can be deterred by controlling channel grade at selected locations. Figure 4.10 shows that grade control structures at Raymond Road or North 1st St, Mill Rd, North 14th St, and Waverly Road prevents channel incision upstream of Raymond Road at the saline wetlands. Channel incision between Mill and Waverly Roads is reduced by approximately 60 percent.

Table 4.2 Magnitude of channel degradation and widening along the modeling reach on Little Salt Creek.

site	model mile	average incision		average widening	
		(ft)	(m)	(ft)	(m)
Raymond Rd	0-0.8	4.8	1.5	2.1	0.6
Mill Rd	1.4-2.3	9.2	2.8	5.1	1.5
N 14th St	2.4-2.9	9.6	2.9	1.3	0.4
Waverly Rd	3.1-3.8	9.8	3.0	1.2	0.4
Near Bluff Rd	3.9-4.5	12.9	3.9	3.8	1.2

5. West Papillion Creek Study Results

5.1 Setup of Simulations

The computer model CONCEPTS was used to study the long-term stability of the North Branch West Papillion Creek and the West Papillion Creek between Fort Street, Douglas County, and West Center Street, Sarpy County. Nine model runs were performed (Table 5.1). To study the sensitivity of the results of the model simulations to input parameters, we varied the following parameters: (1) discharge, observed breakpoint data versus design discharge; (2) Manning *n* of the streambed; (3) critical shear stress of the bed material; and (4) critical shear stress of the bank material. In the case of the first four runs we used a very simple bank stability analysis in which we did not take into account the relative amount of streambank saturation and the pressure applied by the water in the channel. This simplification had only minor effects on the evolution of the modeling reach.

Table 5.1 Simulations performed for the West Papillion Creek study

run	discharge	Manning *n*	critical shear stress of bed material	critical shear stress of bank material (psf)	bank stability analysis
1	16-year breakpoint	0.025	observed	0.17 (8 Pa)	simple
2	16-year breakpoint	0.025	modified	0.17 (8 Pa)	simple
3	16-year breakpoint	0.020	modified	0.17 (8 Pa)	simple
4	16-year breakpoint	0.015	modified	0.17 (8 Pa)	simple
5	16-year breakpoint	0.025	modified	0.17 (8 Pa)	full
6	16-year breakpoint	0.025	modified	0.33 (16 Pa)	full
7	16-year breakpoint	0.025	modified	0.13 (6 Pa)	full
8	1.05-year flood: 278 cfs (7.87 cms)	0.025	modified	0.17 (8 Pa)	full
9	2-year flood: 1380 cfs (39.2 cms)	0.025	modified	0.17 (8 Pa)	full
10[†]	16-year breakpoint	0.025	modified	0.17 (8 Pa)	full
11[‡]	16-year breakpoint	0.025	modified	0.17 (8 Pa)	full

[†]channel stabilization alternative 1, [‡]channel stabilization alternative 2

The discharges used were the 16-year breakpoint discharge derived in section 3, the 1.05-year design discharge of 278 cfs (7.87 cms), and the 2-year design discharge of 1380 cfs (39.2 cms). Manning *n* of the streambed was varied from 0.025 to 0.015.

The critical shear stress to initiate the entrainment of bed material varies significantly along the modeling reach (Table 3.1). Measured data were unavailable for the following reaches: (1) between Fort Street and 168th Street, (2) between Maple Street and Blondo Street, (3) between the most downstream surveyed cross section near Blondo Street and Dodge Street, and (4)

between Dodge Street and West Center Street. Values for these reaches were obtained by interpolating the measured data.

Measured data on critical shear stress to entrain bank material is not available. We may assume that it is similar to that of bed material. However, the latter is as large as 21 psf (100 Pa) along the modeling reach. This is an unreasonable value for moist bank material. Hence, we used a critical shear stress similar to that in the Little Salt Creek study, 0.16 psf (8 Pa). In addition, simulations were carried out with critical shear stresses for bank material of 0.13 psf (6 Pa) and 0.33 psf (16 Pa).

The following parameters were the same for all runs and all cross sections:

- Manning's *n* of streambanks and floodplains were selected as 0.04 and 0.15, respectively.
- Shear-strength parameters, effective cohesion and angle of internal friction, of the bank material were selected as 99.3 psf (4.75 kPa) and 29 degrees, respectively. These values are the average of those measured. The bulk unit weight of the bank material is assumed to be 114.6 lb/ft^3 (18 kN/m^3). This value is a 25 percent increase over the average dry bulk unit weight to include water content of the streambank material. The angle indicating the increase in shear strength for an increase in matric suction is set to 17 degrees. The groundwater table at each streambank was set 3.3 ft (1.0 m) above the bank toe elevation.

Run 1 using the measured erodibility and critical shear stress for the streambed predicted excessive scour of the streambed at the upstream end of the modeling reach upstream and downstream of Fort Street. Even the smallest flow events (those slightly larger than the base-flow discharge of 7.1 cfs (0.20 cms)) exerted shear stresses at the bed exceeding 0.05 psf (2.6 Pa). Therefore, all of the following runs were performed with increased critical shear stresses between Fort and 168th Streets, varying from 0.10 psf (5.0 Pa) to 0.21 psf (10.0 Pa).

In the following sections the distance downstream of the upstream boundary of the modeling reach is referred to as "model mile."

5.2 Sensitivity to Bed Roughness

The shear stress exerted by the flow on the bed depends on the roughness of the bed. It is difficult to determine the roughness of cohesive streambeds if stage profiles for various discharges are unavailable. Conventional methods that relate the resistance parameter Manning's *n* to a characteristic grain size estimate unrealistically small *n* values. Runs were performed for three different values of Manning's *n*: 0.025 (run 2), 0.02 (run 3), and 0.015 (run 4).

Figures 5.1 through 5.3 show the predicted thalweg profiles of the modeling reach at various points of time. The figures show that the streambed is degrading from the inlet of the modeling reach to model mile 2.7 (4.34 km), which is halfway between Maple and Blondo Streets. Further downstream, the streambed is stable because the shear stresses exerted by the flow are smaller than the critical shear stress to entrain the bed material.

The rate at which the degradation progresses with time decreases with decreasing roughness of the bed. Also, the depth of incision slightly decreases with decreasing bed roughness. The maximum simulated channel incision is approximately 11.5 ft (3.5 m) near Fort Street.

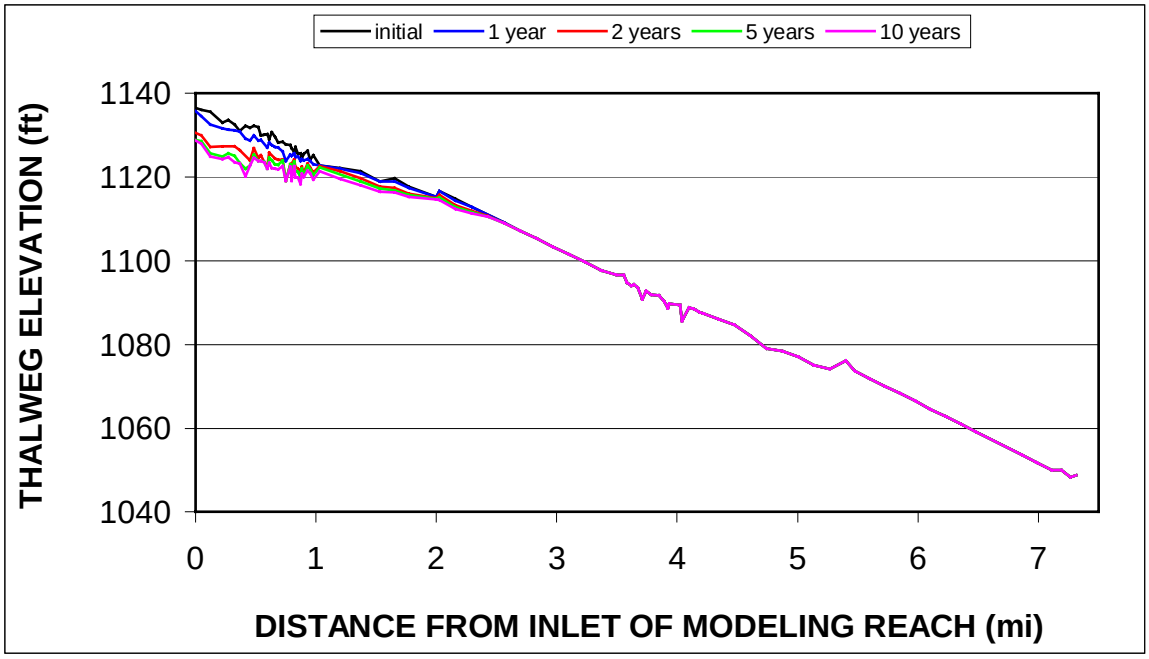

Figure 5.1 Simulated evolution of the thalweg profile, North Branch West Papillion and West Papillion Creeks, for a 16-year period with n=0.025 (run 2).

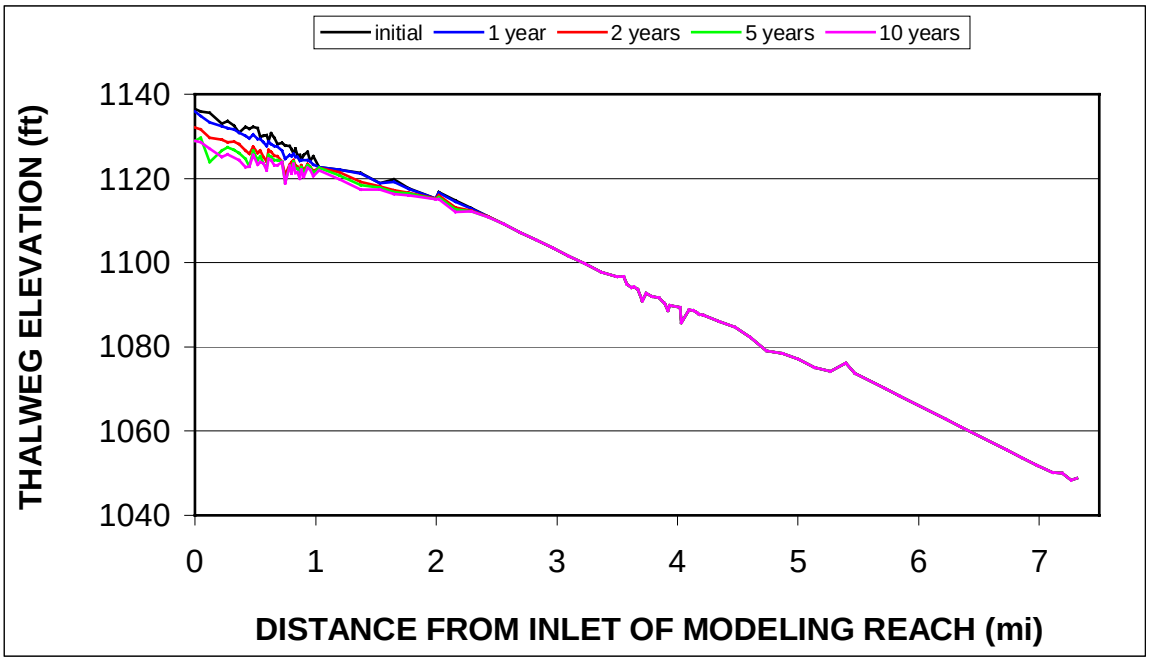

Figure 5.2 Simulated evolution of the thalweg profile, North Branch West Papillion and West Papillion Creeks, for a 16-year period with n=0.02 (run 3).

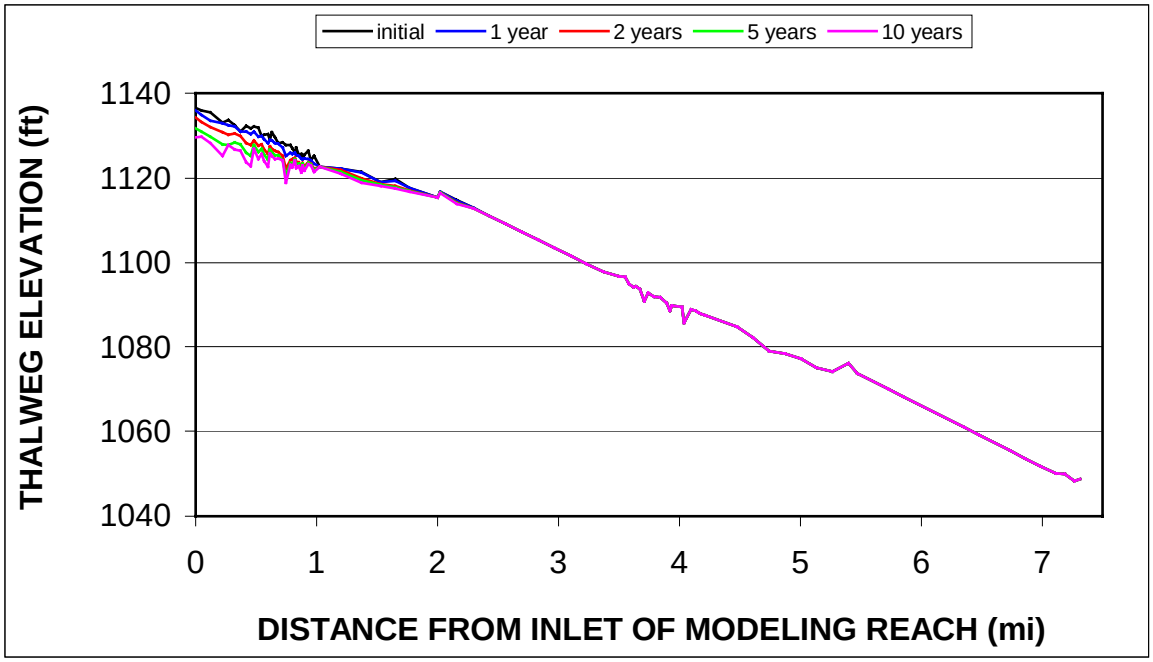

Figure 5.3 Simulated evolution of the thalweg profile, North Branch West Papillion and West Papillion Creeks, for a 16-year period with n=0.015 (run 4).

It is important to note that the depth of incision may be overestimated. We assumed that the critical shear stress to entrain bed material particles and the erodibility coefficient are constant across the depth of the streambed. The jet tests show that critical shear stress increases and erodibility decreases along the modeling reach, which coincides with historical degradation of the streambed. Therefore, we may assume that critical shear stress increases and erodibility decreases at depth. As a result, the channel incision may be smaller than predicted.

Incision leads to a series of bank failures upstream and downstream of Fort Street. Also, several streambanks failed downstream of Blondo Street. Figures 5.4 and 5.5 show the simulated changes in cross-sectional geometry at a cross section upstream and downstream of Fort Street.

Although, the critical shear stresses to entrain bed and bank material are the same, less bank material is entrained than bed material. Osman and Thorne's (1988) method computes the bank material erodibility coefficient as a function of the critical shear stress. The resulting erodibility coefficient is much smaller than that measured of the streambed. Consequently, channel incision prevails over bank retreat at the bank toe.

5.3 Sensitivity to Critical Shear Stress to Entrain Bank Material

Lateral erosion of the bank toe is a function of the local excess shear stress, the difference between the hydraulic shear stress and the critical shear stress. The latter shear stress is a function of bank-material properties and needs to be determined experimentally. Because measured data are unavailable, three runs were made using different values of critical shear stress: (1) run 5, $\tau_c = 0.17$ psf (8.0 Pa); (2) run 6, $\tau_c = 0.33$ psf (16.0 Pa); and (3) run 7, $\tau_c = 0.13$ psf (6.0 Pa). In these runs, bank-stability analysis takes into account the effects of pore-water and confining pressures on the factor of safety.

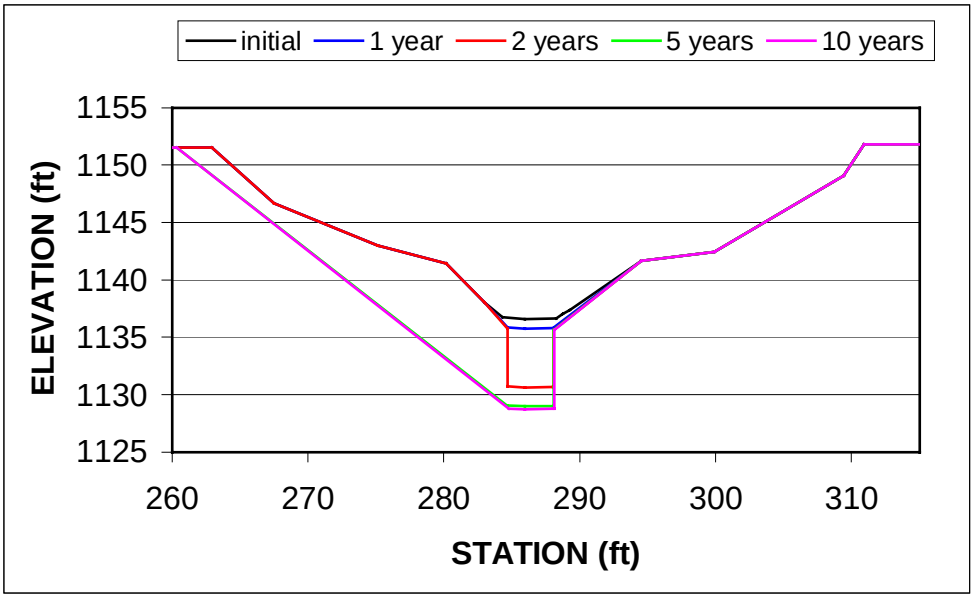

Figure 5.4 Computed changes in geometry of cross section 1 upstream of Fort Street, North Branch West Papillion Creek (model mile 0), for a 16-year period with *n*=0.025 (run 2).

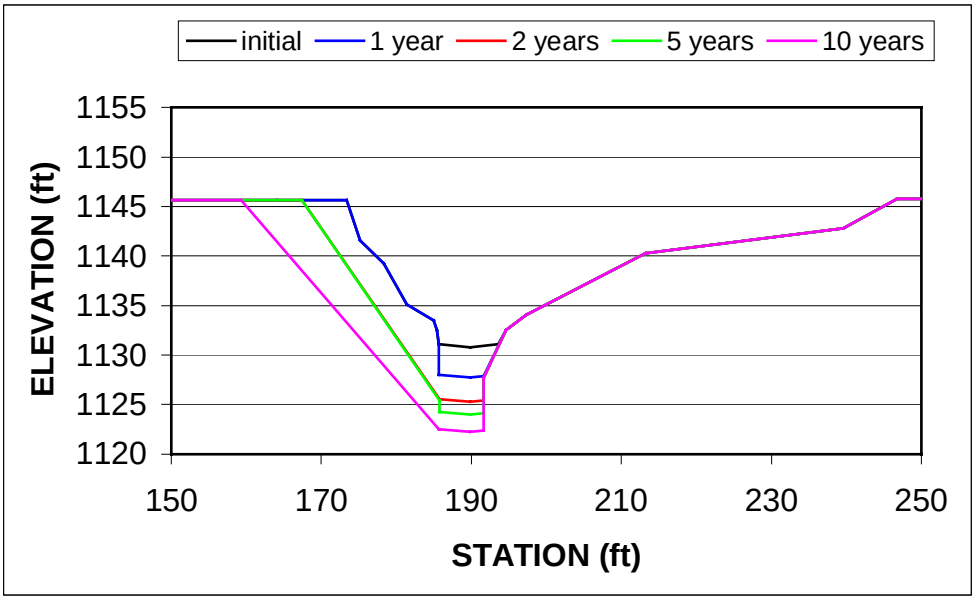

Figure 5.5 Computed changes in geometry of cross section 7 downstream of Fort Street, North Branch West Papillion Creek (model mile 0.63 (1.01 km)), for a 16-year period with *n*=0.025 (run 2).

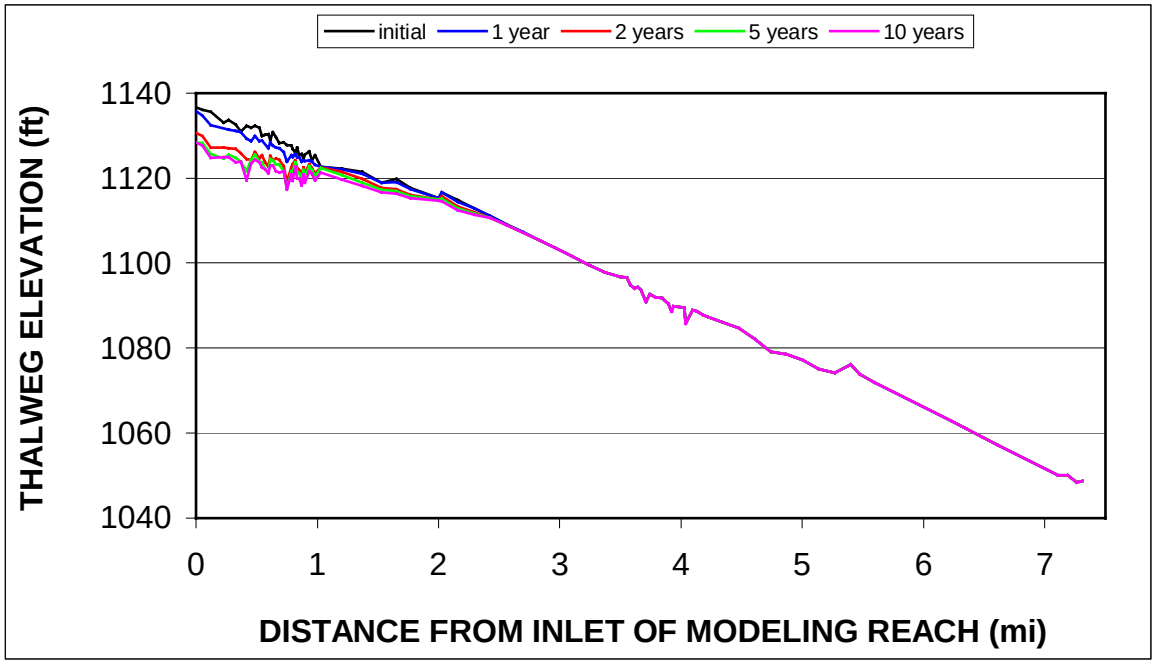

Figure 5.6 Simulated evolution of the thalweg profile, North Branch West Papillion and West Papillion Creeks, for a 16-year period with bank τ_c=0.17 psf (8 Pa) (run 5).

Figures 5.6 through 5.8 show the predicted thalweg profiles of the modeling reach at various points of time. The figures show that incision increases with decreasing critical shear stress. The average depth of degradation upstream of Fort Street after 10 years is: 8.1 ft (2.5 m) for $\tau_c = 0.33$ psf (run 6), 9.0 ft (2.8 m) for $\tau_c = 0.17$ psf (run 5), and 10.2 ft (3.1 m) for $\tau_c = 0.13$ psf (run 7).

Most banks that failed in run 2 are also failing in run 5. However, the timing of failure differs. Because matric suction in the unsaturated part of the streambank increases the apparent shear strength of the bank material, a higher bank is needed for bank failure to occur. Therefore, the channel needs to incise more in run 5 than in run 2 to initiate failures (see Figures 5.9 and 5.10). The weight of the failure block is the driving force of bank failure. The dimensions of the failure block are a function of bank height and angle of the slip surface. Figures 5.9 and 5.10 show that the banks are not only higher but also have a flatter slip-surface angles (cf. Figures 5.4 and 5.5 of run 2). This results in an increase in the weight of the failure block needed to offset the increase in apparent shear strength of the bank material due to matric suction. The flatter angle of the slip surface increases the widening rate on the average by 40 percent.

Figures 5.11 and 5.12 show the computed changes in geometry for the same cross sections in case or run 7 ($\tau_c = 0.13$ psf). Lowering the critical shear stress by 25 percent causes the lateral erosion to increase from 1.3 ft (0.4 m) to 12.2 ft (3.7 m) for cross section 1 upstream of Fort Street and from 0.4 ft (0.1 m) to 7.5 ft (2.3 m) for cross section 7 downstream of Fort Street after 10 years. As a consequence, the widening rate at the top of the bank also increases. The average widening rates are: (1) $\tau_c = 0.17$ psf, 4.1 ft (1.3 m); and (2) $\tau_c = 0.13$ psf, 6.0 ft (1.8 m). This

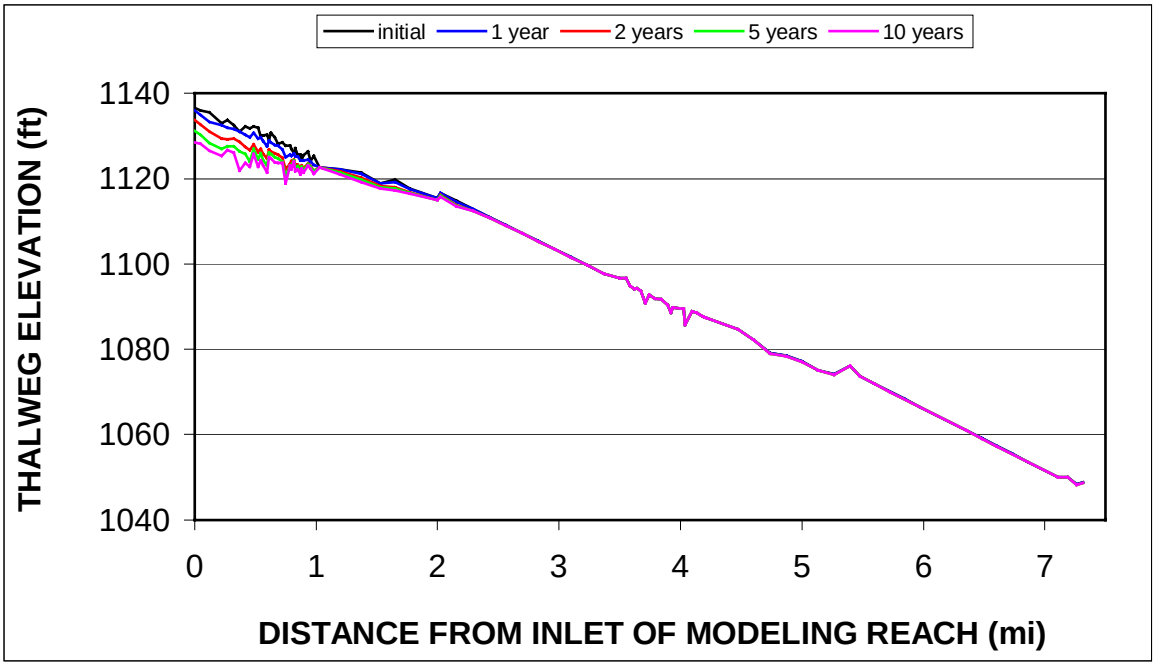

Figure 5.7 Simulated evolution of the thalweg profile, North Branch West Papillion and West Papillion Creeks, for a 16-year period with bank τ_c=0.33 psf (16 Pa) (run 6).

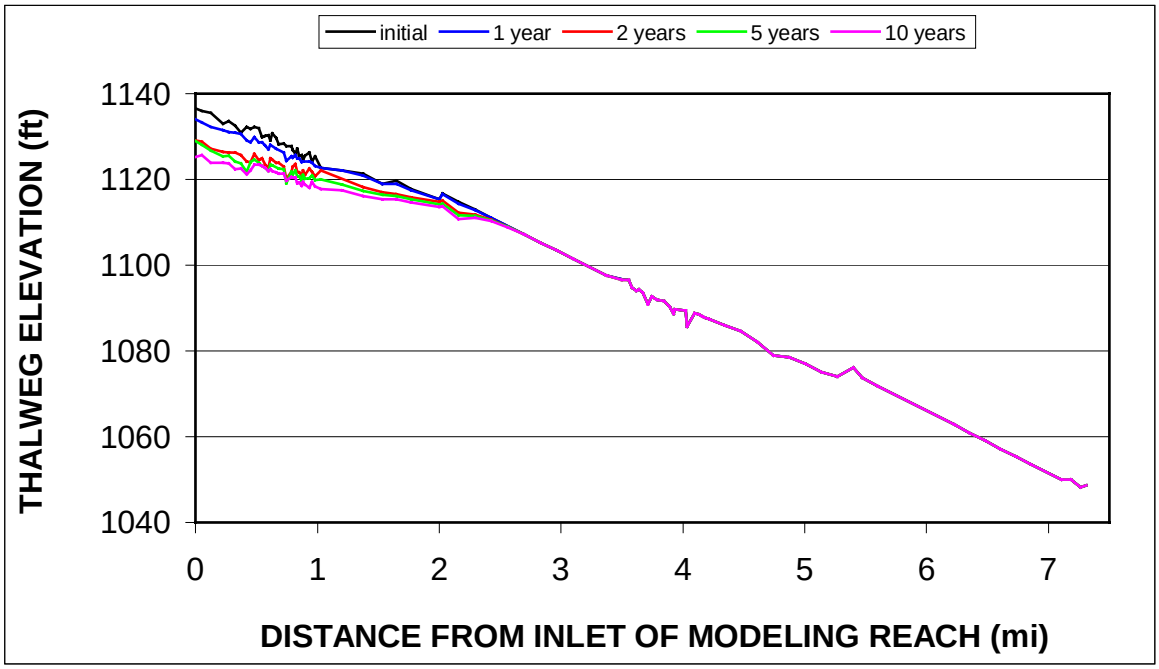

Figure 5.8 Simulated evolution of the thalweg profile, North Branch West Papillion and West Papillion Creeks, for a 16-year period with bank τ_c=0.13 psf (6 Pa) (run 7).

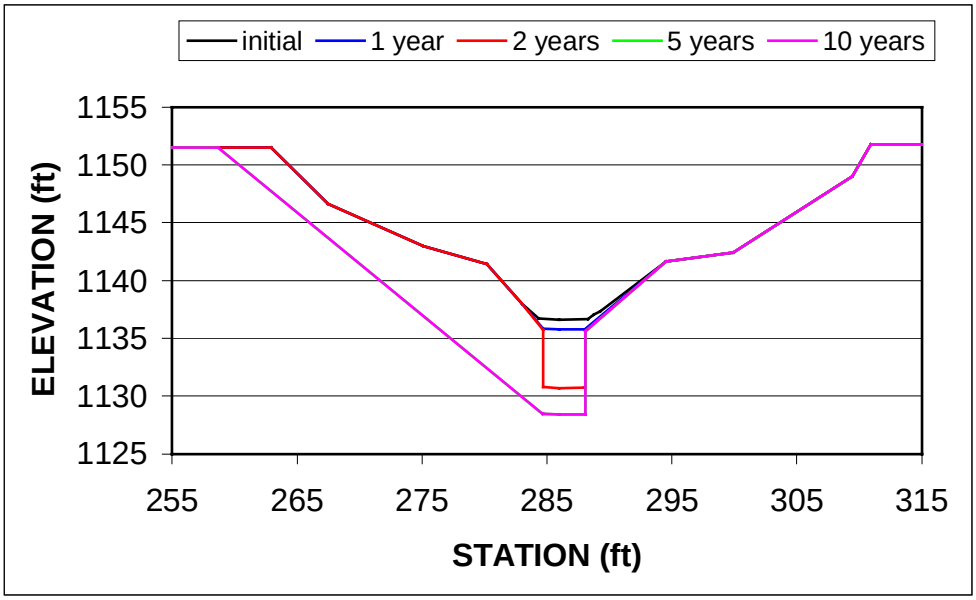

Figure 5.9 Computed changes in geometry of cross section 1 upstream of Fort Street, North Branch West Papillion Creek (model mile 0), for a 16-year period with τ_c=0.33 psf (16 Pa) (run 6).

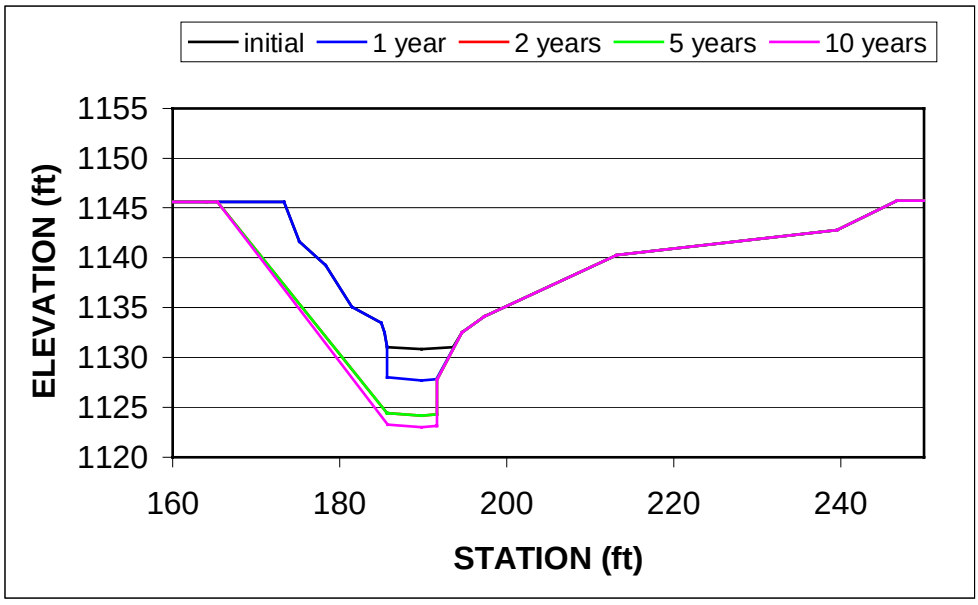

Figure 5.10 Computed changes in geometry of cross section 7 downstream of Fort Street, North Branch West Papillion Creek (model mile 0.63 (1.01 km)), for a 16-year period with τ_c=0.33 psf (16 Pa) (run 6).

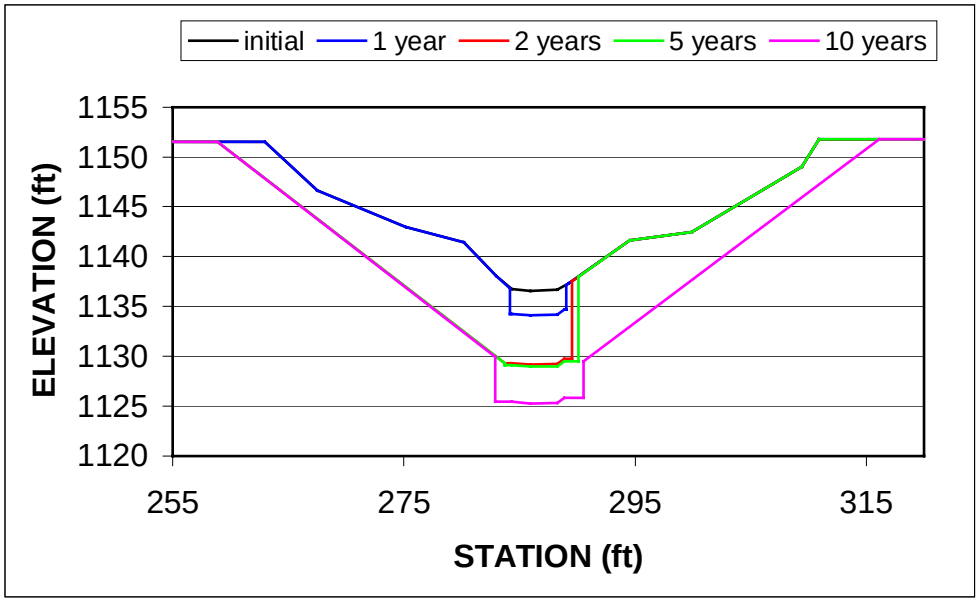

Figure 5.11 Computed changes in geometry of cross section 1 upstream of Fort Street, North Branch West Papillion Creek (model mile 0), for a 16-year period with τ_c=0.13 psf (6 Pa) (run 7).

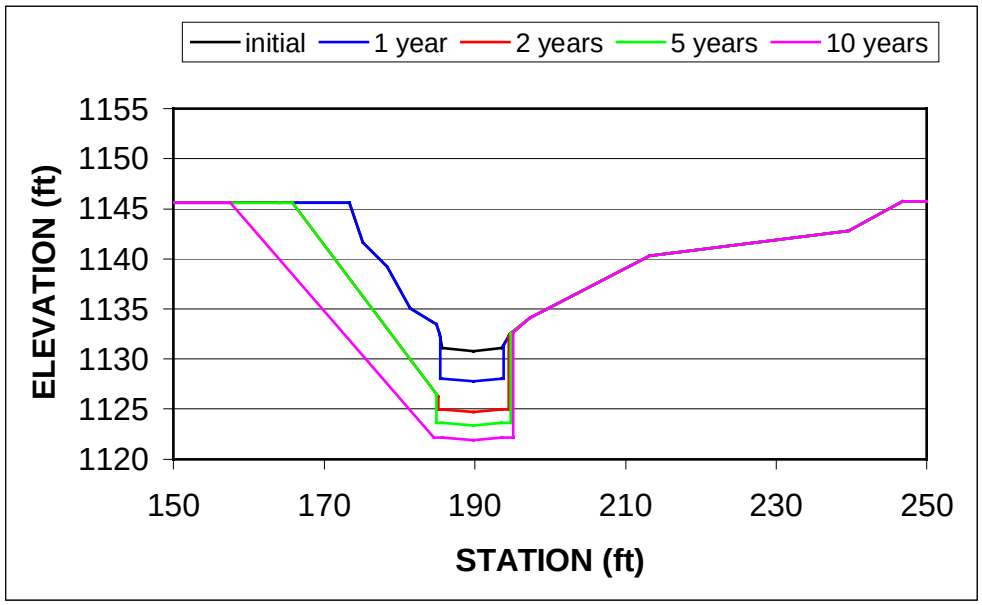

Figure 5.12 Computed changes in geometry of cross section 7 downstream of Fort Street, North Branch West Papillion Creek (model mile 0.63 (1.01 km)), for a 16-year period with τ_c=0.13 psf (6 Pa) (run 7).

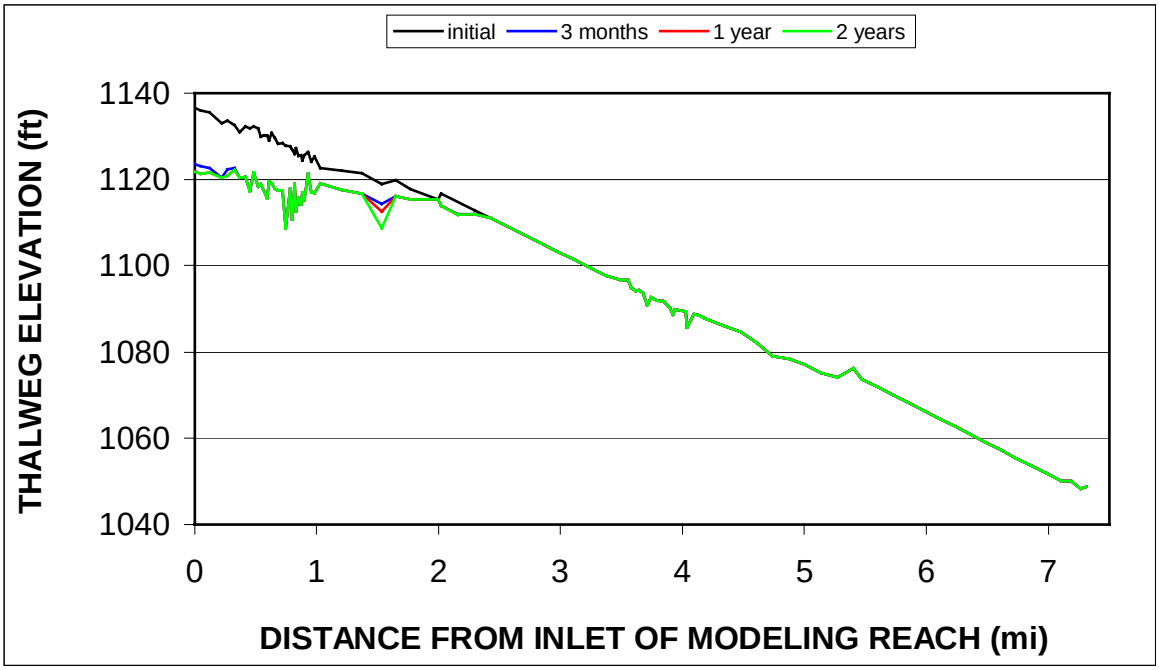

Figure 5.13 Simulated evolution of the thalweg profile, North Branch West Papillion and West Papillion Creeks, for a 2-year period and the 1.05-year discharge (run 8).

is mainly caused by failures of both banks of a cross section (run 7) as opposed to only one of the banks of a cross section (run 5).

5.4 Sensitivity to Imposed Discharge

Commonly, the stability of a channel is determined by using a project or design flood representing the channel forming discharge, which usually coincides with the 1.5-year to 2-year runoff event. However, this theory is highly empirical and may not predict the correct quasi-dynamic equilibrium of the channel. Simulating each runoff event, although computationally more expensive, is more accurate. For comparison, two runs were made with different design floods (the following flow rates are at the upstream boundary of the modeling reach): (1) run8, 1.05-year discharge of 278 cfs (7.87 cms); and (2) run 9, 2-year discharge of 1380 cfs (39.2 cms).

Figures 5.13 and 5.14 show the predicted thalweg profiles of the modeling reach at various points in time. The equilibrium channels differ greatly with those from runs using breakpoint data.

In case of the 1.05-year discharge we obtain an equilibrium channel geometry after approximately two years. Incision occurs from the upstream boundary to model mile 2.43 (3.91 km) where the bed shear stress becomes smaller than the critical bed shear stress of 0.38 psf (18 Pa). This cross section is located downstream of Maple Street.

In case of the 2-year flood, the bed slope reduces to near zero between the upstream boundary and model mile 3.24 (5.21 km) where the critical shear stress is 0.86 psf (41 Pa). This cross section is located upstream of Blondo Street.

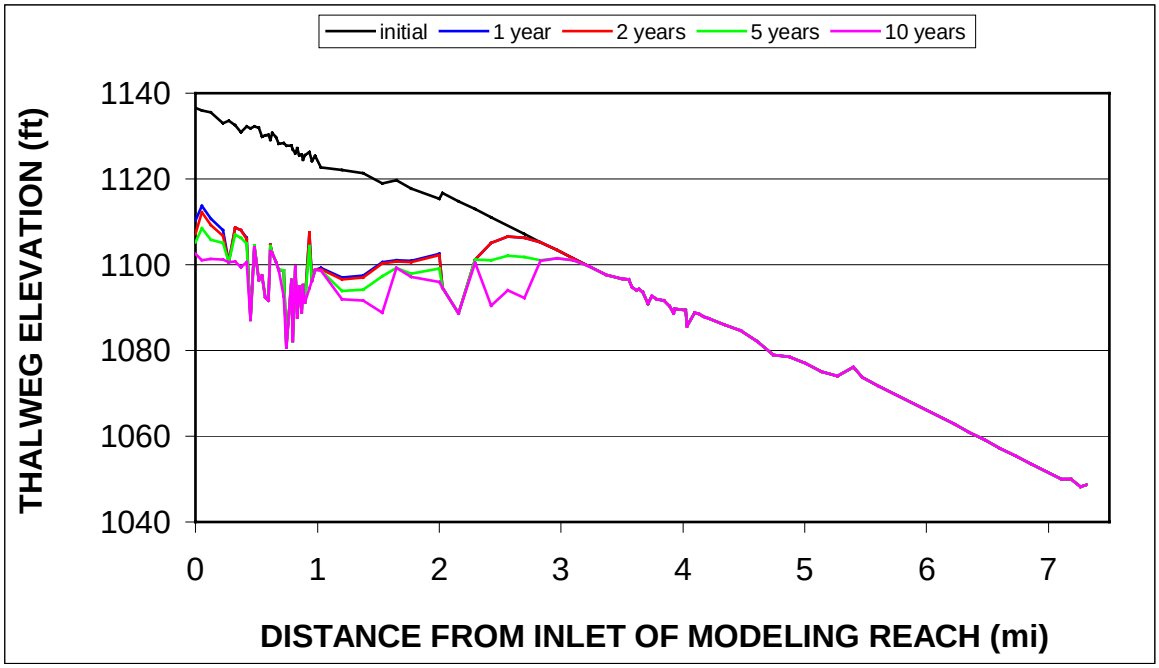

Figure 5.14 Simulated evolution of the thalweg profile, North Branch West Papillion and West Papillion Creeks, for a 16-year period and the 2-year discharge (run 9).

5.5 Stabilization Alternatives

The above simulations show that the North Branch West Papillion Creek will incise upstream of Maple Street using the historic 16-year (1965-1977, 1997-1999) discharge record and the observed erodibility of the surface of the streambed. Two stream-channel stabilization alternatives have been evaluated: (1) the grade at the bridge crossings at Fort, 168th, and Maple Streets are controlled; and (2) in addition to the streambed controls of alternative (1), control structures are added halfway between the upstream boundary and Fort Street, and halfway between Fort and 168th Streets. Figures 5.15 and 5.16 show the simulated evolution of the thalweg profile.

Modeling results show that although incision is reduced by the control structures in their upstream vicinity, the magnitude of erosion further upstream of the structures is the same as without control structures (cf. Figure 5.6, run 5). The average amount of incision upstream of Fort Street reduced from 9.1 ft (2.8 m) for run 5 to 5.8 ft (1.8 m) for run 10 and 4.4 ft (1.3 m) for run 11. The average incision between Fort Street and model mi 1 (1.6 km) reduced from 6.5 ft (2.0 m) for run 5 to 5.9 ft (1.8 m) for run 10 and 4.7 ft (1.4 m) for run 11. The maximum amount of incision upstream of Fort Street is 12.8 ft (3.9 m) for run 5, 9.8 ft (3.0 m) for run 10, and 8.2 ft (2.5 m) for run 11. The maximum amount of incision between Fort Street and model mile 1 (1.6 km) is 10.4 ft (3.2 m) for run 5, 11.4 ft (3.5 m) for run 10, and 9.4 ft (2.9 m) for run 11. It appears that the incision is mainly determined by the erodibility of the streambed, and therefore, cannot be sufficiently controlled by these stabilization alternatives along the entire section between Fort and 168th Streets.

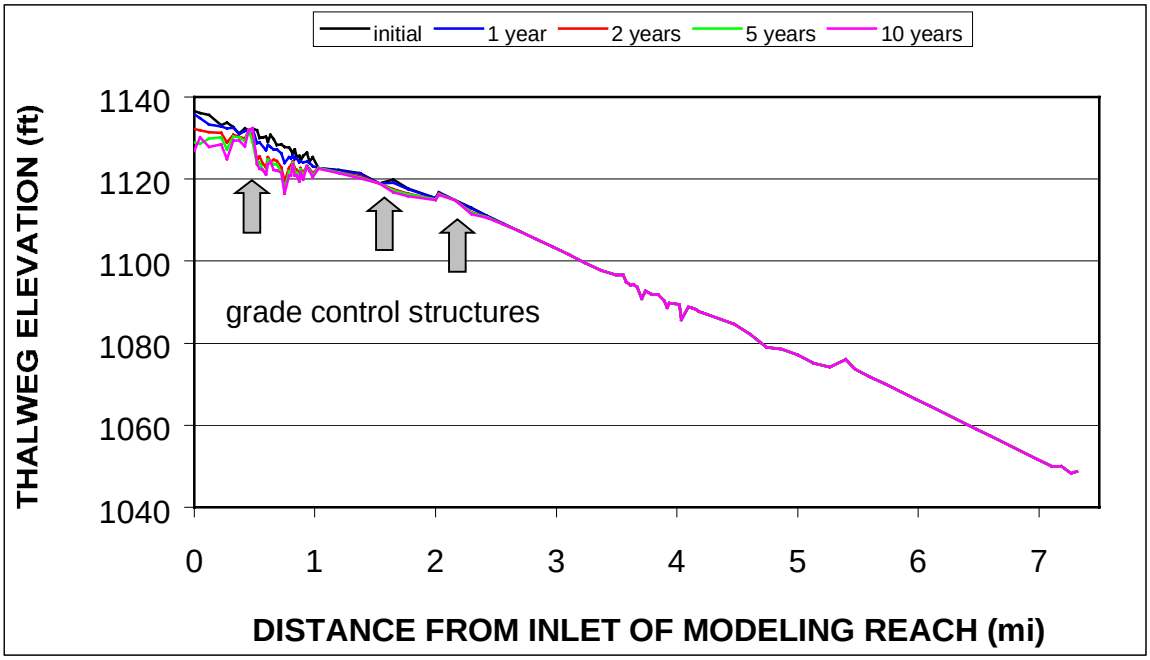

Figure 5.15 Simulated evolution of the thalweg profile, North Branch West Papillion and West Papillion Creeks, for a 16-year period and grade control structures at model miles 0.5 (0.8 km), 1.5 (2.5 km), and 2.2 (3.5 km) (run 10).

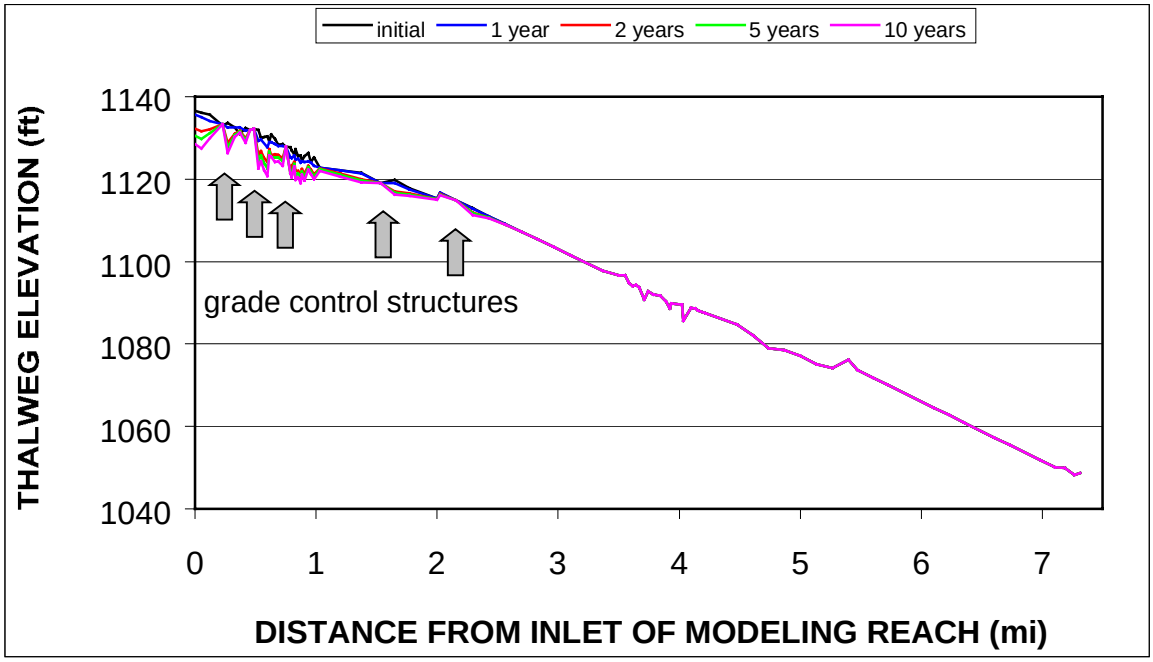

Figure 5.16 Simulated evolution of the thalweg profile, North Branch West Papillion and West Papillion Creeks, for a 16-year period and grade control structures at model miles 0.2 (0.4 km), 0.5 (0.8 km), 0.8 (1.2 km), 1.5 (2.5 km), and 2.2 (3.5 km) (run 11).

These stabilization measures, however, significantly reduce the number of streambank failures. Twenty-five simulated streambank failures were recorded over a 16-year simulation period without any stabilization measures (run 5), whereas only 15 streambanks failed for stabilization alternative 1 and 5 streambanks failed for stabilization alternative 2.

5.6 Effect of Streambank Water-Content on Factor of Safety

Model runs 1 through 11 show that the channel bed is stable between Blondo and West Center Streets. The bank stability-analysis assumed that the groundwater table is located 3.3 ft (1.0 m) above the streambed. Consequently, the negative pore-water pressures or matric suction in the unsaturated part of the streambank are sufficiently large to prevent mass wasting (factor of safety greater than one). However, streambank failure has recently occurred along this section of the modeling reach.

Rainfall and lawn irrigation adjacent to the channel will increase the water content of the streambank, consequently reducing matric suction. Figures 5.17 and 5.18 show the effect of (partial) loss of matric suction on factor of safety for streambanks of cross sections surveyed downstream of Blondo and Dodge Streets. The factor of safety of three of the left banks becomes smaller than 1 and these banks may fail. Two other left banks and two right banks have factors of safety smaller than 1.15 in case of a full loss of matric suction and may fail if the groundwater table moves upward in case of prolonged wetting of the streambank.

5.7 Summary and Interpretation

Table 5.2 summarizes the amount of channel incision and widening along the modeling reach on North Branch West Papillion Creek over a 16-year period using discharge data for 1965-1977

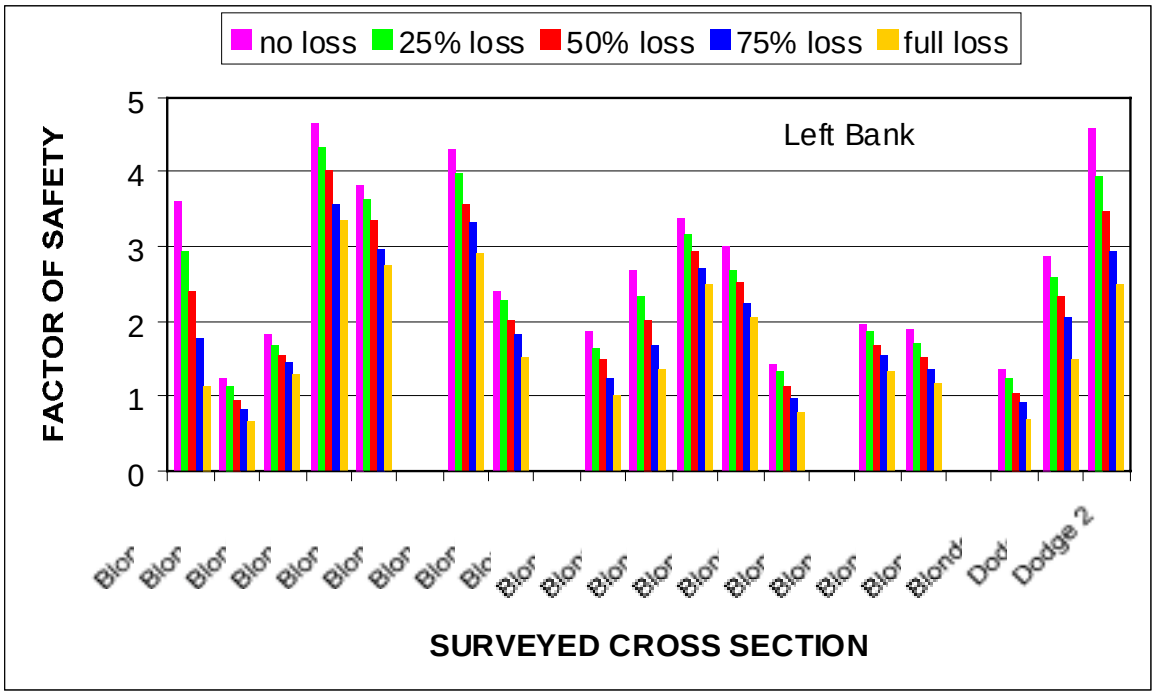

Figure 5.17 The influence of matric suction on the factor of safety of the left bank of cross sections surveyed downstream of Blondo and Dodge Streets.

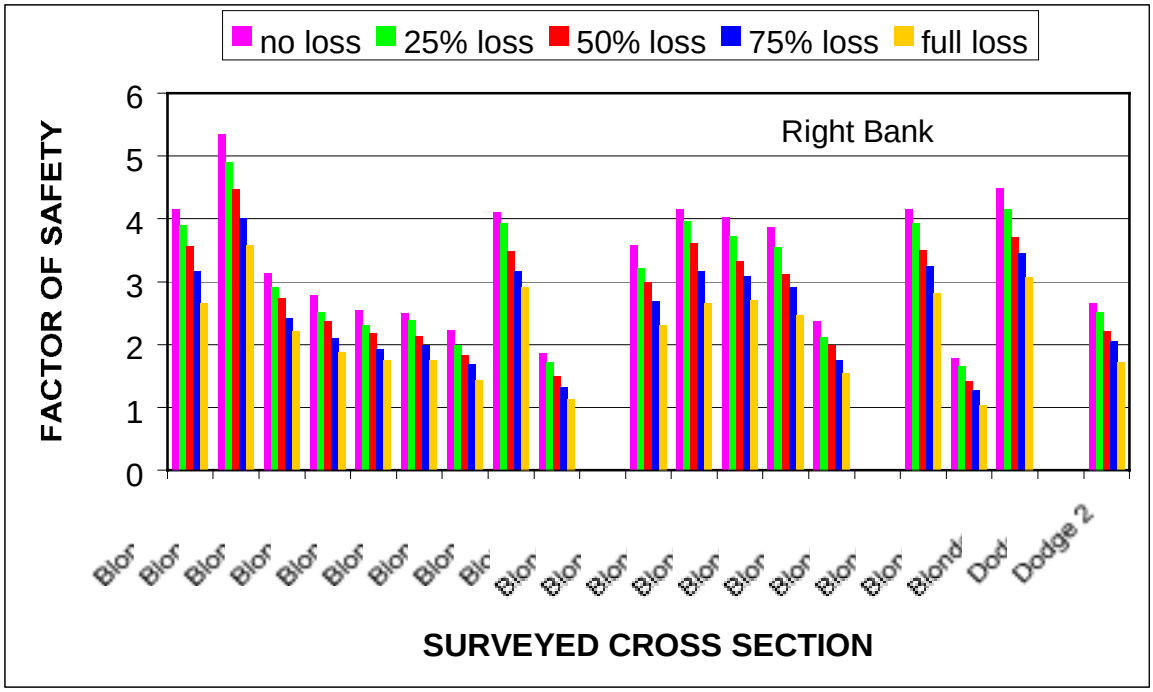

Figure 5.18 The influence of matric suction on the factor of safety of the right bank of cross sections surveyed downstream of Blondo and Dodge Streets.

and 1997-1999. The morphology of the modeling reach is governed by the erodibility of the streambed material. Along the section between Fort and 168th Streets, the shear stresses exerted by the flow on the channel bed are larger than the critical shear stress necessary to entrain bed material measured by the jet-test device. As a result, the North Branch West Papillion Creek incises upstream of 168th Street (for example Figure 5.6). The resulting increase in bank heights leads to a series of bank failures upstream and downstream of Fort Street (Figures 5.4 and 5.5).

Grade control structures may partially alleviate the incision of the streambed (Figures 5.15 and 5.16). The average channel incision is reduced by approximately 25% in case of stabilization alternative 1 and 40% in case of channel stabilization alternative 2 (section 5.5). However, the maximum channel incision upstream of the different grade control structures is only reduced by approximately 10% in case of channel stabilization alternative 1 and 25% in case of channel stabilization alternative 2. Simulations (runs 10 and 11) show that grade control structures are more effective in reducing the number of streambank failures; there is a reduction of 40% in case of stabilization alternative 1 and 80% in case of stabilization alternative 2.

Simulations with the channel stabilization measures also show that the grade control structures at 168th and Maple Streets may not be needed for the spectrum of flow events that occurred during the period 1965-1977 and 1997-1999. However, the expected increase in discharge due to ongoing urbanization upstream of Maple Street will result in increased shear stresses exerted on the channel bed. Figures 5.13 (1.05-year discharge) and 5.14 (2-year discharge) show that larger discharges produce greater shear stresses on the streambed, causing greater incision and extending the incision in this case from model mile 2.43 (3.91 km) to model mile 3.24 (5.21 km).

Downstream of Blondo Street, the erodibility of the streambed material becomes sufficiently large to resist the shear stresses exerted by the flow, inhibiting incision and therefore heightening

of the streambanks. However, these streambanks may still fail if the water content of the streambanks becomes too large (Figures 5.17 and 5.18), for example by rainfall, prolonged wetting, or lawn irrigation.

Table 5.2 Magnitude of channel degradation and widening along the modeling reach on North Branch West Papillion Creek.

site	model mile	average incision (run 5)		average widening (run 7)	
		(ft)	(m)	(ft)	(m)
Upstream of Fort Street	0-0.75	9.1	2.8	4.4	2.8
Downstream of Fort Street	0.75-1.5	6.5	2.0	9.3	1.4

6. Conclusions and Recommendations

6.1 Conclusions

The CONCEPTS numerical model was used to simulate the evolution of: (1) Little Salt Creek between Raymond and Bluff Roads, Lancaster County, Nebraska; and (2) North Branch West Papillion and West Papillion Creeks between Fort and West Center Streets, Douglas County, Nebraska. These creeks have incised and widened, and are threatening saline wetlands (Little Salt Creek) and urban infrastructure (West Papillion Creek) adjacent to the channels.

Field studies were carried out to determine the erodibility of the surface of the streambed and the shear strength of streambank material. Data on bed and bank roughness were not available. Therefore, simulations were performed for a range of Manning's *n* values. A 30-year breakpoint discharge record was constructed for Little Salt Creek and a 16-year breakpoint discharge record for West Papillion Creek. These discharge records were then used to predict future channel geometries.

The modeling reach along Little Salt Creek incised over its entire length. Over a 60-year period the incision varied from 5 ft (1.5 m) upstream of Raymond Road to 14 ft (4.3 m) near Bluff Road. Bank failures occurred along the entire length, widening the channel about 2 ft upstream of Raymond Road. The largest amount of widening, 10 ft (3.0 m), occurred between Raymond Road and Mill Road.

The modeling reach along the North Branch West Papillion and West Papillion Creeks incised along its upper end. Halfway between Maple and Blondo Streets the resistance of the streambed to shear stresses exerted by the flow became sufficiently large to prevent erosion of the streambed. The incision near Fort Street is approximately 11.5 ft (3.5 m) and reduces to zero downstream of Maple Street. The average widening at the bank top is about 4.1 ft (1.3 m) near Fort Street. However, a 25% reduction of the critical shear stress to entrain bank-material particles will lead to a 50% increase in the widening rate of the channel.

The above conclusions should be interpreted with care. The main parameters determining future evolution of the modeling reaches are the erodibility of the streambed material and the critical shear stress (τ_c) at which erosion commences. These parameters were measured at the surface of the streambed and assumed constant across the depth of the streambed. Commonly the bed becomes firmer and more resistant to erosion away from its surface.

Cores collected upstream of Raymond Road along Little Salt Creek show that the bed becomes firm to very firm 1 ft (0.3 m) down. Furthermore, the lower end of the modeling reach along West Papillion Creek has previously incised exposing soils much more resistant to erosion ($\tau_c \approx 2$ psf (100 Pa) versus $\tau_c \approx 0.1$ psf (5 Pa)). The incision of Little Salt Creek and the North Branch West Papillion Creek may, therefore, be regarded as upper limits of expected incisions.

6.2 Recommendations

Controlling the streambed of the Little Salt Creek at the following bridge crossings is recommended: Raymond Road, North 1st Street, Mill Road, North 14th Street, and Waverly Road. This would significantly reduce channel incision of Little Salt Creek. Channel incision upstream of Raymond Road would be prevented, thus protecting the saline wetlands. Incision

upstream of Mill Road and Waverly Road is reduced from 9.2 ft (2.8 m) to 2.5 ft (0.8 m) and from 9.8 ft (3.0 m) to 4.1 ft (1.2 m), respectively.

It is recommended to thoroughly examine the nature of the channel bed of the North Branch West Papillion Creek upstream of Maple Street. Present data on the erodibility of the surface of the streambed are inadequate to accurately simulate the evolution of this creek and therefore propose mitigation measures. The increase in resistance to erosion downward the streambed must be determined. Controlling the streambed of the North Branch West Papillion Creek at selected locations (Figure 5.16) only reduces erosion in the upstream vicinity of the control structures. Using present data shows that installing grade control structures 0.38 mi (0.6 km) upstream of Fort Street, at Fort Street, and halfway between Fort and 168th Streets, would reduce average channel incision by approximately 40 percent. However, the maximum channel incision is only reduced by 25 percent.

Considerations should be given to prevent extensive wetting of the streambanks along the North Branch West Papillion and West Papillion Creeks downstream of Maple Street. Although the streambed is stable, an increase in water content of the streambank material will lead to a sufficient loss of matric suction to cause mass failure of several streambanks (Figures 5.17 and 5.18).

REFERENCES

Arulanandan, K., Gillogley, E., and Tully, R. 1980. "Development of a quantitative method to predict critical shear stress and rate of erosion of natural undisturbed cohesive soils," *Report GL-80-5*, U.S. Army Corps of Engineers, Waterways Experiment Station, Vicksburg, MS.

Brice, J. C. 1966. 'Erosion and deposition in the loess mantled Great Plains, Medicine Creek Drainage Basin, Nebraska,' *U.S. Geological Survey Professional Paper 352-H*, 255-339.

Cunge, J. A., Holly Jr., F. M., and Verwey, A. 1980. *Practical Aspects of Computational River Hydraulics*, Pitman Publishing Inc., Boston, MA.

Hanson, G. J. 1990. 'Surface erodibility of earthen channels at high stresses. Part II – Developing an in-situ testing device,' *Transactions of the ASAE*, **33**(1), 132-137.

Langendoen, E. J. 2000. 'CONCEPTS – Conservational channel evolution and pollutant transport system,' *Software Manual*, US Department of Agriculture, Agricultural Research Service, National Sedimentation Laboratory, Oxford, MS (in preparation).

Leopold, L. B. 1994. *A View of the River*, Harvard University Press, Cambridge, MA.

Lower Platte South Natural Resources District 1999. *Resources Corner Newsletter*, Fall 1999.

Luttenegger, J. A. and Hallberg, B. R. 1981. 'Borehole shear test in geotechnical investigations,' *American Society of Testing Materials*, Special Publication, **740**, 566-578.

Moore, C. T. 1917. 'Drainage districts in southeastern Nebraska,' *Miscellaneous Papers*, E. H. Barbour, ed., Nebraska Geological Survey, **7**(17), 125-164.

Osman, A. M. and Thorne, C. R. 1988. 'Riverbank stability analysis. I: Theory,' *J. Hydr. Eng.*, **114**, 134-150.

Simon, A., Curini, A., Darby, S. E., and Langendoen, E. J. 1999. 'Streambank mechanics and the role of bank and near-bank processes in incised channels,' Incised River Channels, S. E. Darby and A. Simon, eds., John Wiley & Sons Ltd, Chichester, UK, Chapter 6, 123-152.

Simon, A. and Rinaldi, M. 2000. 'Channel instabilities in the loess area of the Midwestern United States,' *J. American Water Resources Association*, **36**(1), 1-18.

APPENDIX I

SURVEYED THALWEG AND CROSS SECTIONS

LITTLE SALT CREEK – SURVEYED THALWEG

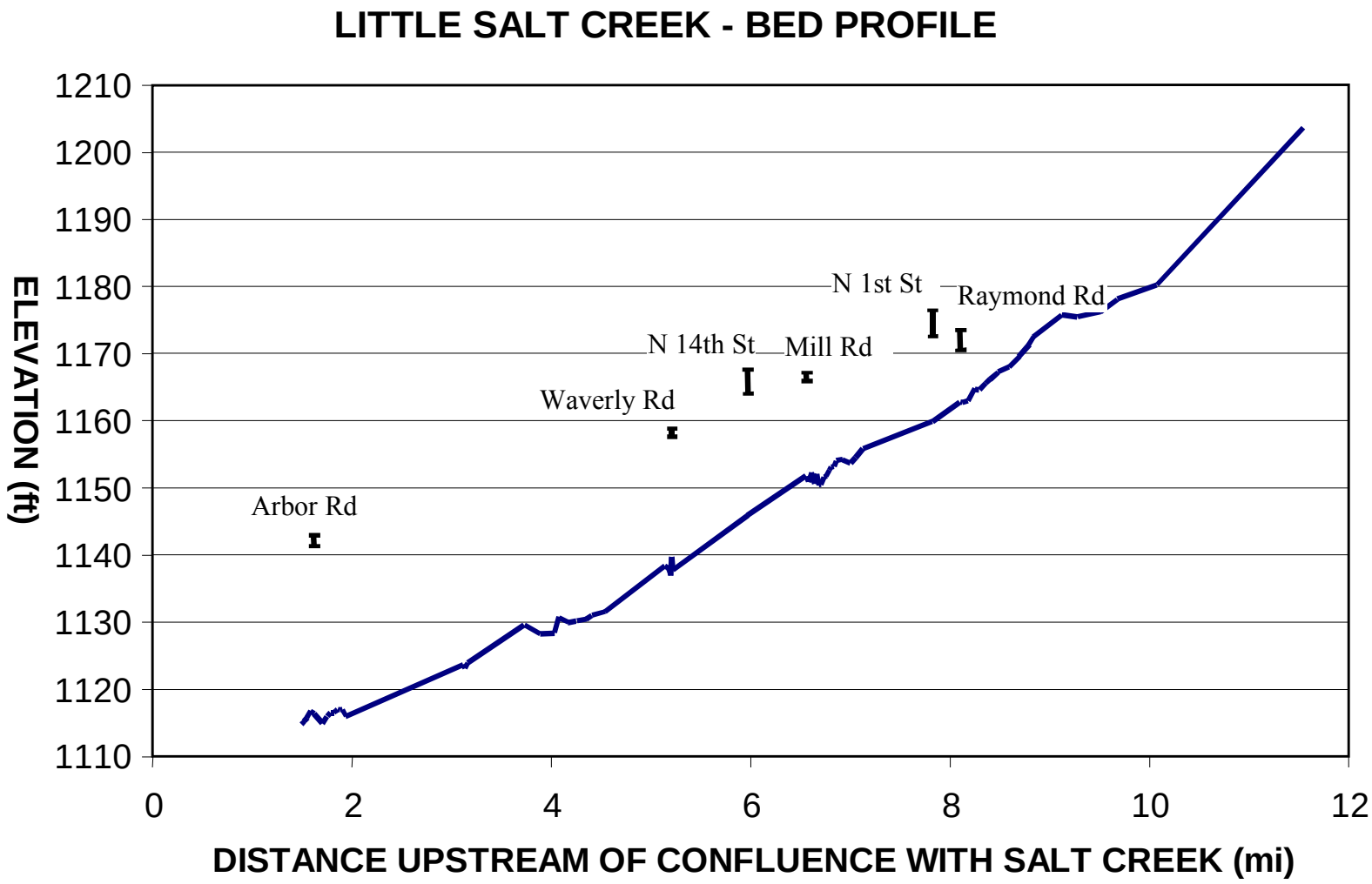

Figure I.1 Graph of surveyed bed profile of the Little Salt Creek and bridge decks.

LITTLE SALT CREEK – CROSS SECTIONS SURVEYED UPSTREAM OF RAYMOND ROAD

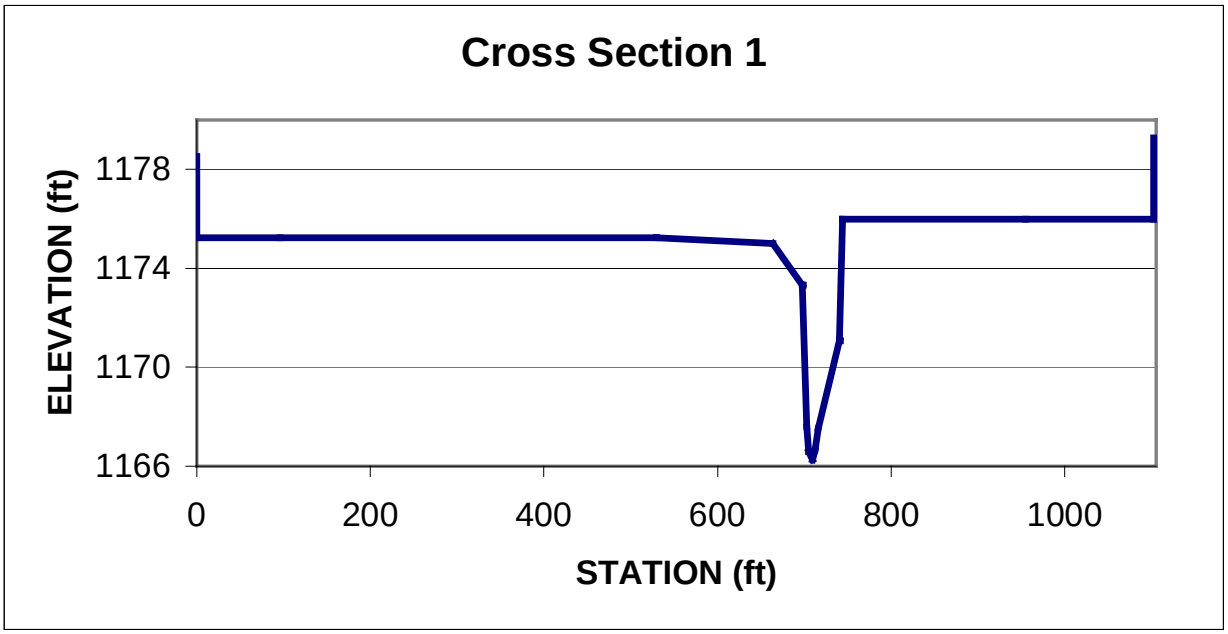

Figure I.2 Graph of surveyed cross section 1 upstream of Raymond Rd 0.00 mi downstream of the upstream boundary of the modeling reach.

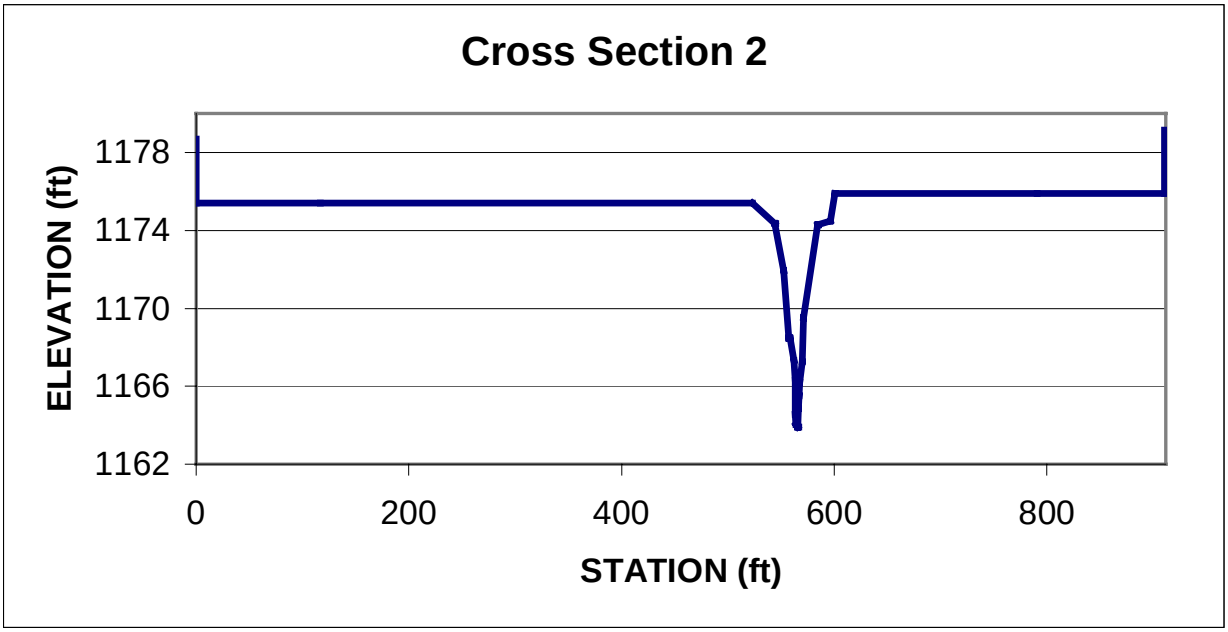

Figure I.3 Graph of surveyed cross section 2 upstream of Raymond Rd 0.04 mi downstream of the upstream boundary of the modeling reach.

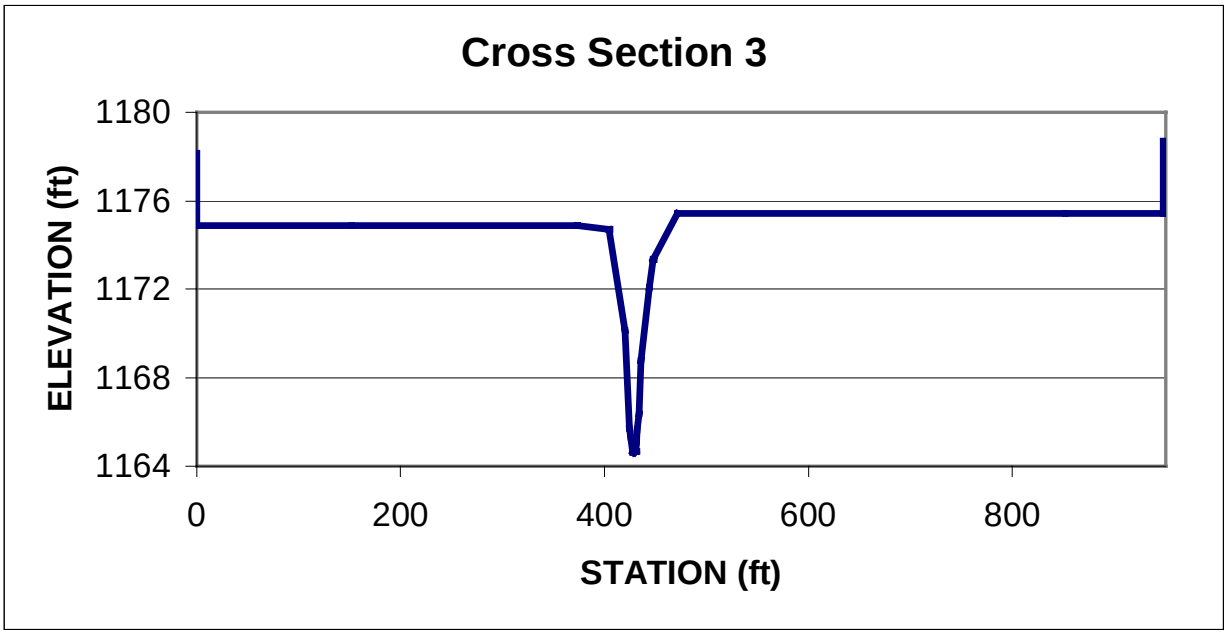

Figure I.4 Graph of surveyed cross section 3 upstream of Raymond Rd 0.10 mi downstream of the upstream boundary of the modeling reach.

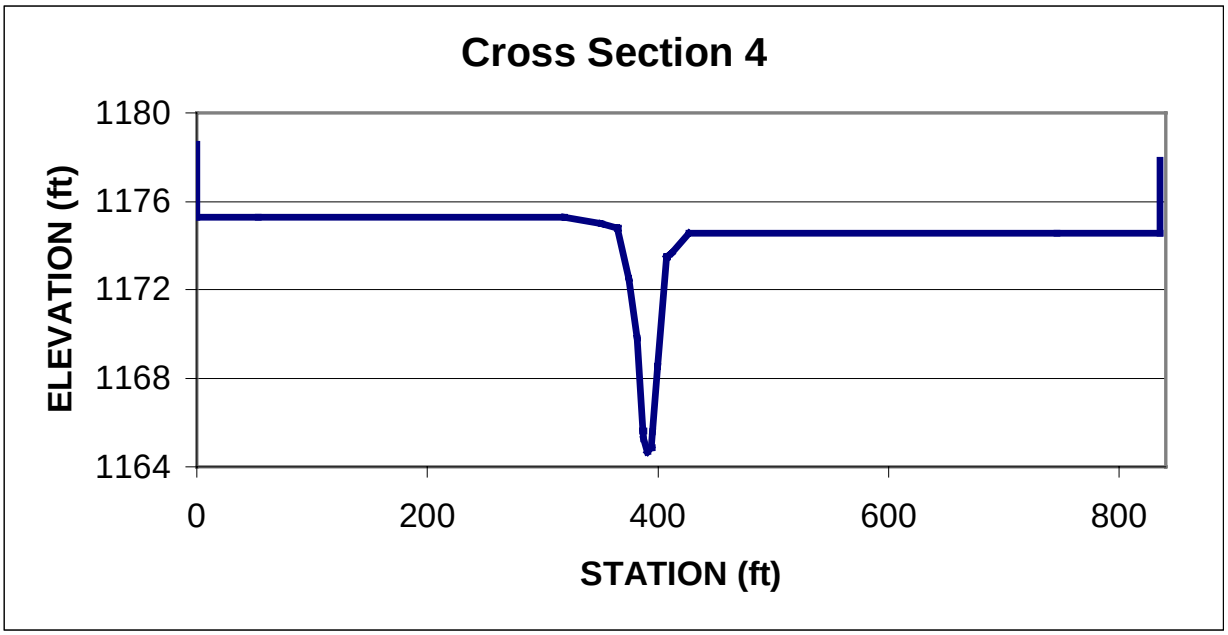

Figure I.5 Graph of surveyed cross section 4 upstream of Raymond Rd 0.13 mi downstream of the upstream boundary of the modeling reach.

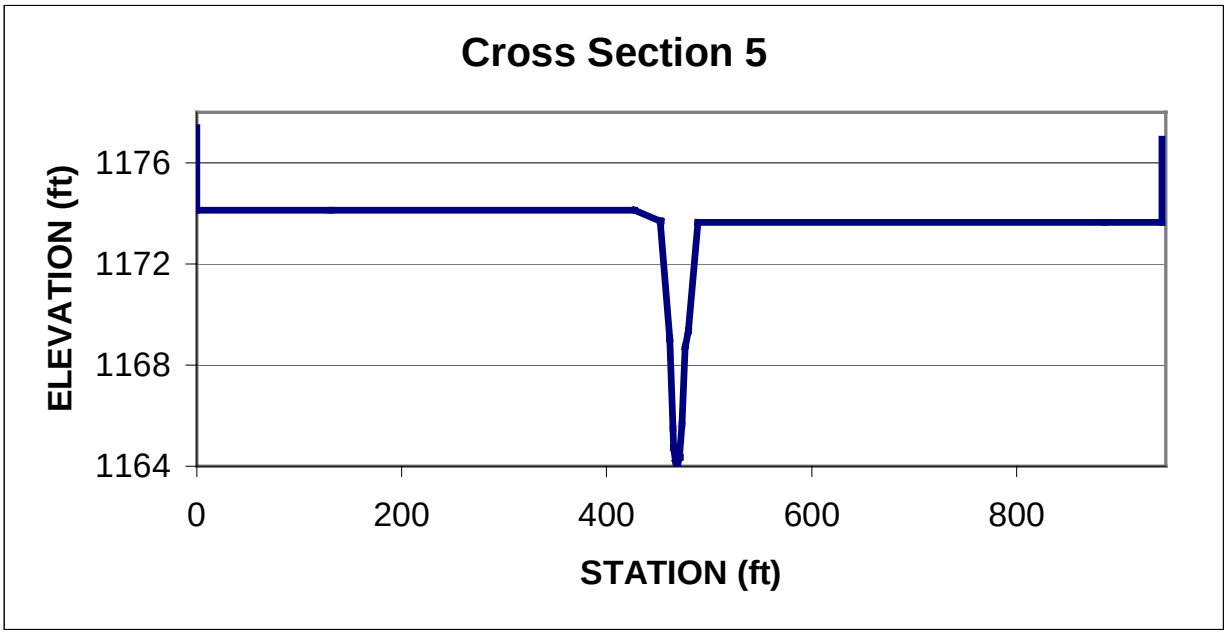

Figure I.6 Graph of surveyed cross section 5 upstream of Raymond Rd 0.18 mi downstream of the upstream boundary of the modeling reach.

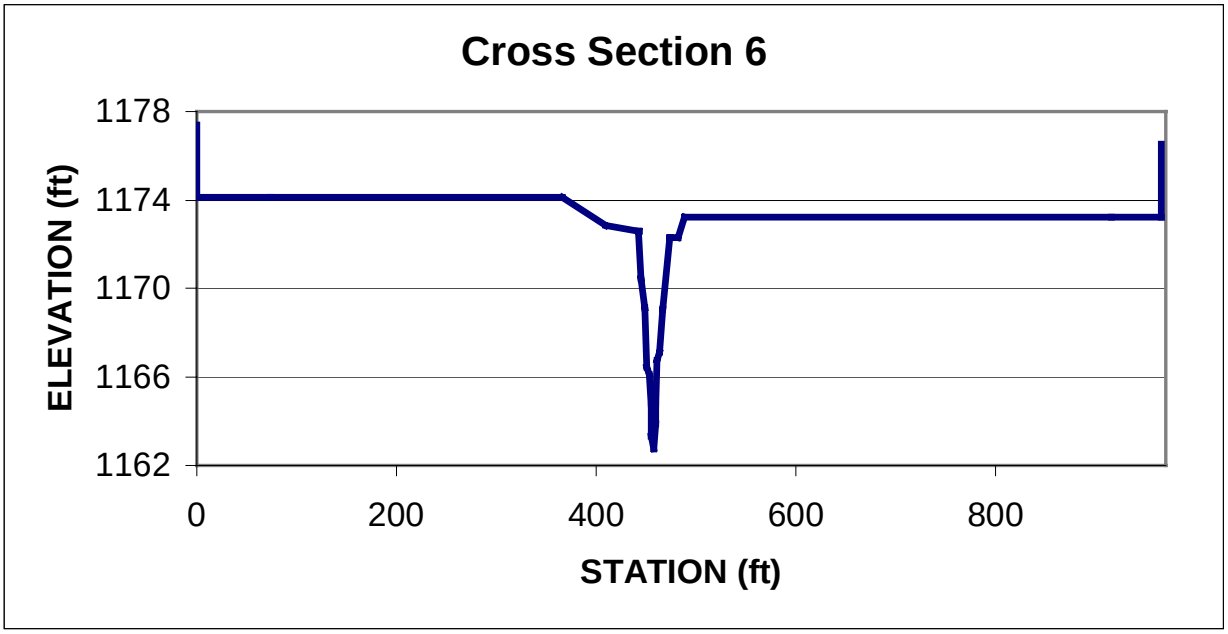

Figure I.7 Graph of surveyed cross section 6 upstream of Raymond Rd 0.22 mi downstream of the upstream boundary of the modeling reach.

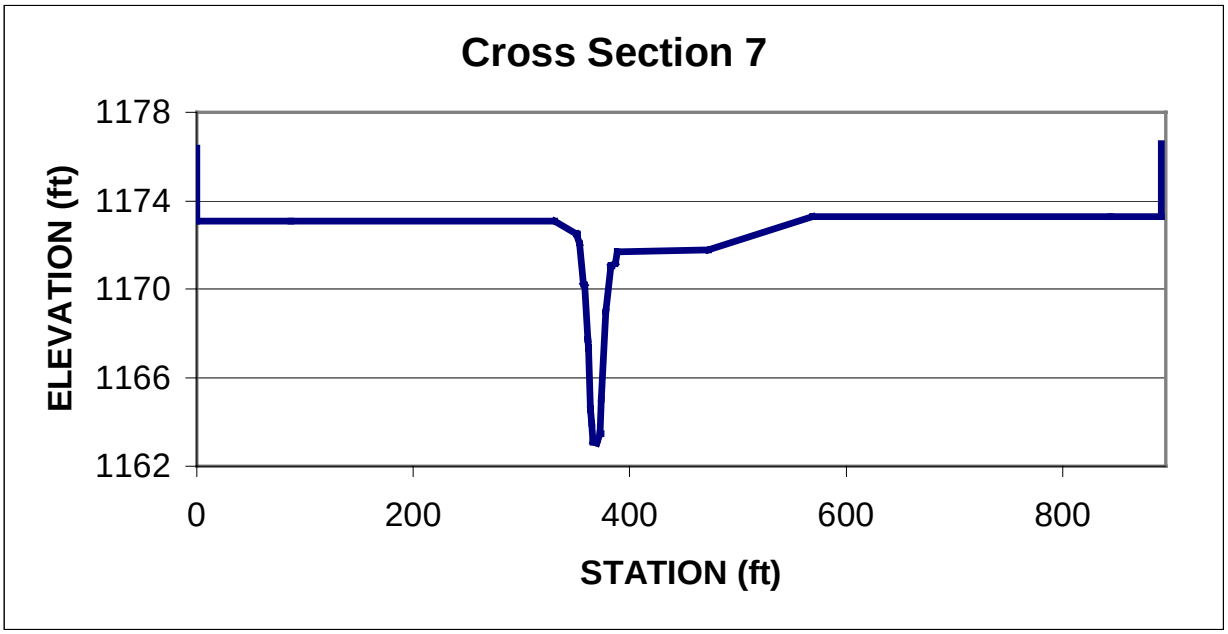

Figure I.8 Graph of surveyed cross section 7 upstream of Raymond Rd 0.27 mi downstream of the upstream boundary of the modeling reach.

LITTLE SALT CREEK – CROSS SECTIONS SURVEYED UPSTREAM OF MILL ROAD

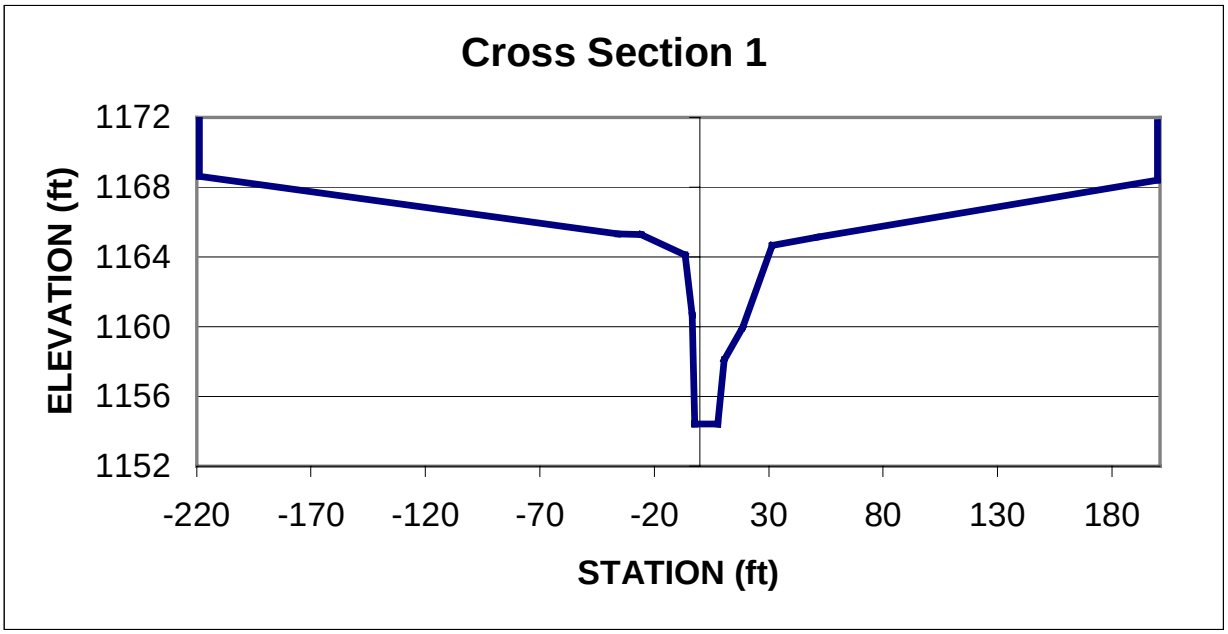

Figure I.9 Graph of surveyed cross section 1 upstream of Mill Rd 1.35 mi downstream of the upstream boundary of the modeling reach.

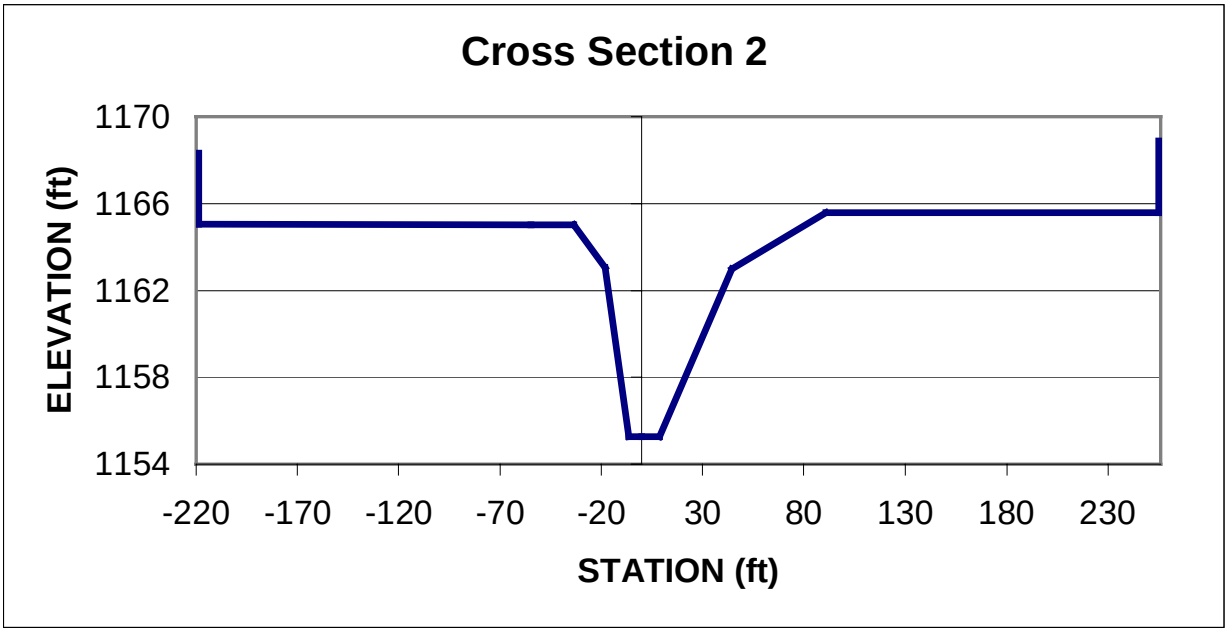

Figure I.10 Graph of surveyed cross section 2 upstream of Mill Rd 1.44 mi downstream of the upstream boundary of the modeling reach.

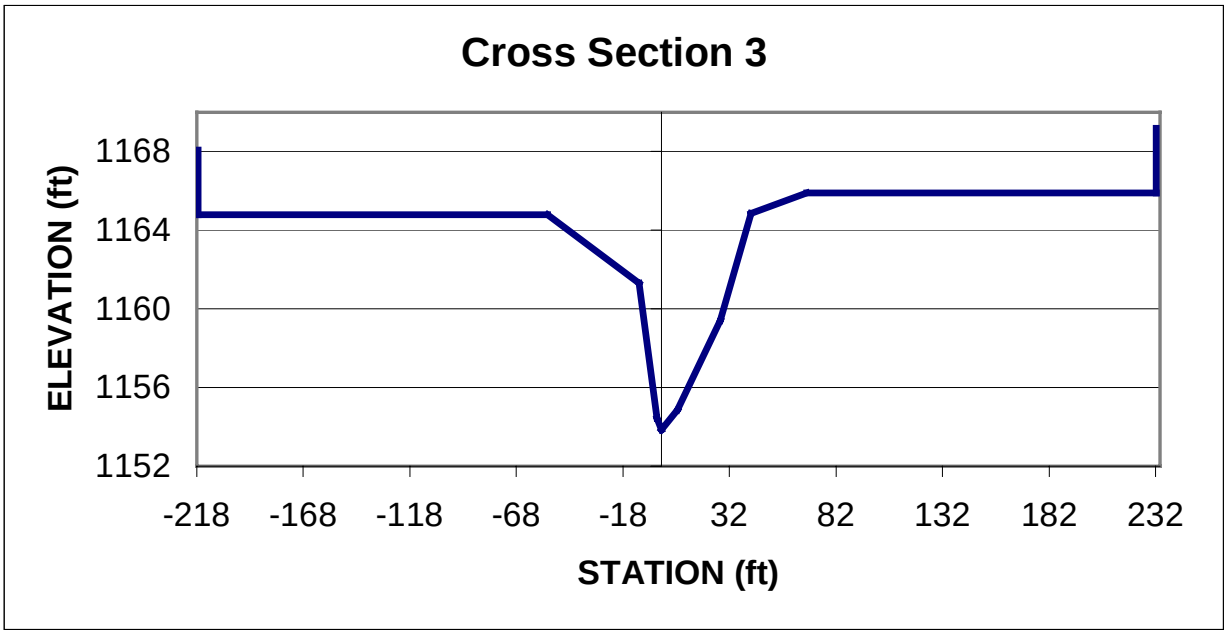

Figure I.11 Graph of surveyed cross section 3 upstream of Mill Rd 1.61 mi downstream of the upstream boundary of the modeling reach.

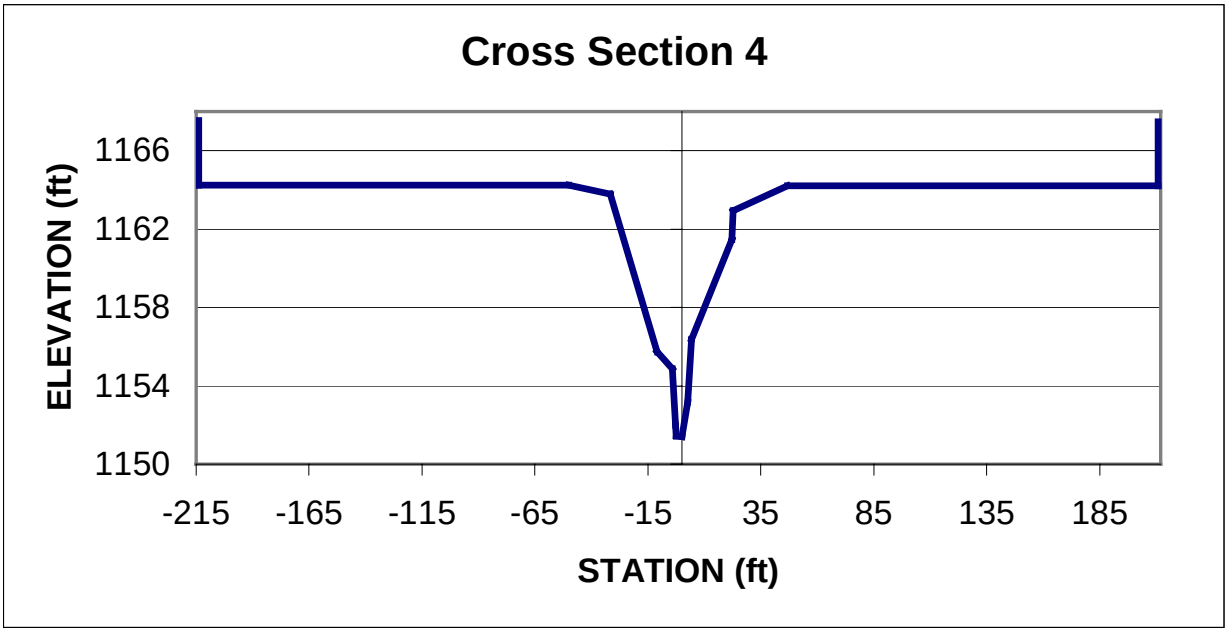

Figure I.12 Graph of surveyed cross section 4 upstream of Mill Rd 1.77 mi downstream of the upstream boundary of the modeling reach.

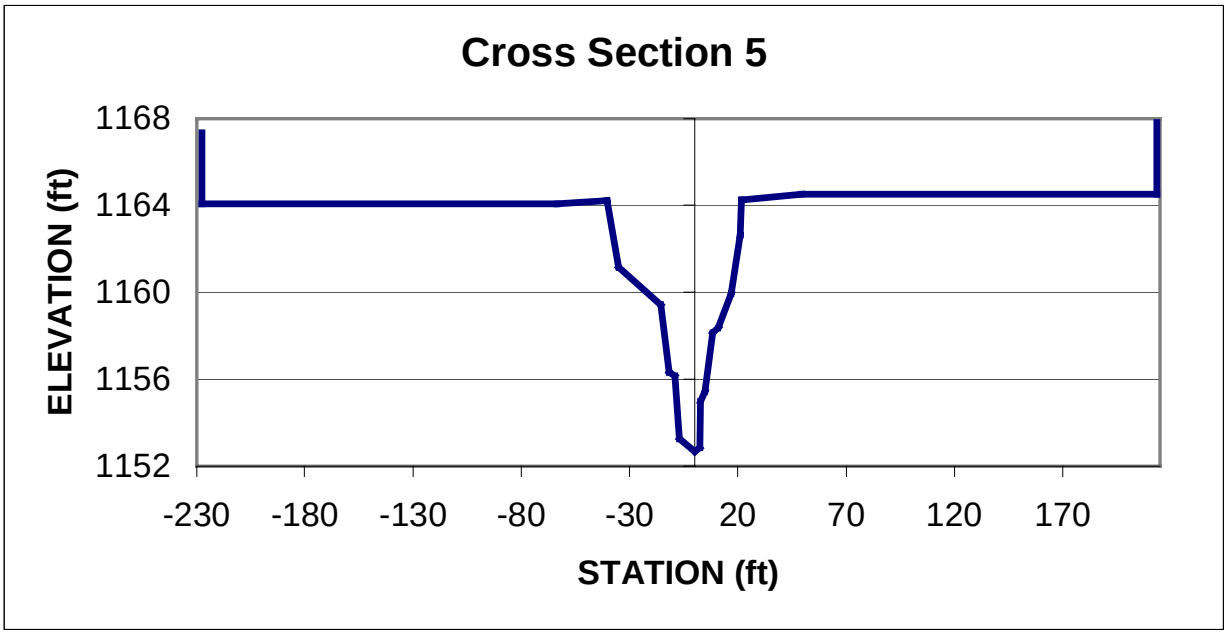

Figure I.13 Graph of surveyed cross section 5 upstream of Mill Rd 1.82 mi downstream of the upstream boundary of the modeling reach.

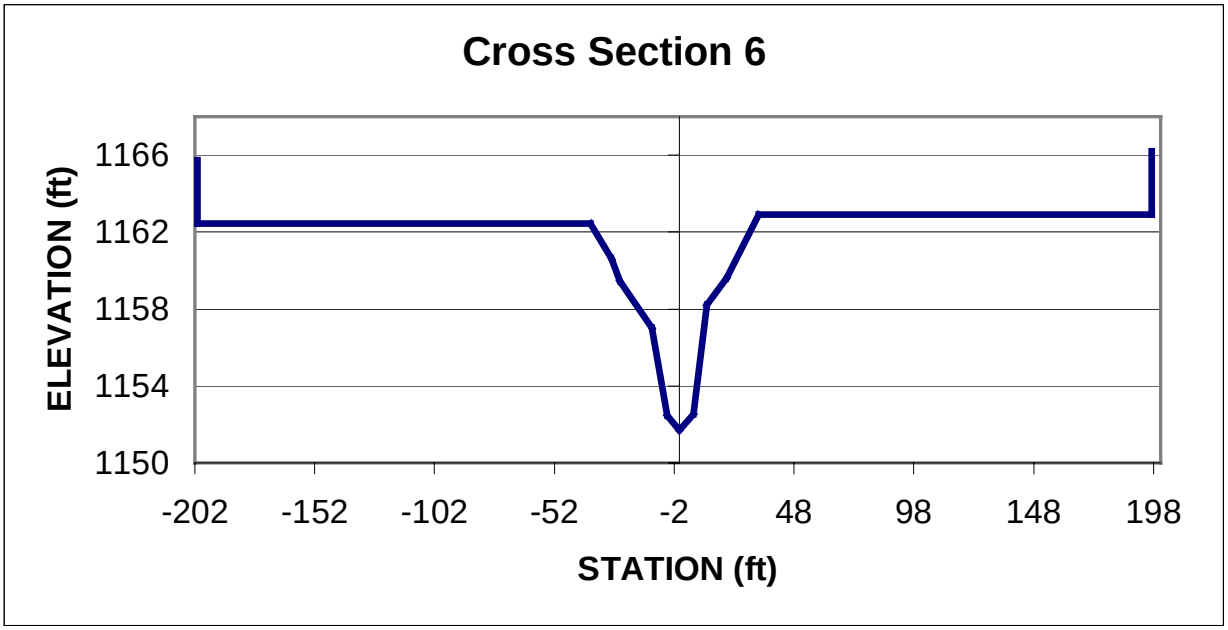

Figure I.14 Graph of surveyed cross section 6 upstream of Mill Rd 1.93 mi downstream of the upstream boundary of the modeling reach.

LITTLE SALT CREEK – CROSS SECTIONS SURVEYED NEAR BLUFF ROAD

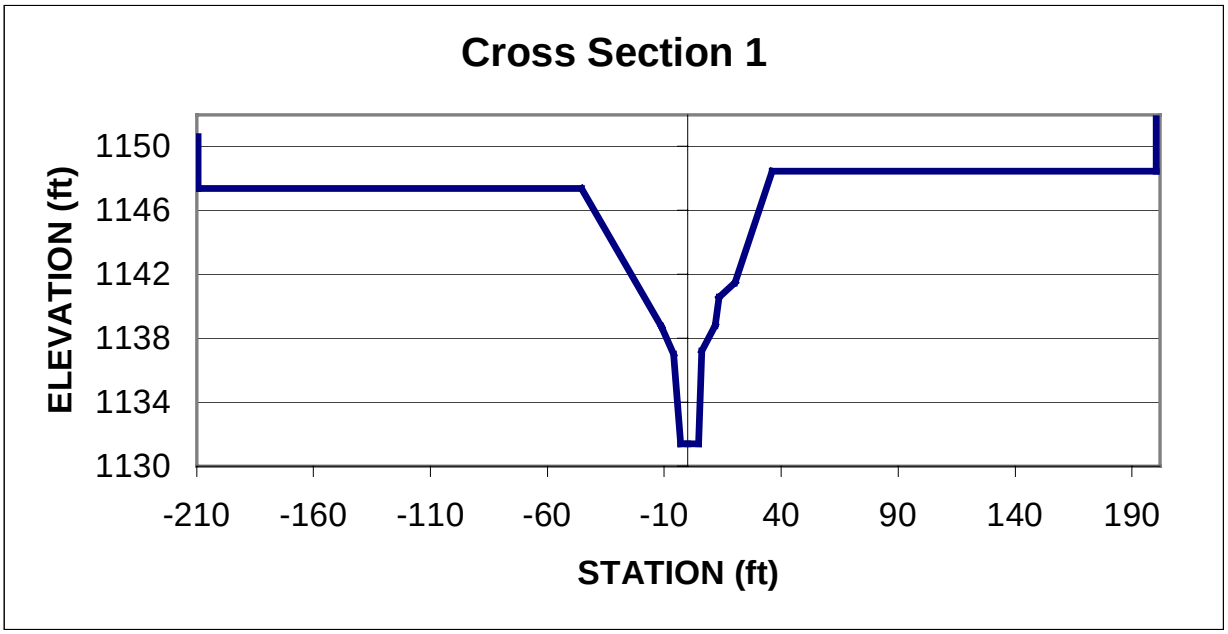

Figure I.15 Graph of surveyed cross section 1 near Bluff Rd 4.15 mi downstream of the upstream boundary of the modeling reach.

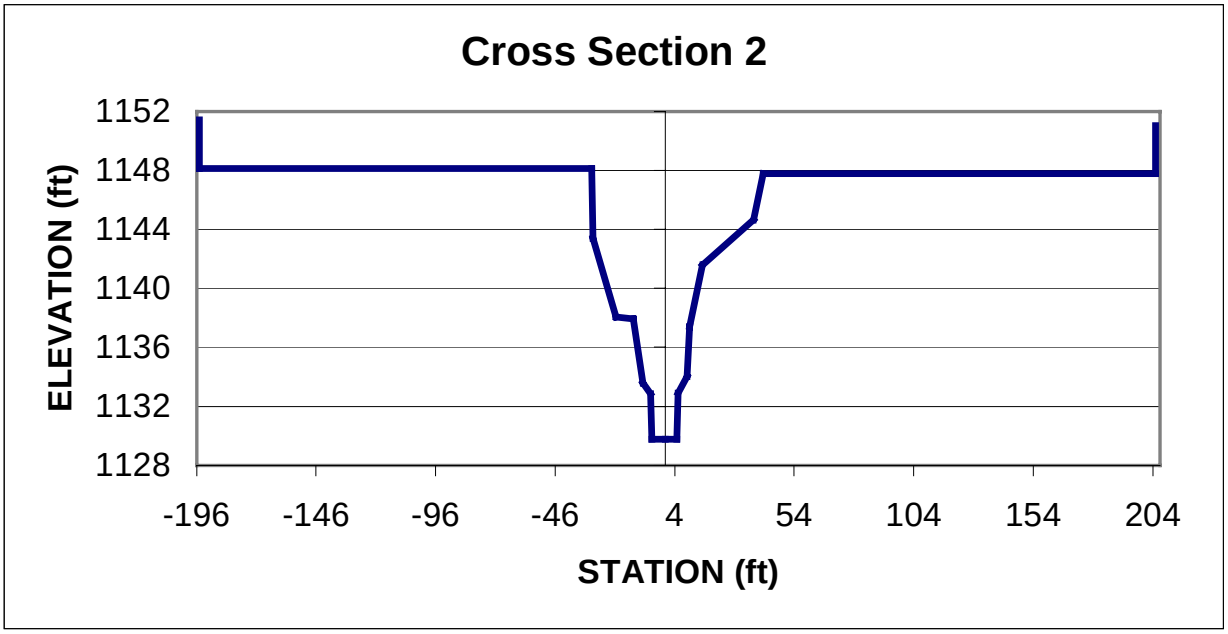

Figure I.16 Graph of surveyed cross section 2 near Bluff Rd 4.33 mi downstream of the upstream boundary of the modeling reach.

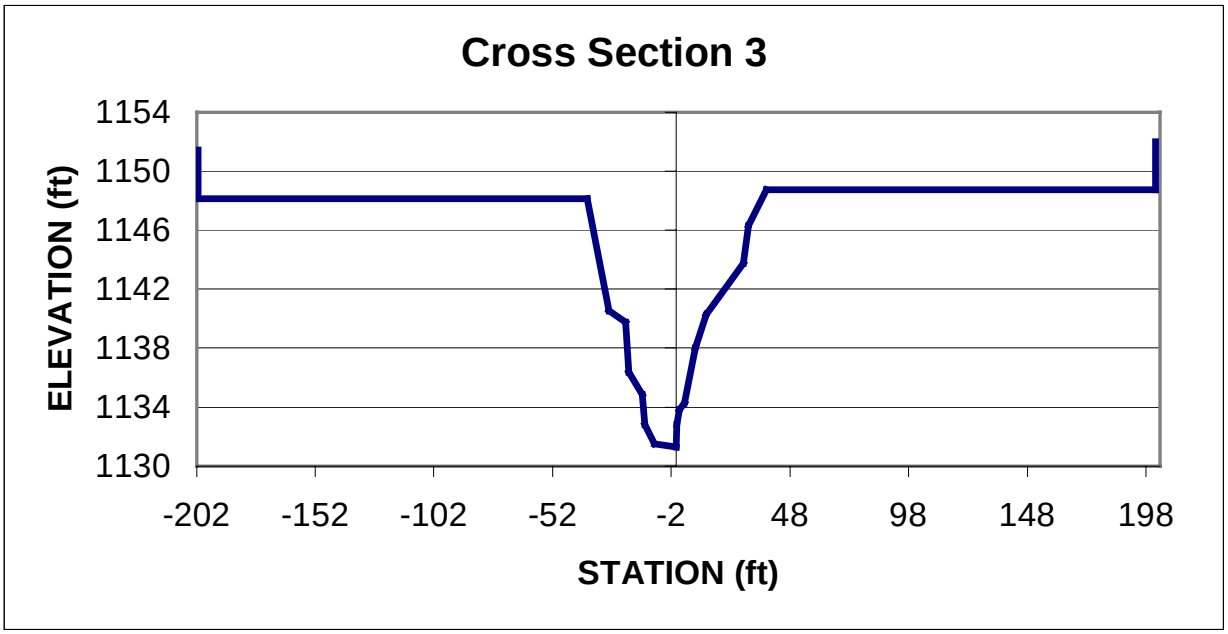

Figure I.17 Graph of surveyed cross section 3 near Bluff Rd 4.42 mi downstream of the upstream boundary of the modeling reach.

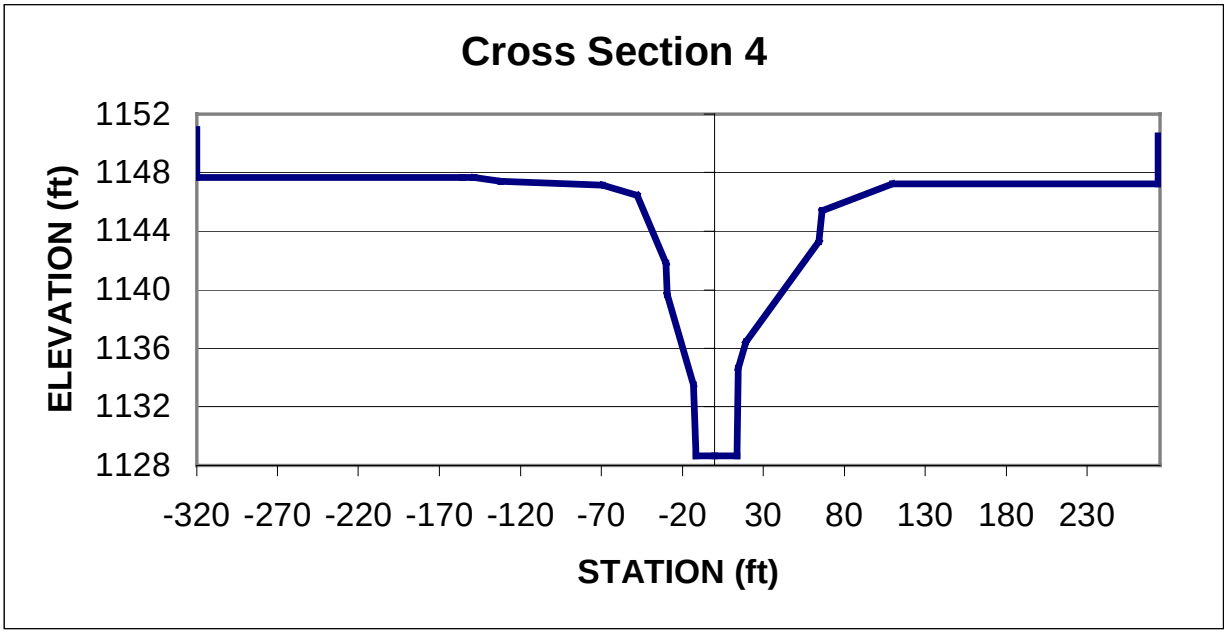

Figure I.18 Graph of surveyed cross section 4 near Bluff Rd 4.66 mi downstream of the upstream boundary of the modeling reach.

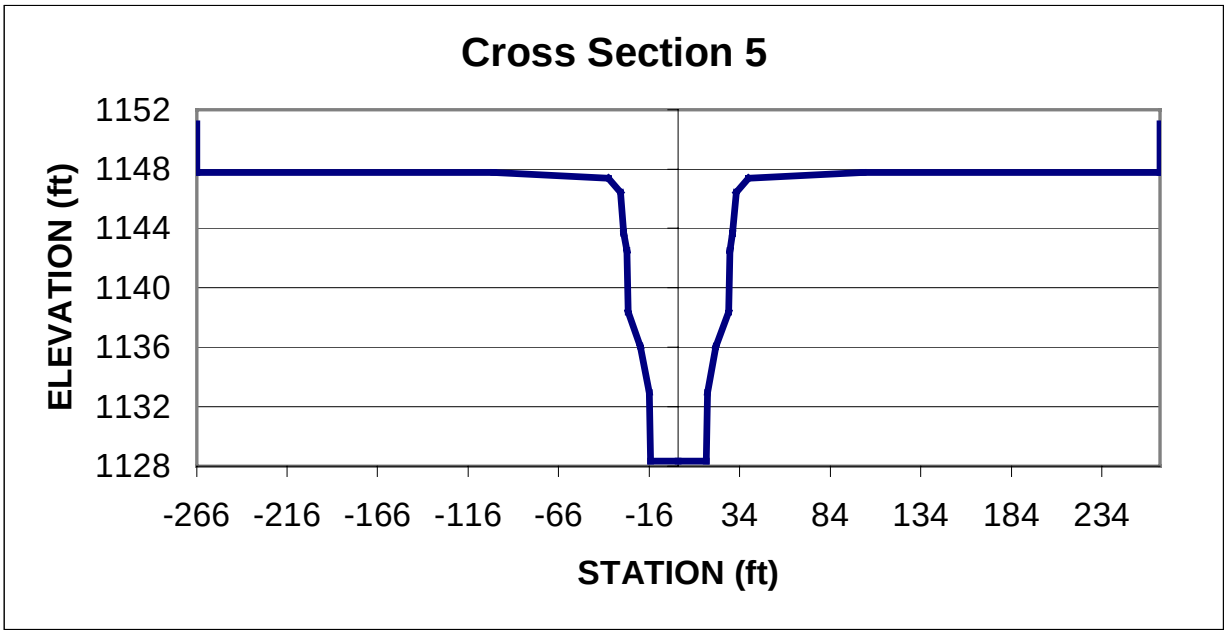

Figure I.19 Graph of surveyed cross section 5 near Bluff Rd 4.72 mi downstream of the upstream boundary of the modeling reach.

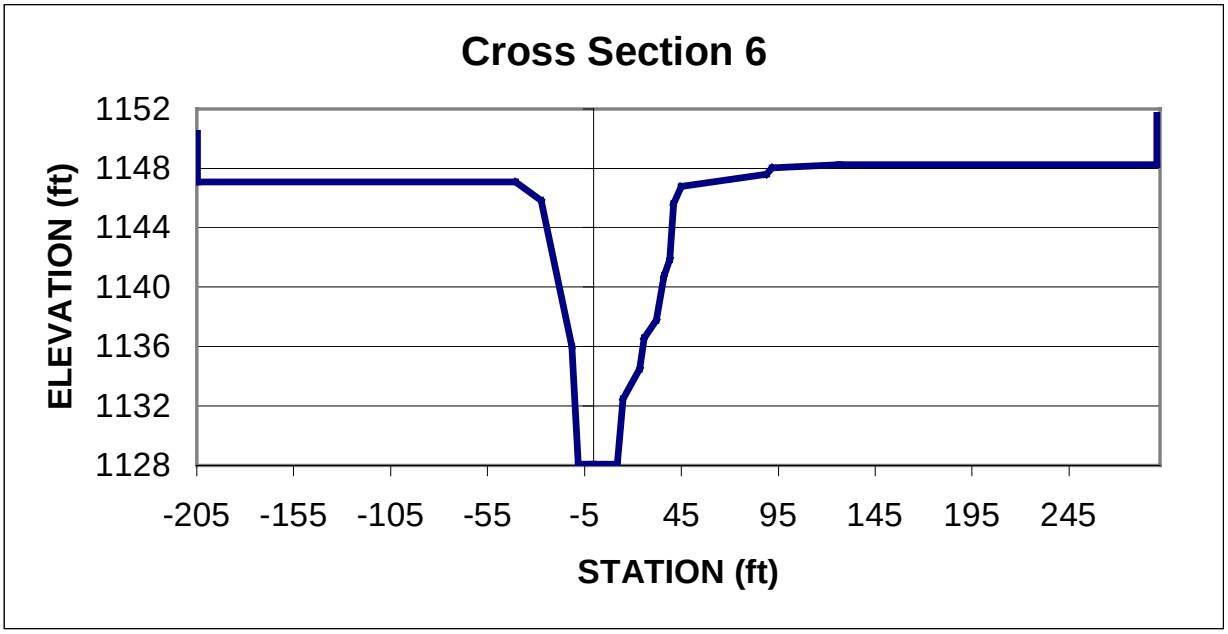

Figure I.20 Graph of surveyed cross section 6 near Bluff Rd 4.80 mi downstream of the upstream boundary of the modeling reach.

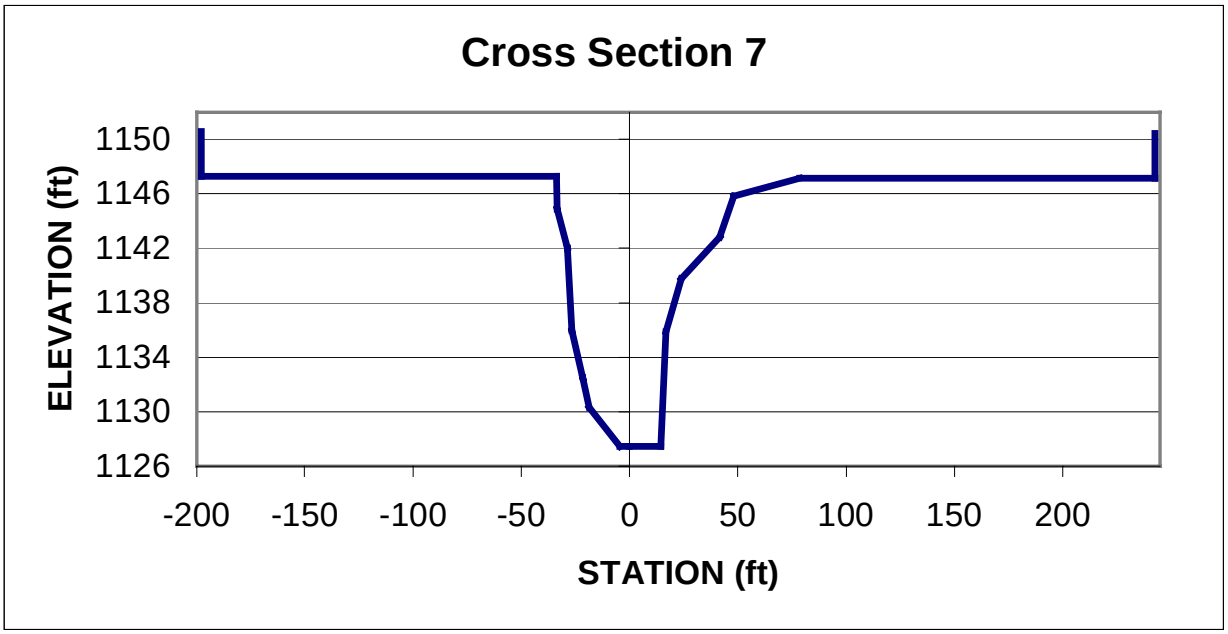

Figure I.21 Graph of surveyed cross section 7 near Bluff Rd 4.88 mi downstream of the upstream boundary of the modeling reach.

WEST PAPILLION CREEK – SURVEYED BED PROFILE

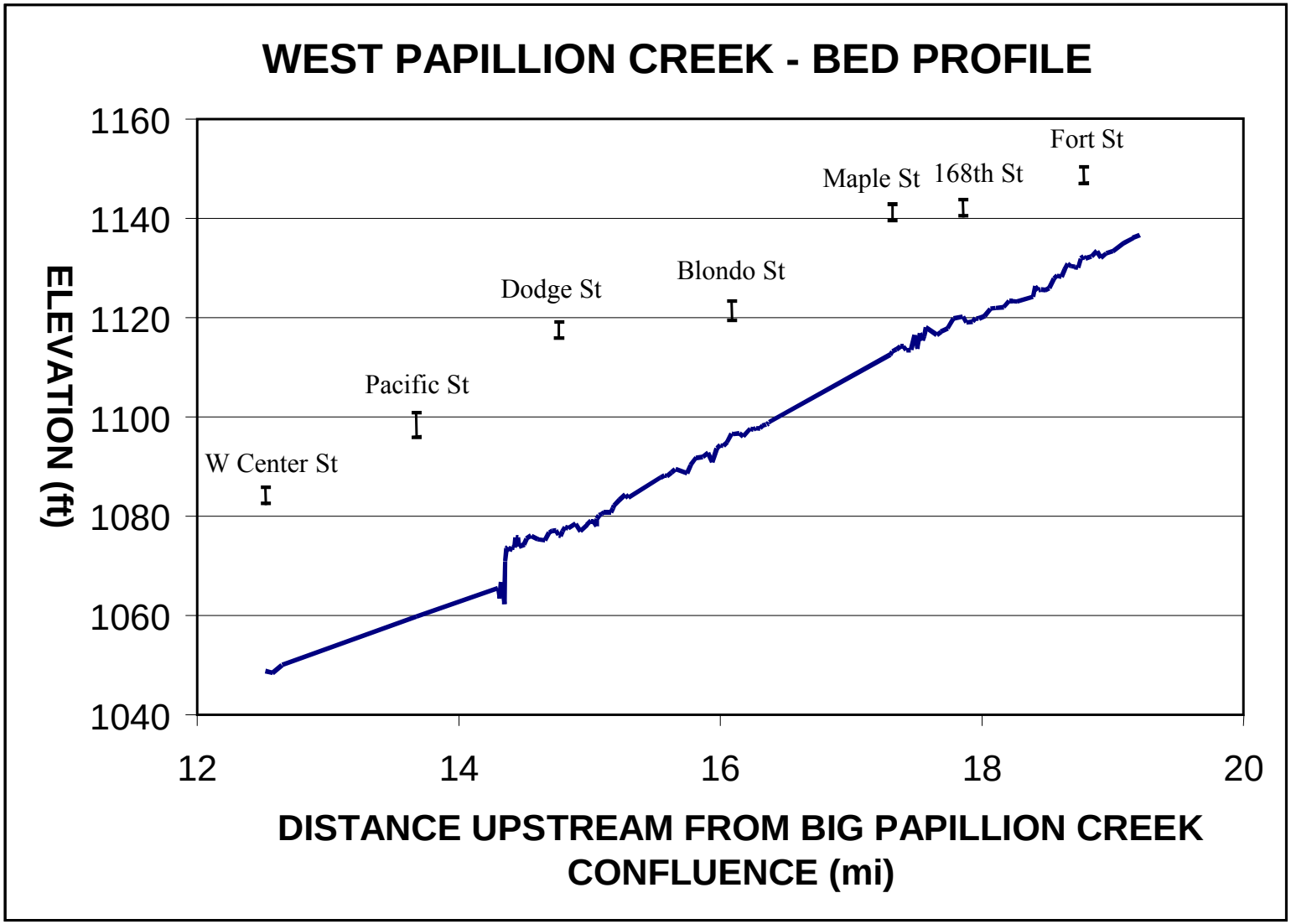

Figure I.22 Graph of surveyed bed profile of the West Papillion Creek and North Branch West Papillion Creek, and bridge decks.

NORTH BRANCH WEST PAPILLION CREEK – CROSS SECTIONS SURVEYED
UPSTREAM OF FORT STREET

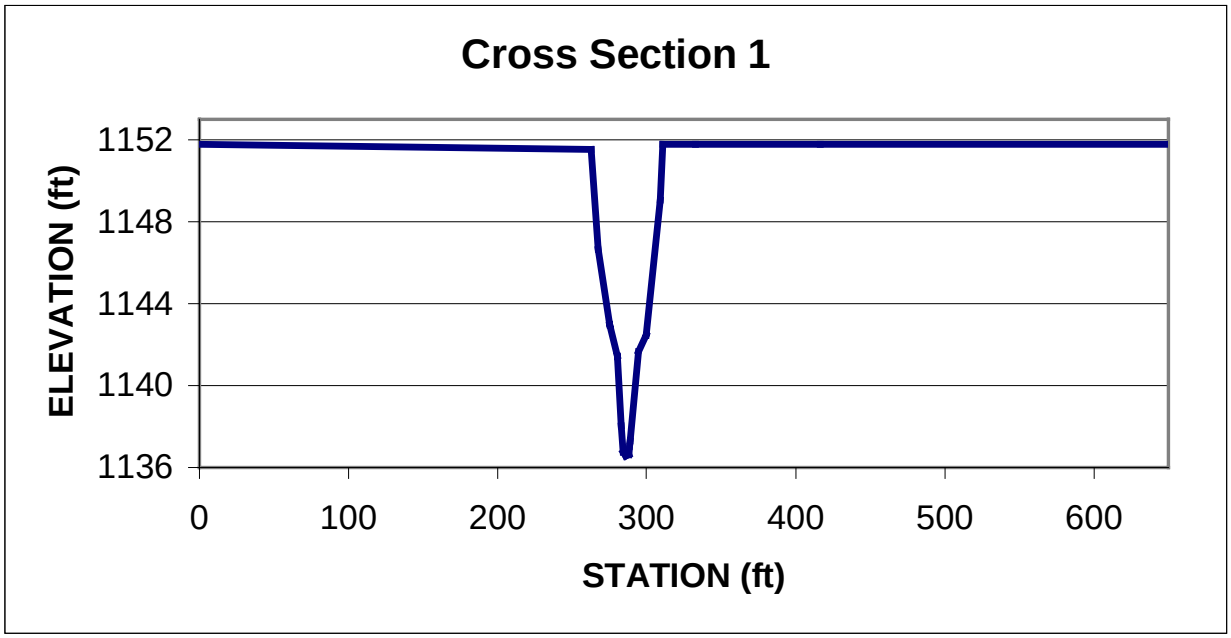

Figure I.23 Graph of surveyed cross section 1 upstream of Fort St 0.00 mi downstream of the upstream boundary of the modeling reach.

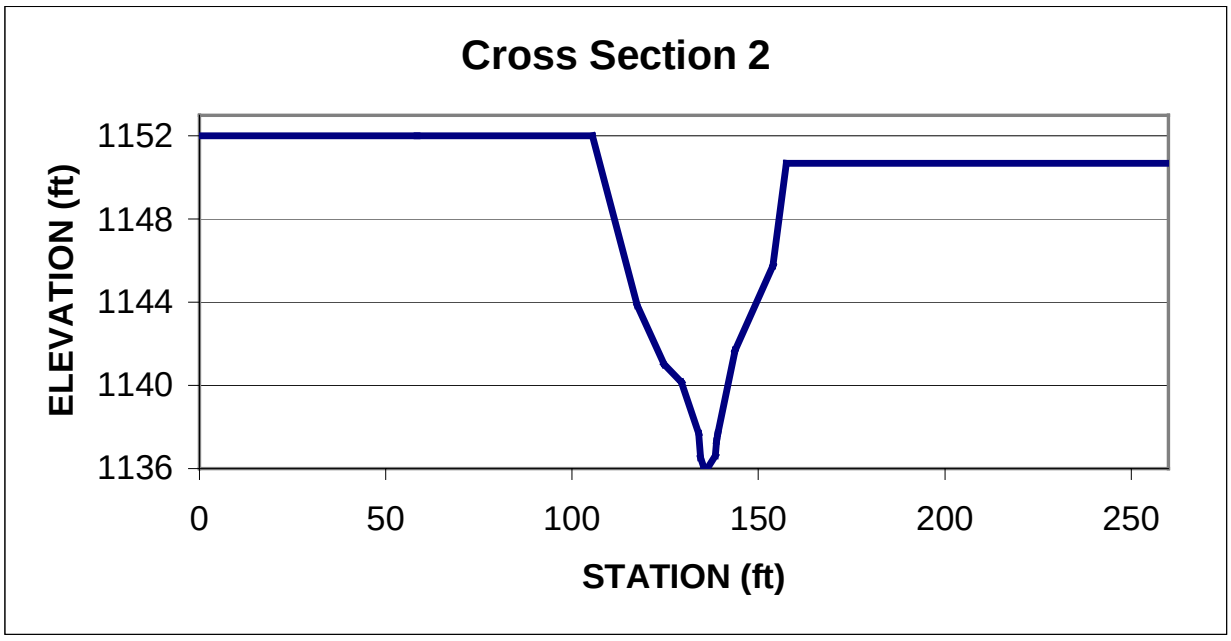

Figure I.24 Graph of surveyed cross section 2 upstream of Fort St 0.05 mi downstream of the upstream boundary of the modeling reach.

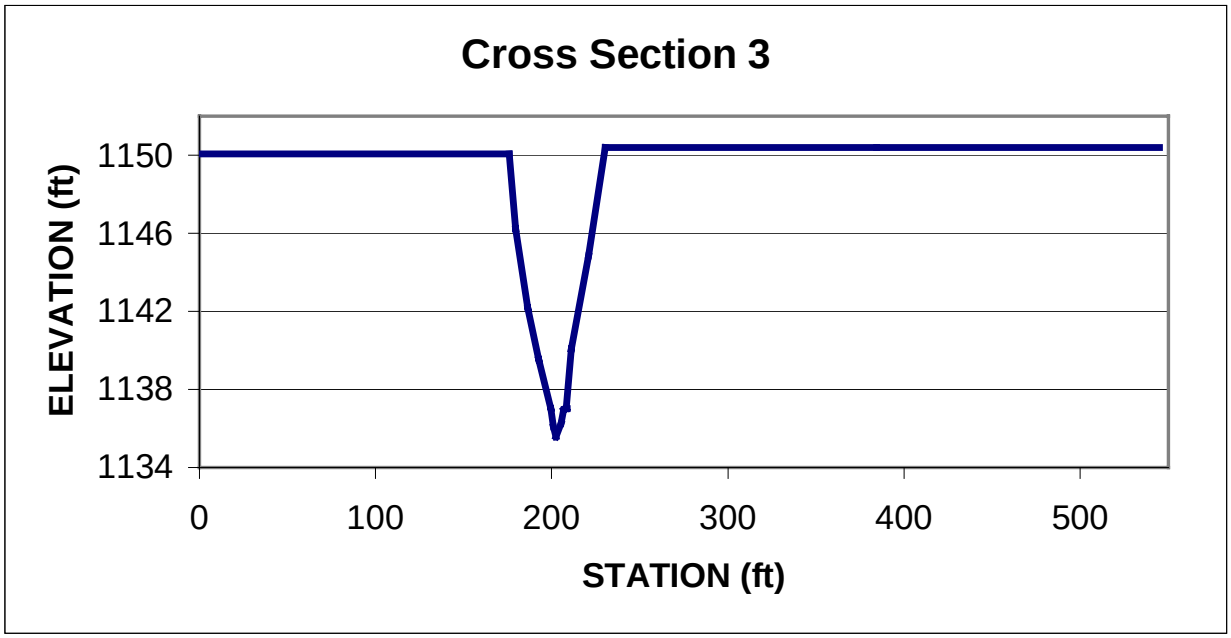

Figure I.25 Graph of surveyed cross section 3 upstream of Fort St 0.12 mi downstream of the upstream boundary of the modeling reach.

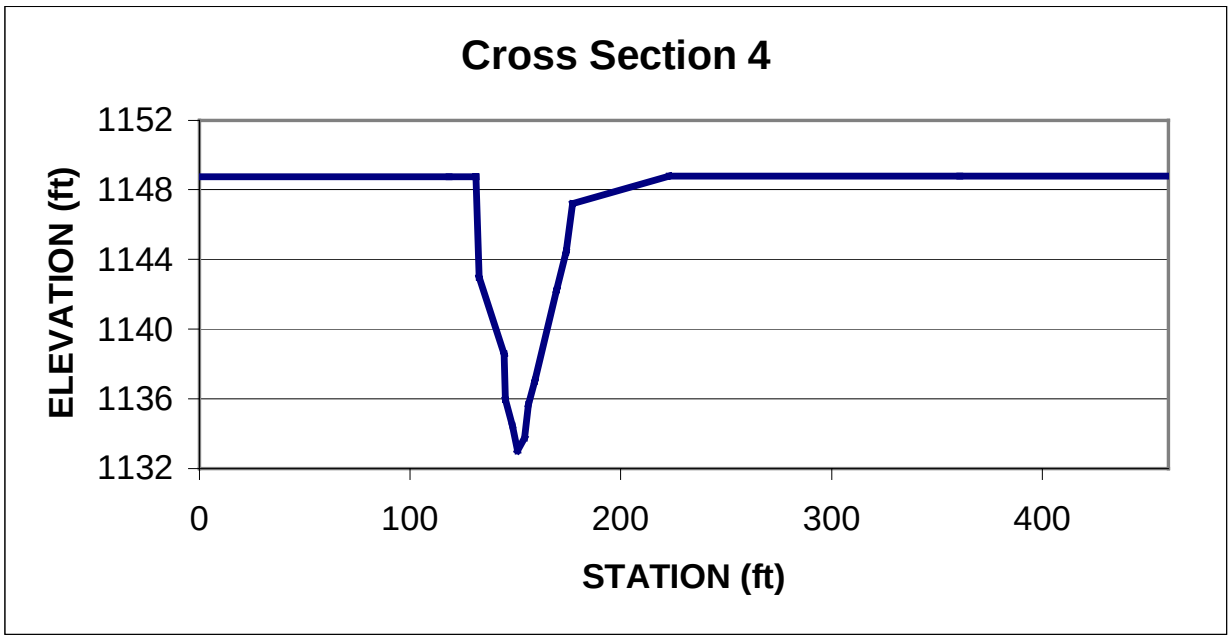

Figure I.26 Graph of surveyed cross section 4 upstream of Fort St 0.22 mi downstream of the upstream boundary of the modeling reach.

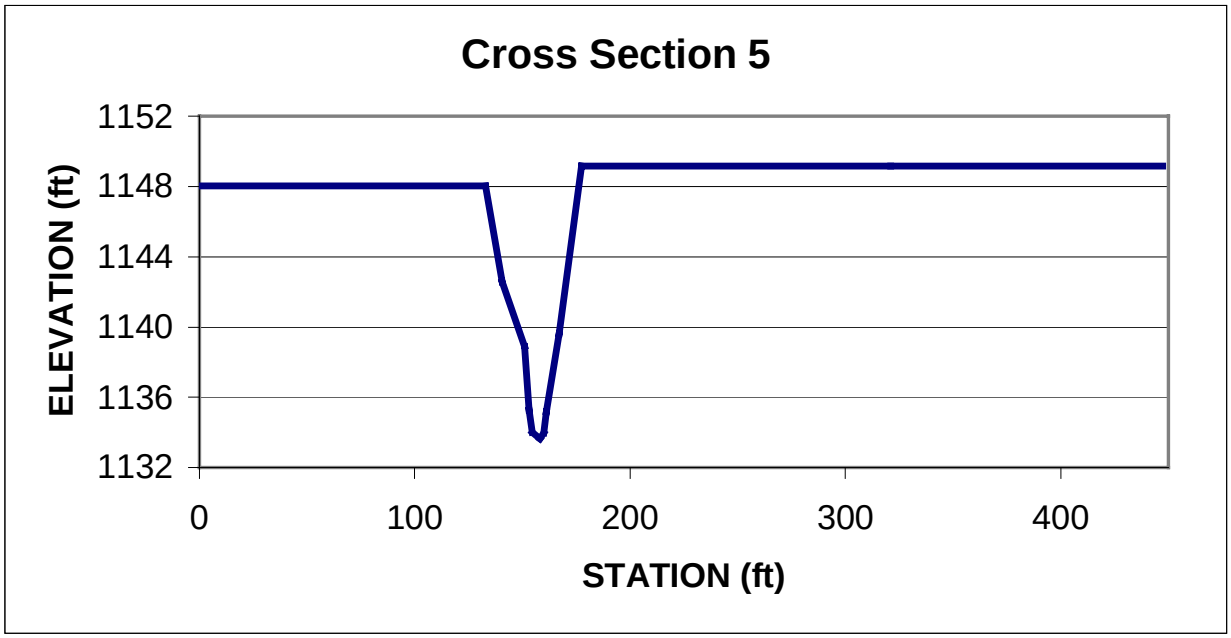

Figure I.27 Graph of surveyed cross section 5 upstream of Fort St 0.27 mi downstream of the upstream boundary of the modeling reach.

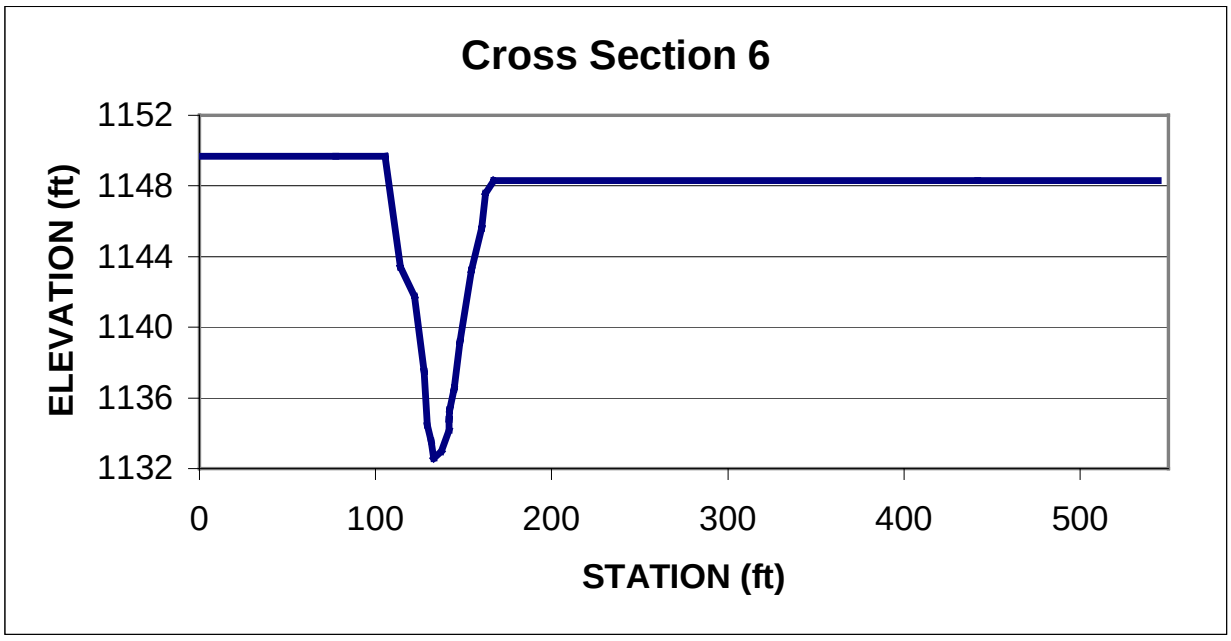

Figure I.28 Graph of surveyed cross section 6 upstream of Fort St 0.33 mi downstream of the upstream boundary of the modeling reach.

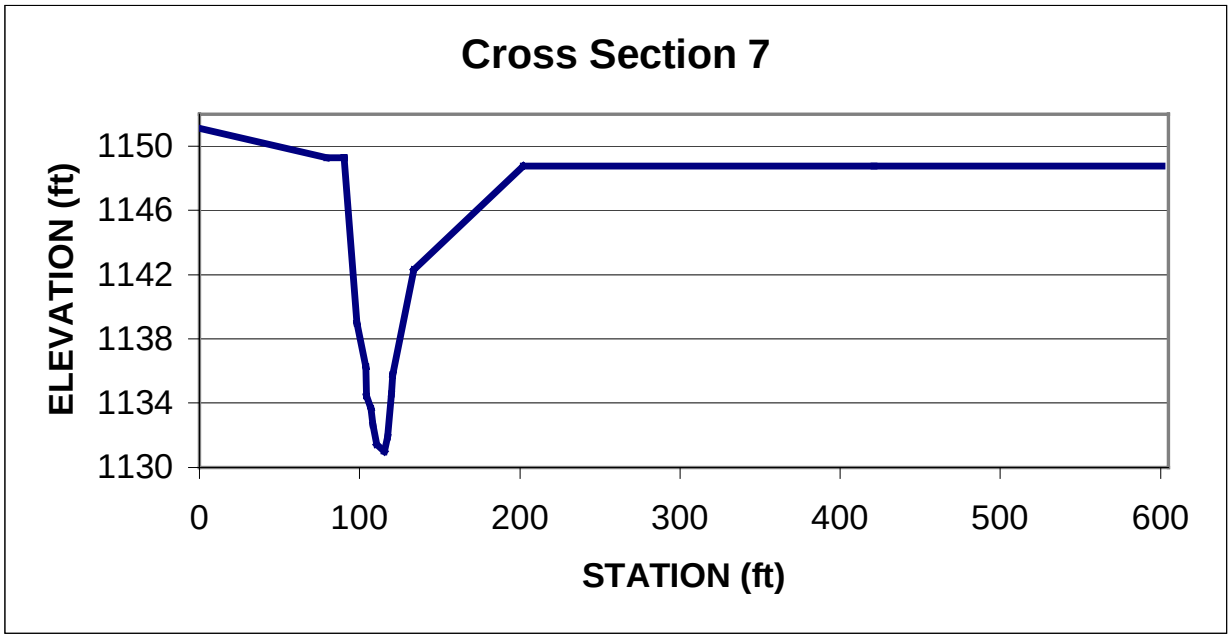

Figure I.29 Graph of surveyed cross section 7 upstream of Fort St 0.37 mi downstream of the upstream boundary of the modeling reach.

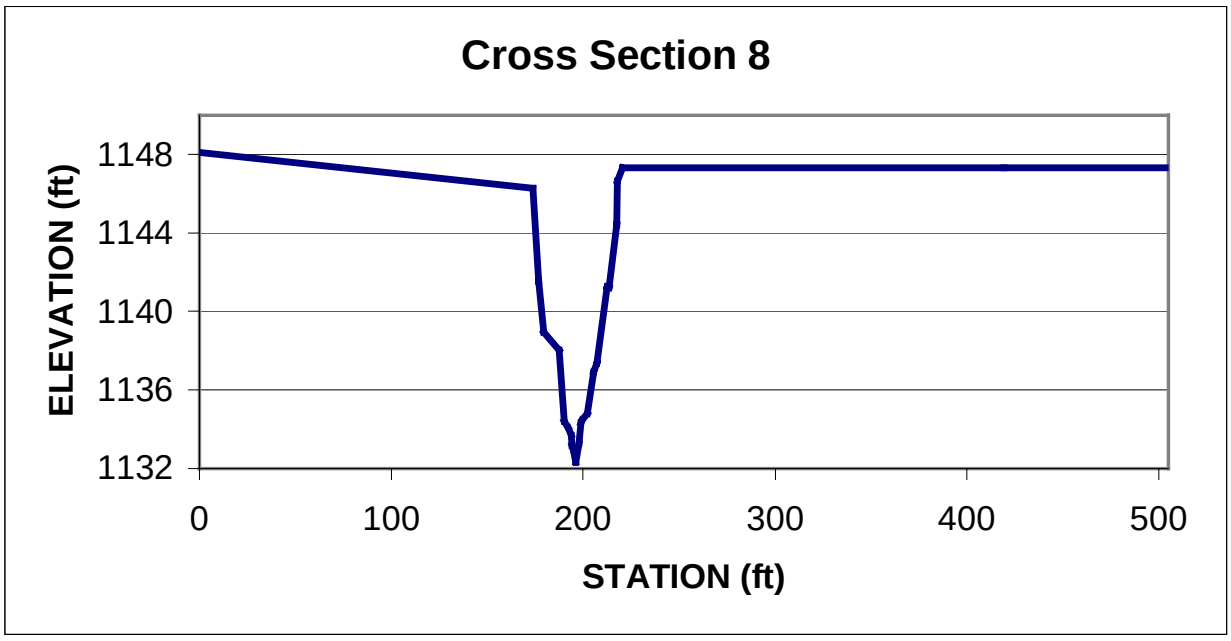

Figure I.30 Graph of surveyed cross section 8 upstream of Fort St 0.42 mi downstream of the upstream boundary of the modeling reach.

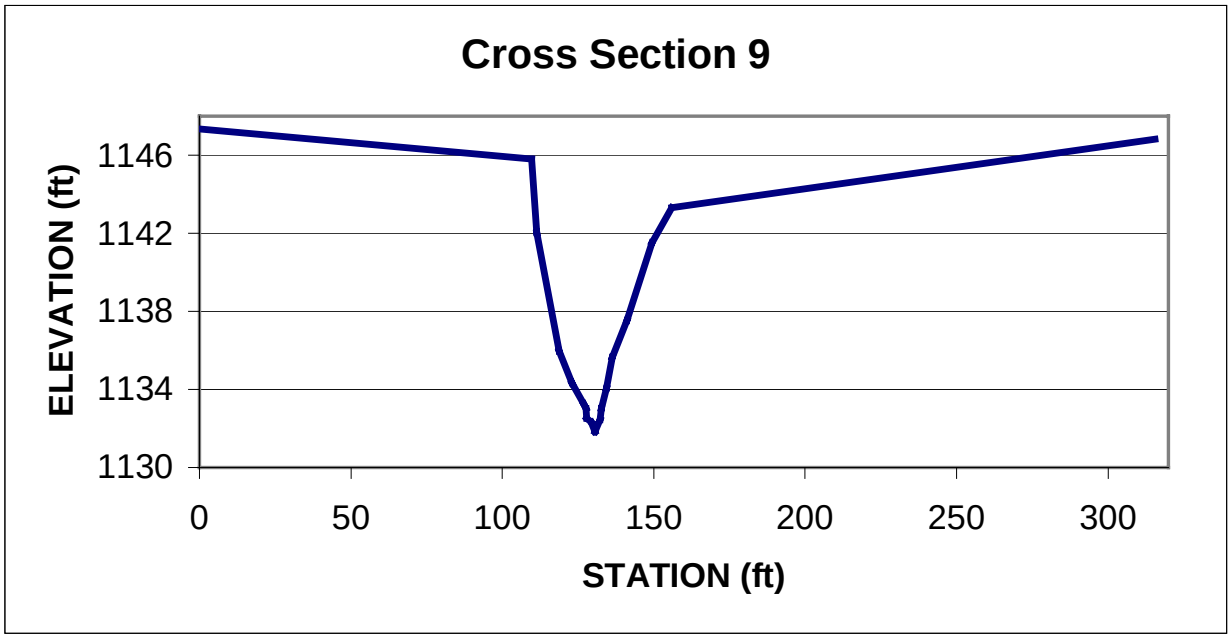

Figure I.31 Graph of surveyed cross section 9 upstream of Fort St 0.45 mi downstream of the upstream boundary of the modeling reach.

NORTH BRANCH WEST PAPILLION CREEK – CROSS SECTIONS SURVEYED DOWNSTREAM OF FORT STREET

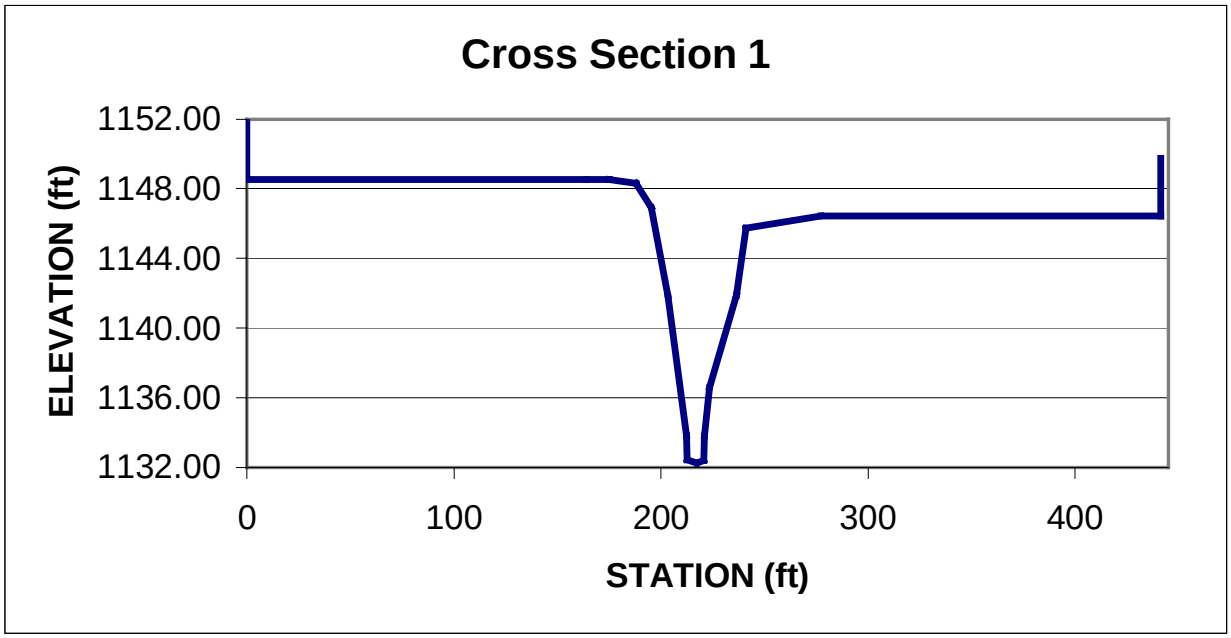

Figure I.32 Graph of surveyed cross section 1 downstream of Fort St 0.48 mi downstream of the upstream boundary of the modeling reach.

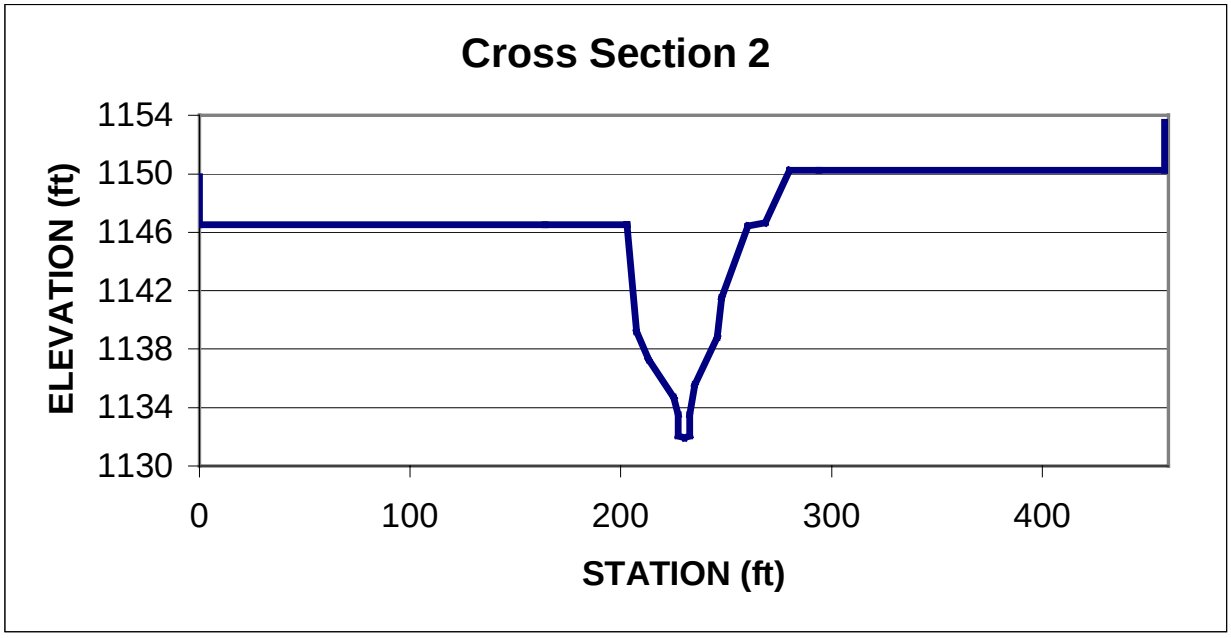

Figure I.33 Graph of surveyed cross section 2 downstream of Fort St 0.52 mi downstream of the upstream boundary of the modeling reach.

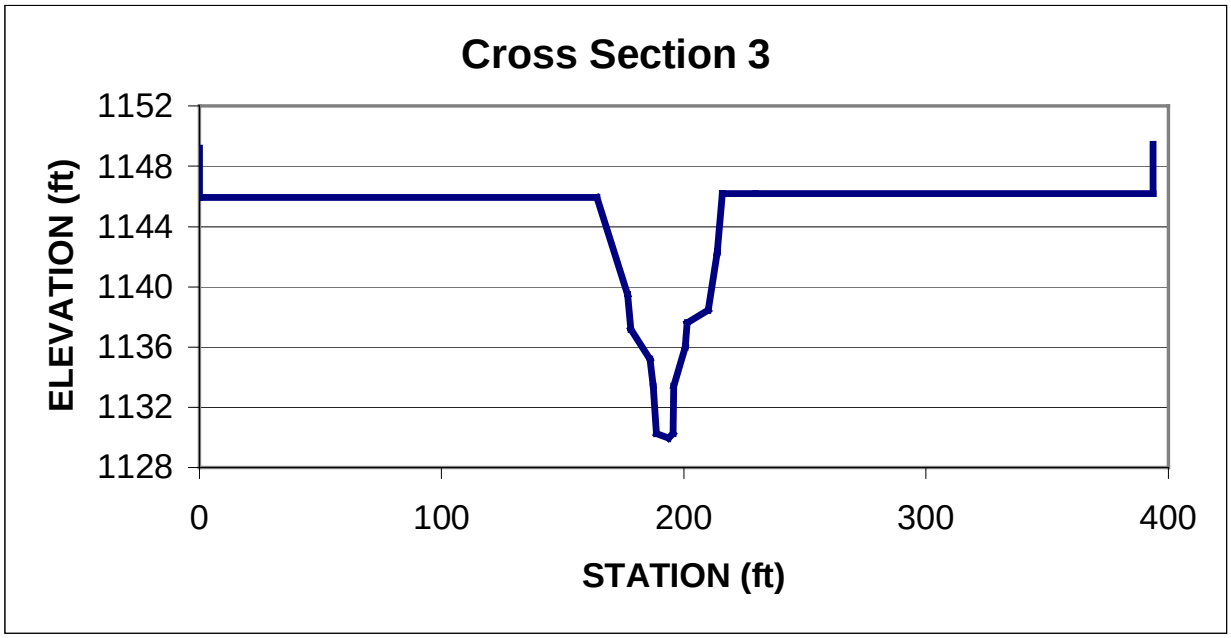

Figure I.34 Graph of surveyed cross section 3 downstream of Fort St 0.54 mi downstream of the upstream boundary of the modeling reach.

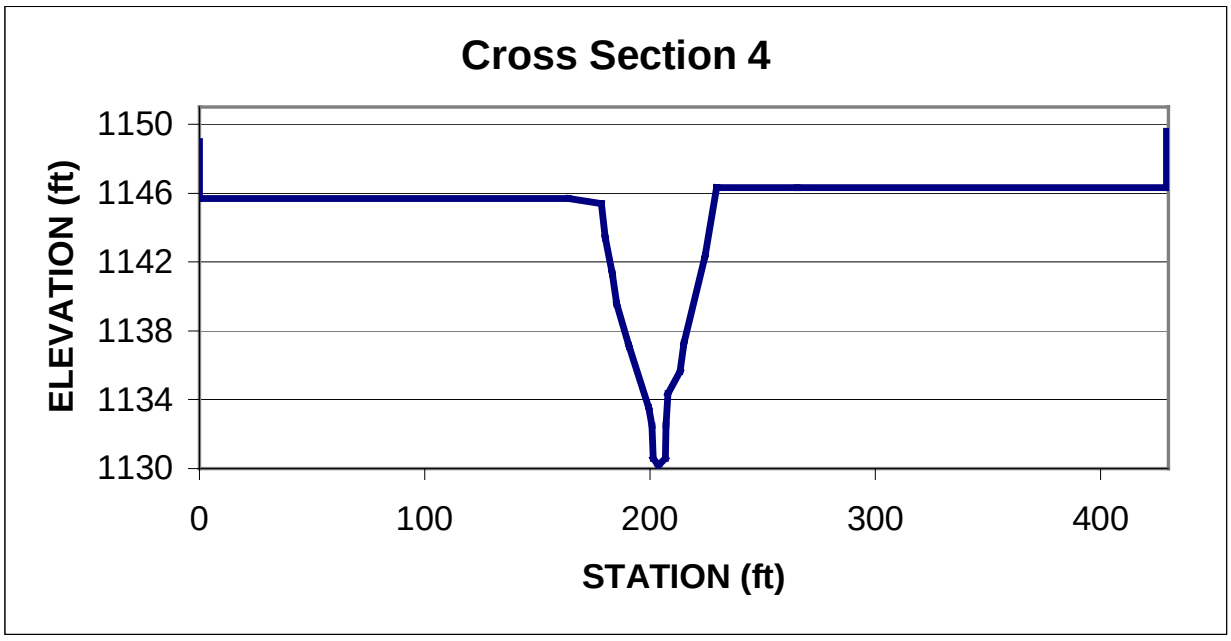

Figure I.35 Graph of surveyed cross section 4 downstream of Fort St 0.57 mi downstream of the upstream boundary of the modeling reach.

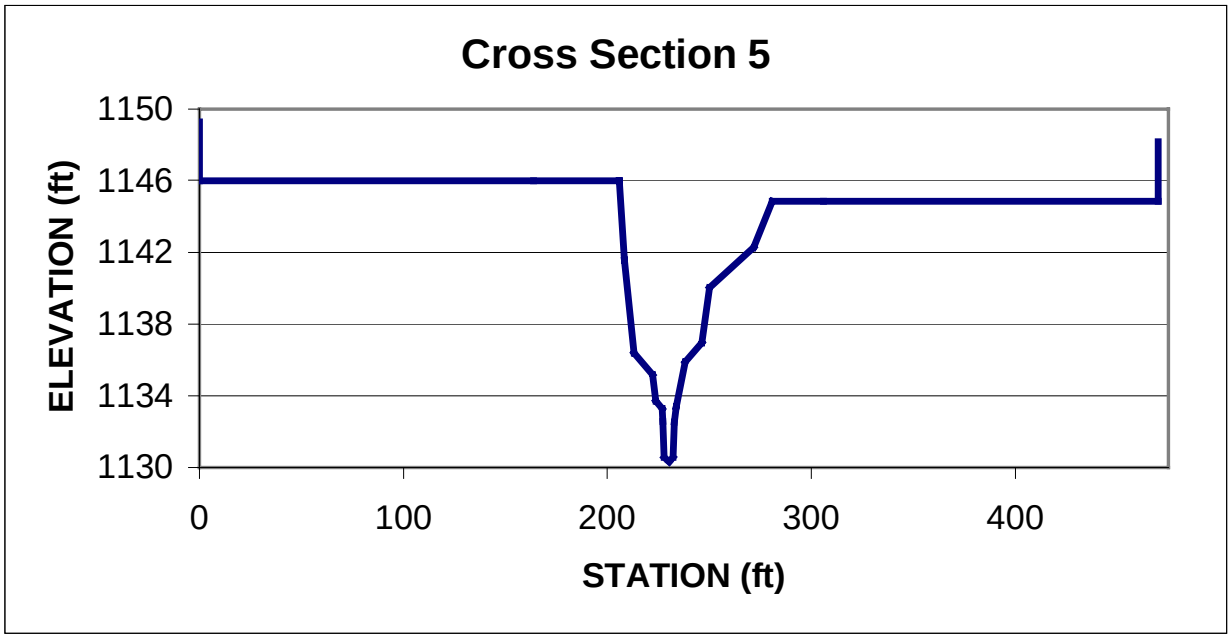

Figure I.36 Graph of surveyed cross section 5 downstream of Fort St 0.60 mi downstream of the upstream boundary of the modeling reach.

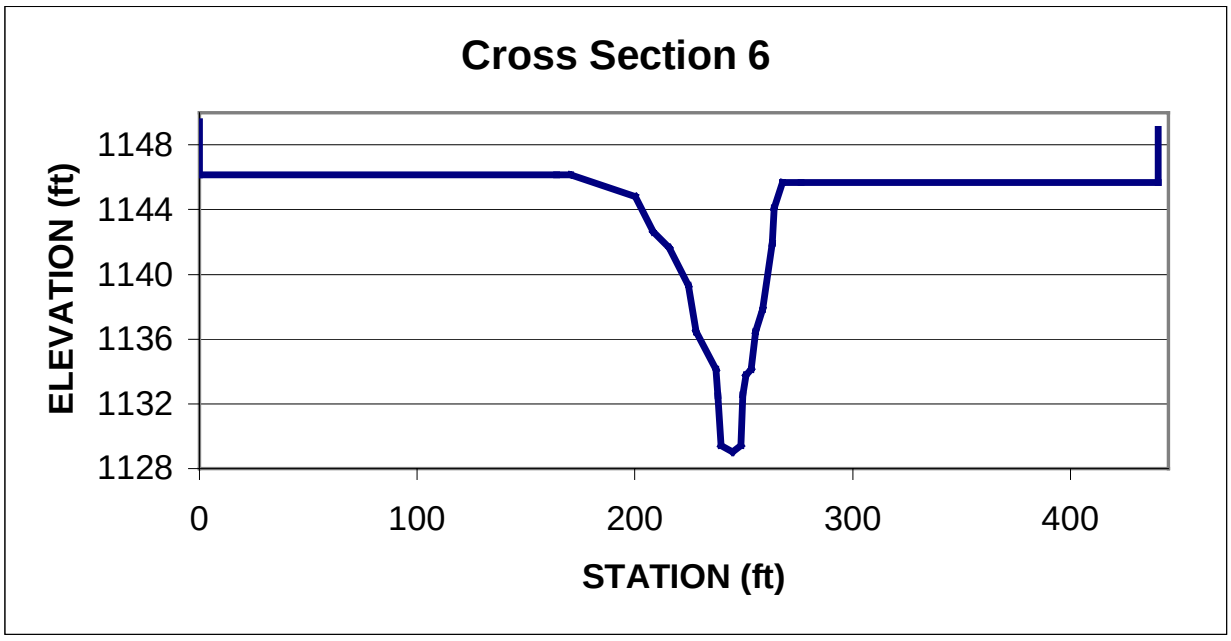

Figure I.37 Graph of surveyed cross section 6 downstream of Fort St 0.61 mi downstream of the upstream boundary of the modeling reach.

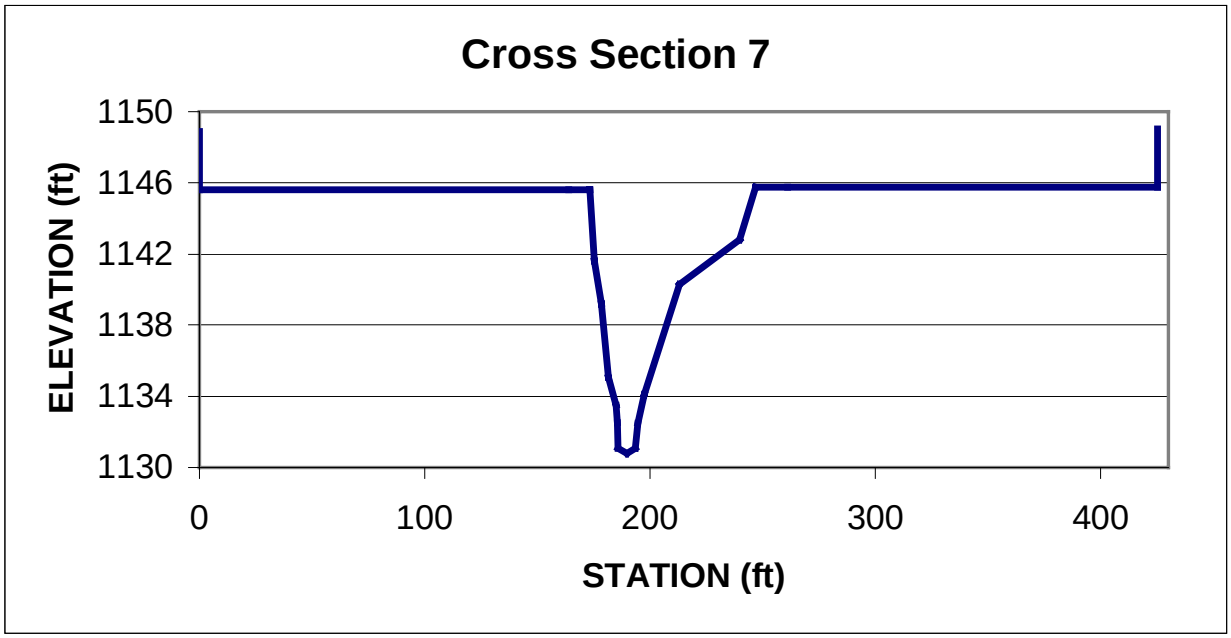

Figure I.38 Graph of surveyed cross section 7 downstream of Fort St 0.63 mi downstream of the upstream boundary of the modeling reach.

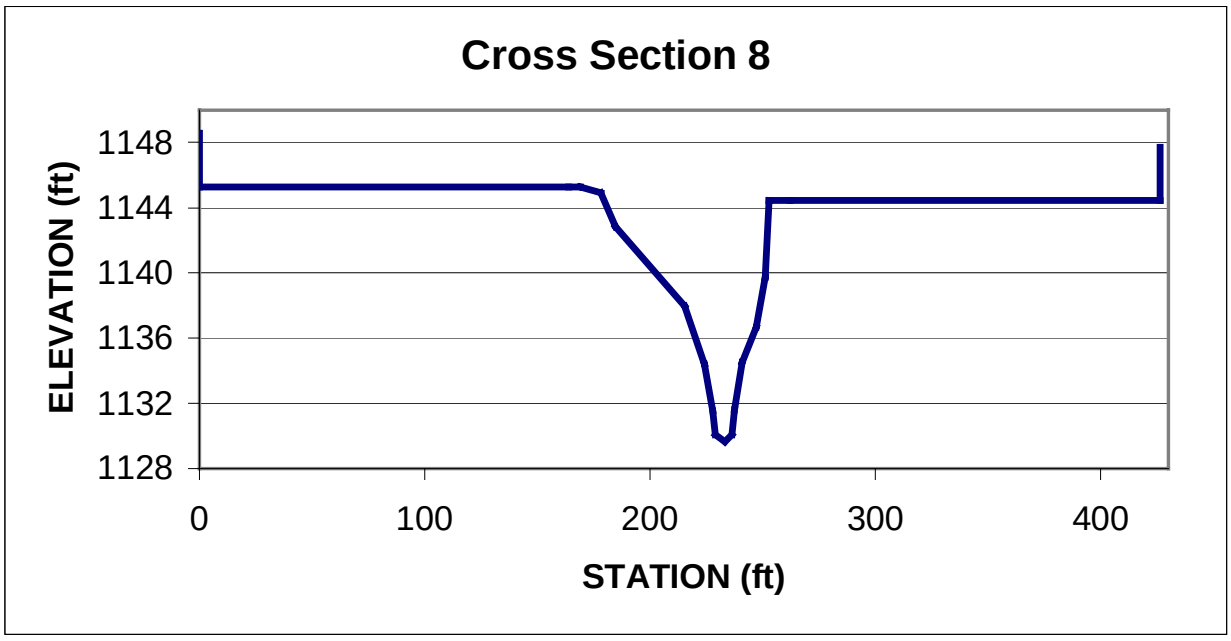

Figure I.39 Graph of surveyed cross section 8 downstream of Fort St 0.66 mi downstream of the upstream boundary of the modeling reach.

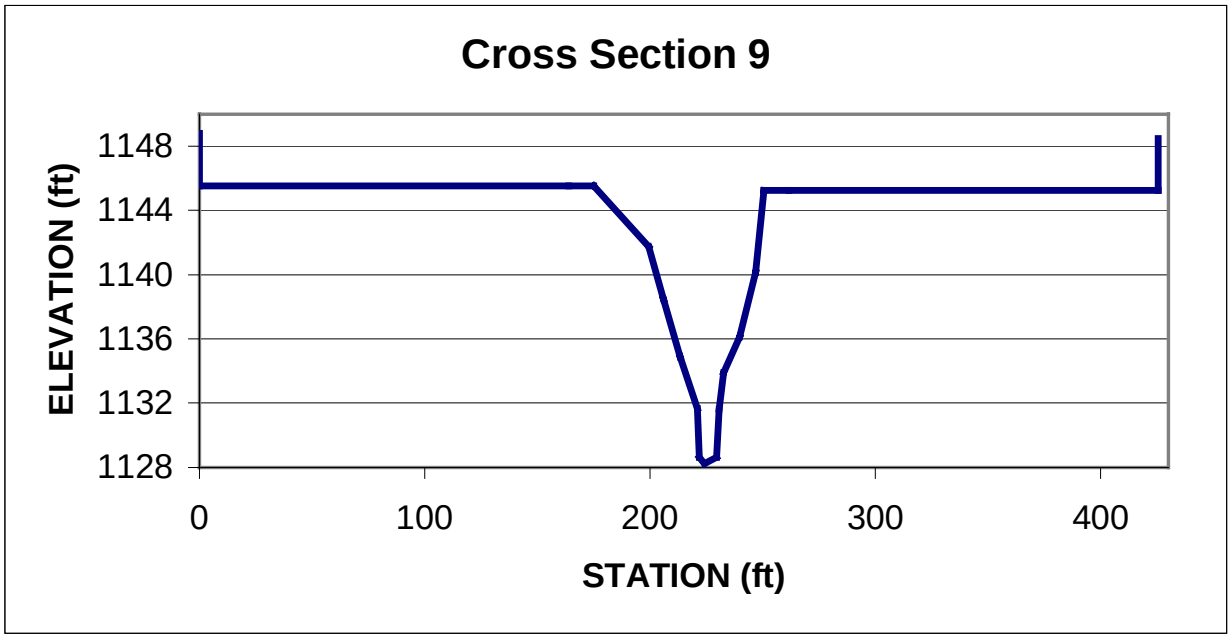

Figure I.40 Graph of surveyed cross section 9 downstream of Fort St 0.68 mi downstream of the upstream boundary of the modeling reach.

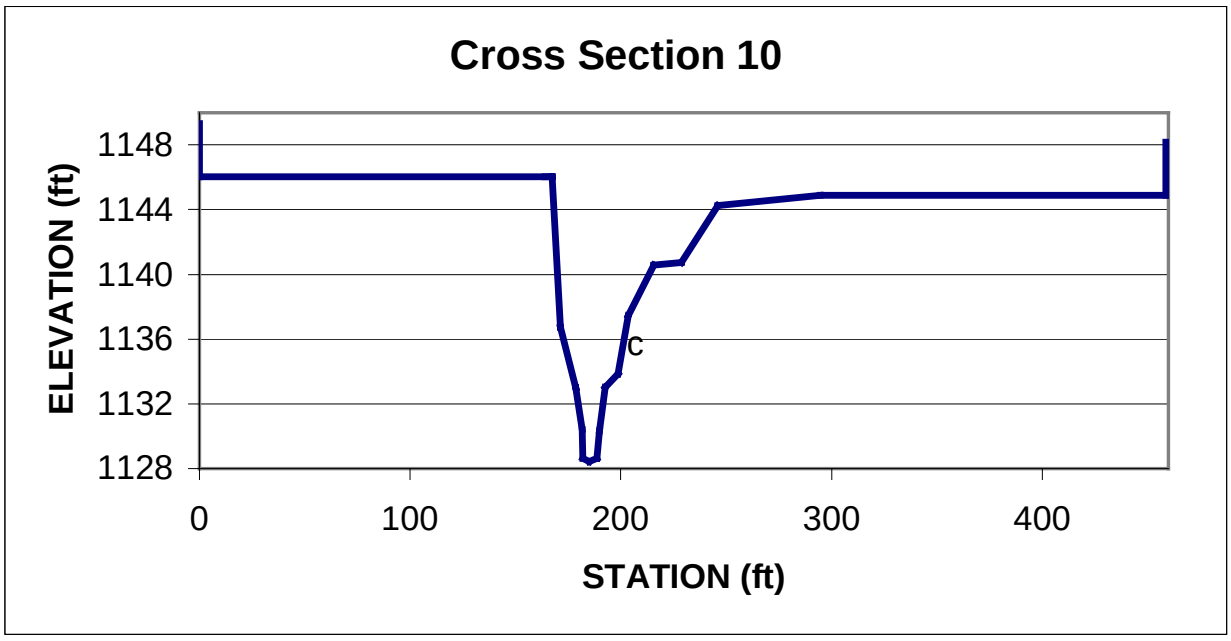

Figure I.41 Graph of surveyed cross section 10 downstream of Fort St 0.72 mi downstream of the upstream boundary of the modeling reach.

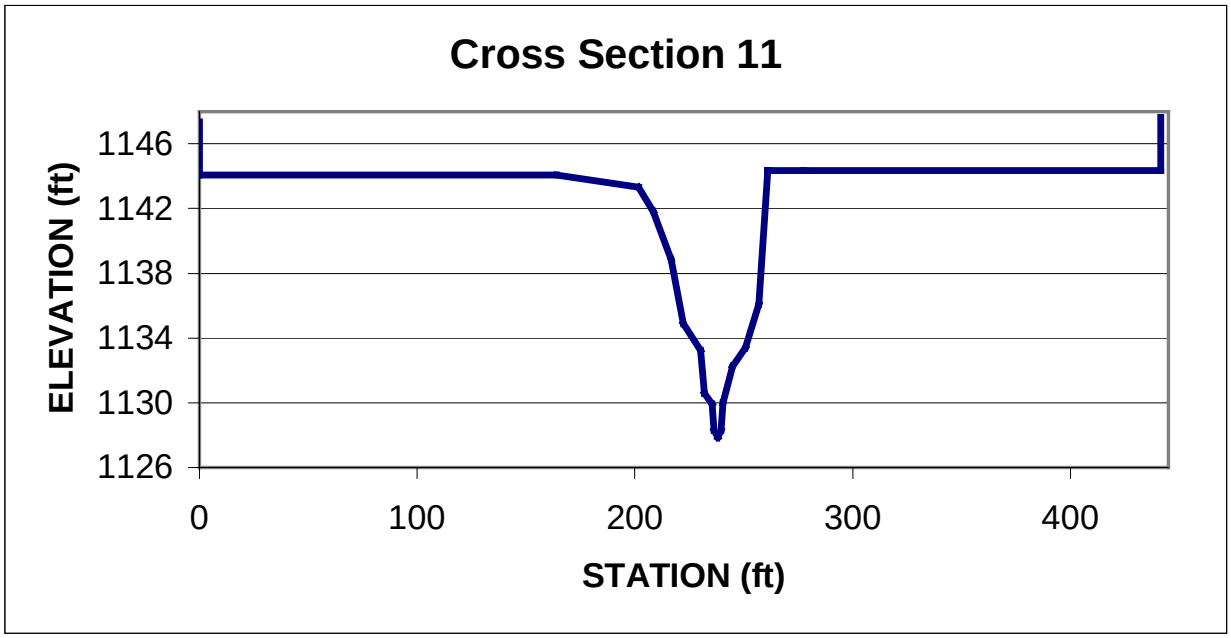

Figure I.42 Graph of surveyed cross section 11 downstream of Fort St 0.75 mi downstream of the upstream boundary of the modeling reach.

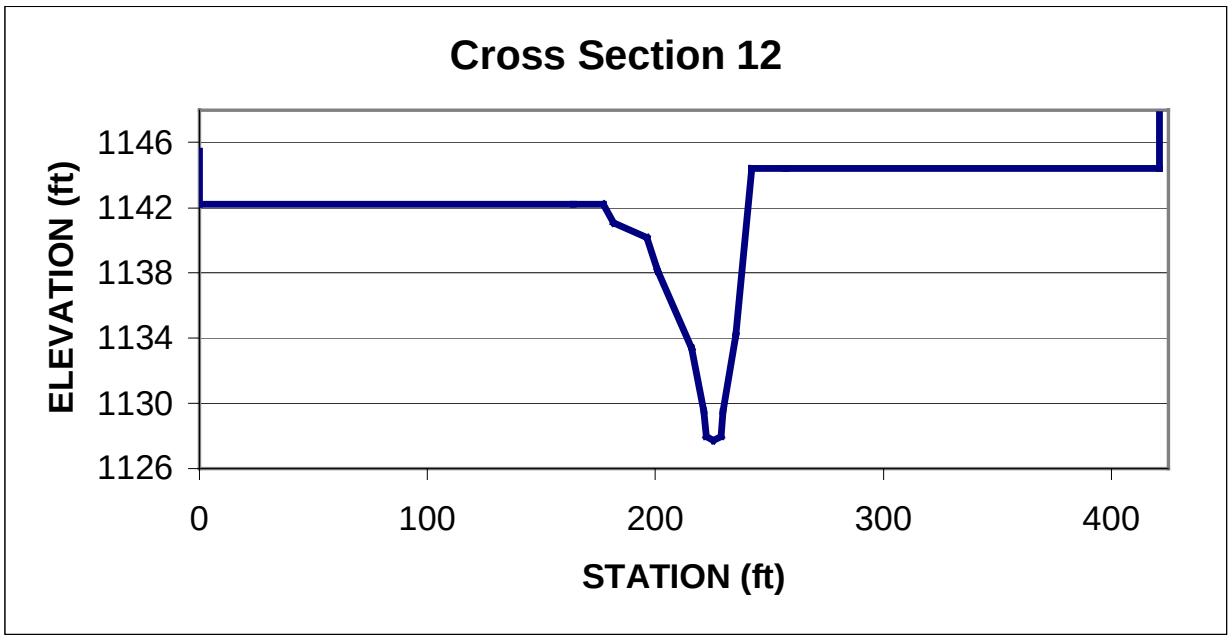

Figure I.43 Graph of surveyed cross section 12 downstream of Fort St 0.79 mi downstream of the upstream boundary of the modeling reach.

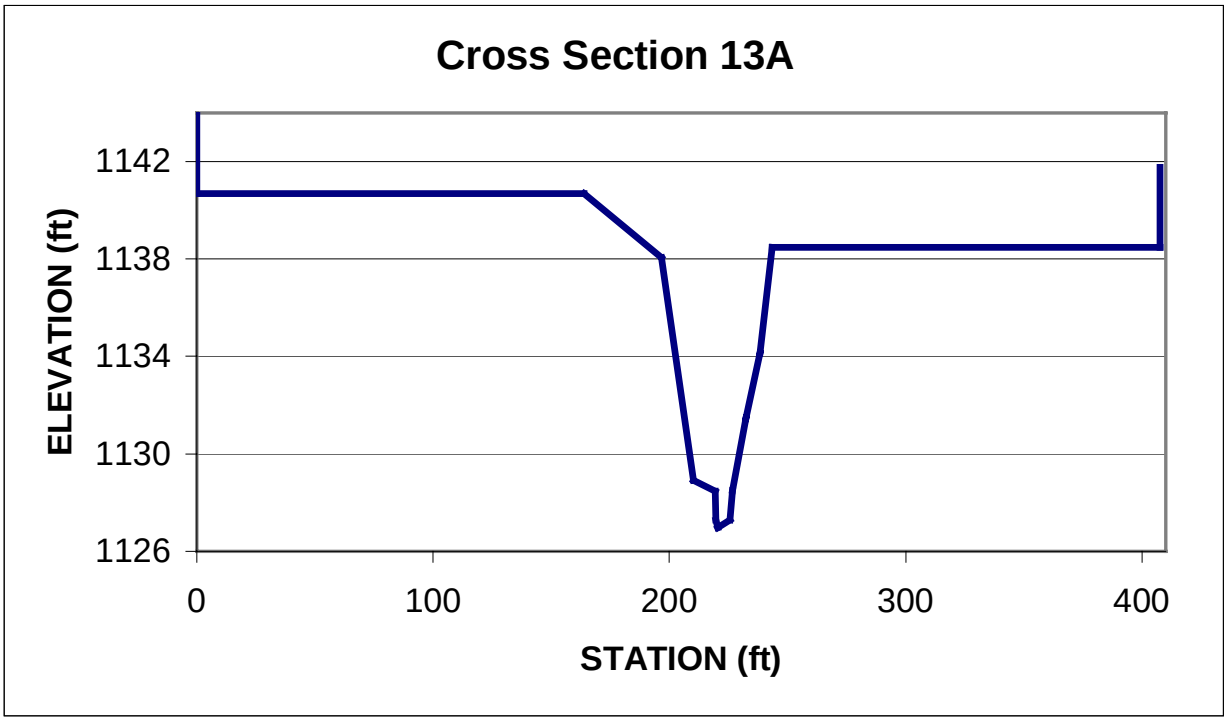

Figure I.44 Graph of surveyed cross section 13A downstream of Fort St 0.80 mi downstream of the upstream boundary of the modeling reach.

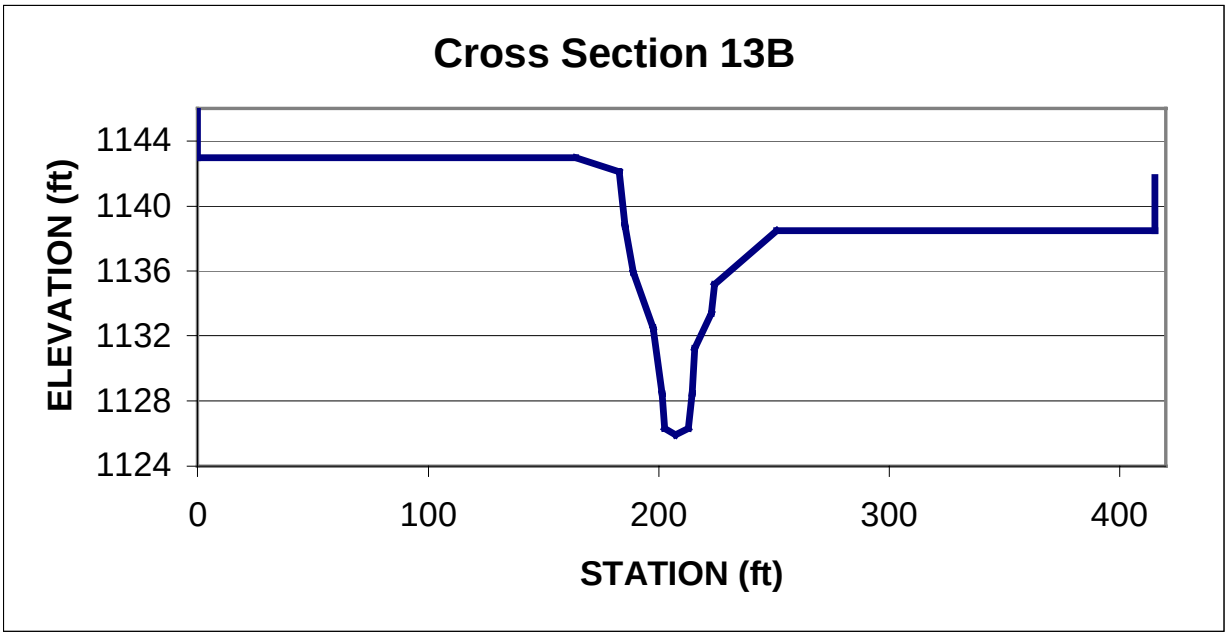

Figure I.45 Graph of surveyed cross section 13B downstream of Fort St 0.82 mi downstream of the upstream boundary of the modeling reach.

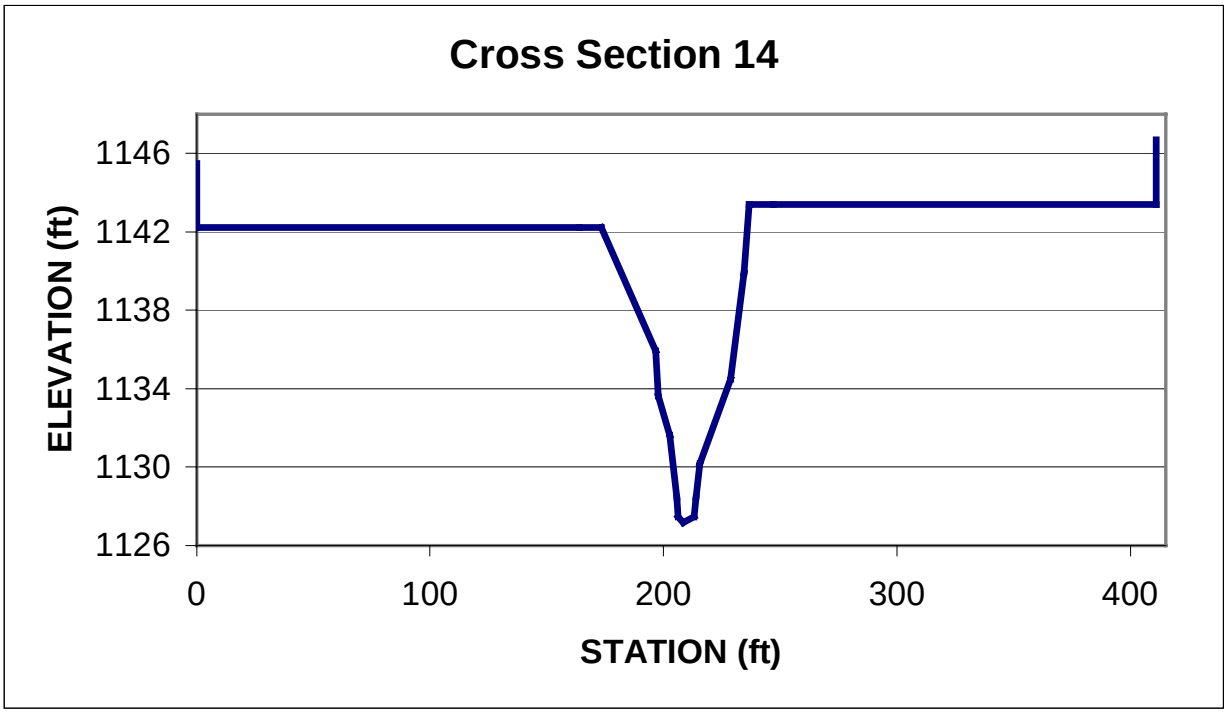

Figure I.46 Graph of surveyed cross section 14 downstream of Fort St 0.83 mi downstream of the upstream boundary of the modeling reach.

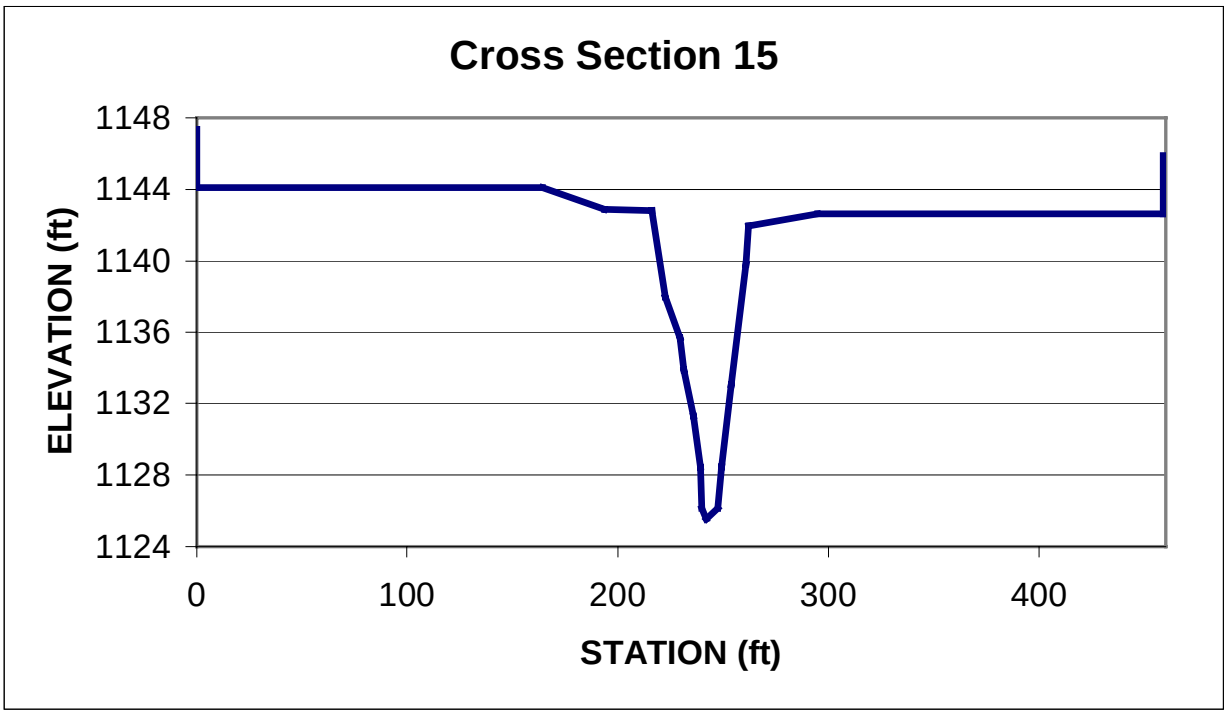

Figure I.47 Graph of surveyed cross section 15 downstream of Fort St 0.85 mi downstream of the upstream boundary of the modeling reach.

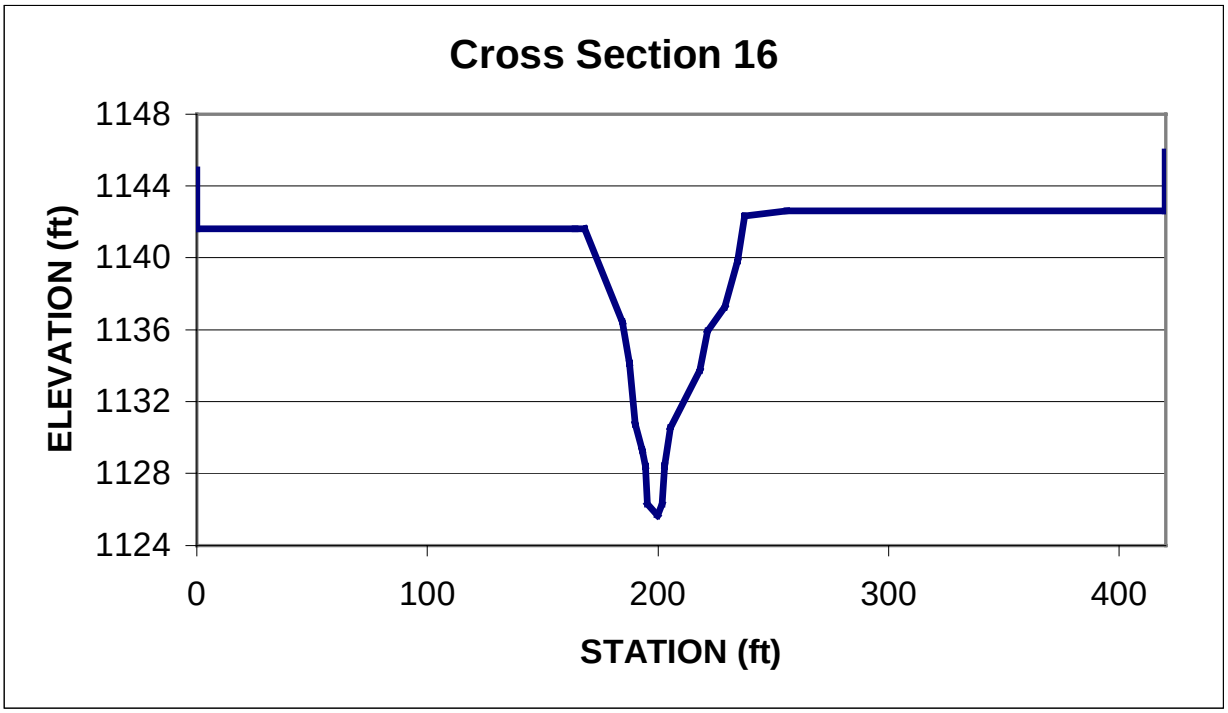

Figure I.48 Graph of surveyed cross section 16 downstream of Fort St 0.87 mi downstream of the upstream boundary of the modeling reach.

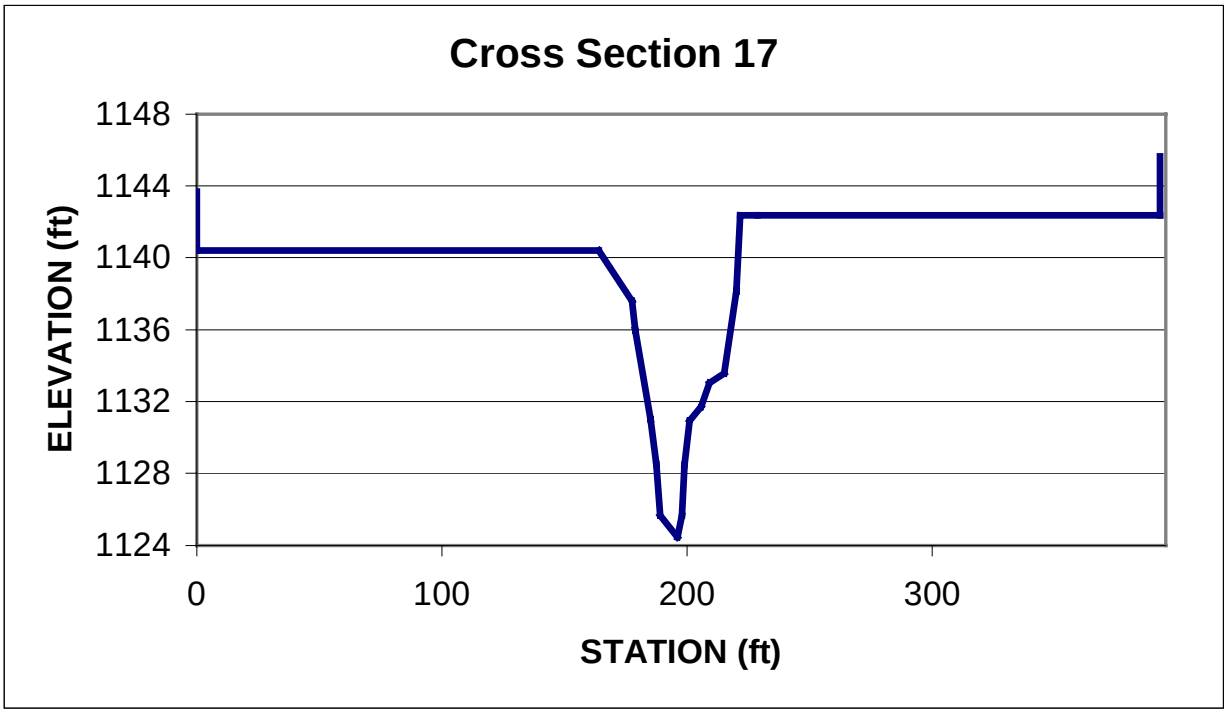

Figure I.49 Graph of surveyed cross section 17 downstream of Fort St 0.88 mi downstream of the upstream boundary of the modeling reach.

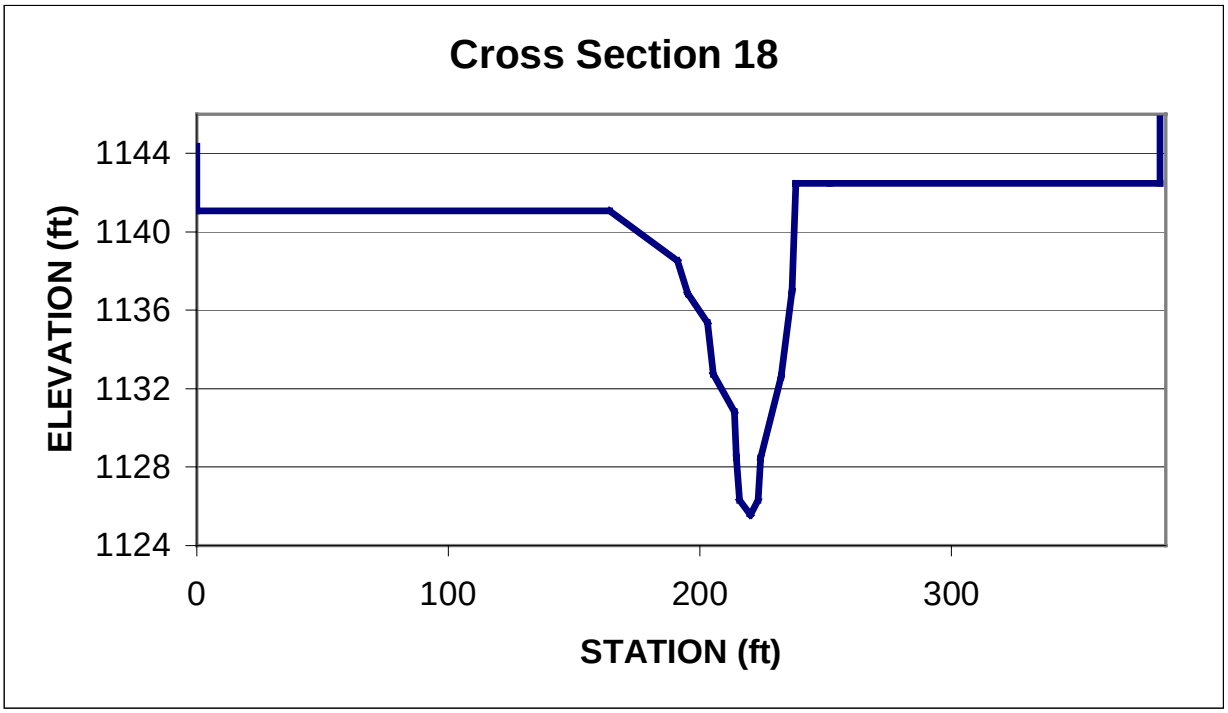

Figure I.50 Graph of surveyed cross section 18 downstream of Fort St 0.90 mi downstream of the upstream boundary of the modeling reach.

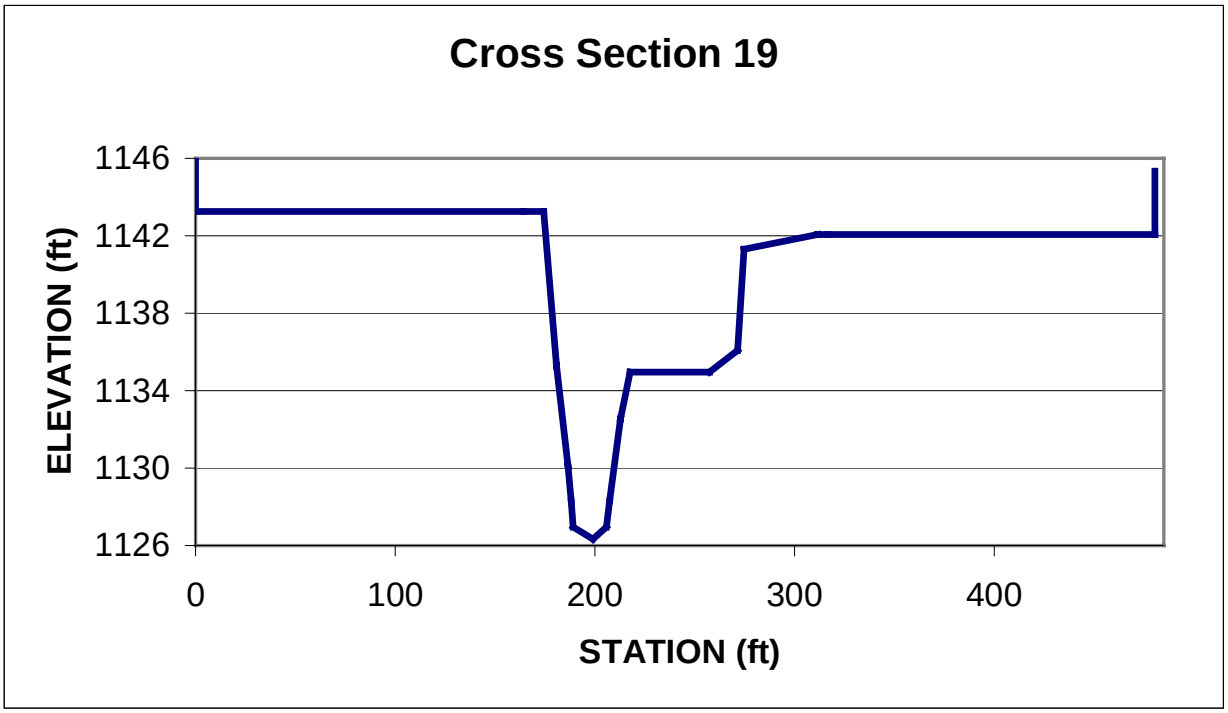

Figure I.51 Graph of surveyed cross section 19 downstream of Fort St 0.93 mi downstream of the upstream boundary of the modeling reach.

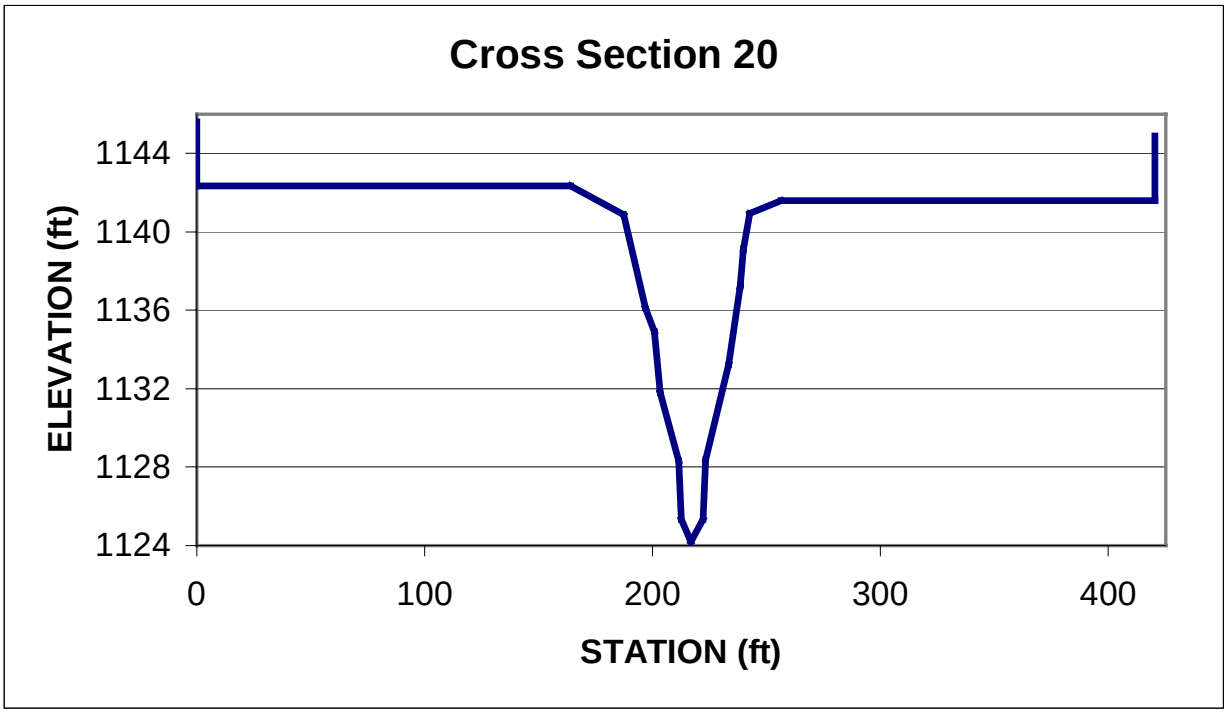

Figure I.52 Graph of surveyed cross section 20 downstream of Fort St 0.95 mi downstream of the upstream boundary of the modeling reach.

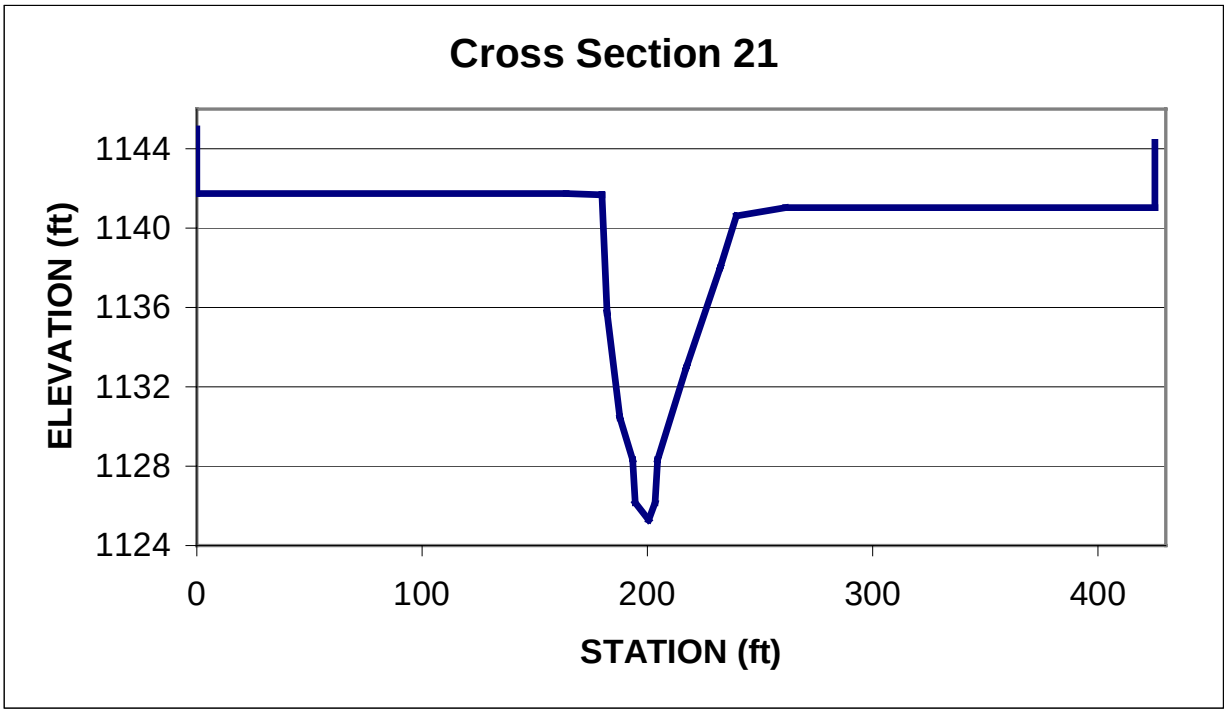

Figure I.53 Graph of surveyed cross section 21 downstream of Fort St 0.98 mi downstream of the upstream boundary of the modeling reach.

NORTH BRANCH WEST PAPILLION CREEK – CROSS SECTIONS SURVEYED NEAR 168TH STREET

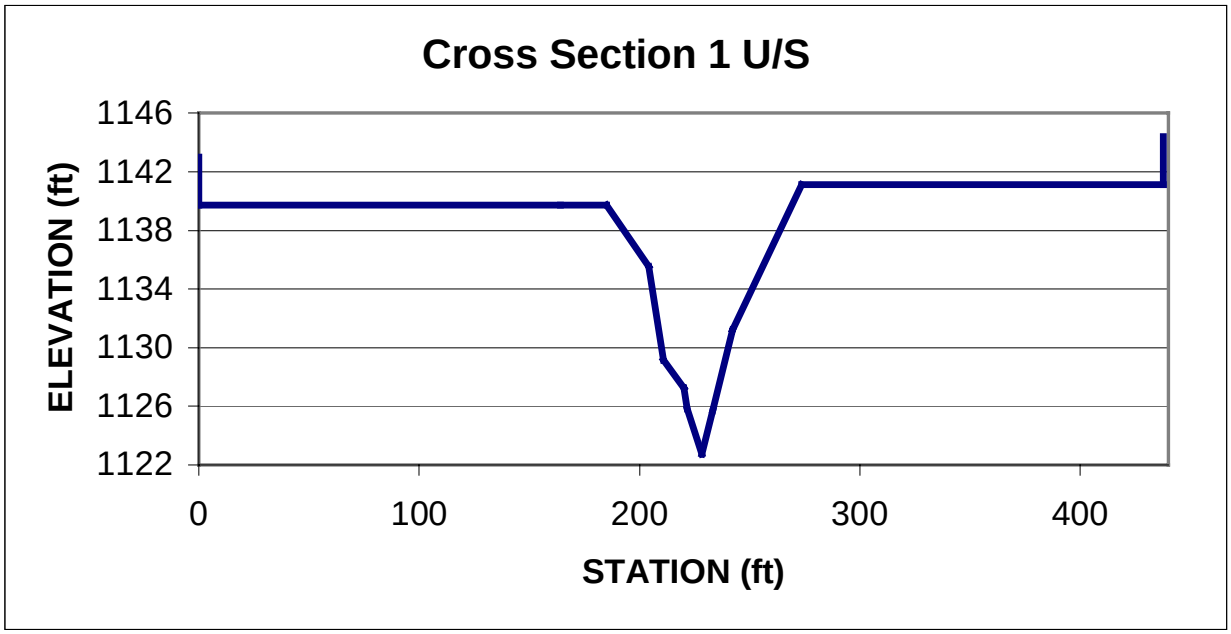

Figure I.54 Graph of surveyed cross section 1 upstream of 168th St 1.03 mi downstream of the upstream boundary of the modeling reach.

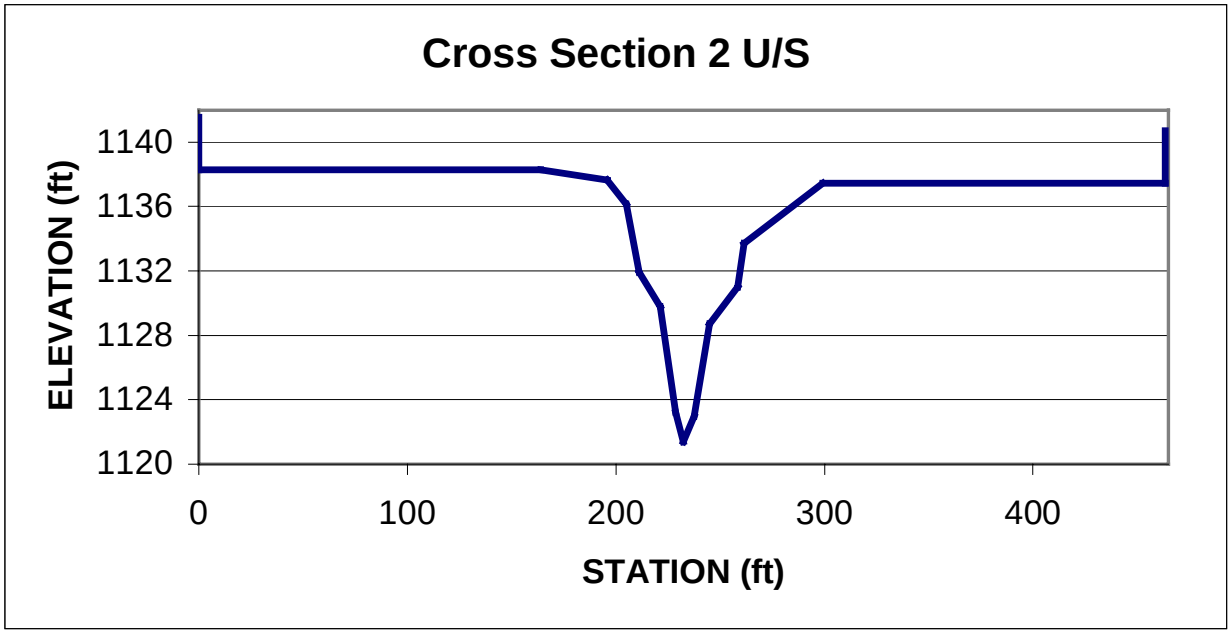

Figure I.55 Graph of surveyed cross section 2 upstream of 168th St 1.37 mi downstream of the upstream boundary of the modeling reach.

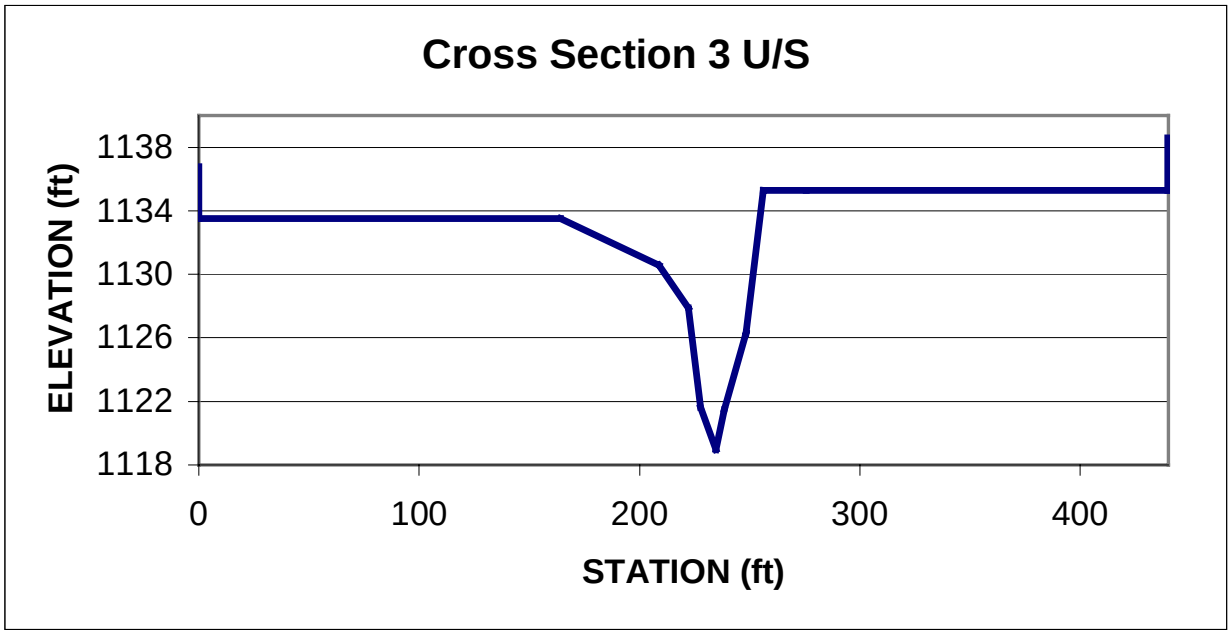

Figure I.56 Graph of surveyed cross section 3 upstream of 168th St 1.53 mi downstream of the upstream boundary of the modeling reach.

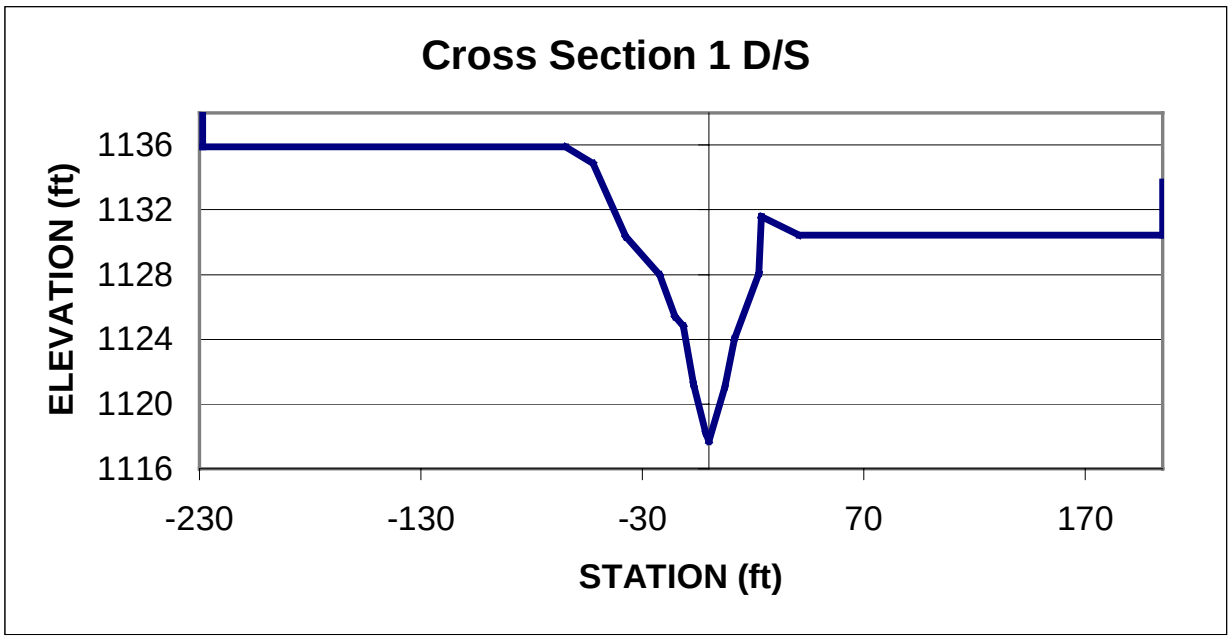

Figure I.57 Graph of surveyed cross section 1 downstream of 168th St 1.77 mi downstream of the upstream boundary of the modeling reach.

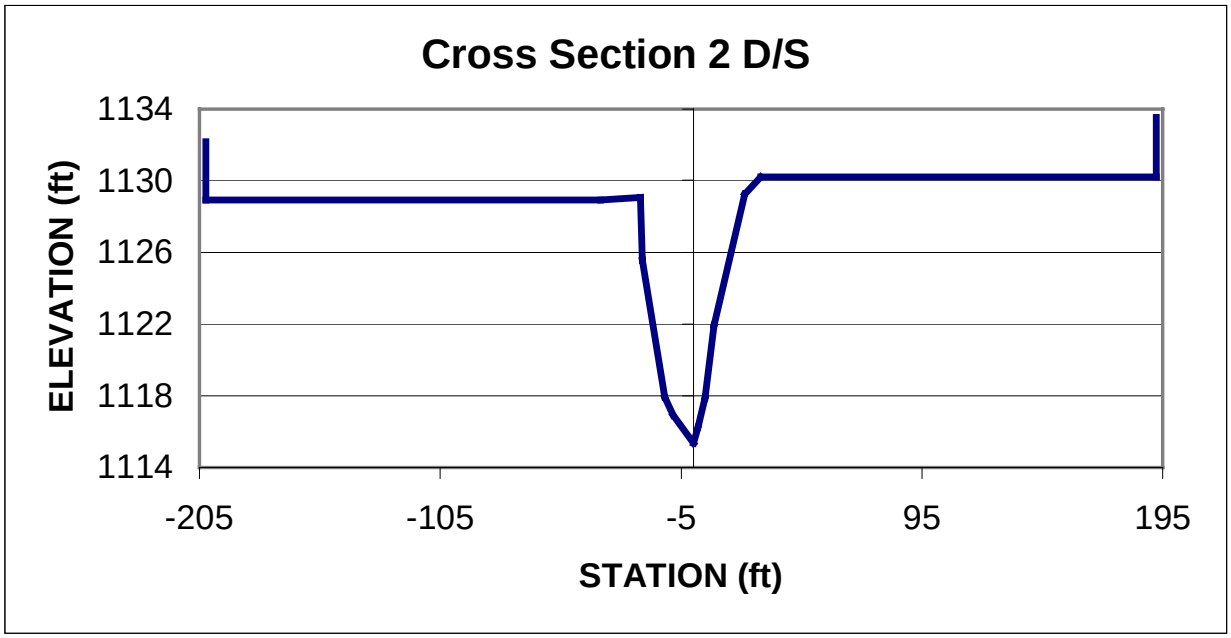

Figure I.58 Graph of surveyed cross section 2 downstream of 168th St 2.00 mi downstream of the upstream boundary of the modeling reach.

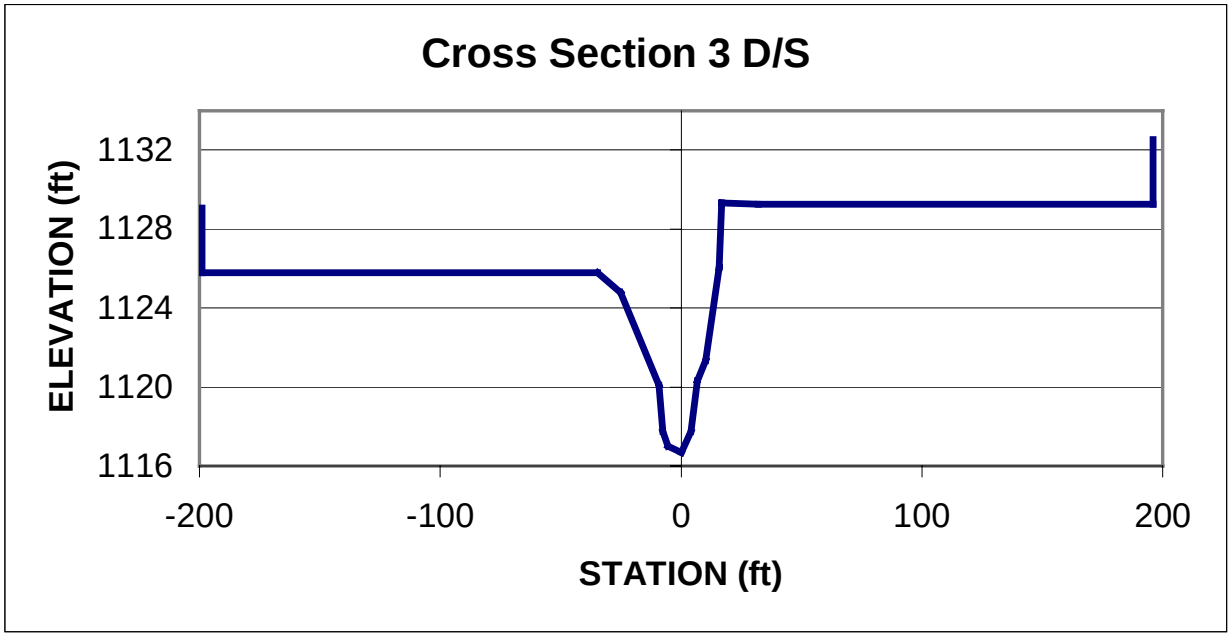

Figure I.59 Graph of surveyed cross section 3 downstream of 168th St 2.02 mi downstream of the upstream boundary of the modeling reach.

NORTH BRANCH WEST PAPILLION CREEK – CROSS SECTIONS SURVEYED DOWNSTREAM OF BLONDO ST

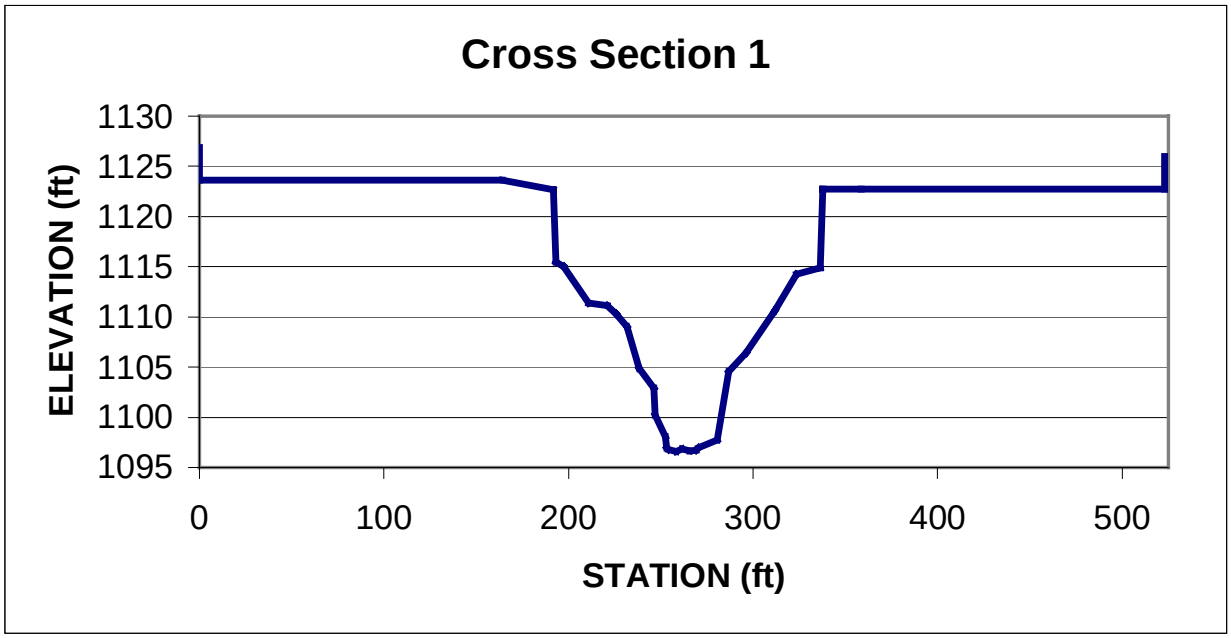

Figure I.60 Graph of surveyed cross section 1 downstream of Blondo St 3.55 mi downstream of the upstream boundary of the modeling reach.

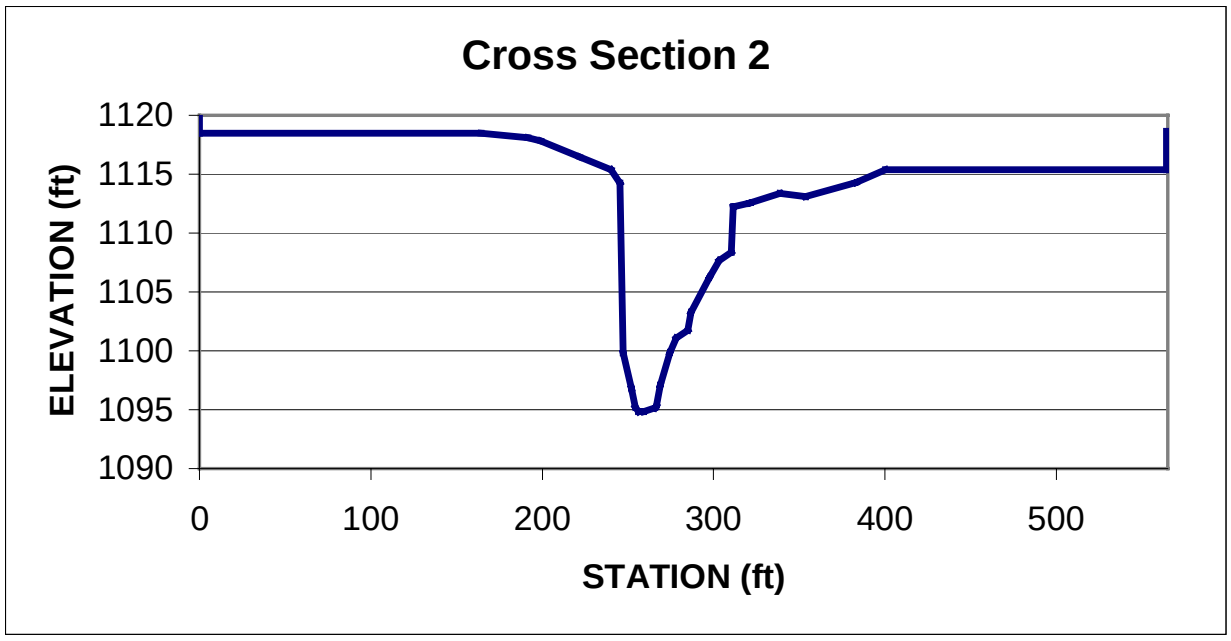

Figure I.61 Graph of surveyed cross section 2 downstream of Blondo St 3.58 mi downstream of the upstream boundary of the modeling reach.

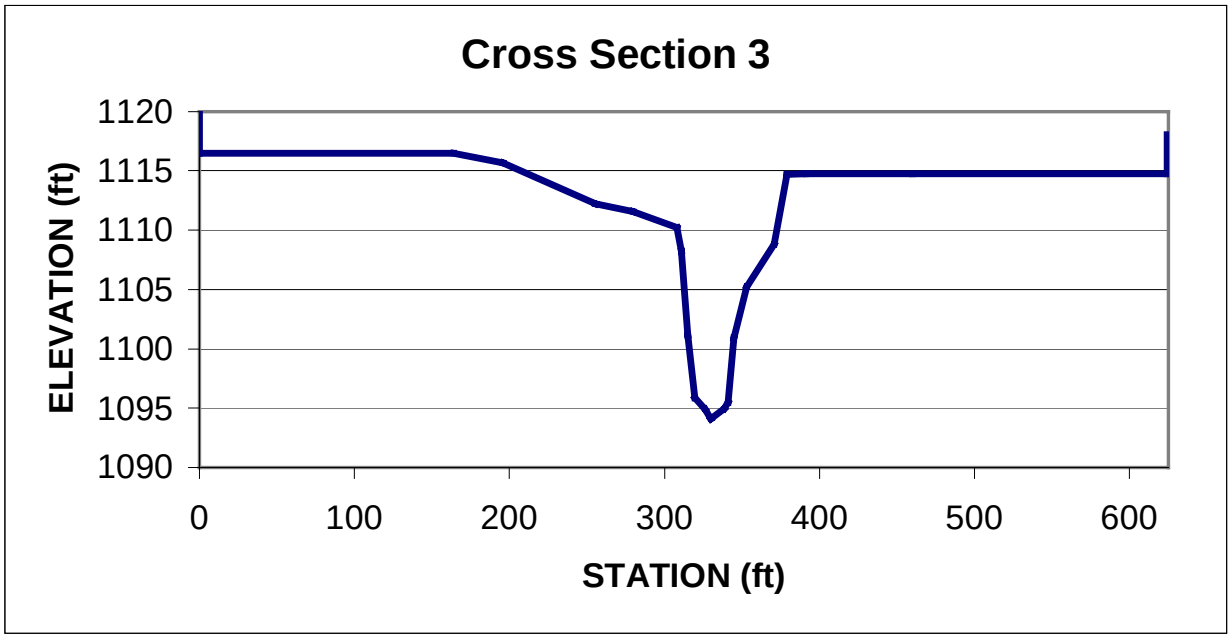

Figure I.62 Graph of surveyed cross section 3 downstream of Blondo St 3.62 mi downstream of the upstream boundary of the modeling reach.

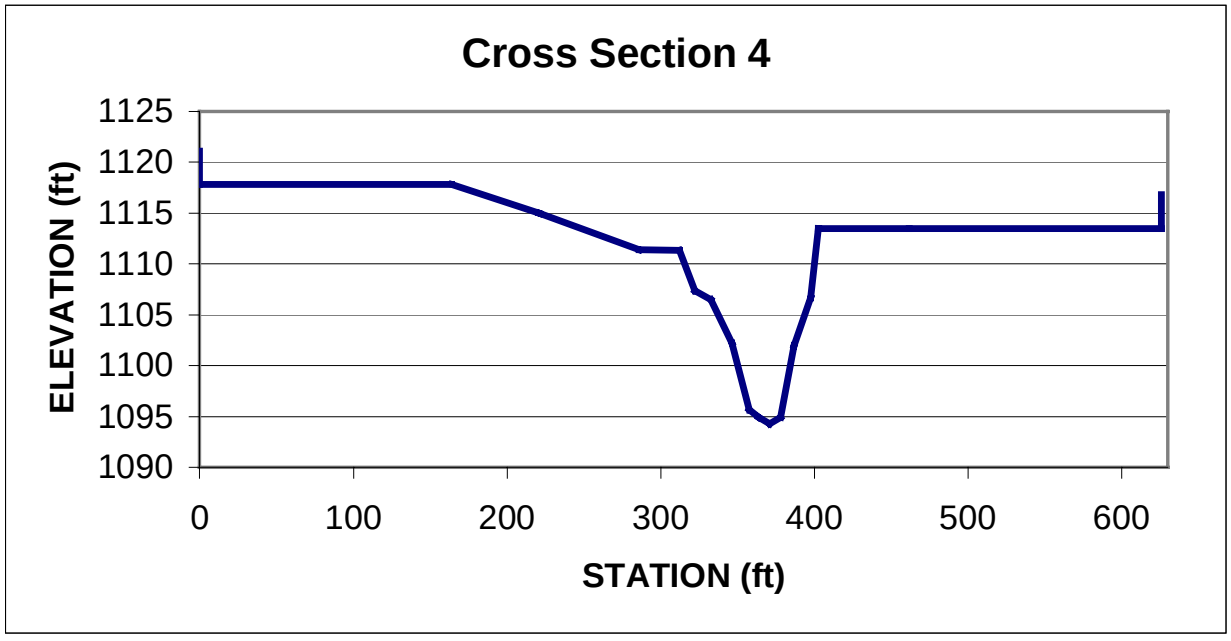

Figure I.63 Graph of surveyed cross section 4 downstream of Blondo St 3.64 mi downstream of the upstream boundary of the modeling reach.

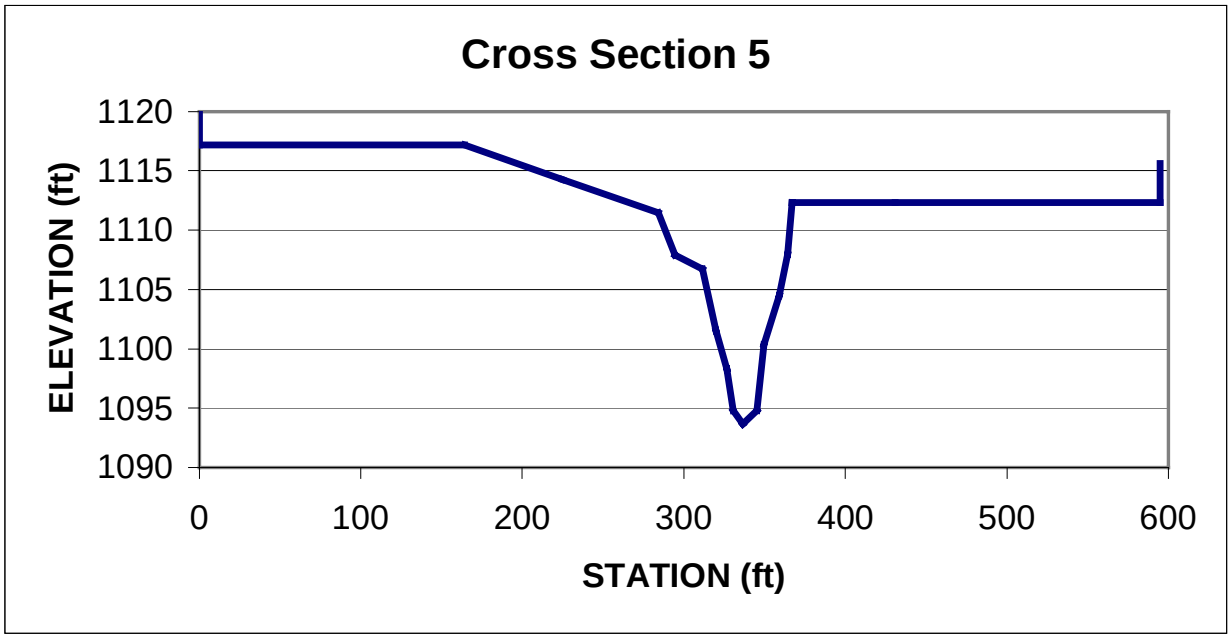

Figure I.64 Graph of surveyed cross section 5 downstream of Blondo St 3.67 mi downstream of the upstream boundary of the modeling reach.

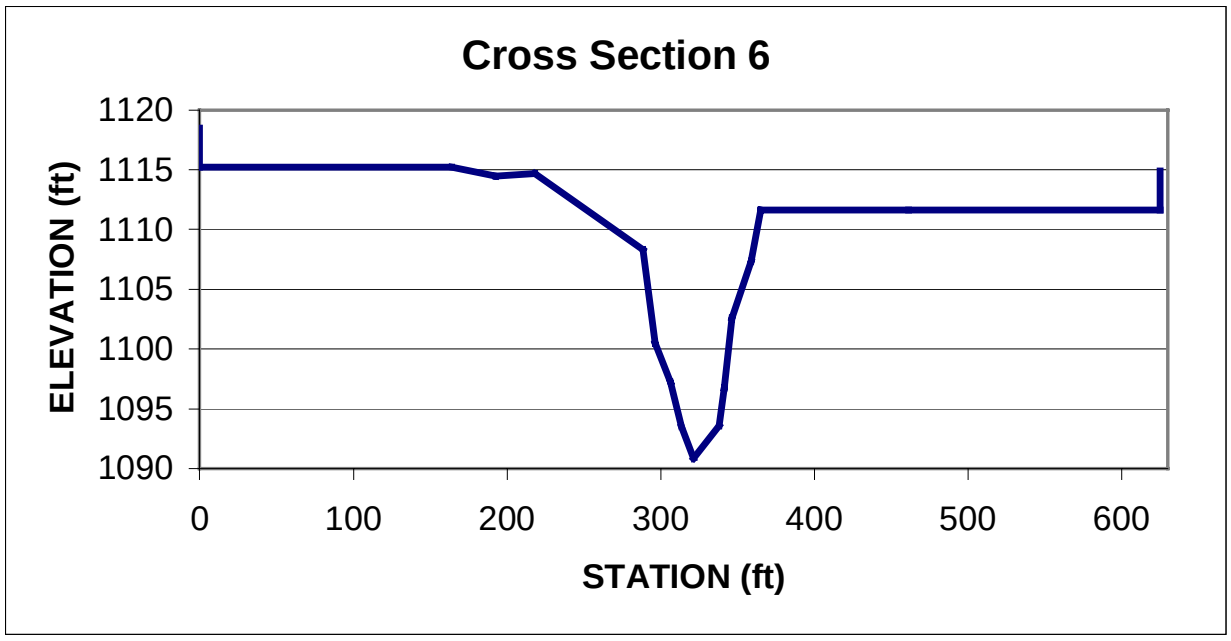

Figure I.65 Graph of surveyed cross section 6 downstream of Blondo St 3.71 mi downstream of the upstream boundary of the modeling reach.

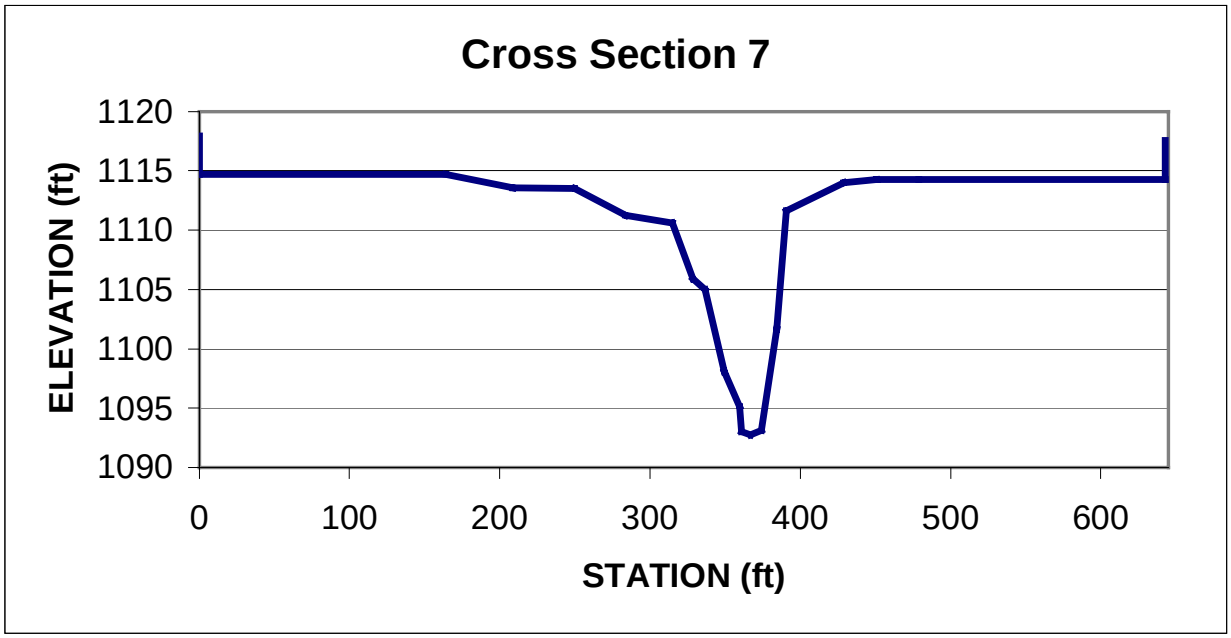

Figure I.66 Graph of surveyed cross section 7 downstream of Blondo St 3.74 mi downstream of the upstream boundary of the modeling reach.

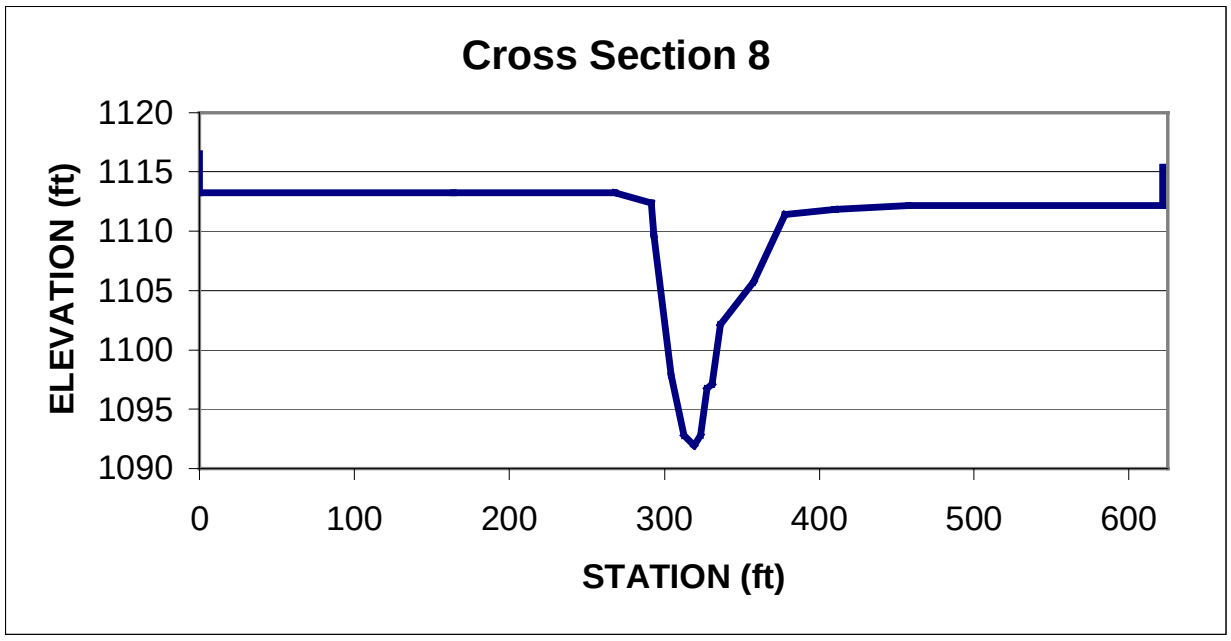

Figure I.67 Graph of surveyed cross section 8 downstream of Blondo St 3.79 mi downstream of the upstream boundary of the modeling reach.

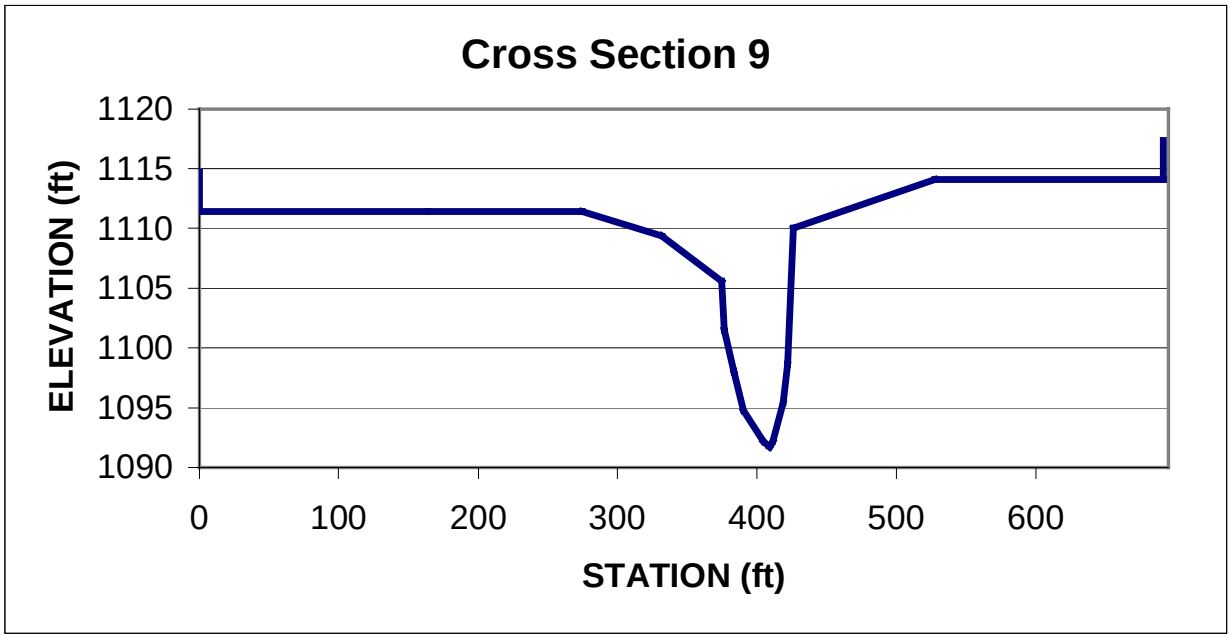

Figure I.68 Graph of surveyed cross section 9 downstream of Blondo St 3.85 mi downstream of the upstream boundary of the modeling reach.

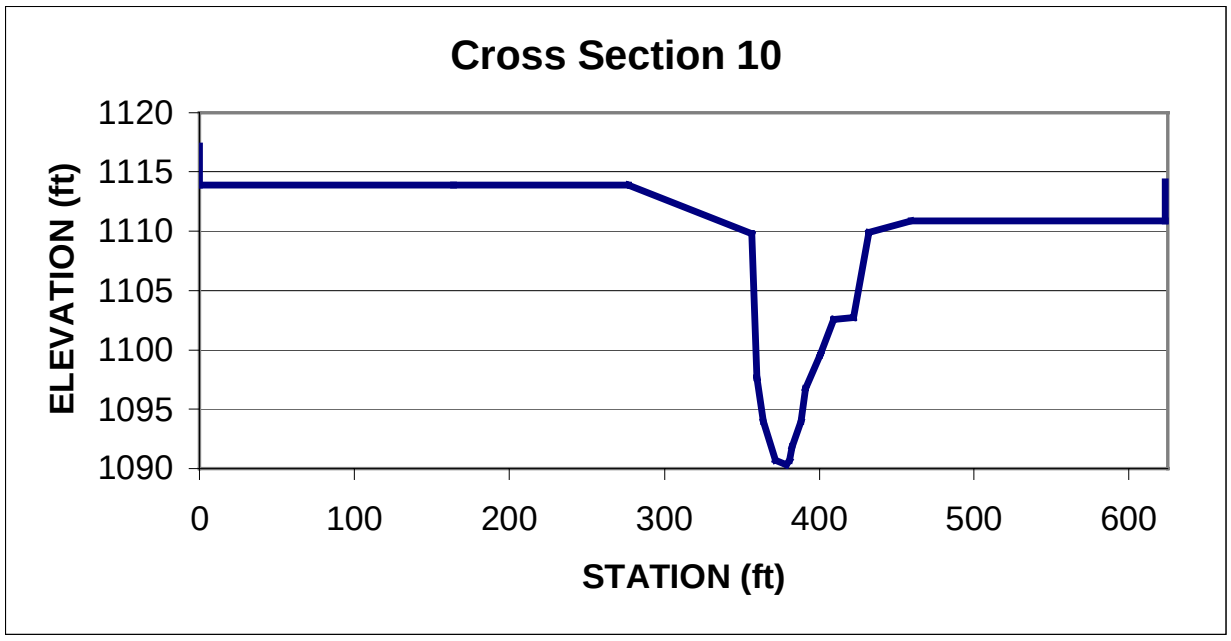

Figure I.69 Graph of surveyed cross section 10 downstream of Blondo St 3.89 mi downstream of the upstream boundary of the modeling reach.

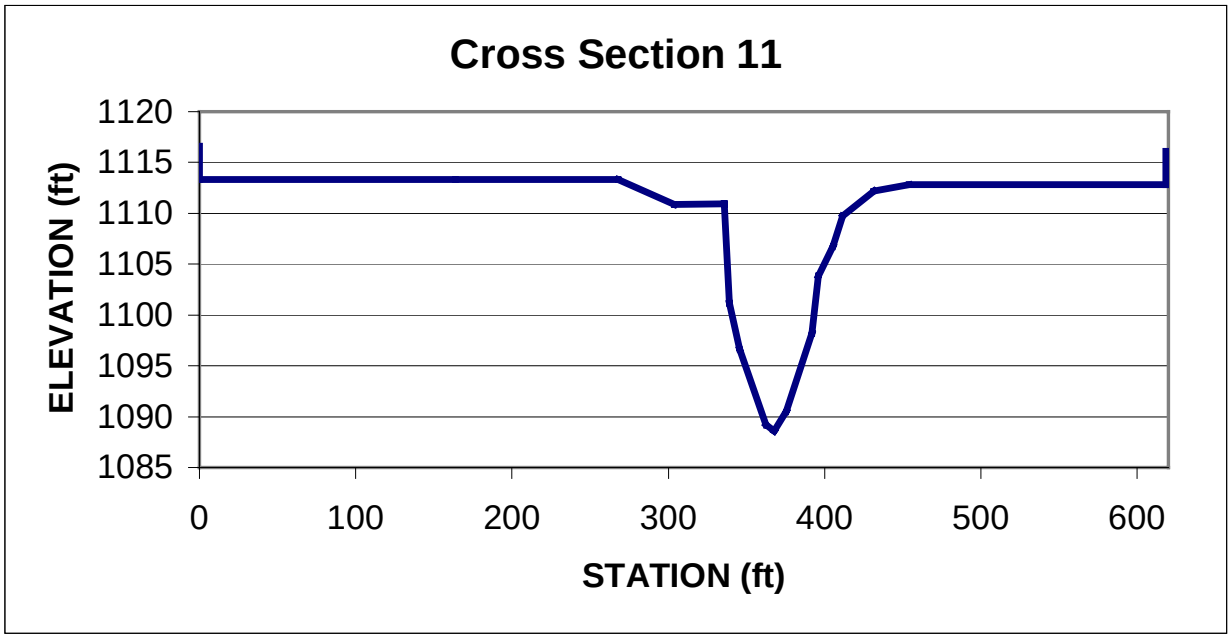

Figure I.70 Graph of surveyed cross section 11 downstream of Blondo St 3.92 mi downstream of the upstream boundary of the modeling reach.

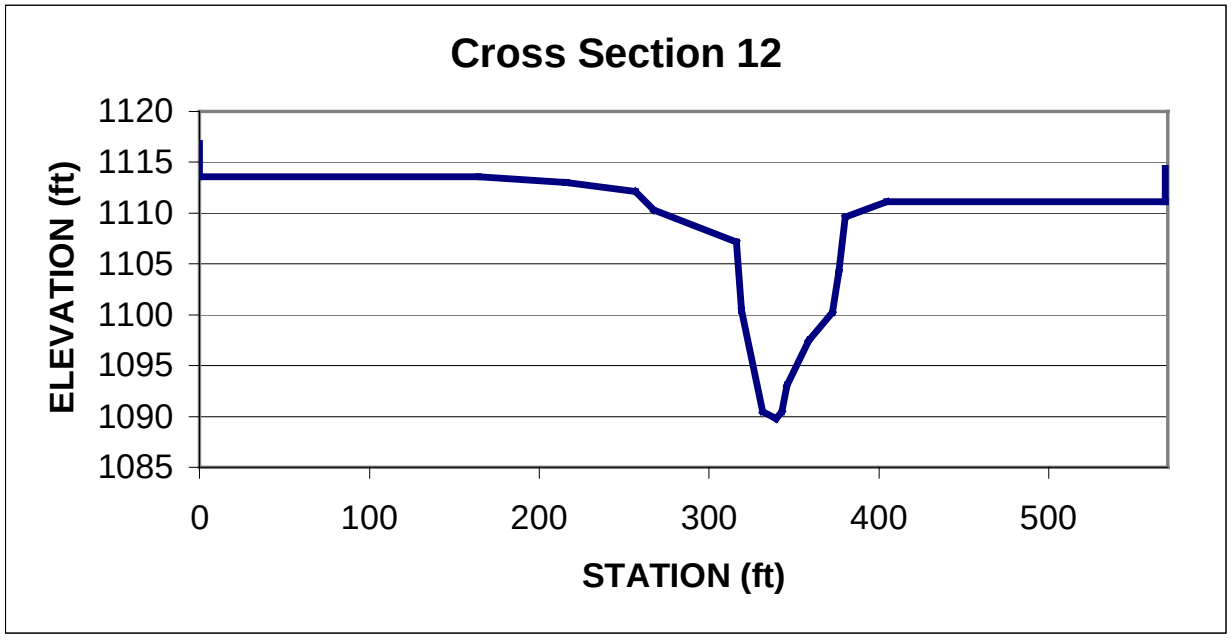

Figure I.71 Graph of surveyed cross section 12 downstream of Blondo St 3.94 mi downstream of the upstream boundary of the modeling reach.

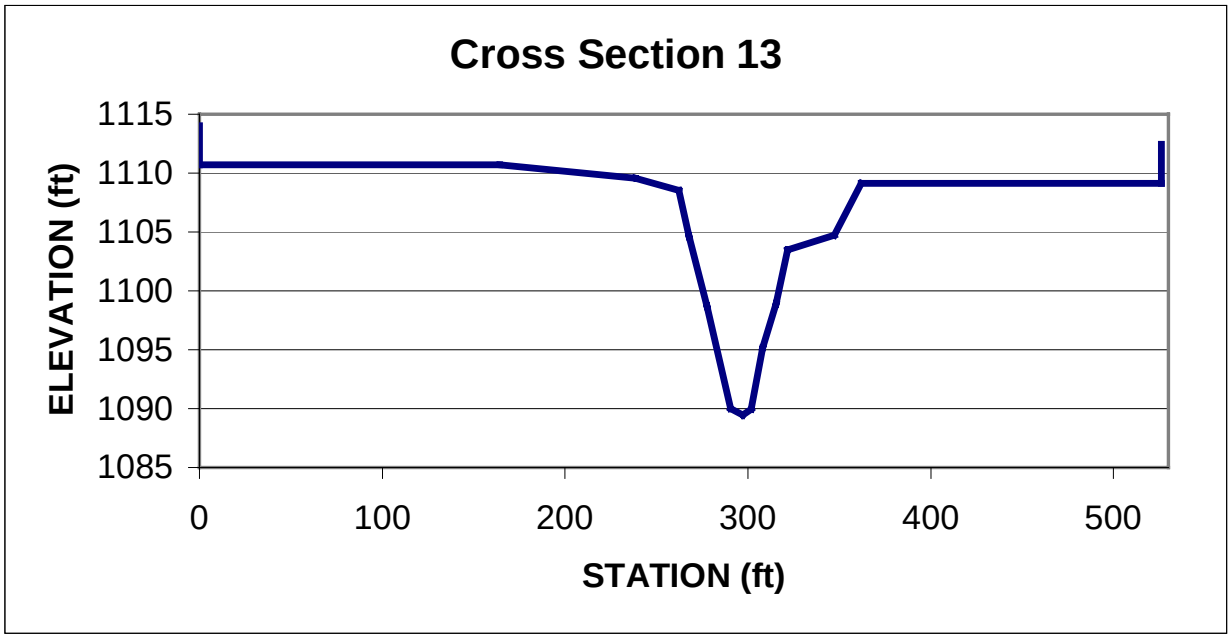

Figure I.72 Graph of surveyed cross section 13 downstream of Blondo St 4.02 mi downstream of the upstream boundary of the modeling reach.

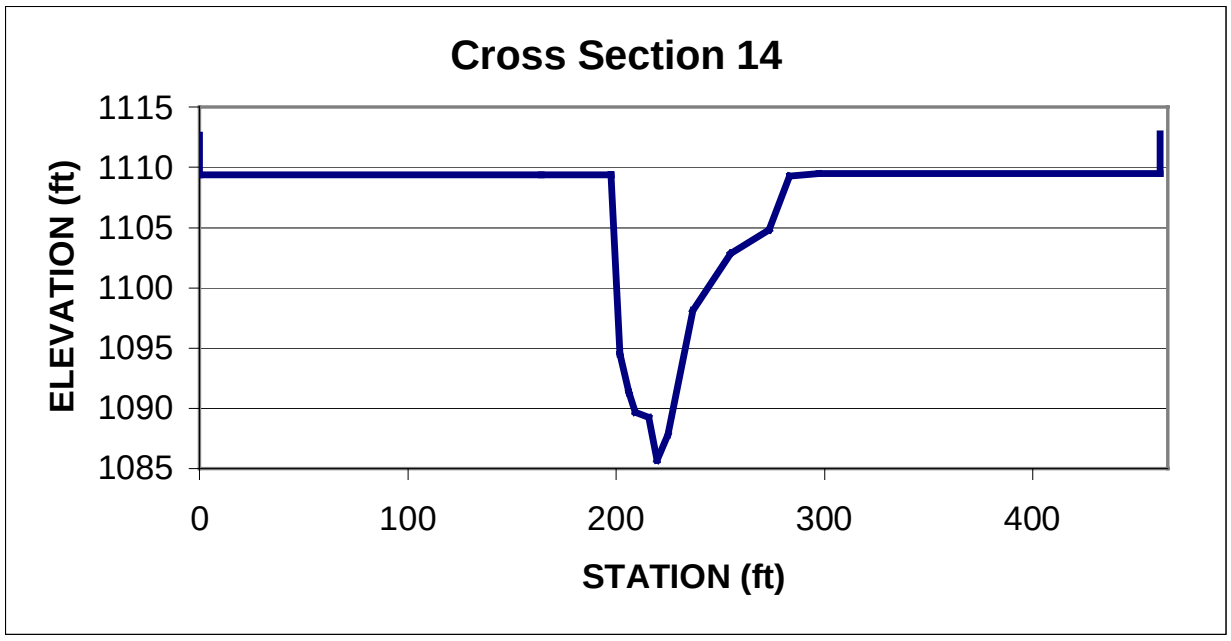

Figure I.73 Graph of surveyed cross section 14 downstream of Blondo St 4.04 mi downstream of the upstream boundary of the modeling reach.

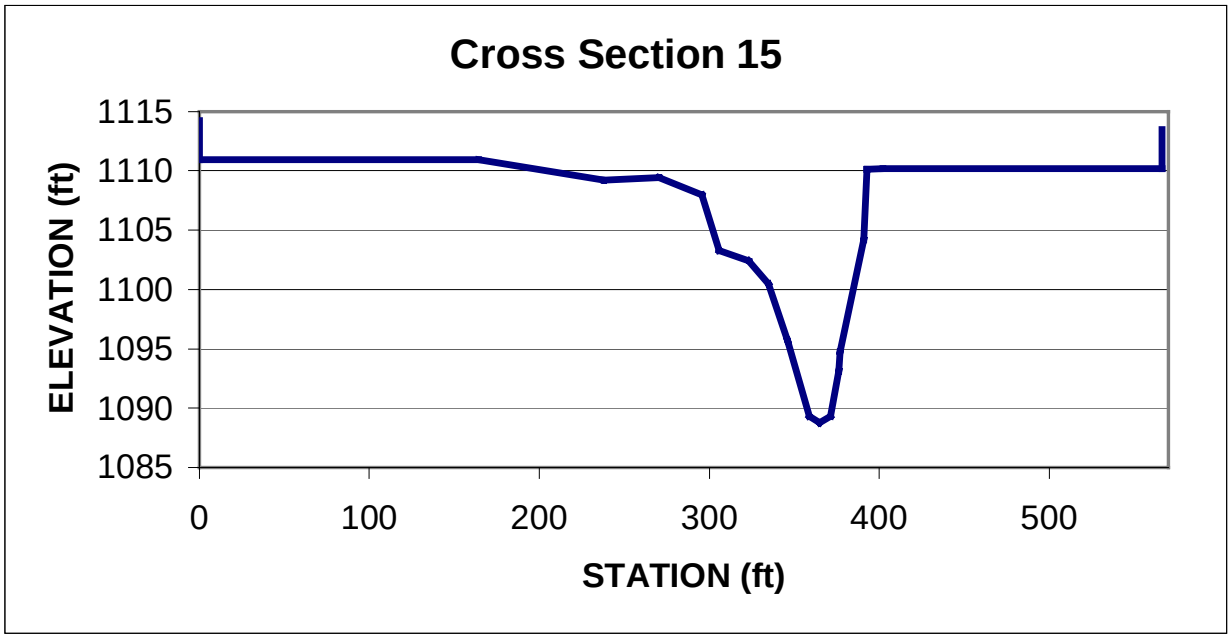

Figure I.74 Graph of surveyed cross section 15 downstream of Blondo St 4.10 mi downstream of the upstream boundary of the modeling reach.

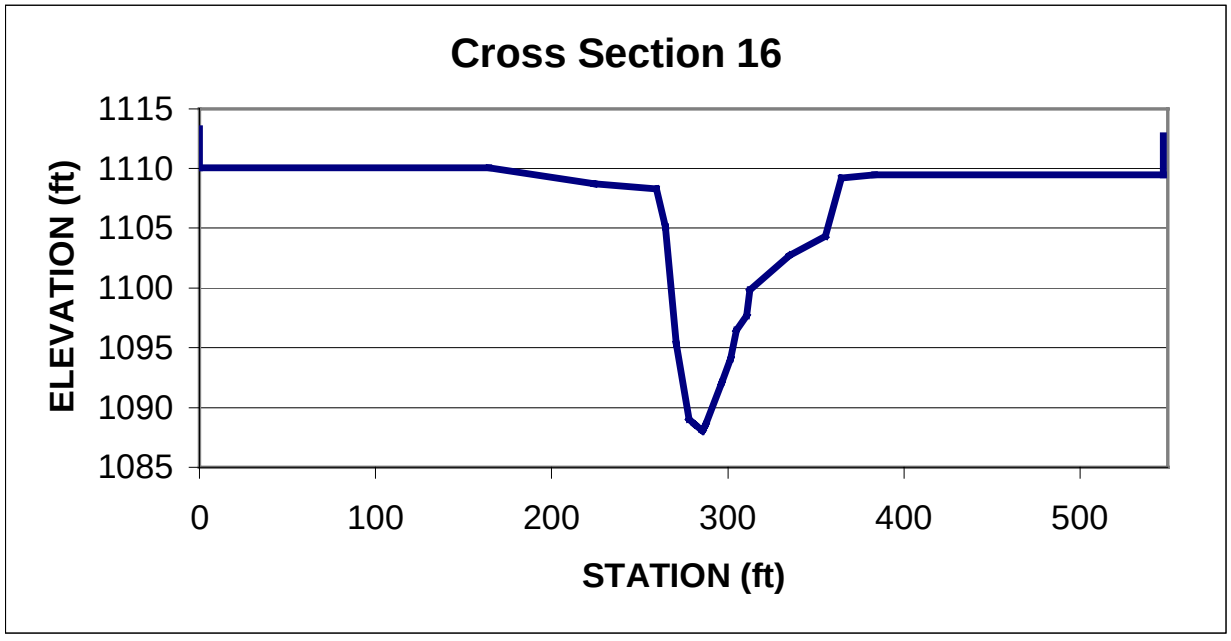

Figure I.75 Graph of surveyed cross section 16 downstream of Blondo St 4.13 mi downstream of the upstream boundary of the modeling reach.

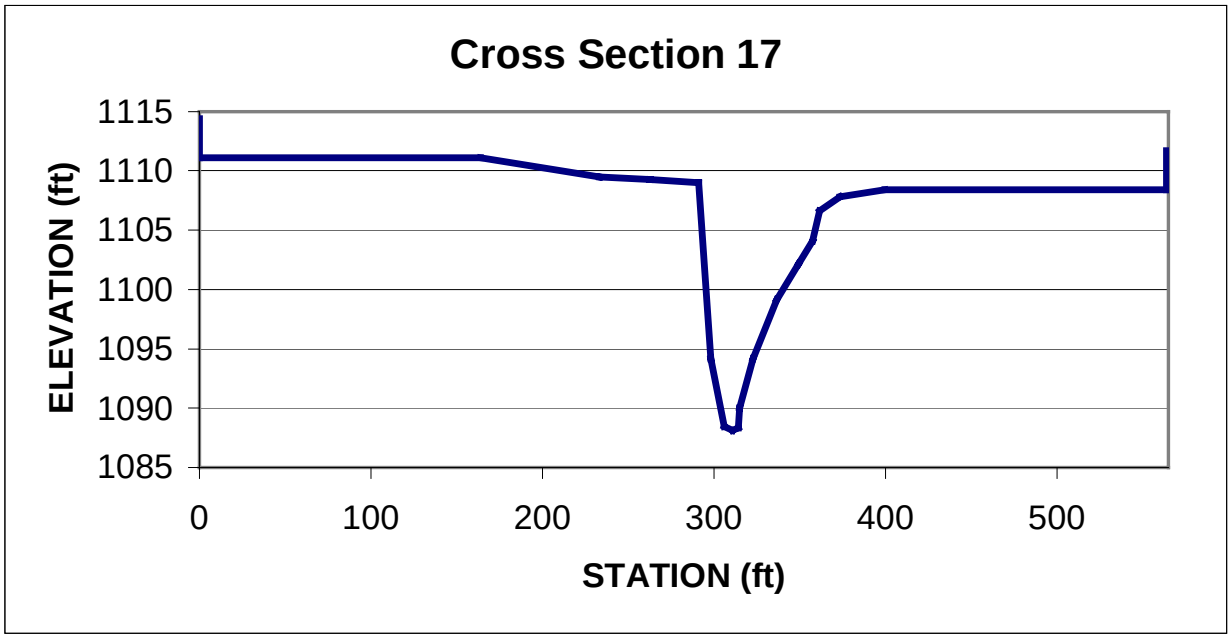

Figure I.76 Graph of surveyed cross section 17 downstream of Blondo St 4.16 mi downstream of the upstream boundary of the modeling reach.

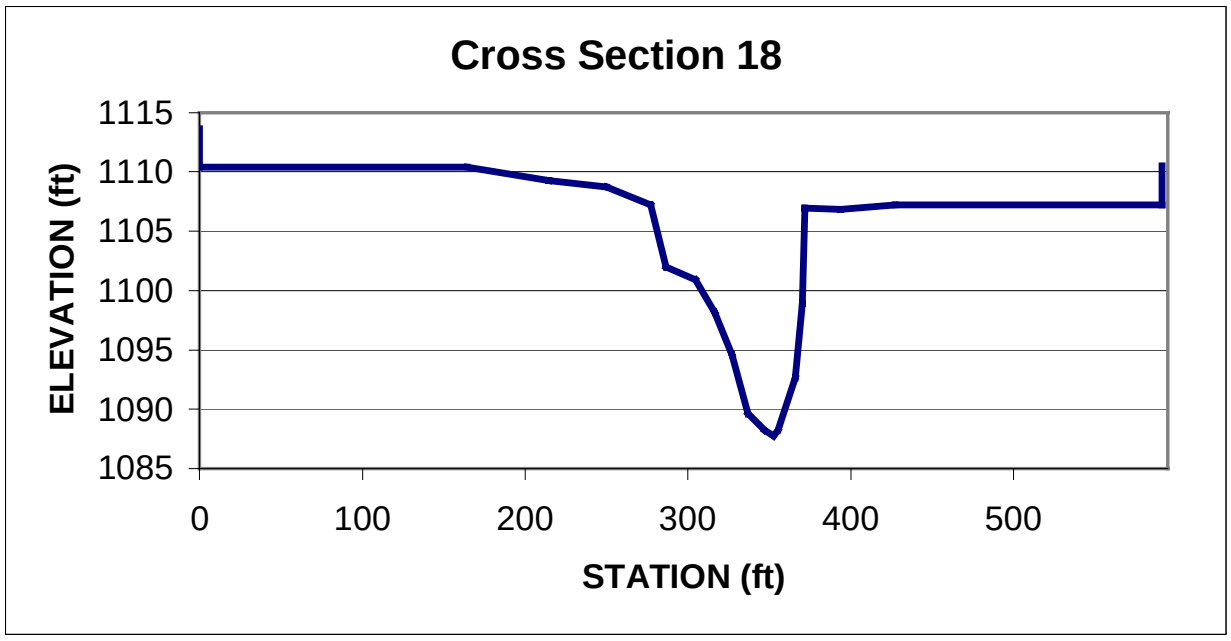

Figure I.77 Graph of surveyed cross section 18 downstream of Blondo St 4.18 mi downstream of the upstream boundary of the modeling reach.

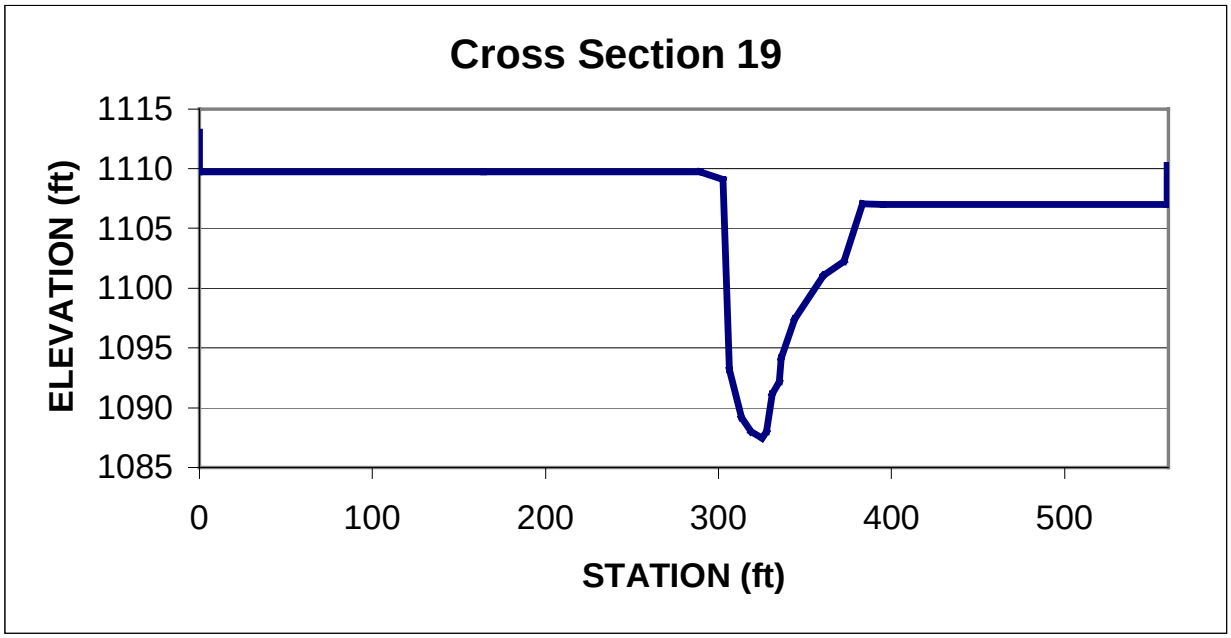

Figure I.78 Graph of surveyed cross section 19 downstream of Blondo St 4.21 mi downstream of the upstream boundary of the modeling reach.

WEST PAPILLION CREEK – CROSS SECTIONS SURVEYED DOWNSTREAM OF DODGE ST

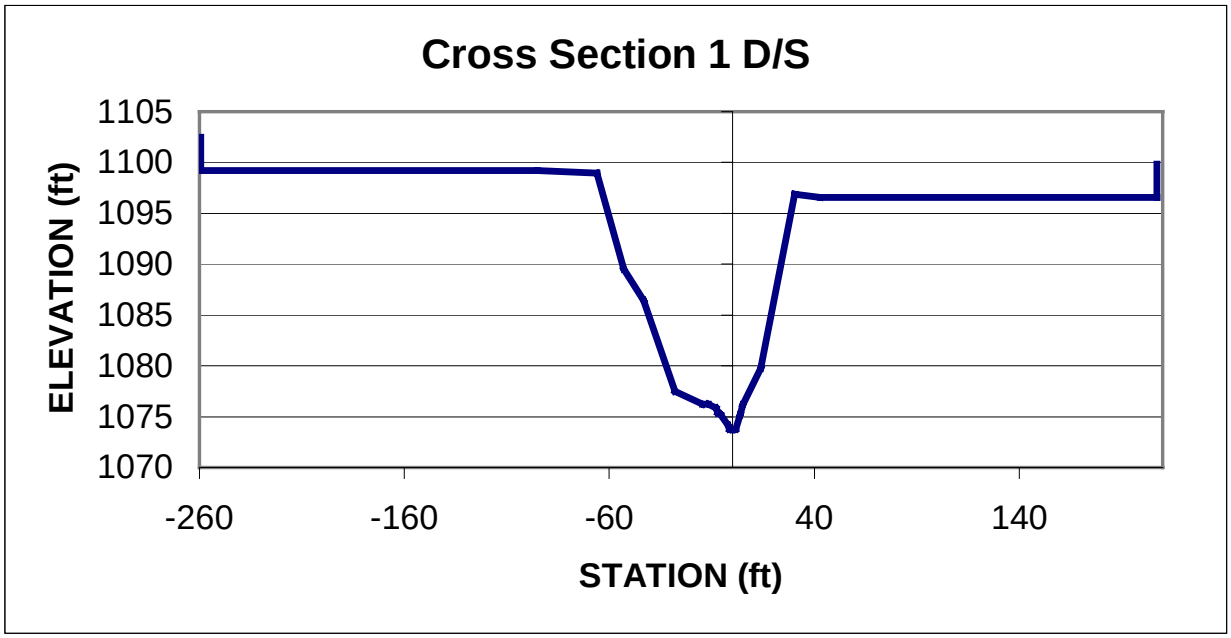

Figure I.79 Graph of surveyed cross section 1 downstream of Dodge St 5.40 mi downstream of the upstream boundary of the modeling reach.

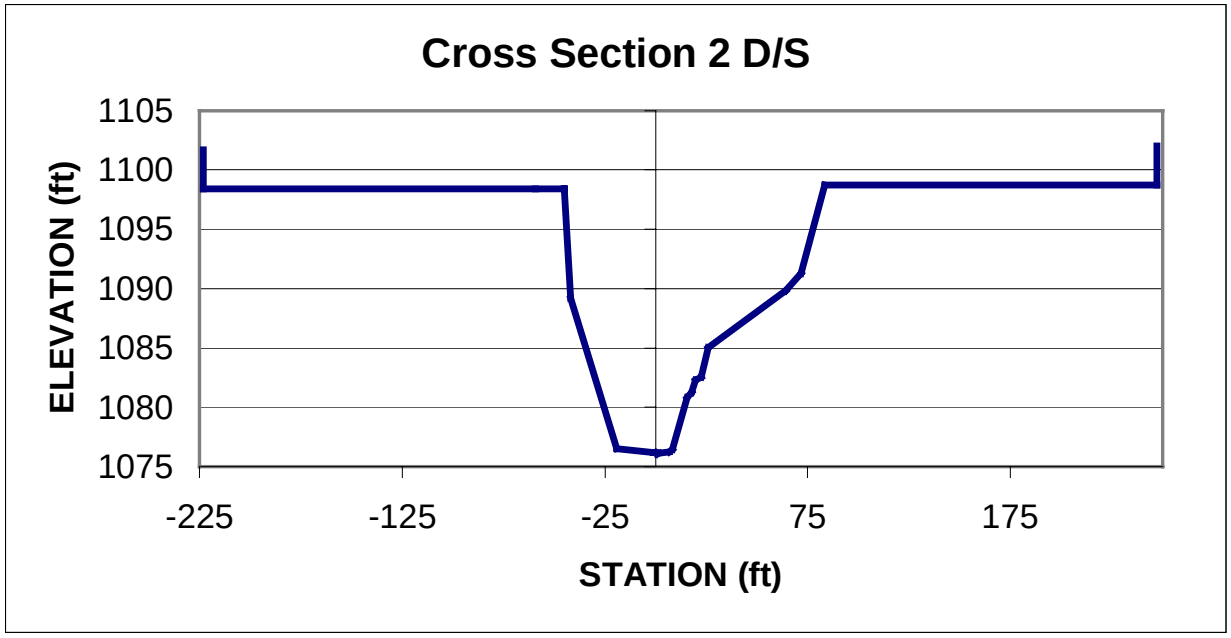

Figure I.80 Graph of surveyed cross section 2 downstream of Dodge St 5.47 mi downstream of the upstream boundary of the modeling reach.

WEST PAPILLION CREEK – CROSS SECTIONS SURVEYED UPSTREAM OF WEST CENTER STREET

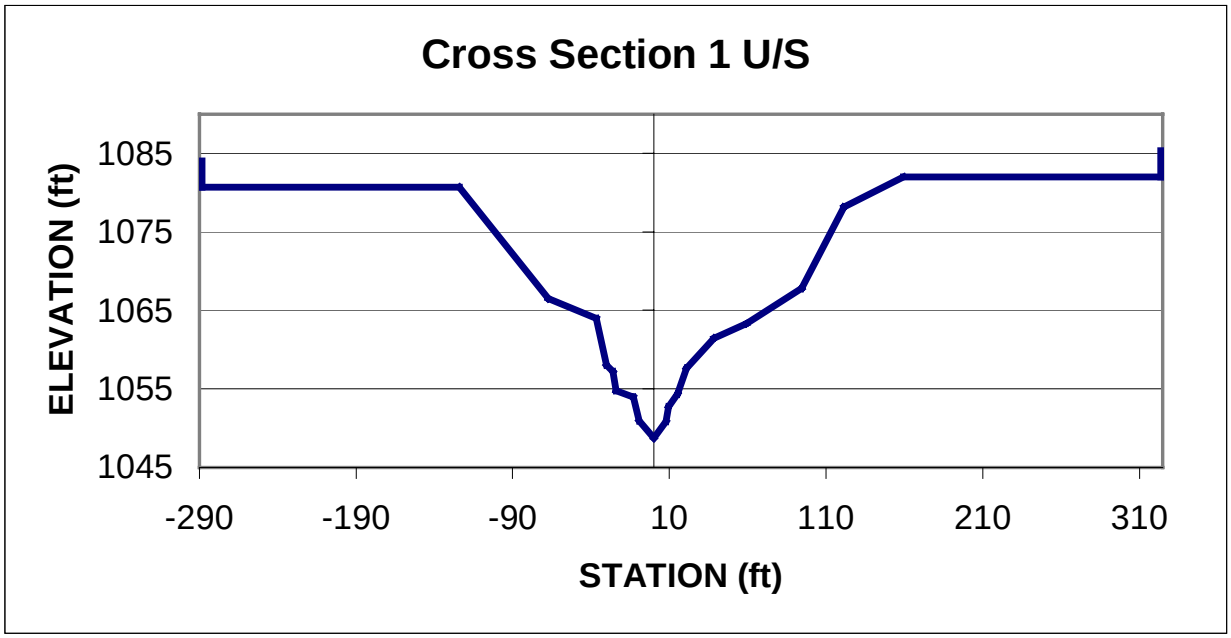

Figure I.81 Graph of surveyed cross section 1 upstream of W Center St 7.11 mi downstream of the upstream boundary of the modeling reach.

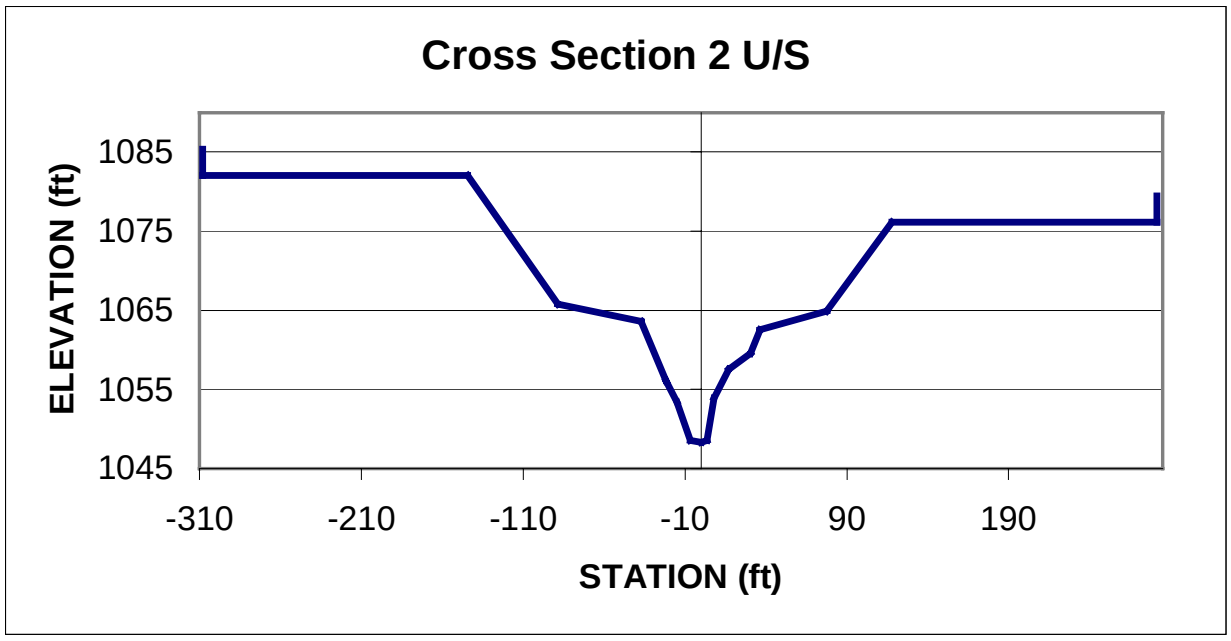

Figure I.82 Graph of surveyed cross section 2 upstream of W Center St 7.19 mi downstream of the upstream boundary of the modeling reach.

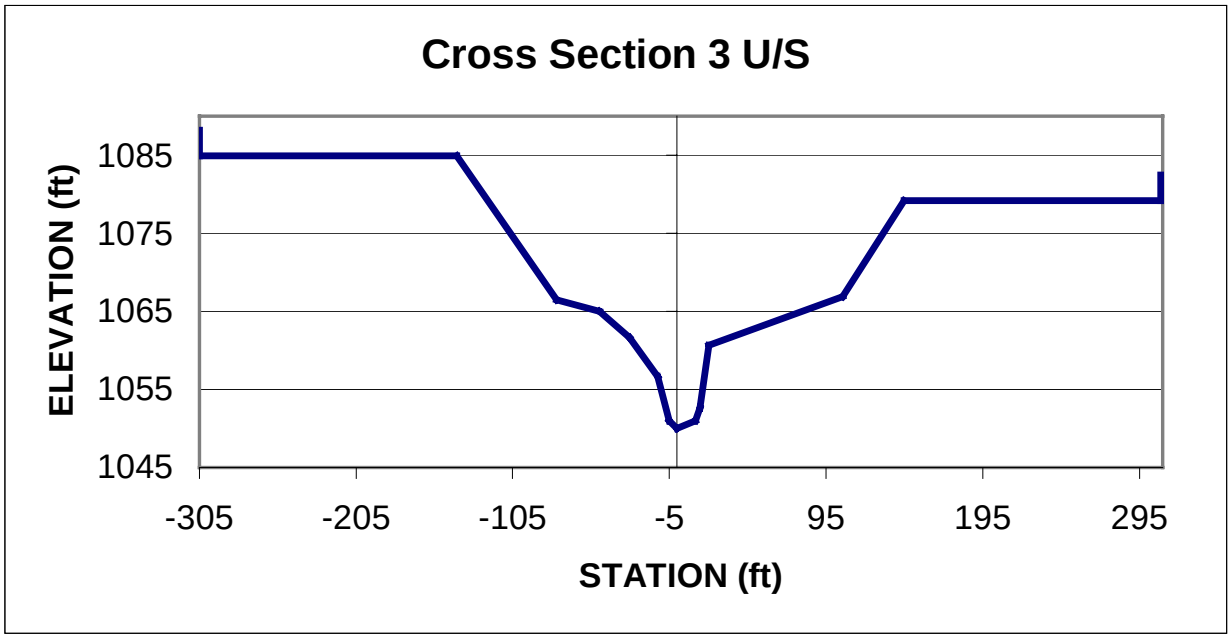

Figure I.83 Graph of surveyed cross section 3 upstream of W Center St 7.26 mi downstream of the upstream boundary of the modeling reach.

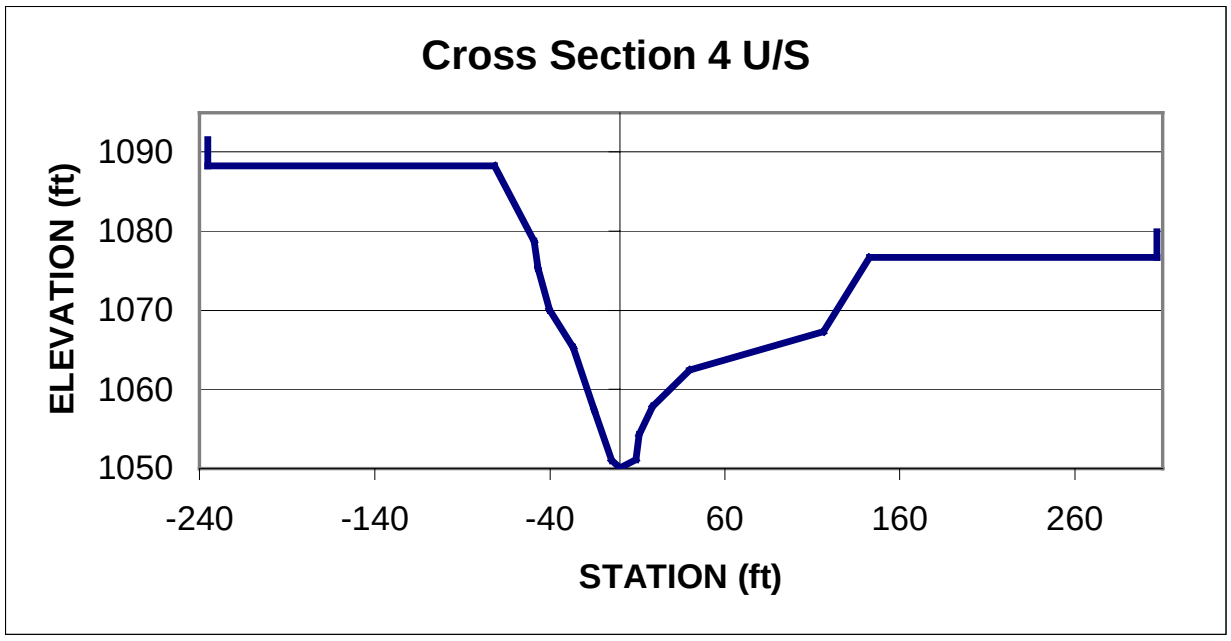

Figure I.84 Graph of surveyed cross section 4 upstream of W Center St 7.31 mi downstream of the upstream boundary of the modeling reach.

APPENDIX II DISCHARGE HYDROGRAPHS

THE LITTLE SALT CREEK – UPSTREAM BOUNDARY OF MODELING REACH

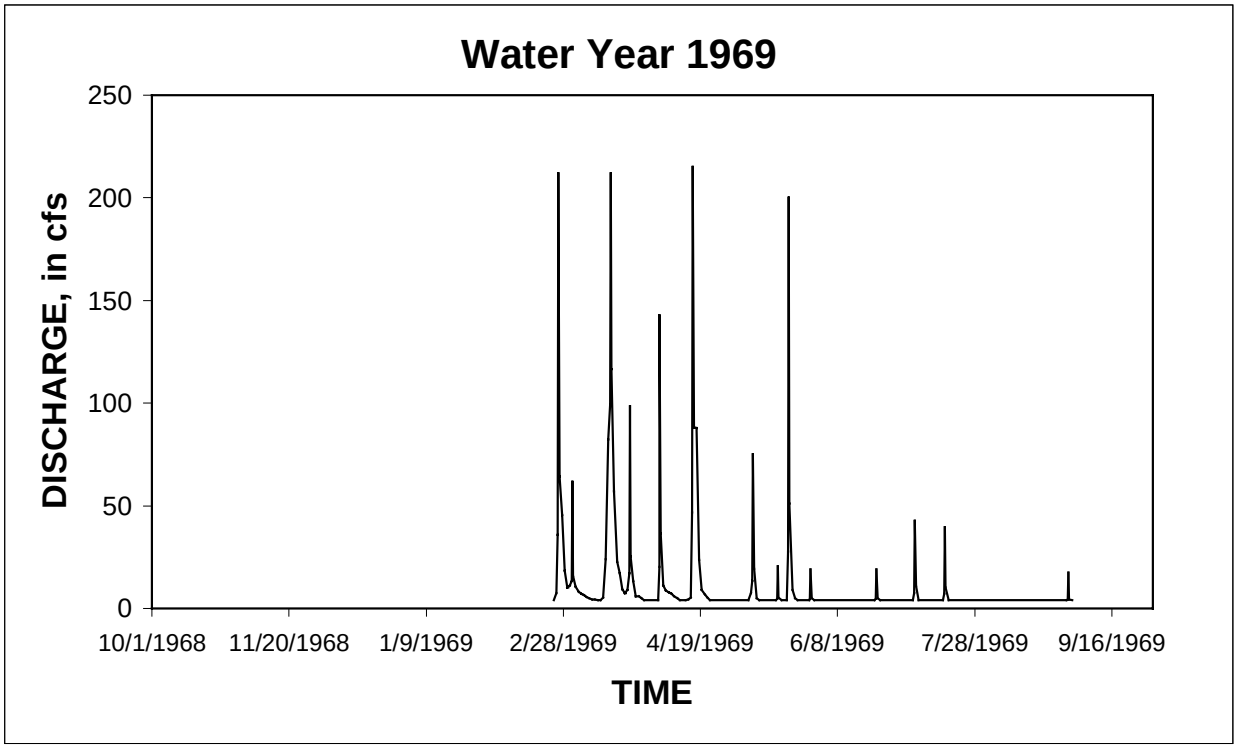

Figure II.1 Discharge hydrograph at the Little Salt Creek (Raymond Rd) for water year 1969.

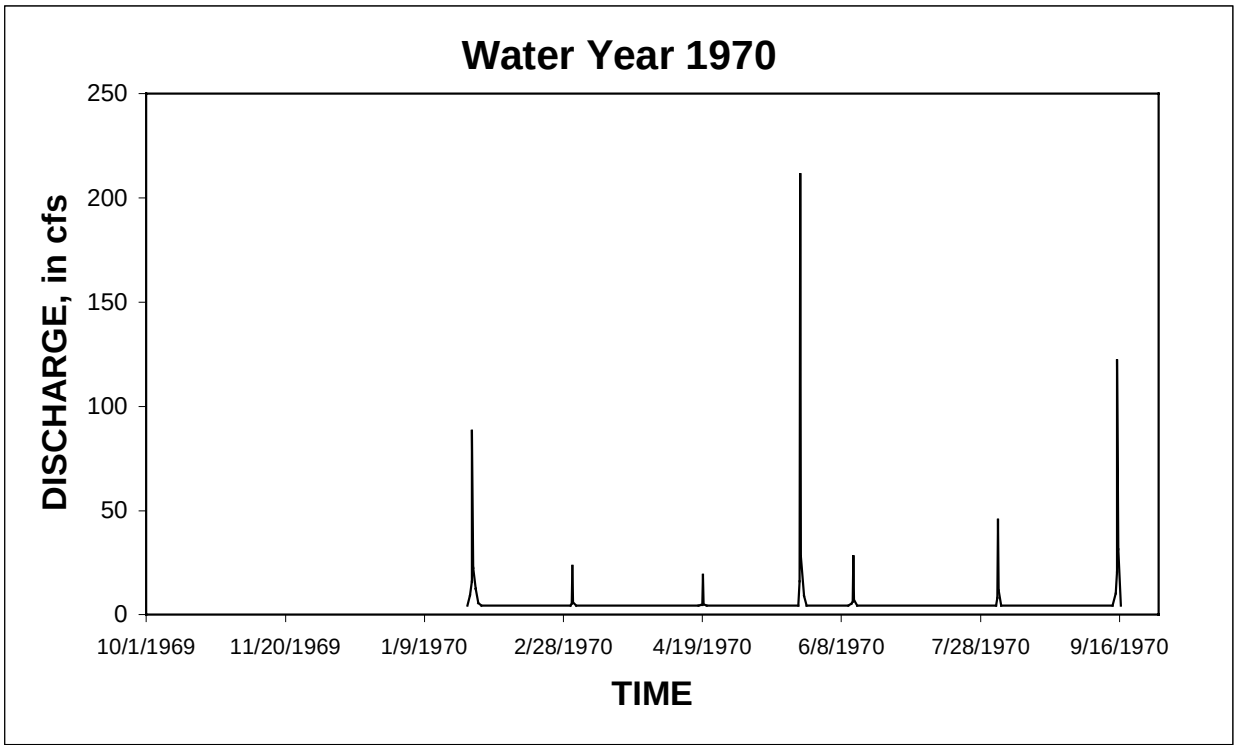

Figure II.2 Discharge hydrograph at the Little Salt Creek (Raymond Rd) for water year 1970.

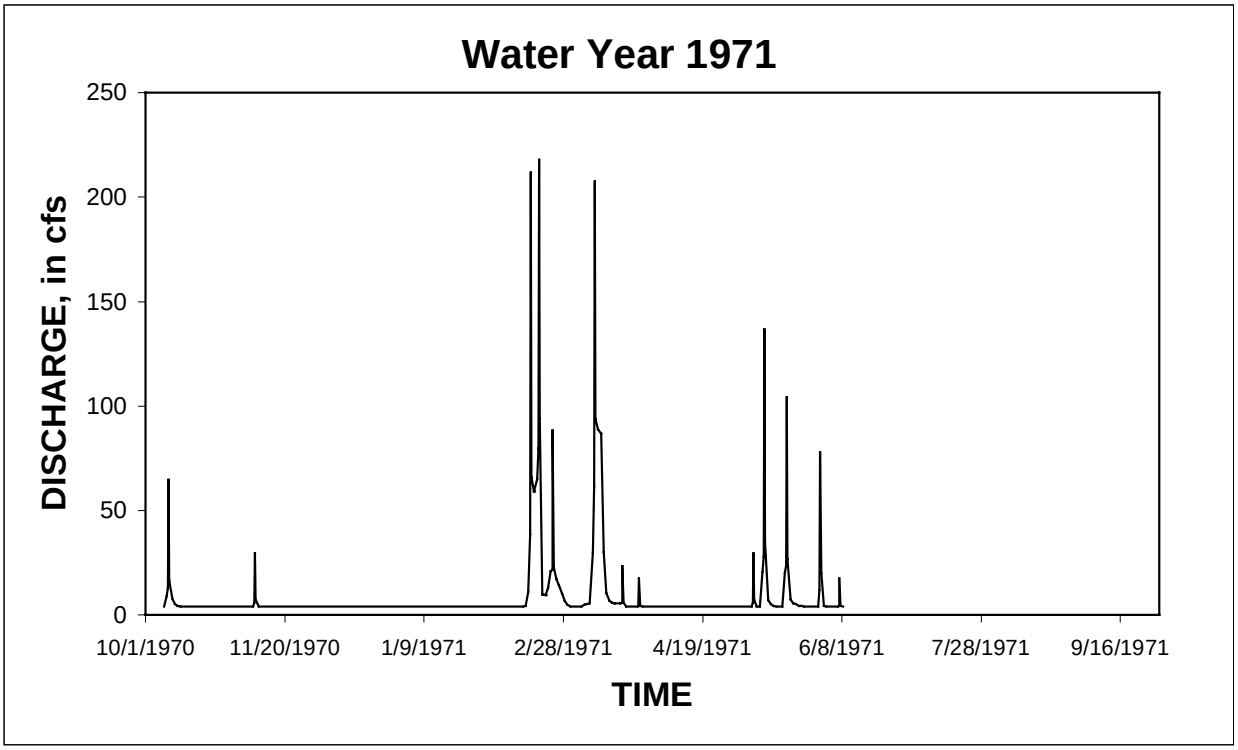

Figure II.3 Discharge hydrograph at the Little Salt Creek (Raymond Rd) for water year 1971.

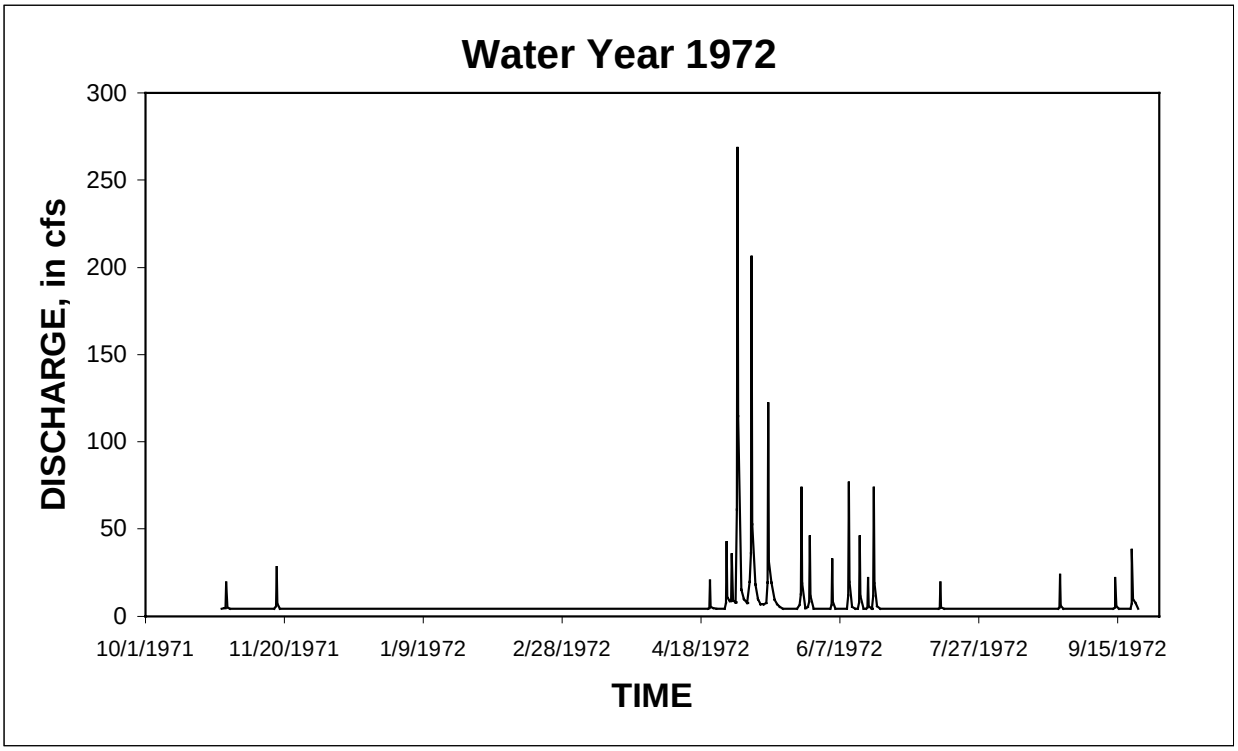

Figure II.4 Discharge hydrograph at the Little Salt Creek (Raymond Rd) for water year 1972.

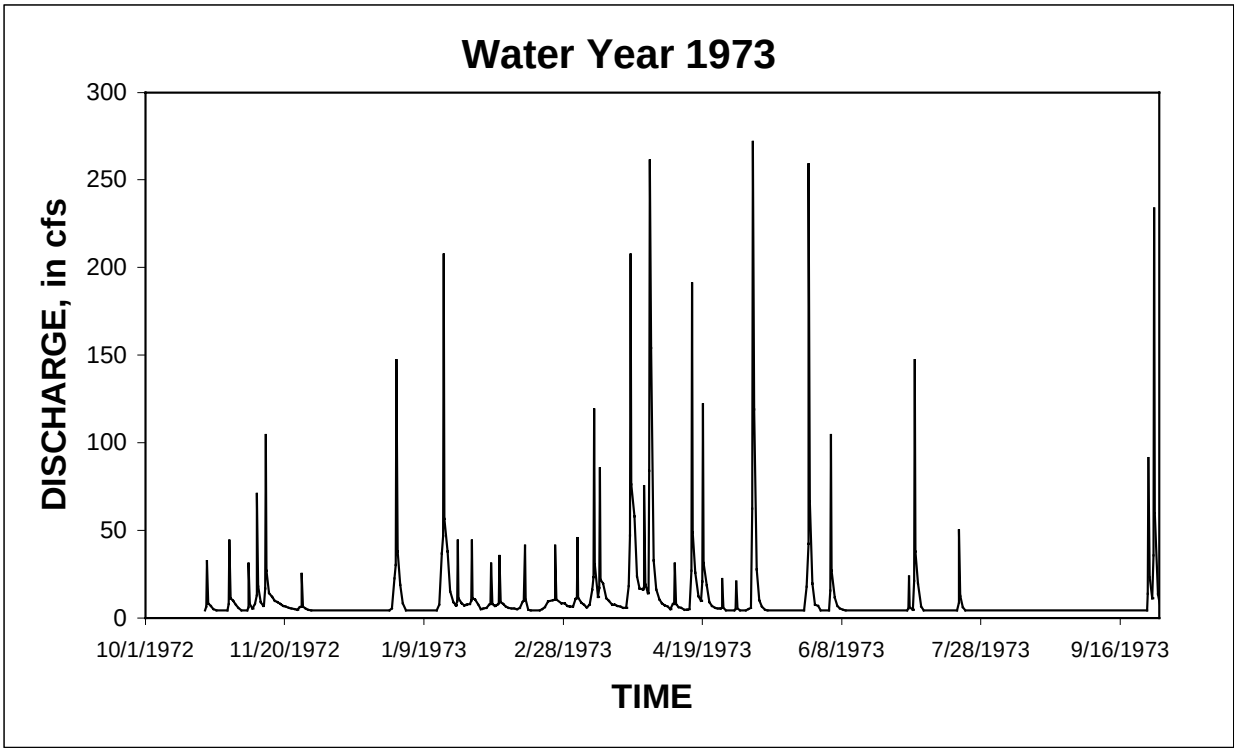

Figure II.5 Discharge hydrograph at the Little Salt Creek (Raymond Rd) for water year 1973.

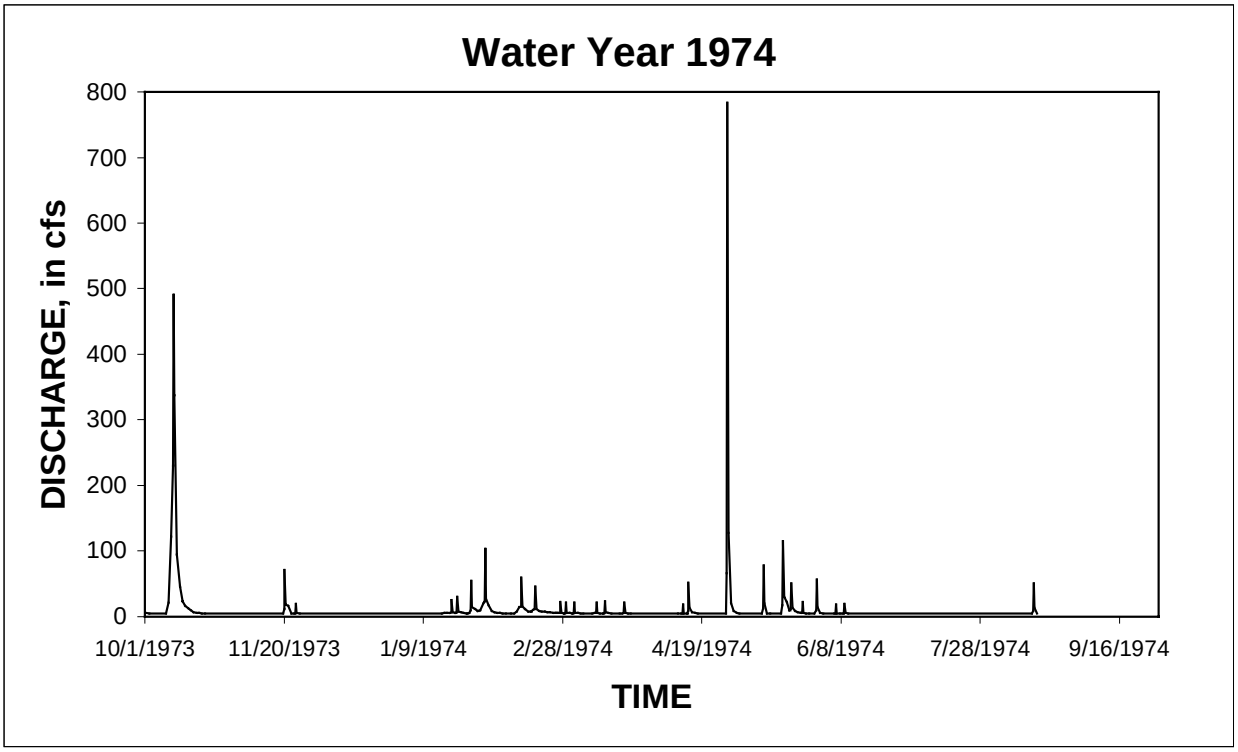

Figure II.6 Discharge hydrograph at the Little Salt Creek (Raymond Rd) for water year 1974.

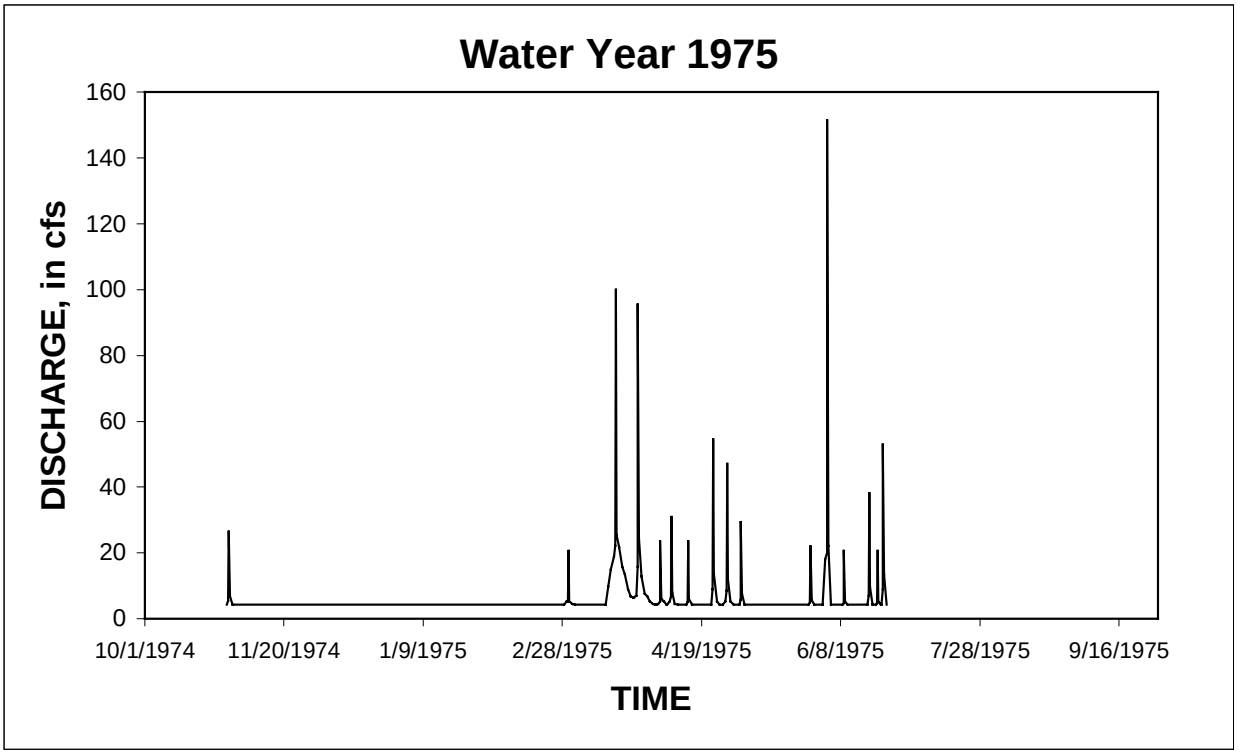

Figure II.7 Discharge hydrograph at the Little Salt Creek (Raymond Rd) for water year 1975.

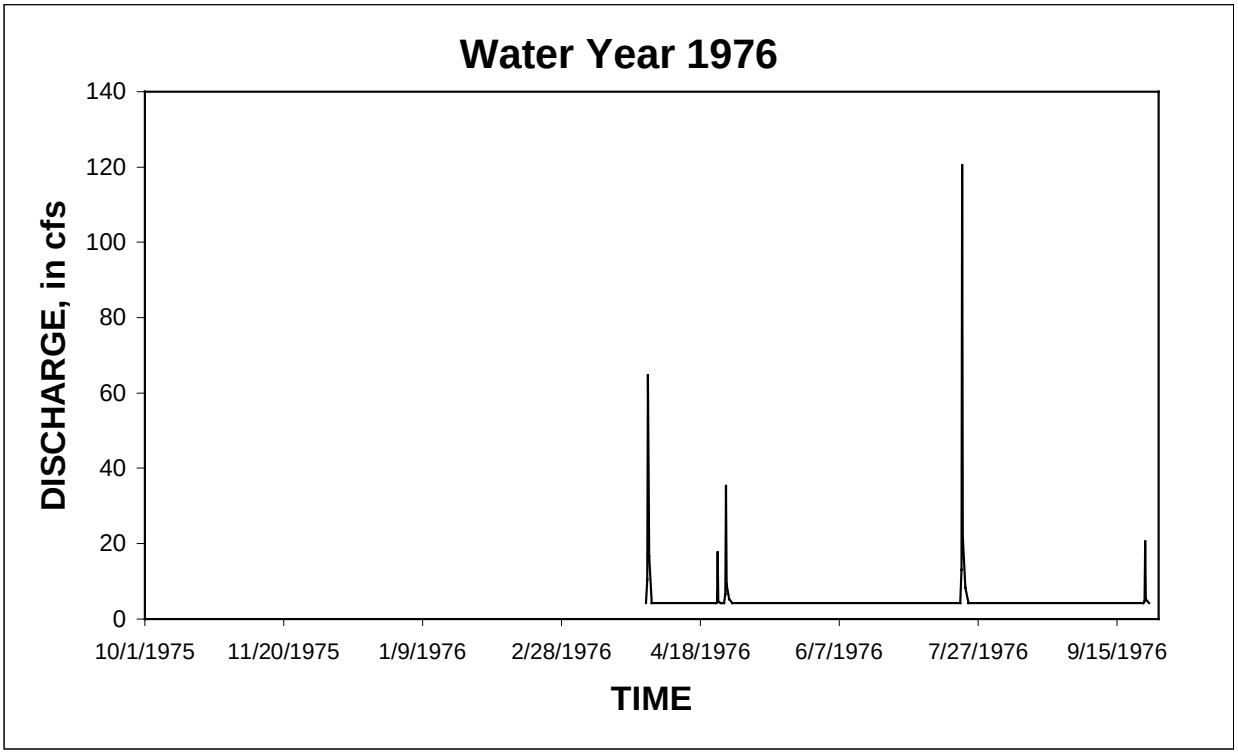

Figure II.8 Discharge hydrograph at the Little Salt Creek (Raymond Rd) for water year 1976.

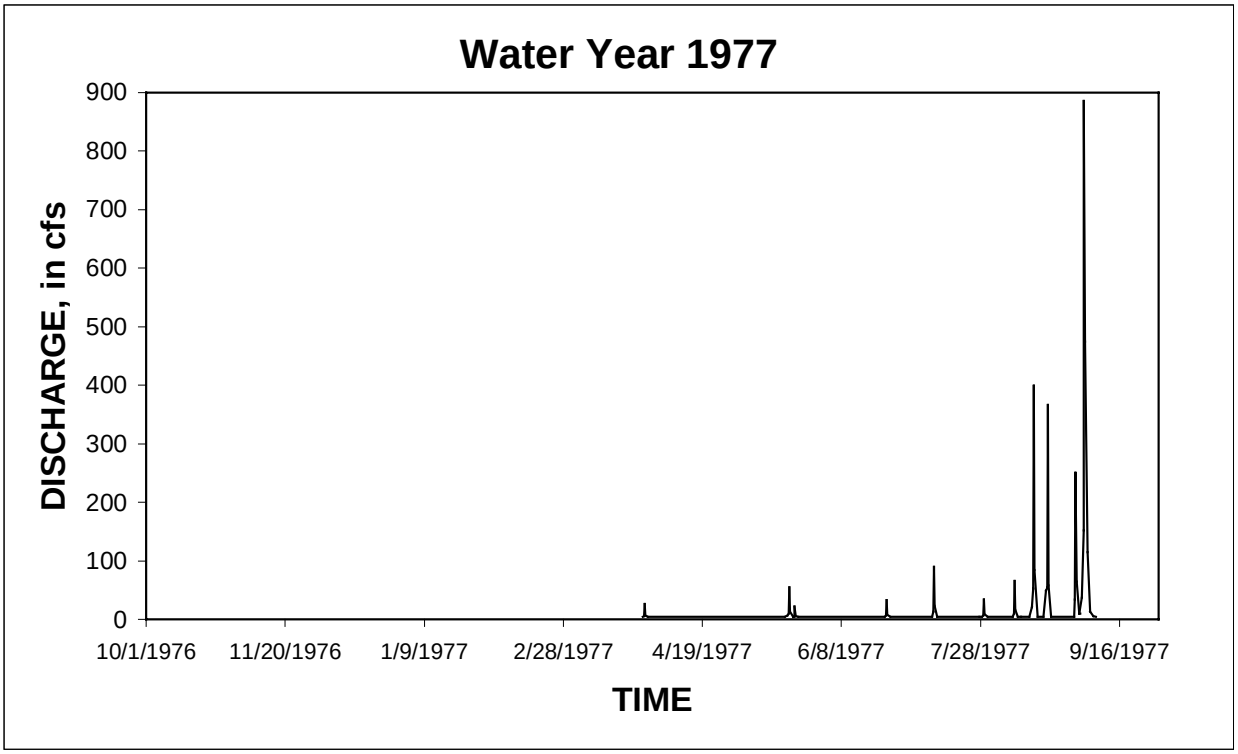

Figure II.9 Discharge hydrograph at the Little Salt Creek (Raymond Rd) for water year 1977.

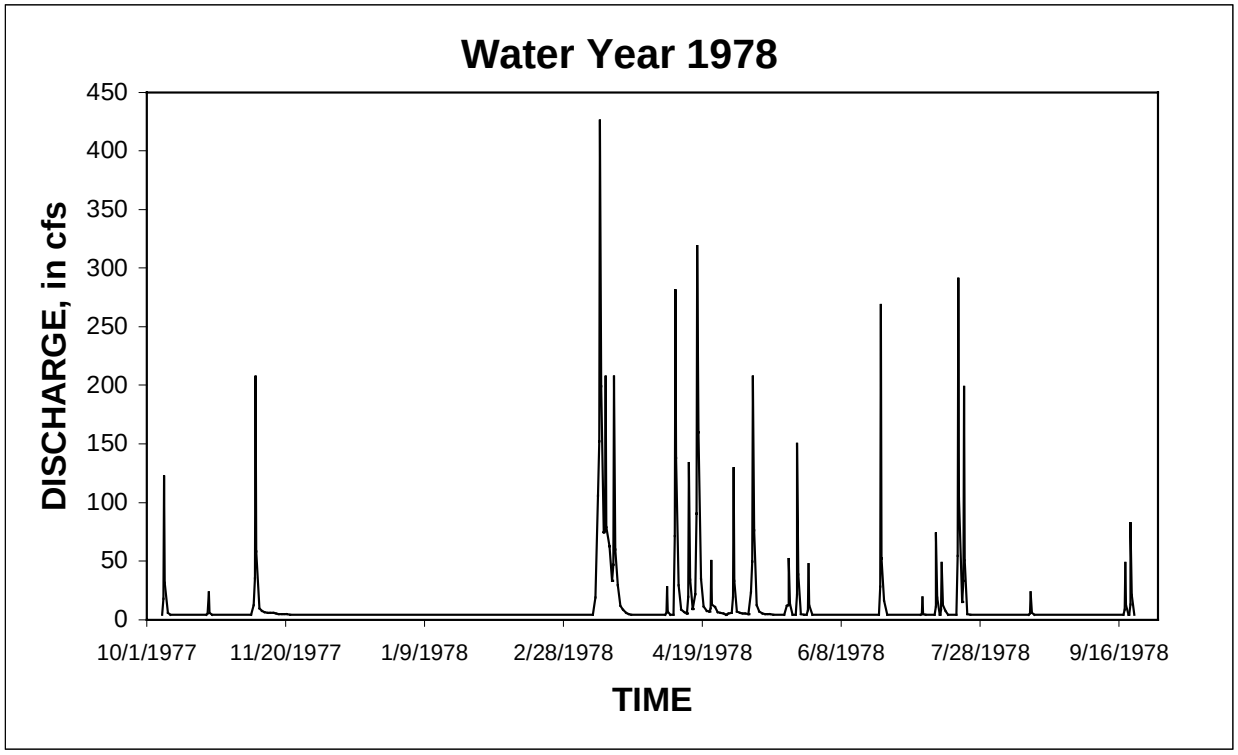

Figure II.10 Discharge hydrograph at the Little Salt Creek (Raymond Rd) for water year 1978.

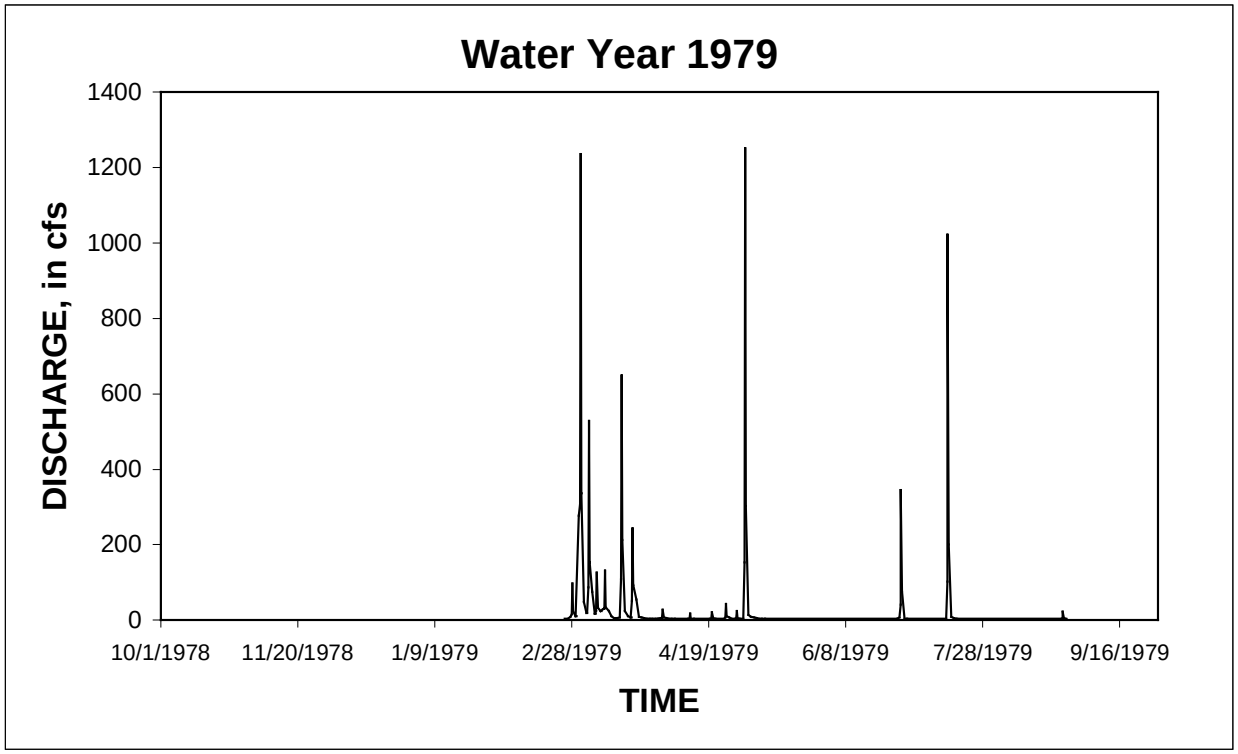

Figure II.11 Discharge hydrograph at the Little Salt Creek (Raymond Rd) for water year 1979.

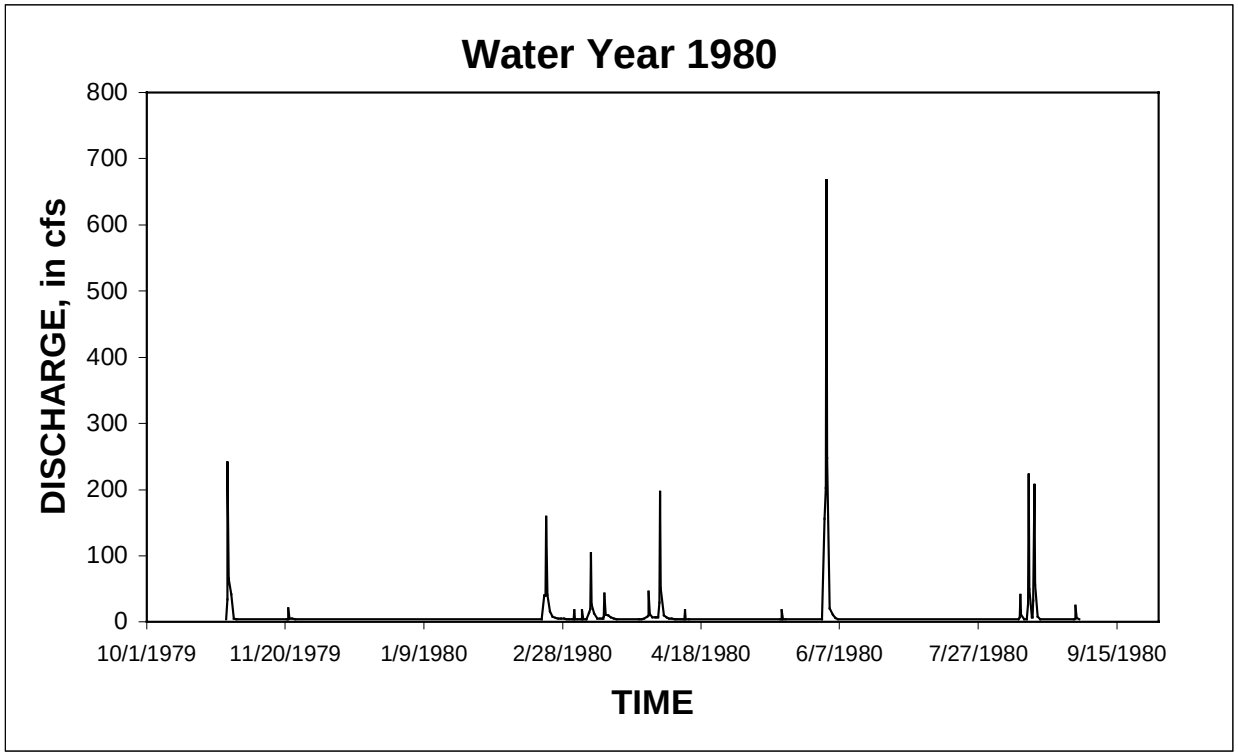

Figure II.12 Discharge hydrograph at the Little Salt Creek (Raymond Rd) for water year 1980.

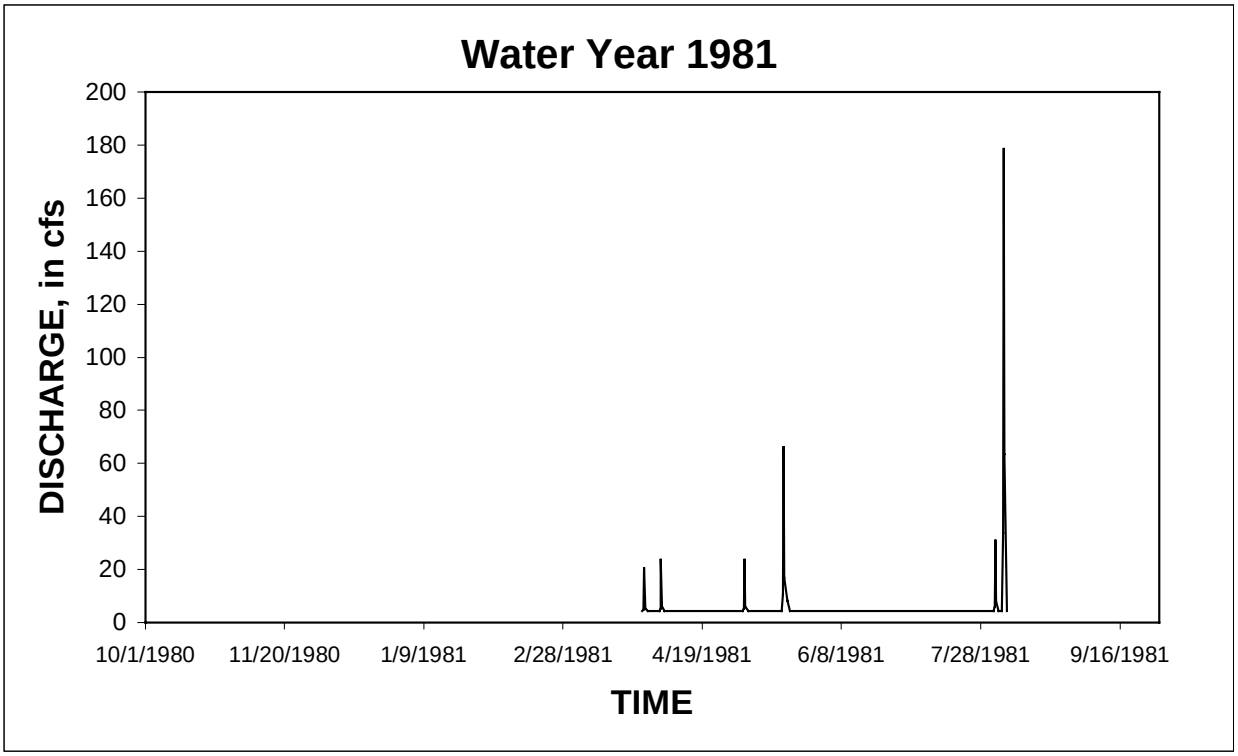

Figure II.13 Discharge hydrograph at the Little Salt Creek (Raymond Rd) for water year 1981.

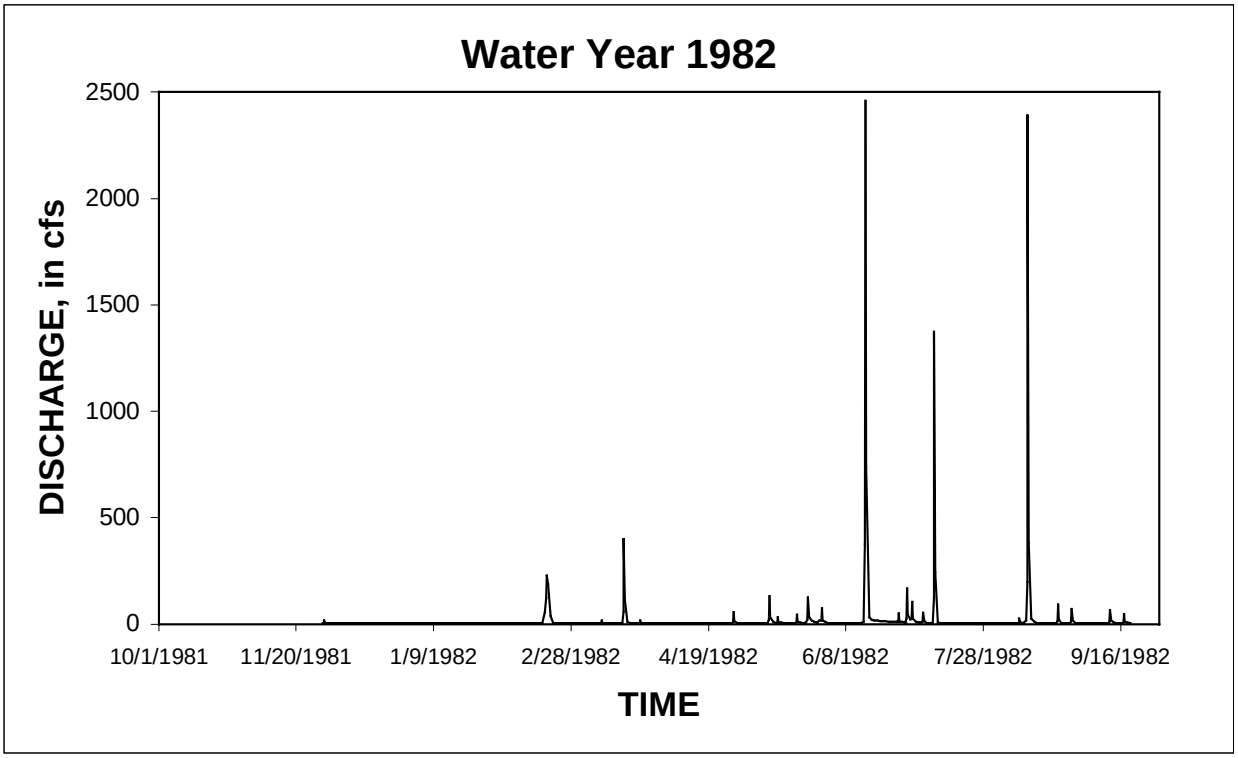

Figure II.14 Discharge hydrograph at the Little Salt Creek (Raymond Rd) for water year 1982.

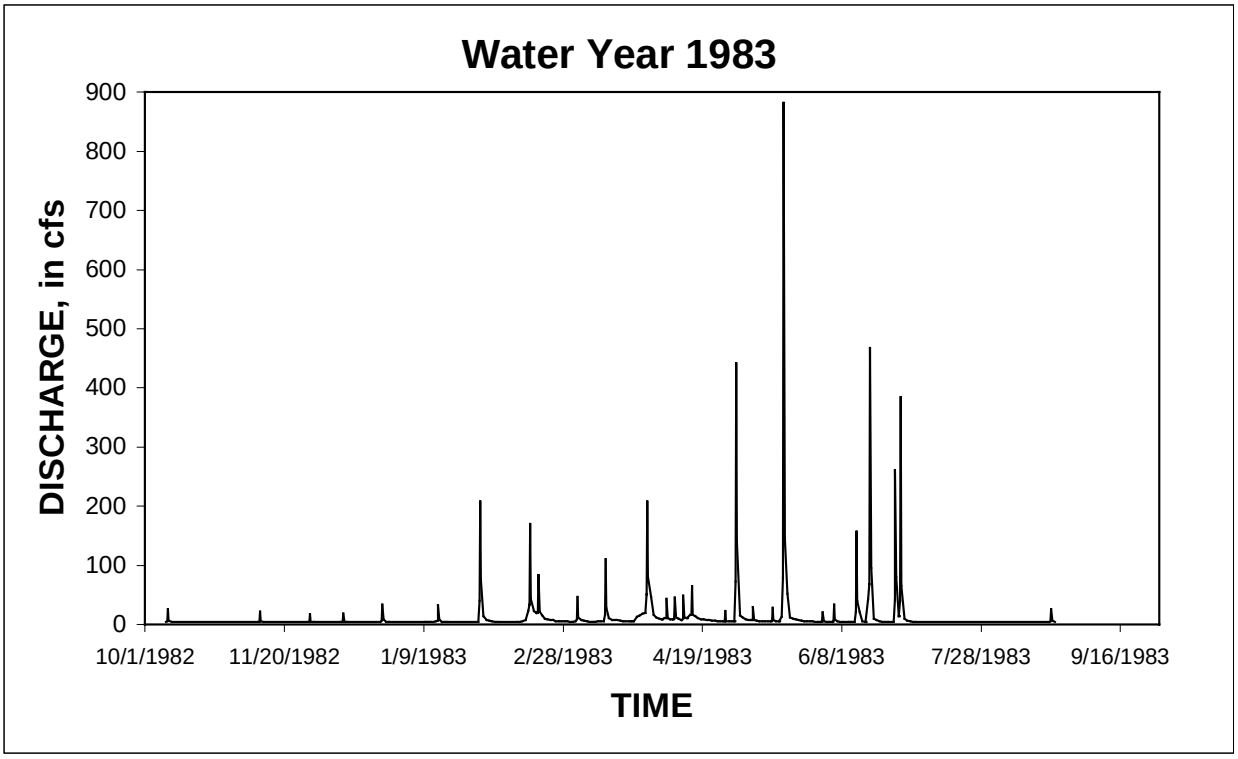

Figure II.15 Discharge hydrograph at the Little Salt Creek (Raymond Rd) for water year 1983.

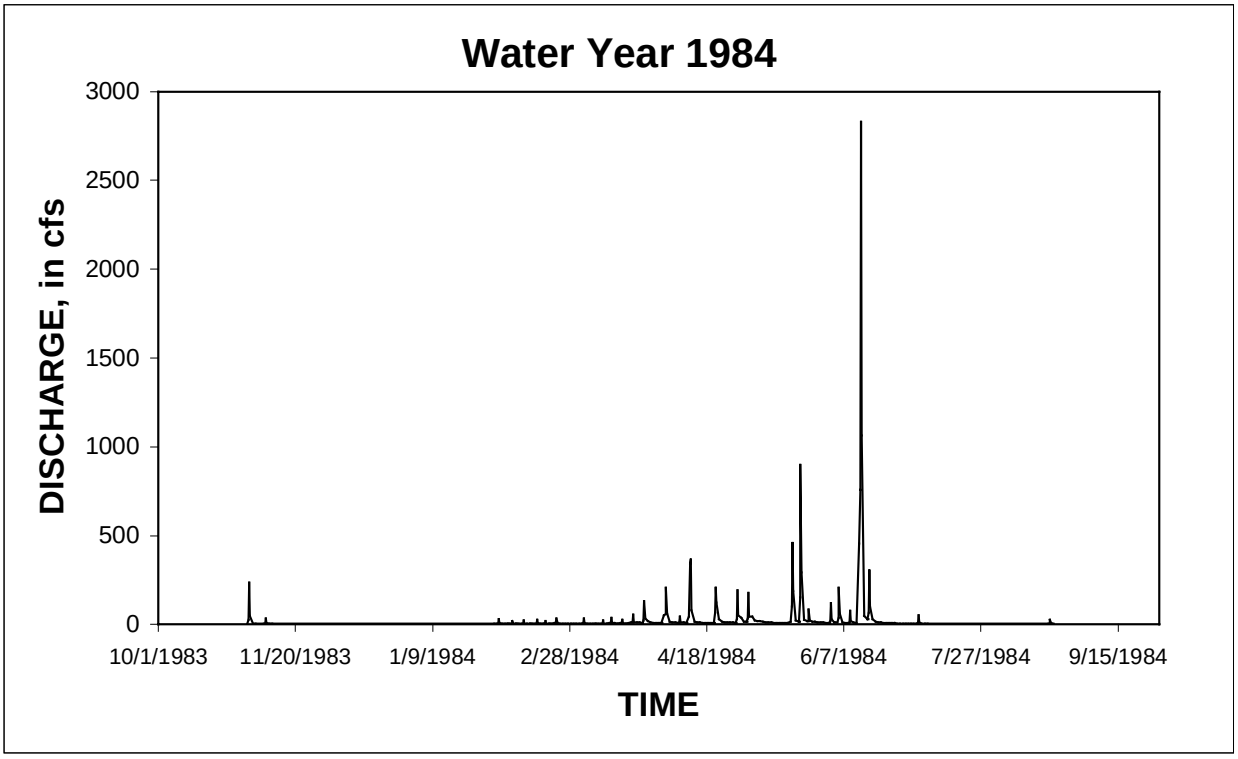

Figure II.16 Discharge hydrograph at the Little Salt Creek (Raymond Rd) for water year 1984.

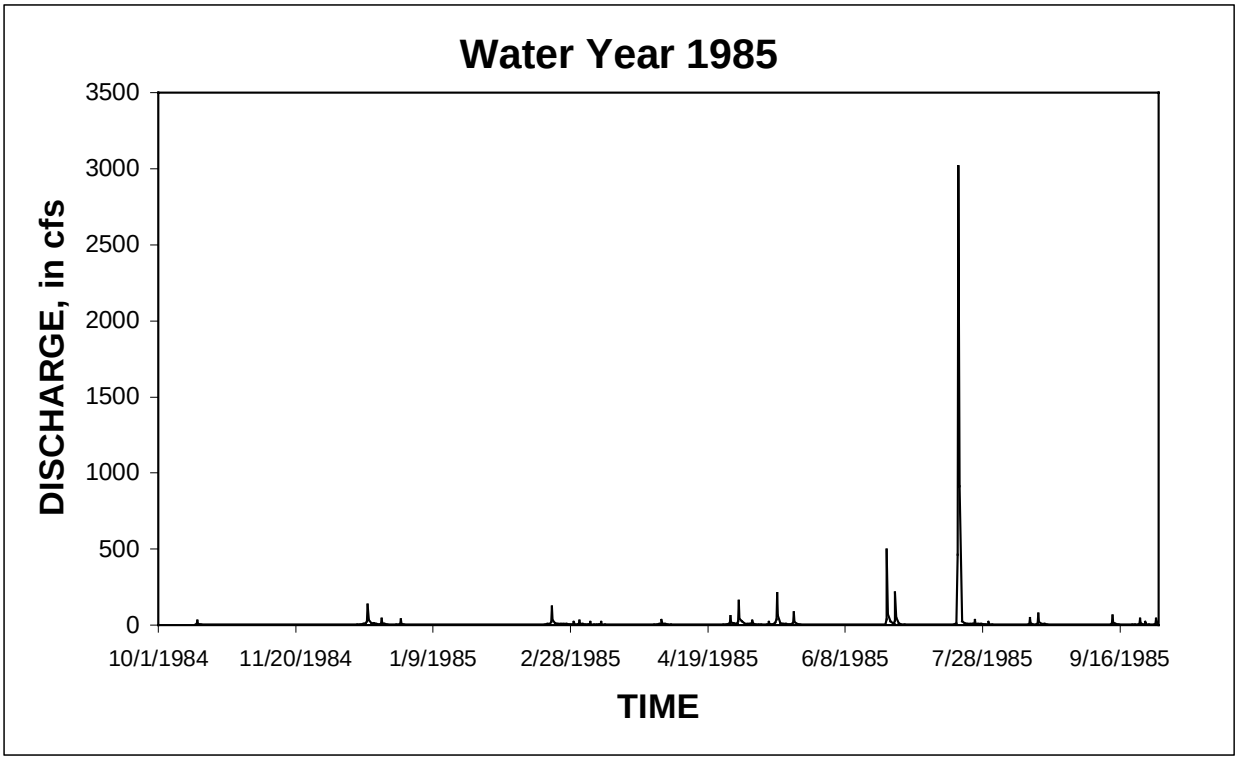

Figure II.17 Discharge hydrograph at the Little Salt Creek (Raymond Rd) for water year 1985.

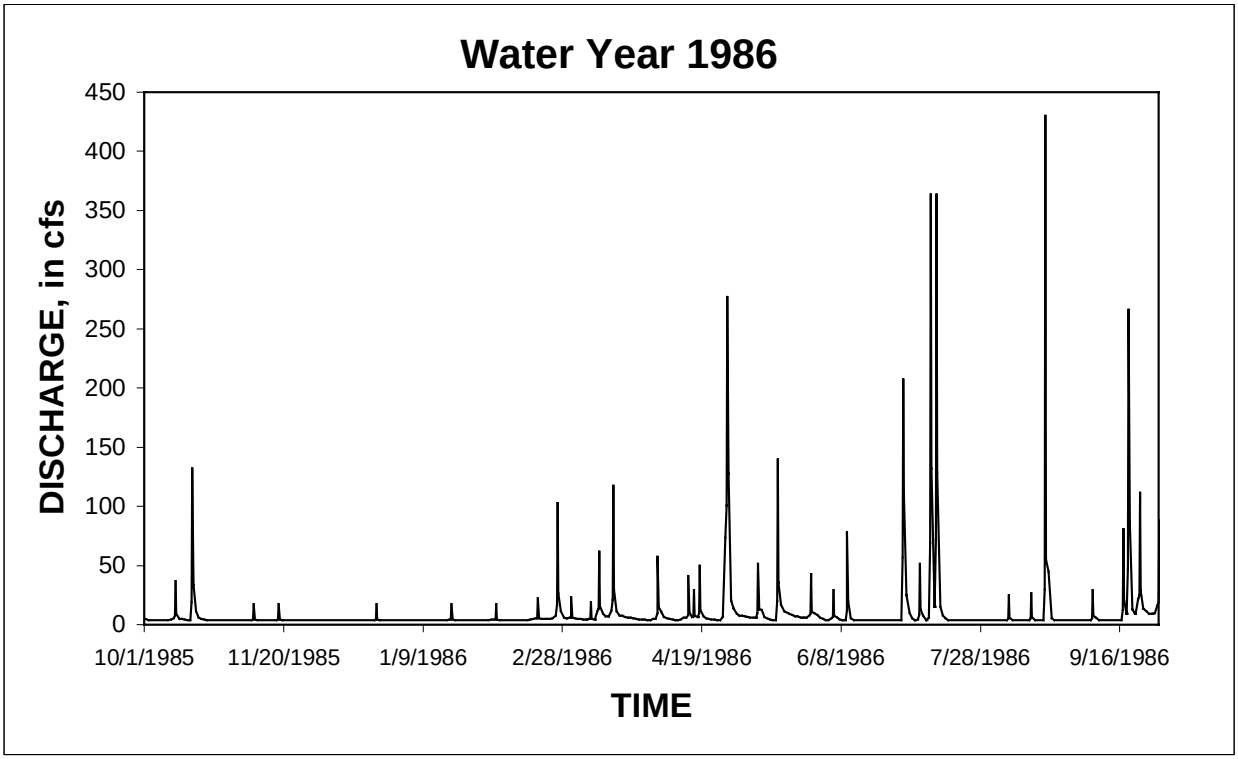

Figure II.18 Discharge hydrograph at the Little Salt Creek (Raymond Rd) for water year 1986.

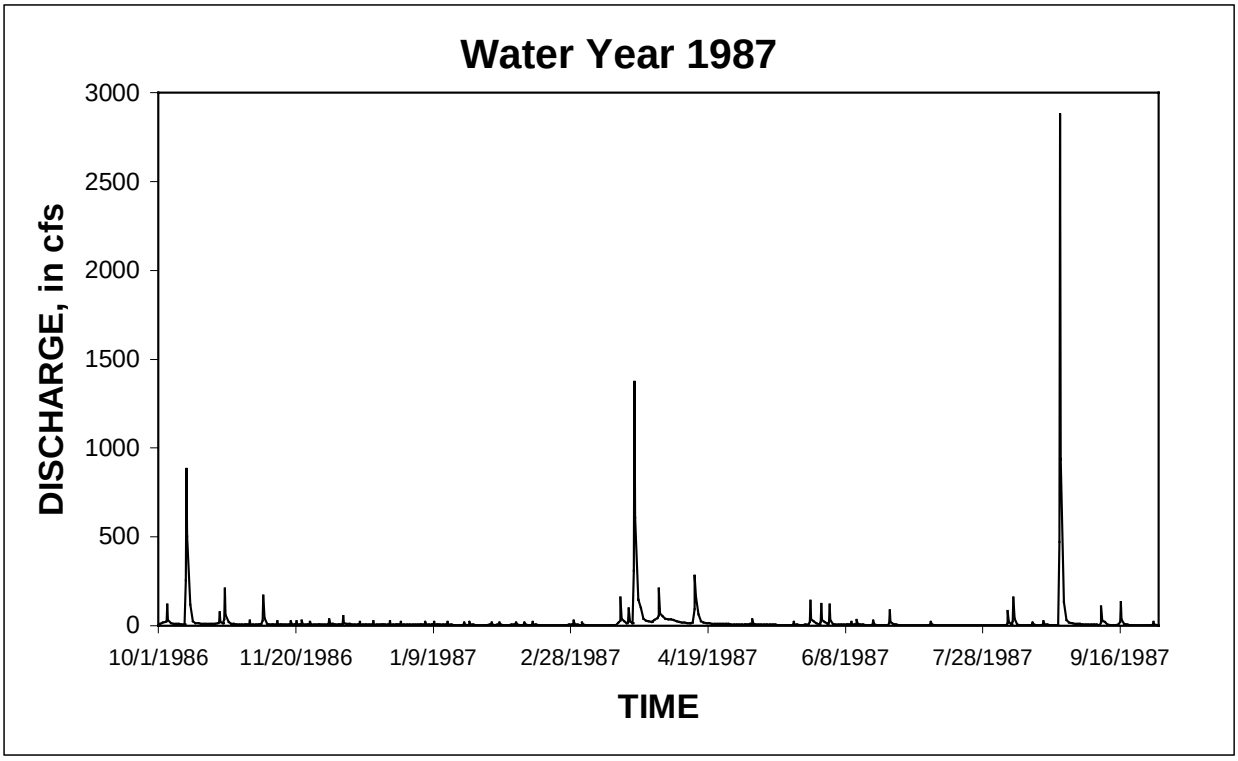

Figure II.19 Discharge hydrograph at the Little Salt Creek (Raymond Rd) for water year 1987.

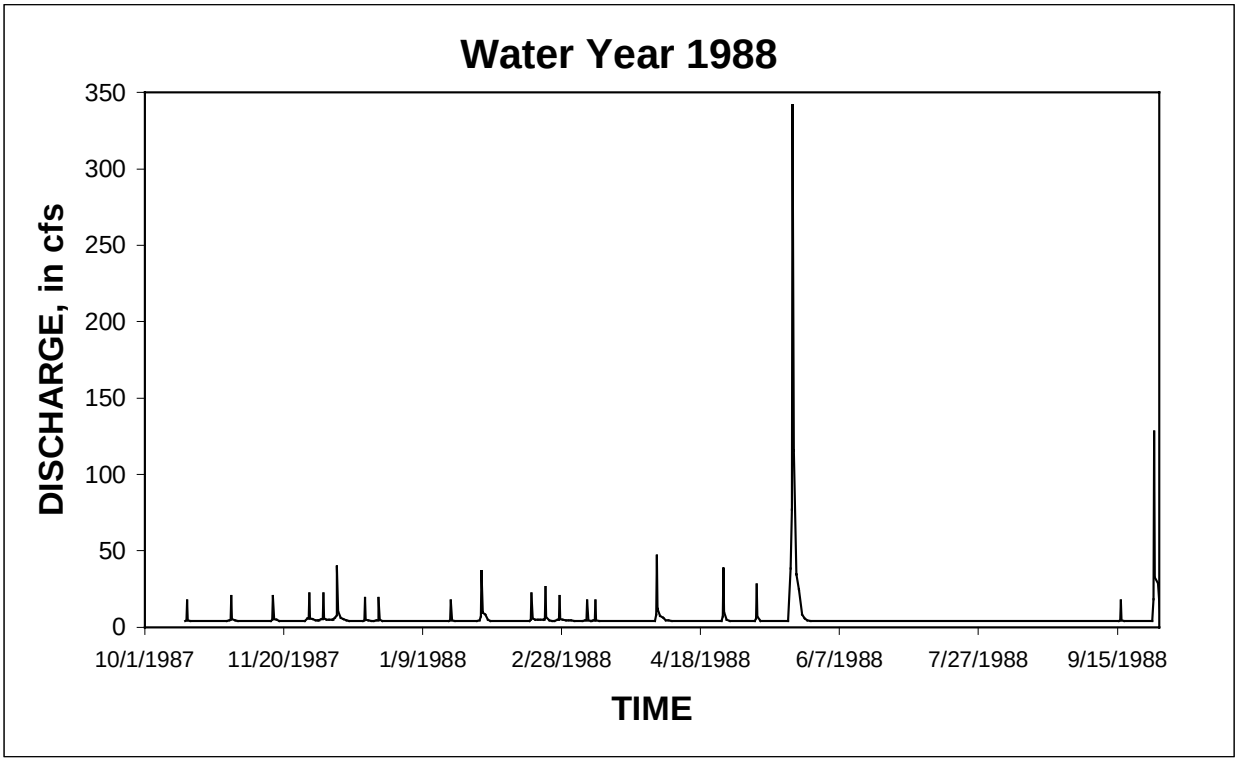

Figure II.20 Discharge hydrograph at the Little Salt Creek (Raymond Rd) for water year 1988.

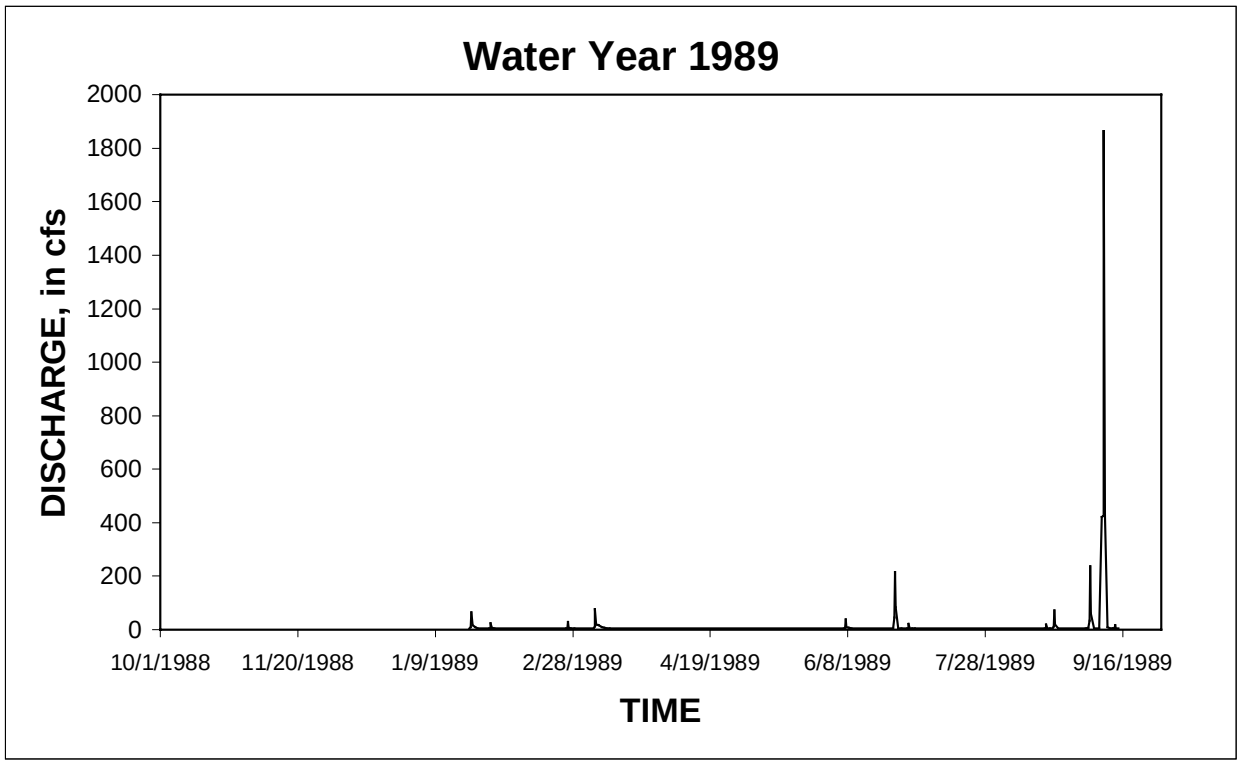

Figure II.21 Discharge hydrograph at the Little Salt Creek (Raymond Rd) for water year 1989.

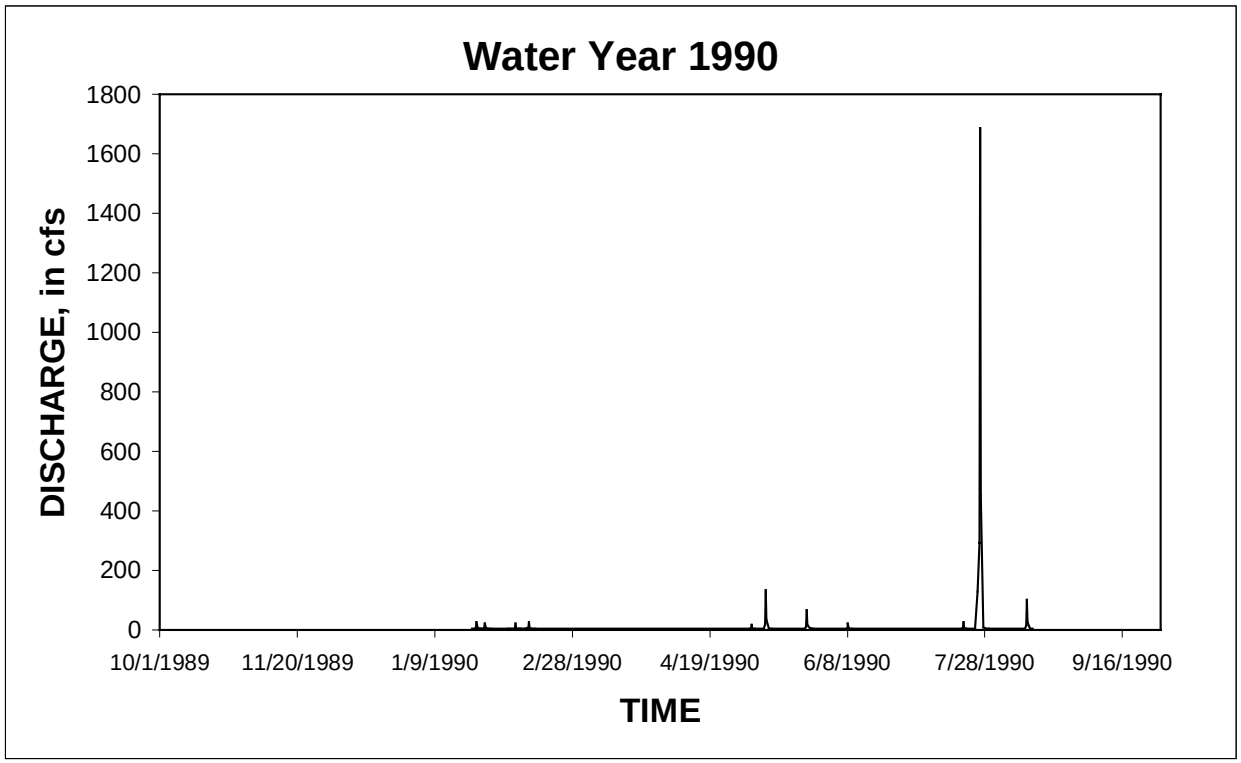

Figure II.22 Discharge hydrograph at the Little Salt Creek (Raymond Rd) for water year 1990.

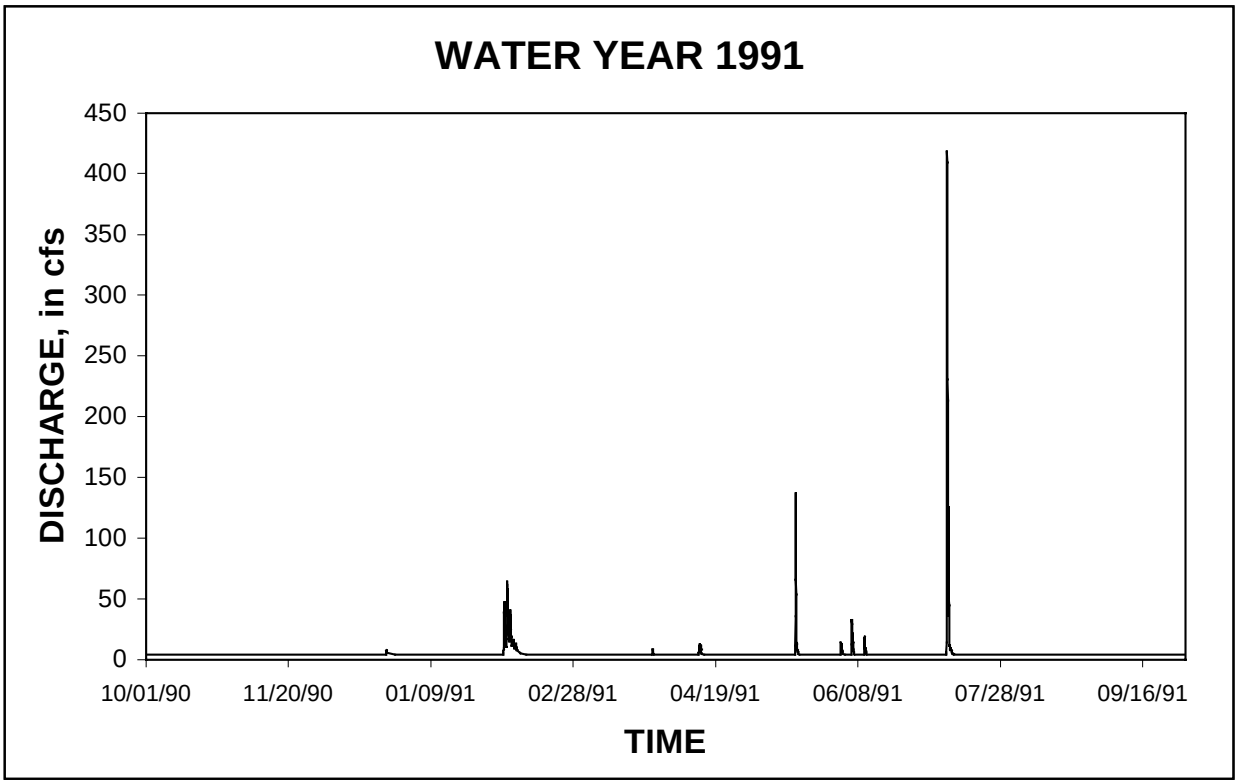

Figure II.23 Discharge hydrograph at the Little Salt Creek (Raymond Rd) for water year 1991.

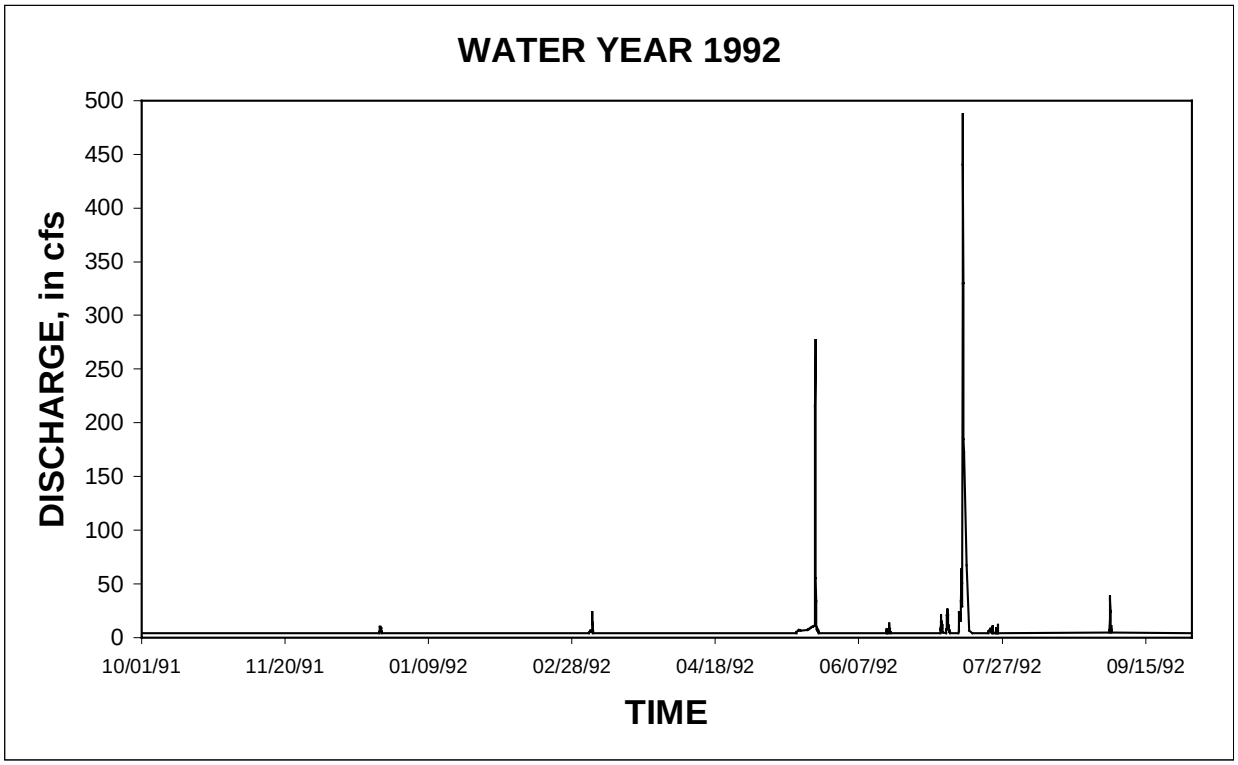

Figure II.24 Discharge hydrograph at the Little Salt Creek (Raymond Rd) for water year 1992.

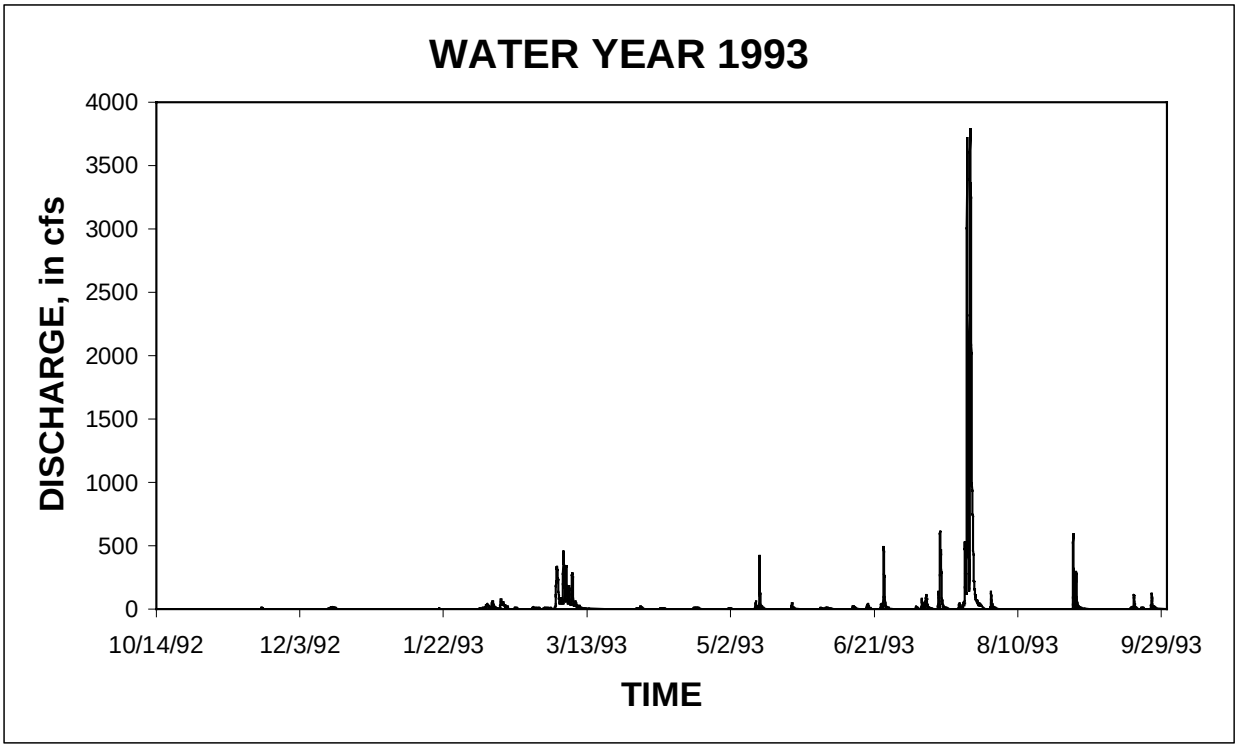

Figure II.25 Discharge hydrograph at the Little Salt Creek (Raymond Rd) for water year 1993.

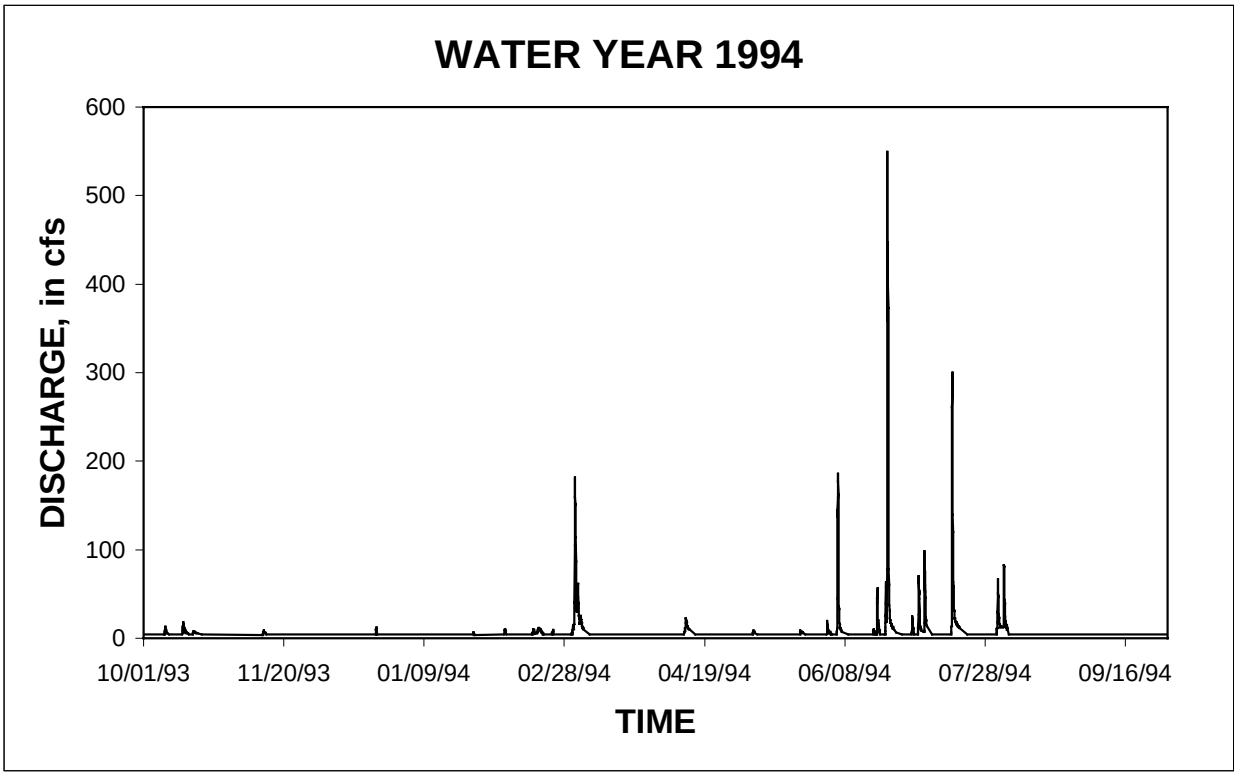

Figure II.26 Discharge hydrograph at the Little Salt Creek (Raymond Rd) for water year 1994.

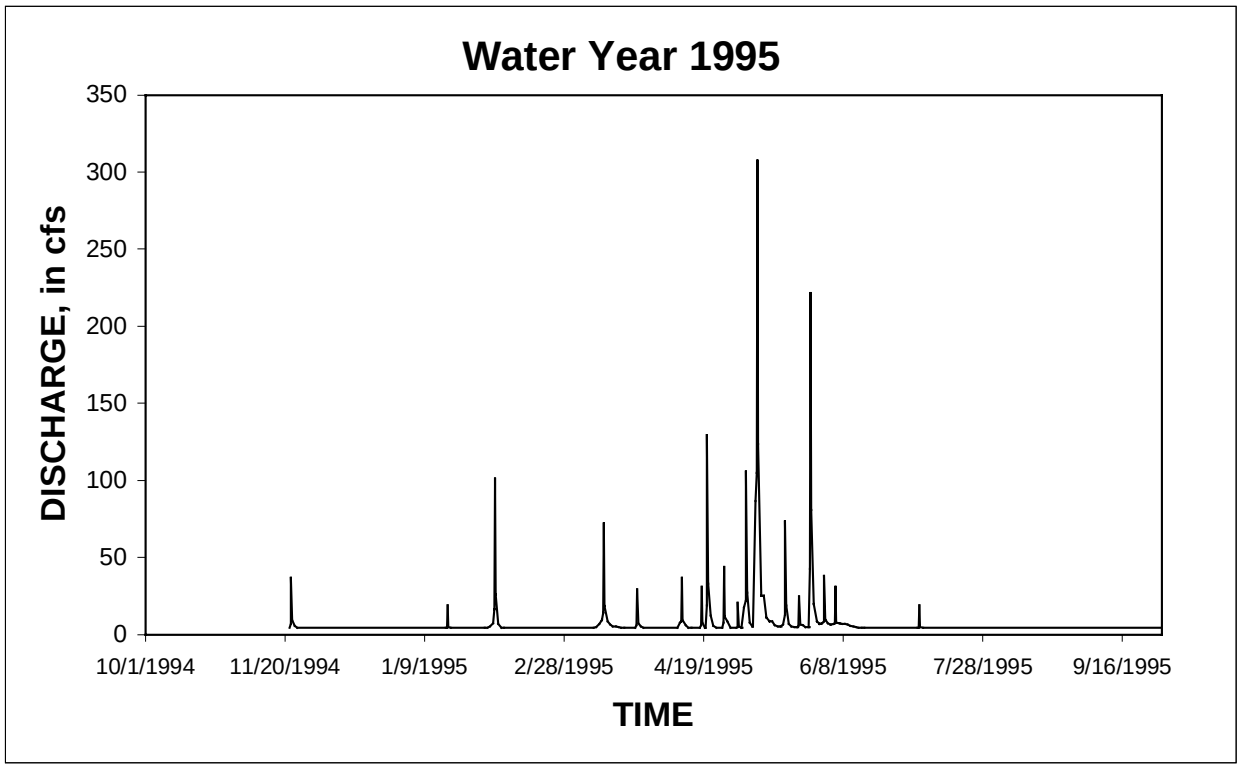

Figure II.27 Discharge hydrograph at the Little Salt Creek (Raymond Rd) for water year 1995.

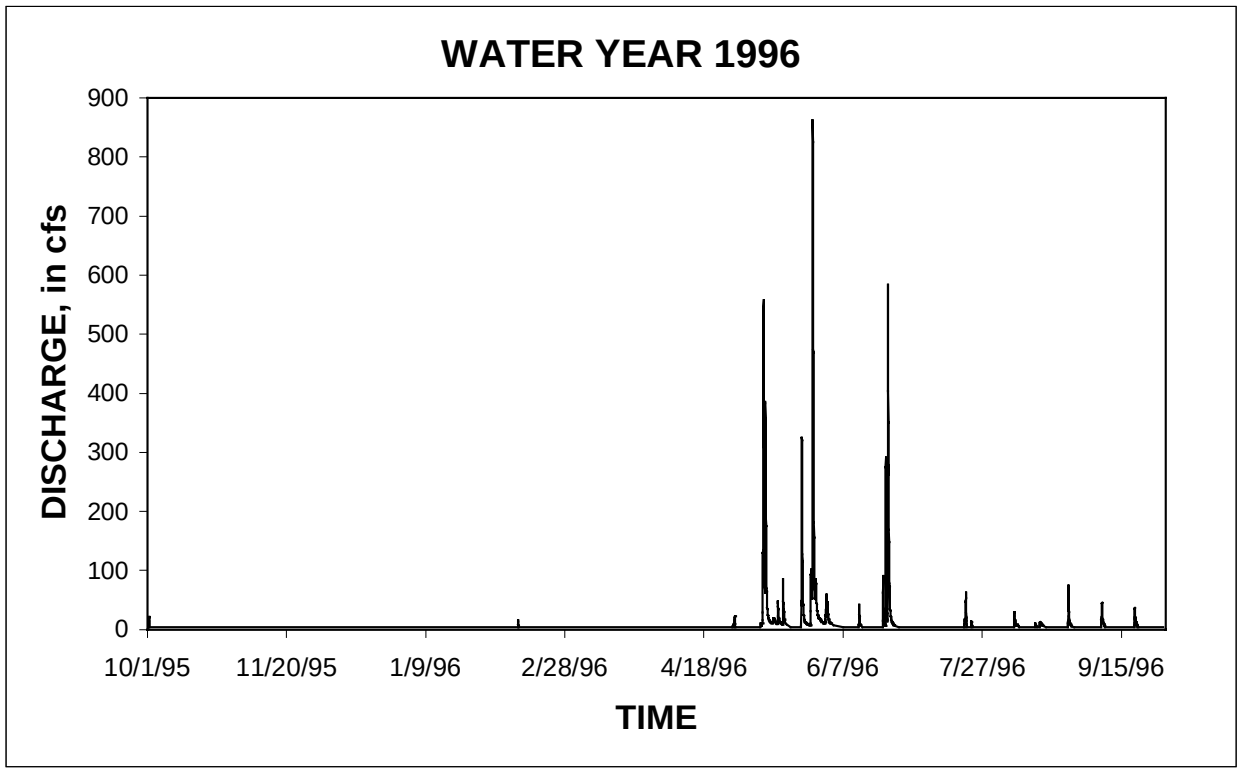

Figure II.28 Discharge hydrograph at the Little Salt Creek (Raymond Rd) for water year 1996.

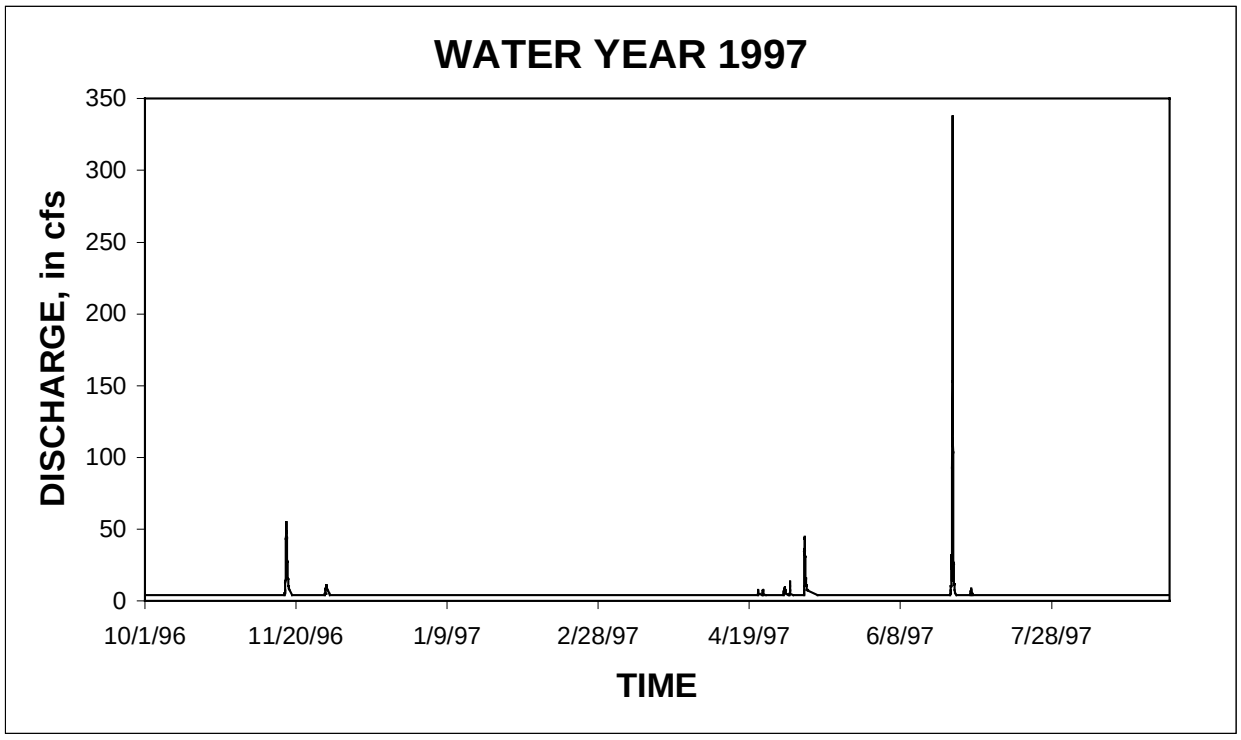

Figure II.29 Discharge hydrograph at the Little Salt Creek (Raymond Rd) for water year 1997.

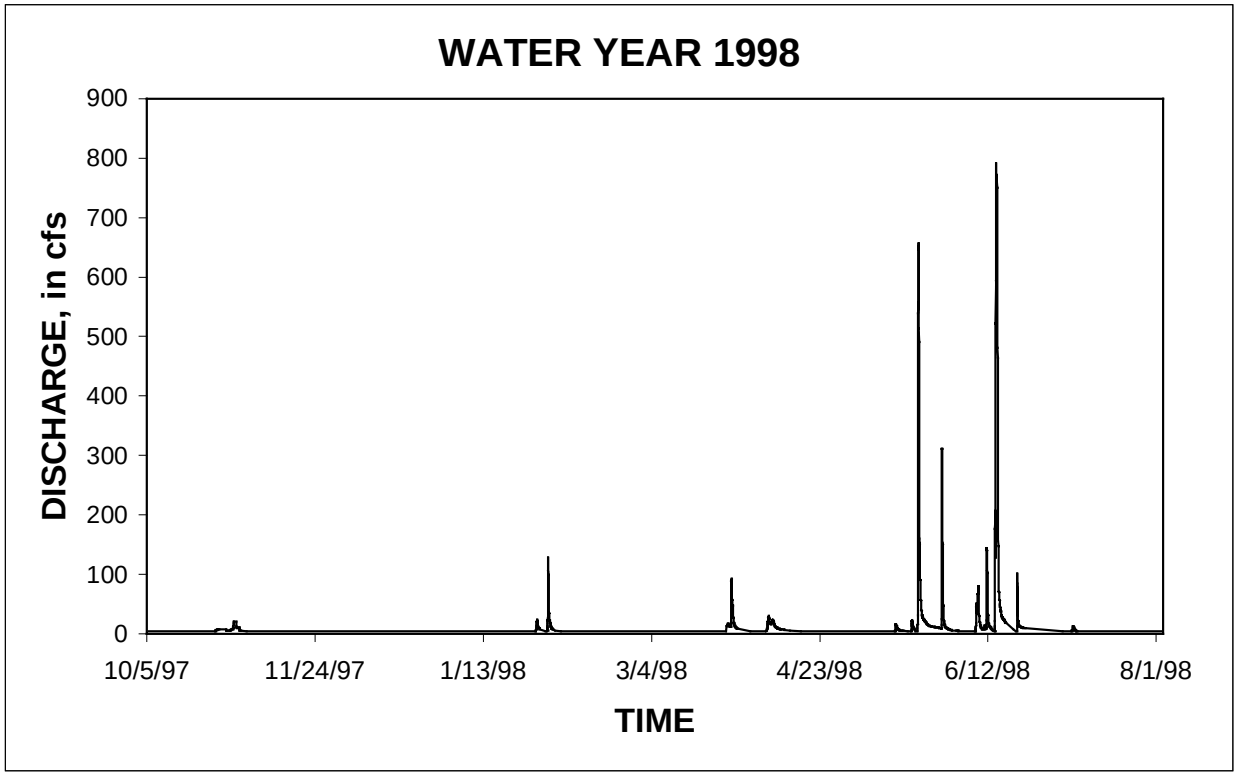

Figure II.30 Discharge hydrograph at the Little Salt Creek (Raymond Rd) for water year 1998.

NORTH BRANCH WEST PAPILLION CREEK – UPSTREAM BOUNDARY OF MODELING REACH

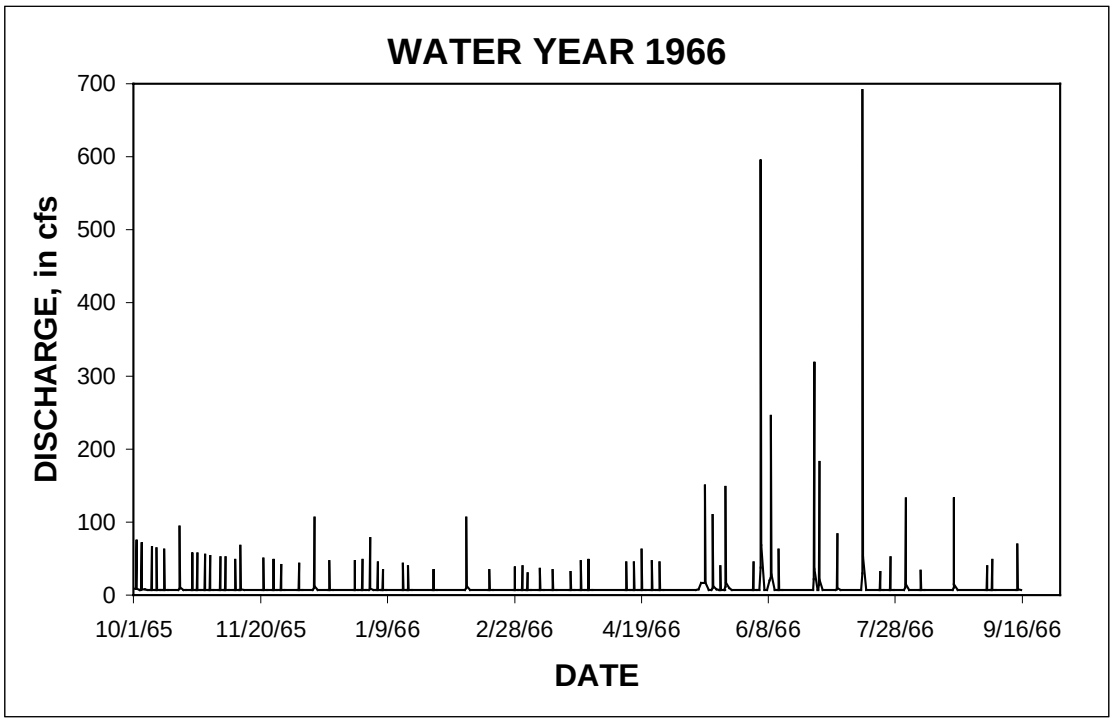

Figure II.31 Discharge hydrograph at the North Branch West Papillion Creek (Fort St) for water year 1966.

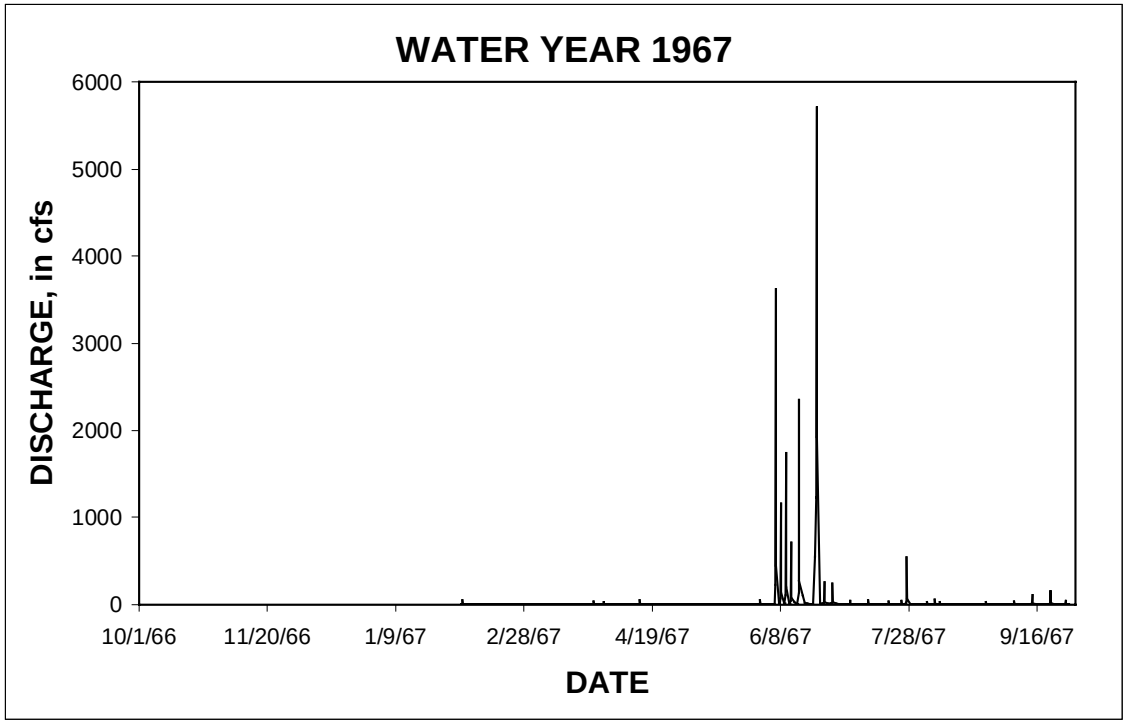

Figure II.32 Discharge hydrograph at the North Branch West Papillion Creek (Fort St) for water year 1967.

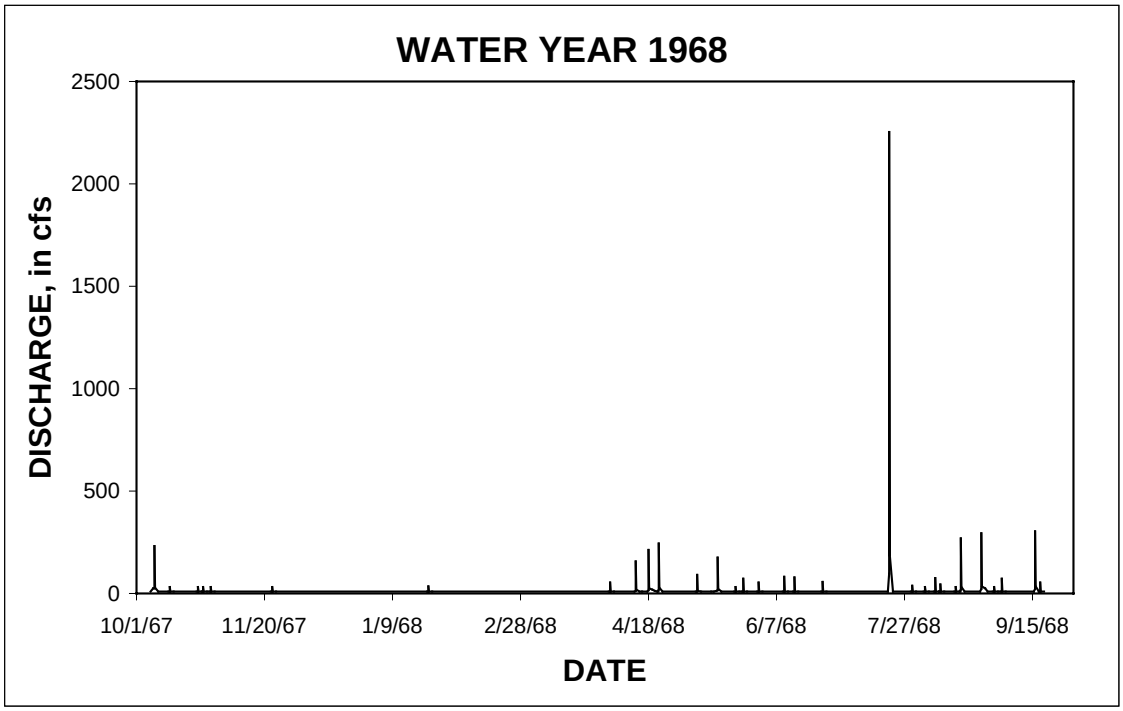

Figure II.33 Discharge hydrograph at the North Branch West Papillion Creek (Fort St) for water year 1968.

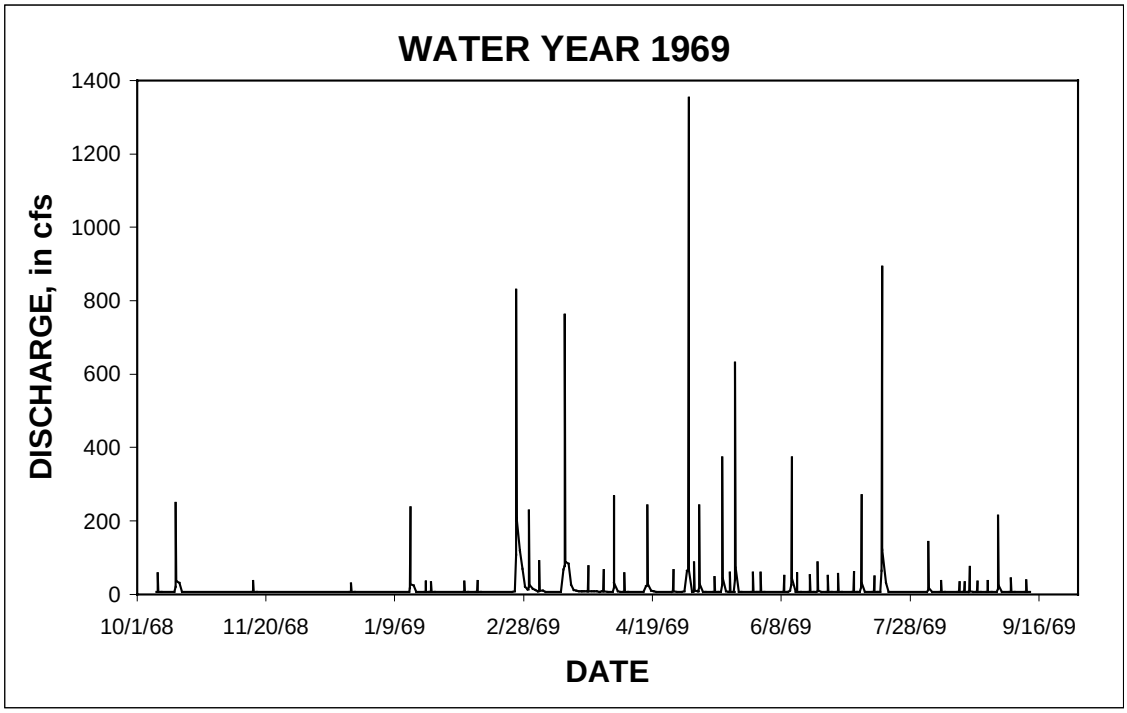

Figure II.34 Discharge hydrograph at the North Branch West Papillion Creek (Fort St) for water year 1969.

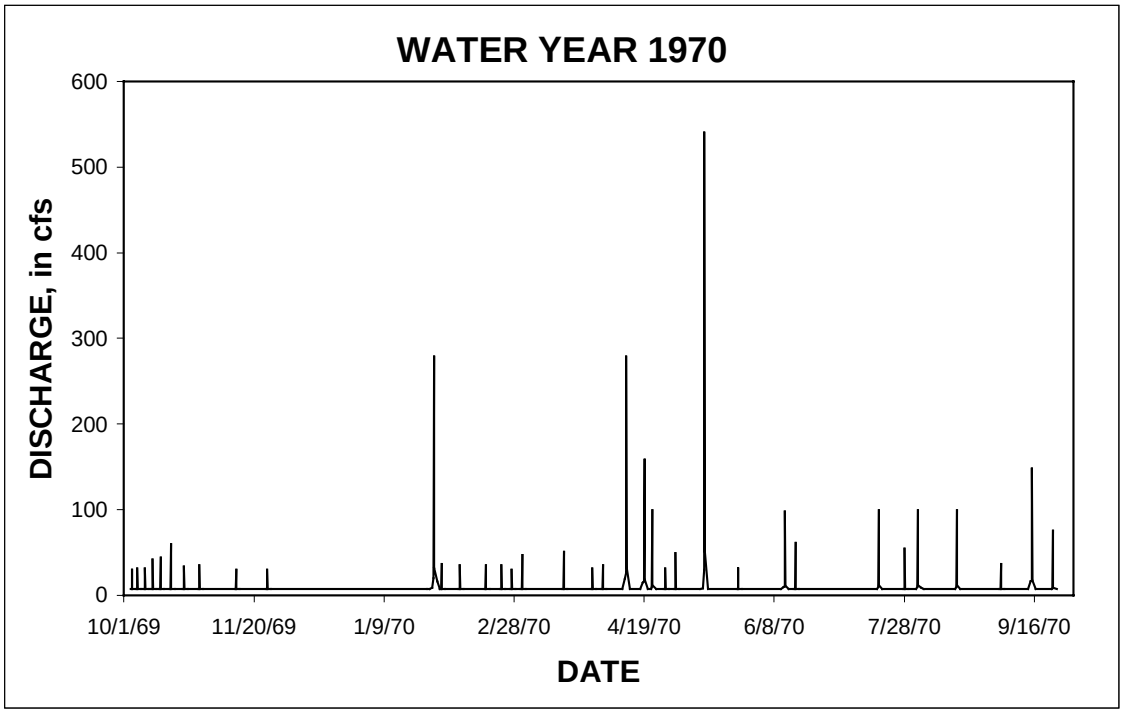

Figure II.35 Discharge hydrograph at the North Branch West Papillion Creek (Fort St) for water year 1970.

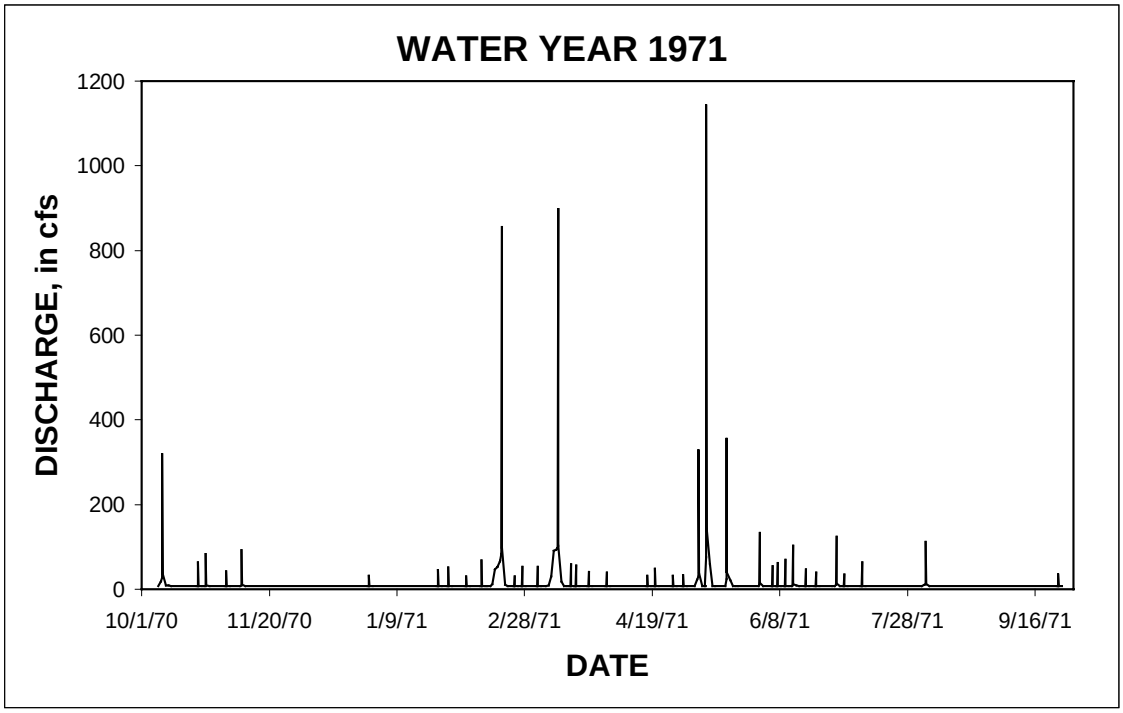

Figure II.36 Discharge hydrograph at the North Branch West Papillion Creek (Fort St) for water year 1971.

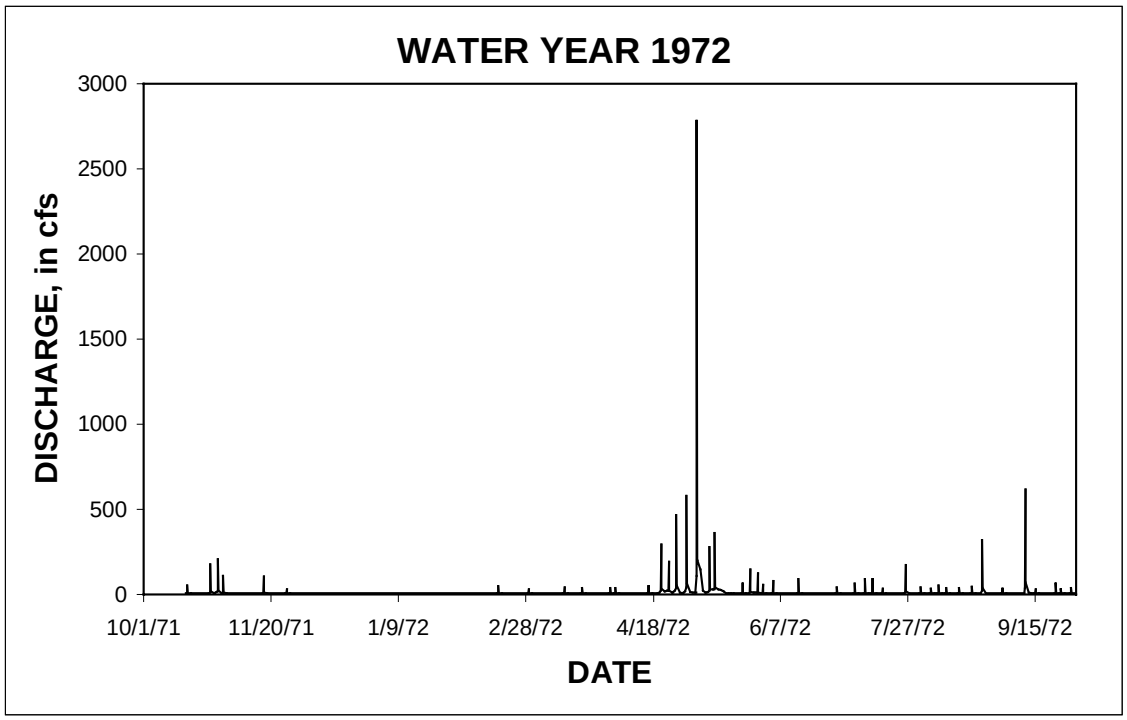

Figure II.37 Discharge hydrograph at the North Branch West Papillion Creek (Fort St) for water year 1972.

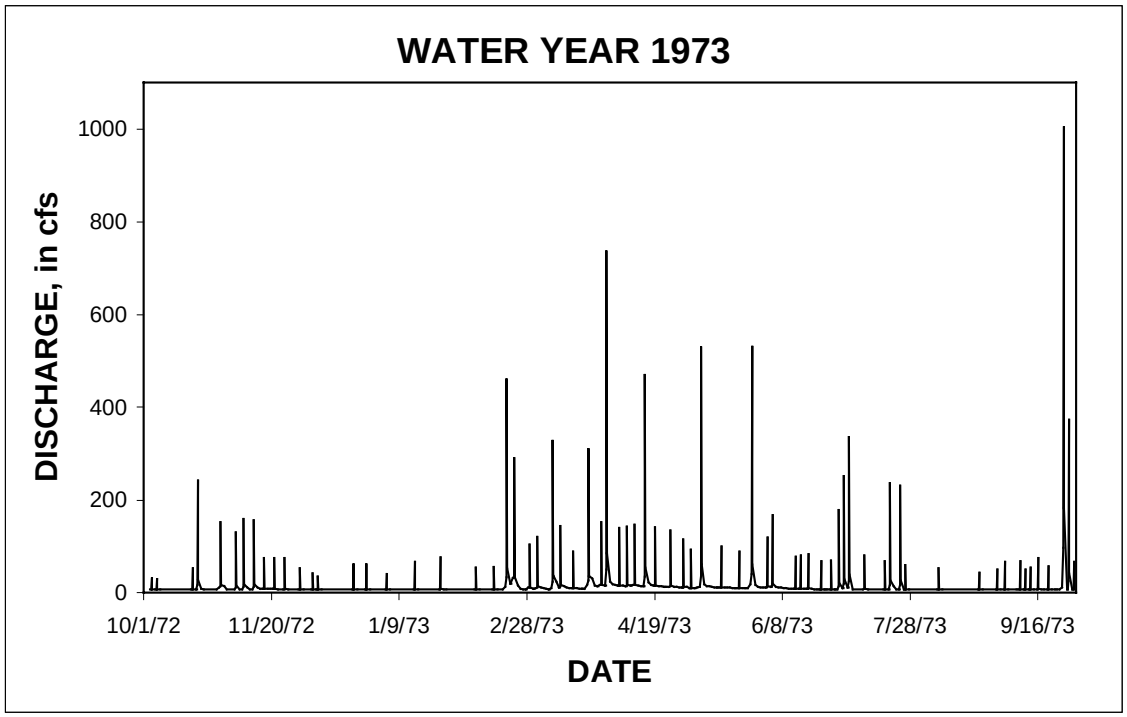

Figure II.38 Discharge hydrograph at the North Branch West Papillion Creek (Fort St) for water year 1973.

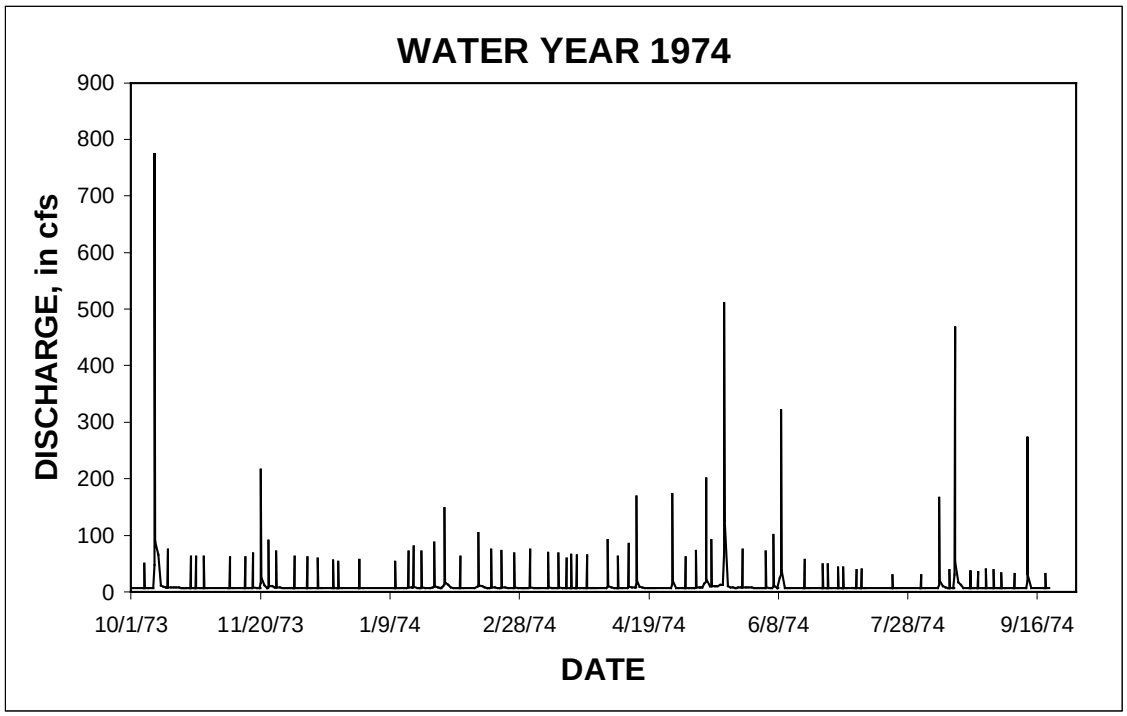

Figure II.39 Discharge hydrograph at the North Branch West Papillion Creek (Fort St) for water year 1974.

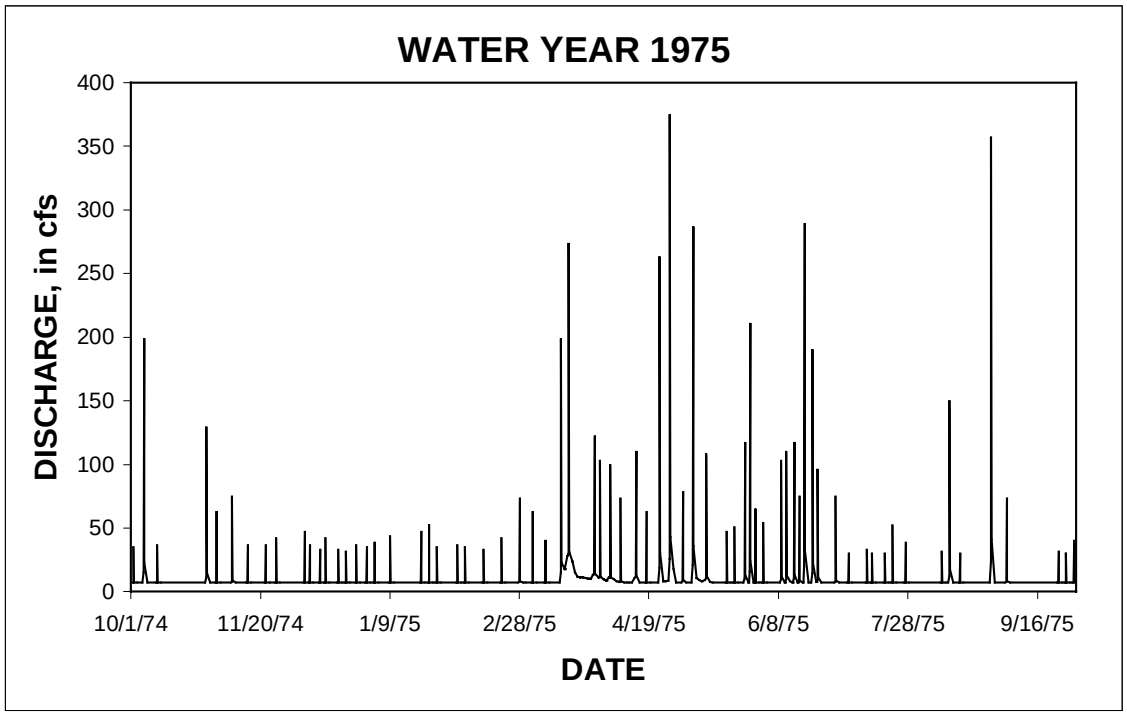

Figure II.40 Discharge hydrograph at the North Branch West Papillion Creek (Fort St) for water year 1975.

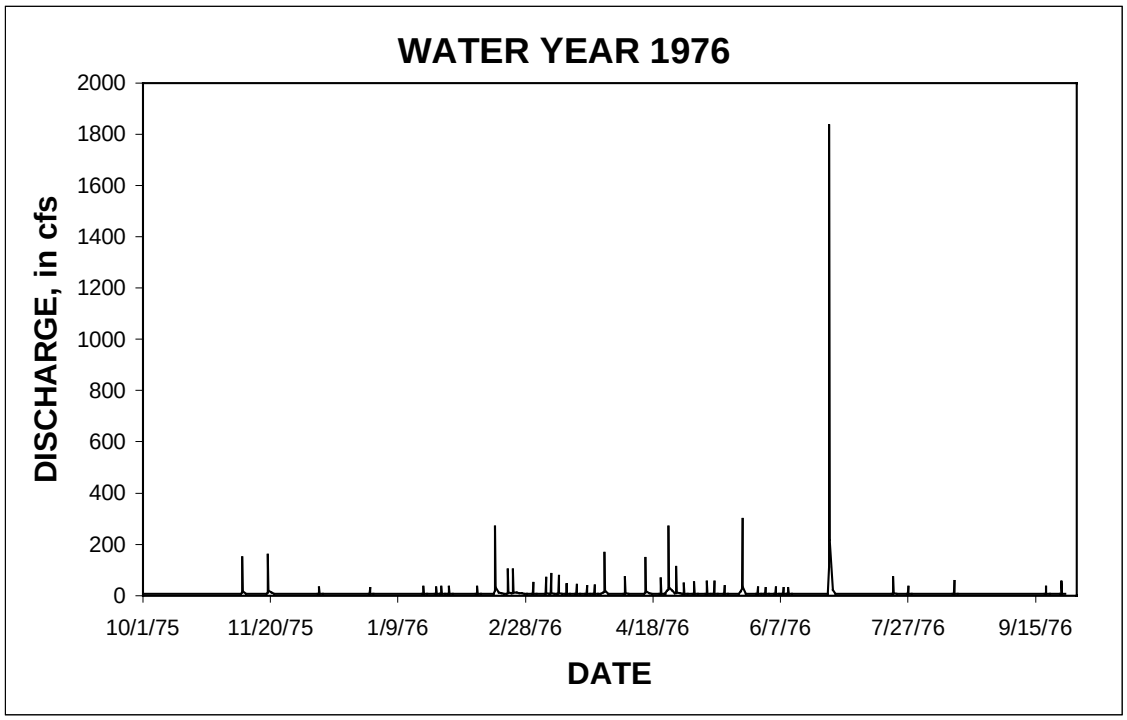

Figure II.41 Discharge hydrograph at the North Branch West Papillion Creek (Fort St) for water year 1976.

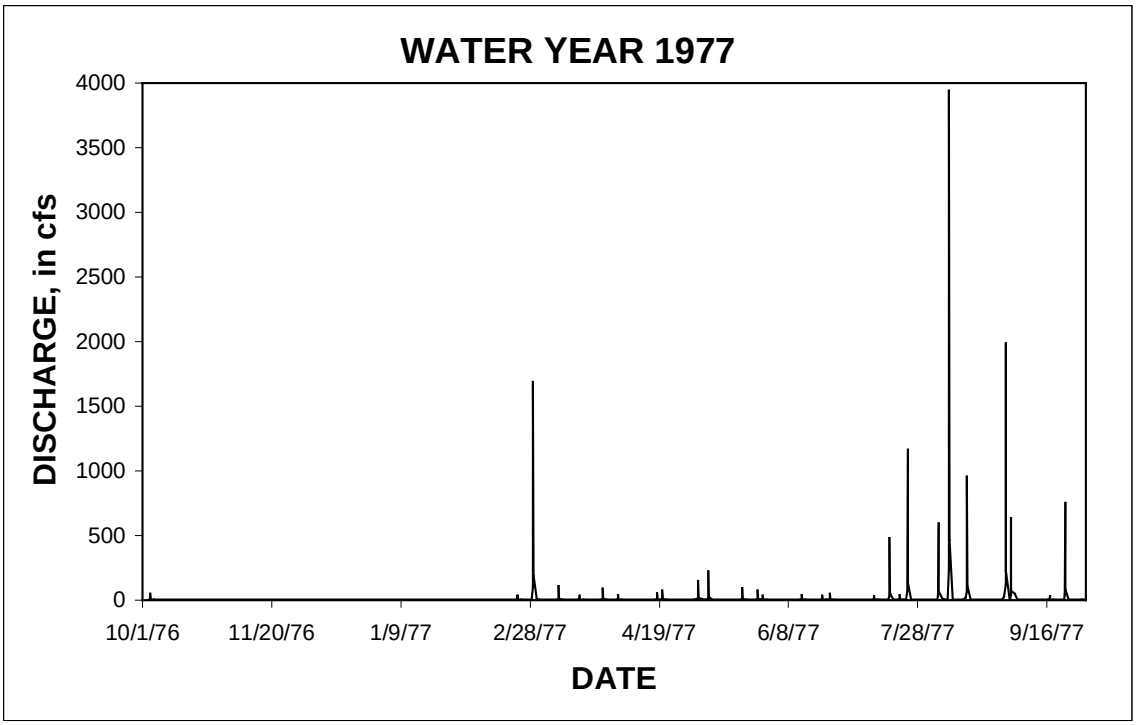

Figure II.42 Discharge hydrograph at the North Branch West Papillion Creek (Fort St) for water year 1977.

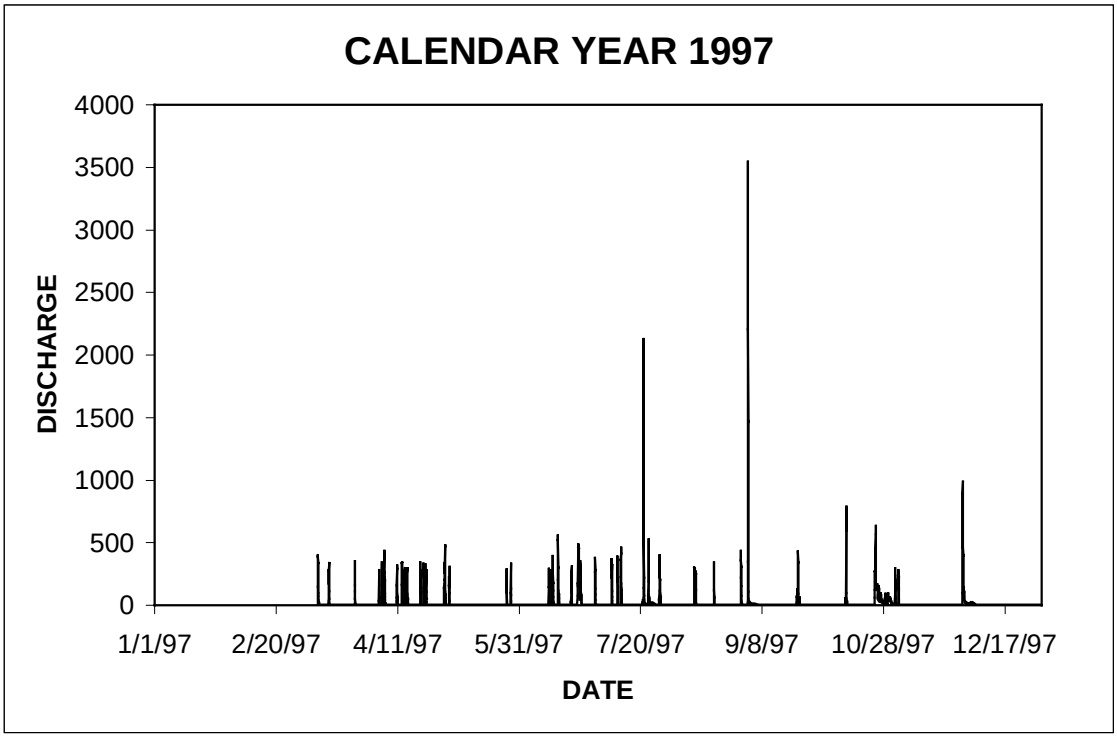

Figure II.43 Discharge hydrograph at the North Branch West Papillion Creek (Fort St) for calendar year 1997.